NASA/TM—2002–211545

Analysis of Graphite-Reinforced Cementitious Composites

R.E. Vaughan
Marshall Space Flight Center, Marshall Space Flight Center, Alabama

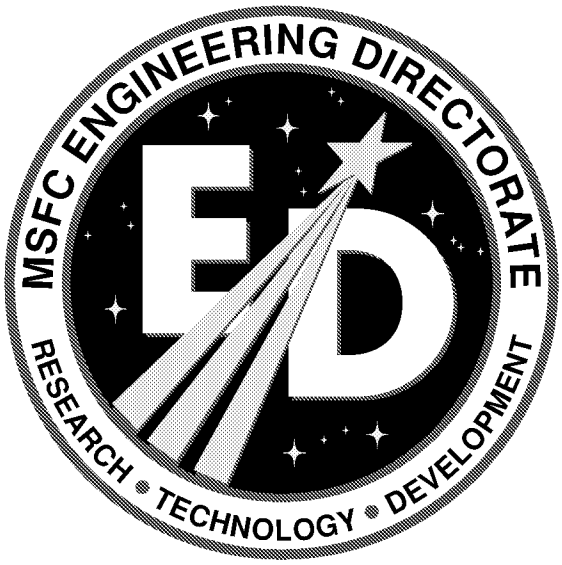

February 2002

The NASA STI Program Office…in Profile

Since its founding, NASA has been dedicated to the advancement of aeronautics and space science. The NASA Scientific and Technical Information (STI) Program Office plays a key part in helping NASA maintain this important role.

The NASA STI Program Office is operated by Langley Research Center, the lead center for NASA's scientific and technical information. The NASA STI Program Office provides access to the NASA STI Database, the largest collection of aeronautical and space science STI in the world. The Program Office is also NASA's institutional mechanism for disseminating the results of its research and development activities. These results are published by NASA in the NASA STI Report Series, which includes the following report types:

- TECHNICAL PUBLICATION. Reports of completed research or a major significant phase of research that present the results of NASA programs and include extensive data or theoretical analysis. Includes compilations of significant scientific and technical data and information deemed to be of continuing reference value. NASA's counterpart of peer-reviewed formal professional papers but has less stringent limitations on manuscript length and extent of graphic presentations.

- TECHNICAL MEMORANDUM. Scientific and technical findings that are preliminary or of specialized interest, e.g., quick release reports, working papers, and bibliographies that contain minimal annotation. Does not contain extensive analysis.

- CONTRACTOR REPORT. Scientific and technical findings by NASA-sponsored contractors and grantees.

- CONFERENCE PUBLICATION. Collected papers from scientific and technical conferences, symposia, seminars, or other meetings sponsored or cosponsored by NASA.

- SPECIAL PUBLICATION. Scientific, technical, or historical information from NASA programs, projects, and mission, often concerned with subjects having substantial public interest.

- TECHNICAL TRANSLATION. English-language translations of foreign scientific and technical material pertinent to NASA's mission.

Specialized services that complement the STI Program Office's diverse offerings include creating custom thesauri, building customized databases, organizing and publishing research results…even providing videos.

For more information about the NASA STI Program Office, see the following:

- Access the NASA STI Program Home Page at ***http://www.sti.nasa.gov***

- E-mail your question via the Internet to help@sti.nasa.gov

- Fax your question to the NASA Access Help Desk at (301) 621–0134

- Telephone the NASA Access Help Desk at (301) 621–0390

- Write to:
  NASA Access Help Desk
  NASA Center for AeroSpace Information
  7121 Standard Drive
  Hanover, MD 21076–1320
  (301)621–0390

NASA/TM—2002–211545

Analysis of Graphite-Reinforced Cementitious Composites

R.E. Vaughan
Marshall Space Flight Center, Marshall Space Flight Center, Alabama

National Aeronautics and
Space Administration

Marshall Space Flight Center • MSFC, Alabama 35812

February 2002

TRADEMARKS

Available from:

NASA Center for AeroSpace Information
7121 Standard Drive
Hanover, MD 21076–1320
(301) 621–0390

National Technical Information Service
5285 Port Royal Road
Springfield, VA 22161
(703) 487–4650

TABLE OF CONTENTS

TABLE OF CONTENTS (Continued)

TABLE OF CONTENTS (Continued)

LIST OF FIGURES

LIST OF FIGURES (Continued)

LIST OF FIGURES (Continued)

LIST OF FIGURES (Continued)

LIST OF FIGURES (Continued)

LIST OF TABLES

LIST OF ACRONYMS

ASTM	American Society for Testing and Materials
TM	Technical Memorandum
UAH	University of Alabama in Huntsville

NOMENCLATURE

*	
A	extensional stiffness matrix (for composite plate theory)
A	total cross-sectional area
A_1	cross-sectional area for region 1
A_2	cross-sectional area for region 2
A_3	cross-sectional area for region 3
A_c	cross-sectional area for the cementitious region
A_{fiber}	cross-sectional area of the fiber
A_g	cross-sectional area for the graphite-reinforced region
A_{matrix}	cross-sectional area for the matrix region
A_{yarn}	cross-sectional area for one graphite yarn
a	dimension
B	coupling stiffness matrix
b	dimension
C	dimension
c	distance from centroid to the outer surface of the material
D	bending stiffness matrix
d	dimension
d_2	incremental thickness
E	Young's modulus (general term)
E_1	low Young's modulus
E_2	high Young's modulus
E_{axial}	axial Young's modulus
$E_{\text{composite}}$	composite Young's modulus

NOMENCLATURE (Continued)

$E_{\text{effective}}$	effective Young's modulus
E_{fiber}	Young's modulus for the fiber
E_{matrix}	Young's modulus for the matrix
$E_{\text{transverse}}$	transverse Young's modulus
E_x	Young's modulus for the x direction
E_y	Young's modulus for the y direction
G	shear modulus
G_{12}	shear modulus for the 1-2 direction
G_{fiber}	shear modulus for fiber
G_{matrix}	shear modulus for matrix
G_{xy}	shear modulus for the x-y direction
h	dimension
h_c	center of the top section
h_g	center of the graphite-reinforced section
I	moment of inertia (general term)
I_c	moment of inertia for cementitious section
I_{c_total}	moment of inertia for cementitious section with respect to composite beam
I_g	moment of inertia for graphite-reinforced section
I_{g_total}	moment of inertia for reinforced section with respect to composite beam
I_{total}	total moment of inertia for composite beam
I_x	moment of inertia for x direction
i	counting increment
K	curvature of a plane curve
K_x	rate of change of the curvature in x direction
K_y	rate of change of the curvature in y direction
k	refers to layers in laminated plate

NOMENCLATURE (Continued)

L	original length
L_{fiber}	fiber material length
L_{matrix}	matrix material length
M	moment
N_x	force in x direction
N_{xy}	shear load
N_y	force in y direction
N_{yarn}	number of yarns
n	number of layers in the plate
o	initial or midplane
P	force or load
P_{fiber}	force in fiber material
P_{matrix}	force in matrix material
Q	stiffness matrix
Q_n	stiffness matrix
$\overline{Q}$	transformed stiffness matrix
$\overline{Q}_n$	transformed stiffness matrix for layer n
R	Reuter's matrix
S	compliance matrix
S_n	compliance matrix for layer n
T	transformation matrix
T^{-1}	inverse of the transformation matrix
T_n	transformation for layer n
t	thickness
t_k	lamina thickness of layer k

NOMENCLATURE (Continued)

u	displacement in x direction
V	load matrix when solving for composite properties
V_{fiber}	volume fraction for fiber
V_{matrix}	volume fraction for matrix
v	displacement in y direction
W	dimension, gauge width
w	dimension width
w_c	width of the cementitious (matrix) section
w_g	width of the graphite-reinforced section
X_{bar}	centroid of beam
x	dimension
xo	initial x dimension
Y_{bar}	centroid location
y	direction
y'	dimension
$\bar{y}'*$	centroid location, weighted section
y_{cal}	calculated deflection
y_{fem}	deflection from finite element model
y_g	centroid graphite section
y_{max}	maximum deflection of beam
y_{test}	actual deflection of beam during test
z	center of the lamina
z'	dimension
$\bar{z}'*$	dimension
z_k	distance from the lamina midplane to the center of the kth layer

NOMENCLATURE (Continued)

β	width of composite beam
γ	shear strain, shear deformation
γ_{0xy}	midplane shear strain
γ_{12}	shear for in the 1-2 coordinate system
γ_{fiber}	shear in the reinforcement fiber
γ_{matrix}	shear in the matrix material
γ_{max}	maximum value of shear strain
γ_{xy}	shear strain in the *x*-*y* coordinate system
Δ	change in
Δ_{error}	error
$\Delta_{\text{shear deflection}}$	error
Δw	total transverse deflection
Δw_{fiber}	fiber deflection
Δw_{matrix}	matrix deflection
δ	deflection
ε	strain (general term)
ε_0	midsurface strain
ε_1	strain in direction 1
ε_2	strain in direction 2
ε_{12}	tensorial strain
$\varepsilon_{\text{axial}}$	strain in fiber
$\varepsilon_{\text{fiber}}$	strain in fiber
$\varepsilon_{\text{matrix}}$	strain in matrix
$\varepsilon_{\text{matrix}_i}$	strain in matrix
$\varepsilon_{\text{trans}}$	strain in transverse direction
ε_x	strain in *x* direction

NOMENCLATURE (Continued)

ε_y	strain in *y* direction
η	elastic modulus ratio, transform section ratio, Young's modulus ratio
θ	slope of a beam in bending (for beam equations)
θ	ply angle (for composite plate equations)
ν_{12}	Poisson's ratio for direction 1-2
$\nu_{\text{composite}}$	Poisson's ratio for composite
ν_{fiber}	Poisson's ratio for the fiber
ν_{matrix}	Poisson's ratio for the matrix
ν_{xy}	Poisson's ratio in *xy* direction
ρ_{fiber}	density of the fiber
ρ_{matrix}	density of the matrix
σ	stress
σ_1	stress in 1 direction
σ_2	stress in 2 direction
σ_{fiber}	fiber stress
σ_{matrix}	matrix stress
σ_x	stress in *x* direction
σ_y	stress in *y* direction
σ_z	stress in *z* direction
τ	shear stress
Ψ	strain valued calculated from least-squares method
ψ	ply angle
ς	measure of reinforcement

TECHNICAL MEMORANDUM

ANALYSIS OF GRAPHITE-REINFORCED CEMENTITIOUS COMPOSITES

1. THE PROBLEM

1.1 Introduction

In research on composite beams, Biszick[1] noted that the transform section method did not accurately predict the behavior of the test articles being considered. Biszick documented that a highly efficient structure; i.e., weight and strain energy, could be developed using a matrix with a very low Young's modulus (E_1) and reinforcement with a very high Young's modulus (E_2). These test articles were cementitious beams reinforced with a graphite mesh. The graphite mesh was used in the same way as steel mesh in conventional reinforced concrete; i.e., the reinforcement reacts on the tensile loads, while the concrete reacts on the compressive loads. Significant differences should be noted between a graphite mesh and a similar steel mesh. First, the graphite mesh has no bending or compression stiffness. The mesh drapes, if not supported, and does not resist a compressive force; i.e., cloth. Second, the graphite appears to be saturated by the cement (matrix), such that an adhesive bond forms between the cement and graphite. The cementitious mix used in the test articles was also unique and exhibited ductile properties. Biszick's research showed conclusively that maintaining a high elastic modulus ratio (η), i.e., $E_{\text{fiber}}/E_{\text{matrix}}$, between the matrix and the reinforcement results in efficient composite structures. It follows then, to fully utilize this discovery, the analytical methods must be understood and developed.

This Technical Memorandum (TM) investigates the analytical methods for the analysis of graphite-reinforced cementitious composites where high η's are employed. A sample problem will demonstrate the transform section method of analysis. A finite element model will then be developed and the results compared to the transform section method of analysis. The errors associated with the transform section method and high η's will be demonstrated. Alternative methods of analysis will then be investigated. The rule of mixtures[2–4] will be applied to a graphite-reinforced cementitious composite to calculate effective material properties. These properties will be introduced into the transform section method and the results compared to finite element methods and beam testing. Laminated composite plate theory will then be discussed and applied to the graphite-reinforced cementitious composite. It will be shown that laminated plate theory for composites can successfully be applied to this type of composite. Extensive experimentation is used to develop the material properties used in the laminated plate theory. Graphite-reinforced cementitious composite beams are analyzed using classical composite methods and compared to finite element methods and experimental results.

1.2 Problem Statement

Section 1.2 illustrates a problem with the analysis of a composite beam that has a high elastic modulus ratio. First, the expression for the moment of inertia (I) is derived in terms of η. The moment of inertia is then used to calculate the deflection of a beam subjected to pure bending. The deflection of the beam is calculated as η ranges from 1 to 1,000. The analysis is then repeated using a finite element model. The conclusion is made that the transform section method of analysis is not accurate for $\eta > 20$.

1.3 Composite Beam

Figure 1 illustrates a beam composed of two different materials. Since the beam is subjected to boundary conditions and loads to produce pure bending between the supports (fig. 2), the transform section property method may be used to determine the deflection in the beam for each of the load cases described in table 1. These results can be compared to those obtained from a finite element model.[5]

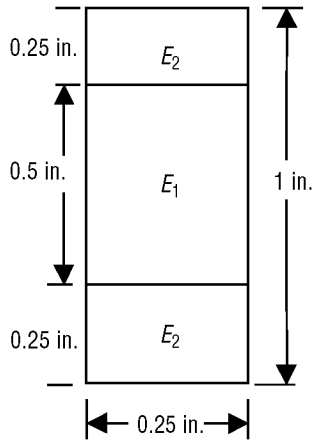

Figure 1. Beam cross section.

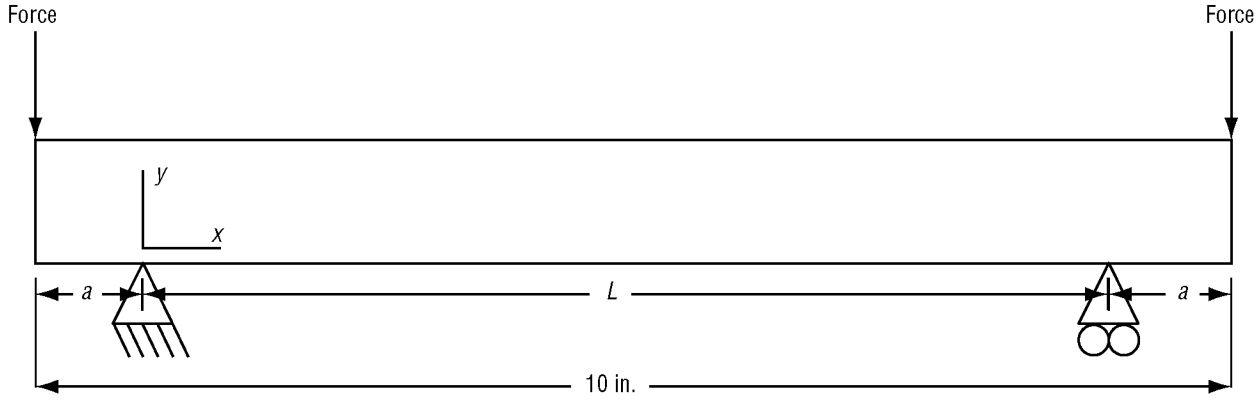

Figure 2. Beam in pure bending.

Table 1. Loads and deflections for transform section method.

Case	E_1	E_2	η	Flange	I_x	Deflection
1	3.00E+07	3.00E+07	1	0.347	0.0289	9.22722E–03
2	1.50E+07	3.00E+07	2	0.694	0.0542	9.84010E–03
3	7.50E+06	3.00E+07	4	1.388	0.1048	1.01781E–02
4	3.00E+06	3.00E+07	10	3.470	0.2566	1.03923E–02
5	2.14E+06	3.00E+07	14	4.858	0.3578	1.04341E–02
6	1.50E+06	3.00E+07	20	6.940	0.5097	1.04657E–02
7	1.00E+06	3.00E+07	30	10.410	0.7627	1.04904E–02
8	7.50E+05	3.00E+07	40	13.880	1.0157	1.05028E–02
9	3.75E+05	3.00E+07	80	27.760	2.0278	1.05215E–02
10	3.00E+05	3.00E+07	100	34.700	2.5338	1.05252E–02
11	2.50E+05	3.00E+07	120	41.640	3.0399	1.05277E–02
12	1.50E+05	3.00E+07	200	69.400	5.0640	1.05327E–02
13	1.36E+05	3.00E+07	220	76.340	5.5701	1.05334E–02
14	1.00E+05	3.00E+07	300	104.100	7.5942	1.05352E–02
15	7.50E+04	3.00E+07	400	138.800	10.1244	1.05364E–02
16	6.00E+04	3.00E+07	500	173.500	12.6547	1.05372E–02
17	5.00E+04	3.00E+07	600	208.200	15.1849	1.05377E–02
18	3.00E+04	3.00E+07	1,000	347.000	25.3057	1.05387E–02

1.4 Analysis Using the Transform Section Method

The equation for the deflection (y_{max}) of a beam (fig. 3) in pure bending can be derived using the elastic curve equations and the boundary conditions:

$$y_{max} = \frac{Pax}{2E_1 I}(L - x) \quad . \tag{1}$$

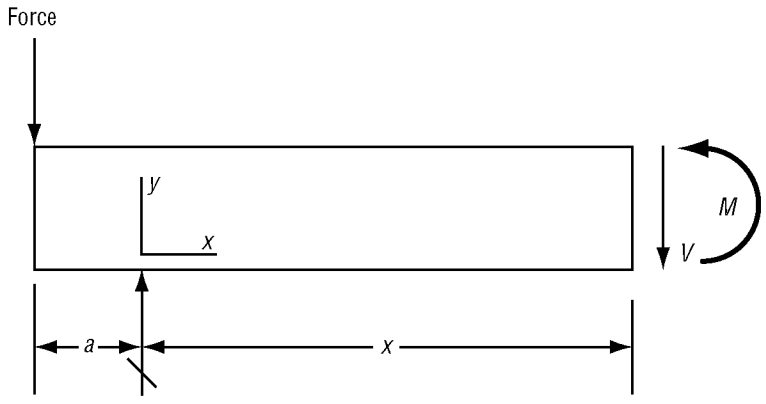

Figure 3. Free-body diagram.

The effective value of the moment of inertia can be calculated using the transform section method;[6] A_1 and A_3 are made from a material with properties of E_2. A_2 is made from a material with properties of E_1. The original cross section of the beam (fig. 4) is modified per the transform section method. The moment of inertia is then calculated from the new geometry and summarized below:

- Material properties of the composite beam: $E_1 = 360 \times 10^3$ lbf/in.^{2}, $E_2 = 30 \times 10^6$ lbf/in.^{2}
- Transform section ratio: $\eta = E_2/E_1$, $\eta = 83.33$
- Width of the composite beam: $\beta = 0.347$ in.
- Moment of inertia calculation:

$$I_1 = \int_{0.25}^{0.5} y^2 \eta\beta \, dy \qquad I_2 = \int_{-0.25}^{0.25} y^2 \beta \, dy \qquad I_3 = \int_{0.5}^{-0.25} y^2 \eta\beta \, dy$$

$$= 3.645 \times 10^{-2} \eta\beta \qquad = 1.0416 \times 10^{-2} \beta \qquad = 3.645 \times 10^{-2} \eta\beta$$

$$I_1 = 1.045 \text{ in.}^4 \qquad I_2 = 0.004 \text{ in.}^4 \qquad I_3 = 1.045 \text{ in.}^4$$

$$I = I_1 + I_2 + I_3 \qquad I = 2.112 \text{ in.}^4$$

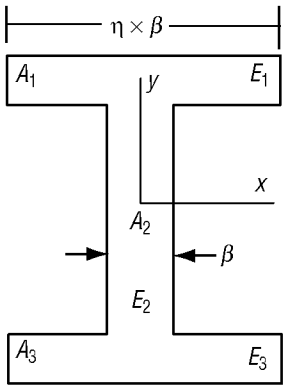

Figure 4. Transform section geometry.

It should be noted that the middle section of the beam (A_2) is independent of η. As η increases, section A_2 becomes insignificant. The expression for I can be written in terms of η as follows:

$$I = 3.645\times10^{-2}\eta\beta + 1.0416\times10^{-2}\beta + 3.645\times10^{-2}\eta\beta$$

$$I = 7.29\times10^{-2}\eta\beta + 1.0416\times10^{-2}\beta \ . \tag{2}$$

Let $\beta = 0.347$ in., then

$$I = 2.53\times10^{-2}\eta + 3.6\times10^{-3} \text{ in.}^4 \tag{3}$$

Now this expression can be substituted into the elastic curve equation:

$$y_{\max} = \frac{Pax}{2E_1(0.00253\eta + 0.0036)}\left(\frac{L}{2}\right) \ . \tag{4}$$

Since $\eta = \dfrac{E_2}{E_1}$,

$$y_{\max} = \frac{Pax}{2E_1\left(0.00253\left(E_2/E_1\right) + 0.0036\right)}\left(\frac{L}{2}\right) \ , \tag{5}$$

so that

$$y_{\max} = \frac{Pax}{0.0506E_2 + 0.0072E_1}\left(\frac{L}{2}\right) \ . \tag{6}$$

Equation (6) is used in a Microsoft® Excel spreadsheet to calculate the deflection for each case. As shown in table 1, E_2 remains constant while E_1 decreases. As the Young's modulus ratio (η) increases from 1 to 1,000, the deflection value increases to 0.015 in. and then becomes essentially constant.

1.5 Analysis Using the Finite Element Method

A finite element model of the beam was generated using the MSC/Nastran finite element code.[5] The model is composed of quad4 plate elements with loads and constraints (fig. 5). The model returned a maximum deflection of 9.19×10^{-3} for $\eta = 1$. The results of the finite element model can be compared to the results from the elastic curve equation for the same case:

$$\text{Error\%} = \left|\frac{Y_{\text{model}} - Y_{\text{equation}}}{Y_{\text{model}}}\right|\times100\% = \left|\frac{0.00919 - 0.00922}{0.00919}\right|\times100\% = 0.39\% \ . \tag{7}$$

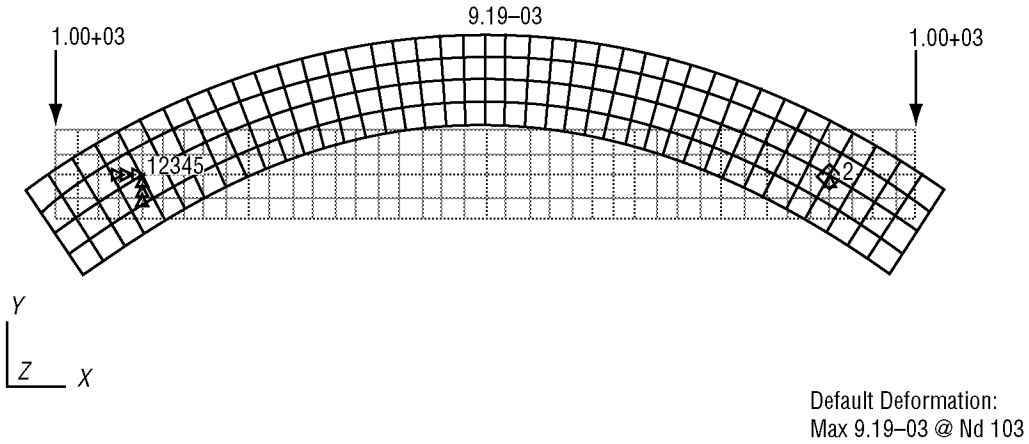

Figure 5. Finite element model.

The analysis of the first case indicates that the transform section method and the finite element model are in good agreement. The finite element model was run for each of the 18 cases. The results were tabulated in the Excel spreadsheet (table 2).

Table 2. Results of the finite element analysis.

Case	E_1	E_2	η	I_x	Deflection	Model	Error (%)
1	3.00E+07	3.00E+07	1	0.0289	9.22722E–03	9.19E–03	–0.39
2	1.50E+07	3.00E+07	2	0.0542	9.84010E–03	9.78E–03	–0.66
3	7.50E+06	3.00E+07	4	0.1048	1.01781E–02	1.01E–02	–1.10
4	3.00E+06	3.00E+07	10	0.2566	1.03923E–02	1.02E–02	–2.01
5	2.14E+06	3.00E+07	14	0.3578	1.04341E–02	1.02E–02	–2.30
6	1.50E+06	3.00E+07	20	0.5097	1.04657E–02	1.02E–02	–2.24
7	1.00E+06	3.00E+07	30	0.7627	1.04904E–02	1.04E–02	–1.29
8	7.50E+05	3.00E+07	40	1.0157	1.05028E–02	1.06E–02	0.51
9	3.75E+05	3.00E+07	80	2.0278	1.05215E–02	1.19E–02	11.88
10	3.00E+05	3.00E+07	100	2.5338	1.05252E–02	1.29E–02	18.16
11	2.50E+05	3.00E+07	120	3.0399	1.05277E–02	1.39E–02	24.15
12	1.50E+05	3.00E+07	200	5.0640	1.05327E–02	1.84E–02	42.76
13	1.36E+05	3.00E+07	220	5.5701	1.05334E–02	1.96E–02	46.26
14	1.00E+05	3.00E+07	300	7.5942	1.05352E–02	2.42E–02	56.54
15	7.50E+04	3.00E+07	400	10.1244	1.05364E–02	2.96E–02	64.44
16	6.00E+04	3.00E+07	500	12.6547	1.05372E–02	3.44E–02	69.35
17	5.00E+04	3.00E+07	600	15.1849	1.05377E–02	3.85E–02	72.59
18	3.00E+04	3.00E+07	1,000	25.3057	1.05387E–02	4.86E–02	78.31

The deflection values from the two methods of analysis are plotted as η increases from 1 to 80. Figure 6 illustrates that the transform sections method of analysis results in a constant deflection as η approaches 20. The finite element model and the transform section method are in reasonable agreement until η reaches 40. Beyond 40 the significant differences in the analysis methods are obvious.

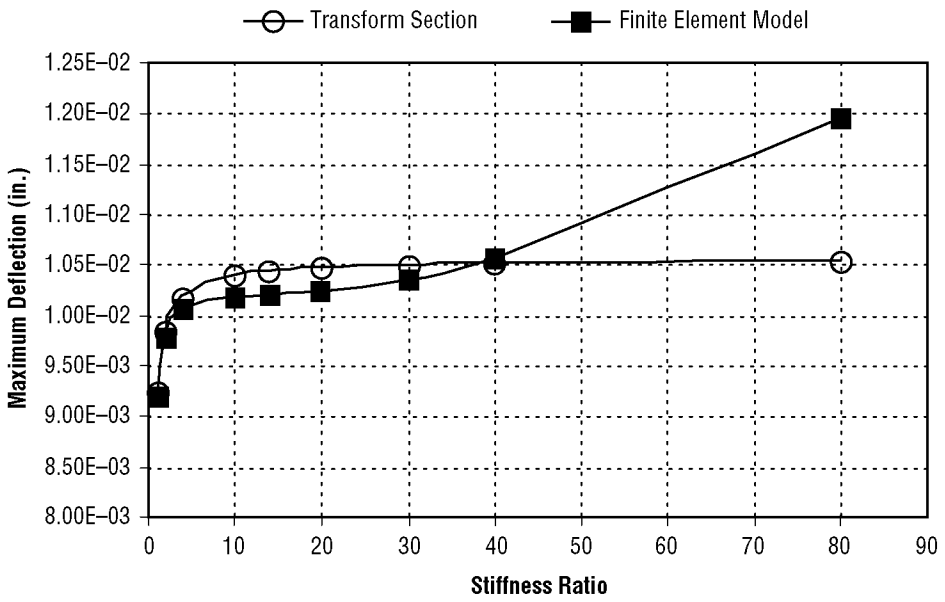

Figure 6. Comparison of transform section method to finite element methods.

This sample problem illustrates the current state of the art for the analysis of graphite-reinforced cementitious materials. This analysis leads to the conclusion that the transform section method of analysis is not adequate for the analysis of graphite-reinforced cementitious composites. The literature search included in section 2 was undertaken to determine an alternate approach.

2. LITERATURE REVIEW

Section 2 provides the background necessary to develop an understanding of the process required to analyze graphite-reinforced cementitious composites. The basic theories used in the analysis are discussed to provide context for subsequent derivation. The material presented here is intended to give the reader a sense of direction for this TM.

2.1 Introduction

A fiber-reinforced material consists of two components: fiber and cement. The cement fills the space around the fibers and keeps them in position. The hardened cement adheres to the fibers, allowing a transfer of load. The type of fiber reinforcement may consist of a variety of materials: steel bars, glass fabric, ceramic whiskers, or carbon strands, to name a few. There are many types of cement as well, including epoxy, polyesters, aluminum alloys, and cementitious materials. In general, the cement material is isotropic while the fibers are longitudinal components that can react to forces along their axes. The fibers are typically much stronger and stiffer than the cement. The material properties of the fiber-reinforced composite are typically orthotropic in nature. The elastic properties of the composite depend on the properties of its constitutive materials, the mix ratio of the components, and the orientation of the fibers.

The literature associated with composite analysis and development covers a phenomenal range of applications, from the *International Space Station* to the common kitchen sink. However, the one common and elusive goal of researchers is to develop a method to predict the elastic properties of a composite from the properties and geometry of the constitutive materials. The purpose of this literature search is to determine which methods will most likely work for the graphite cementious materials being considered in this TM.

2.2 Structural Engineering Approach

The structural engineering approach is illustrated in the transform section method of analysis (sec. 1.3). The most common form of the equation is explained in detail by Beer and Johnston.[6] This approach is often associated with the analysis of steel bars embedded in a concrete matrix. Allen and Haisler[7] modify the approach in a concept referred to as the modulus weighted section properties. In this approach, the beam is divided into discrete homogeneous parts (fig. 7). The modulus weighted section properties are then defined in terms of the Young's modulus ratios as follows:

$$A^* = \sum_{i=1}^{n} \frac{E_i}{E_1} A_i \tag{8}$$

$$\bar{y}'^{*} = \frac{1}{A^*}\sum_{i=1}^{n}\frac{E_i}{E_1}\bar{y}_i' A_i \tag{9}$$

$$\bar{z}'^{*} = \frac{1}{A^*}\sum_{i=1}^{n}\frac{E_i}{E_1}\bar{z}_i' A_i \tag{10}$$

$$I^*_{yy'} = \sum_{i=1}^{n}\frac{E_i}{E_1}\left(I_{y_o y_{oi}} + \bar{z}_i'^2 A_i\right) . \tag{11}$$

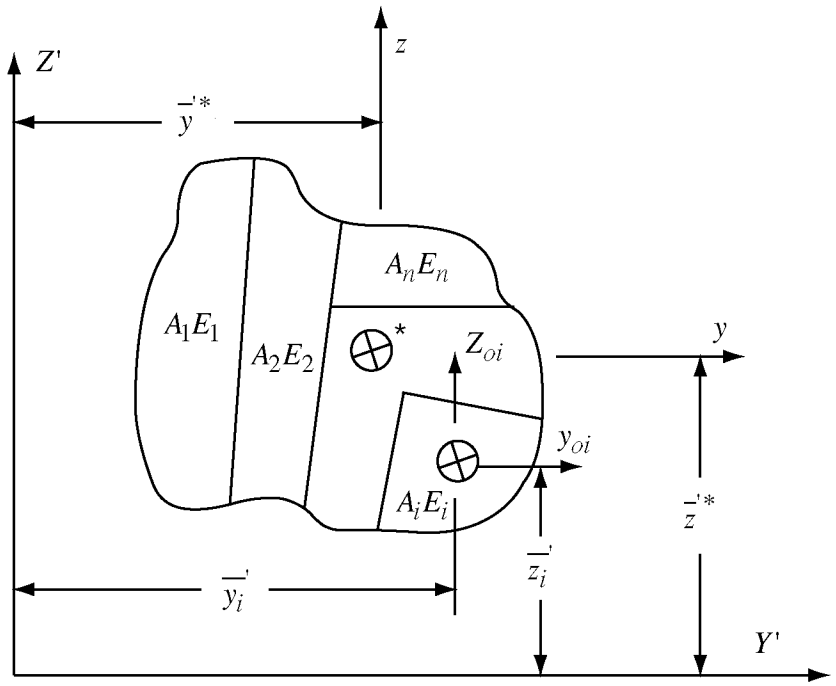

Figure 7. Composite cross section for weight modulus properties.

This method of determining the section properties for a composite beam is considerably more complex than methods described by Beer and Johnston.[6] However, the elastic modulus ratio ($\eta = E_2/E_1$) governs this equation, and as the value of η increases, the accuracy of the method decreases.

Balaguru[2] developed another interesting approach to the analysis of composite beams. Ferrocement is a composite material, consisting primarily of several layers of wire or fiberglass mesh embedded in a cementitious matrix. Balaguru[2] developed an analytical model of the composite beams from the stress-strain curves of the constitutive materials. The model uses section properties calculated

from the transform section method. However, Balaguru takes into account the nonlinear properties of the materials. As the weaker of the materials becomes nonlinear, Young's modulus is recalculated. The new value is used to determine the section properties for the nonlinear load. Balaguru's methods seemed promising for the analysis of the composite considered here; particularly, since the method had been used for the analysis of glass fibers with a cementitious matrix. However, on further investigation,[8] it was found that the analytical method suffered from the same limitations as those encountered with the transform section method. Nonetheless, Balaguru's methods were successfully used with a modified transform section method (sec. 4.13) to determine the deflections of a composite beam considered here.

The common theory used for the structural engineering approach is the transform section method. This approach is the primary cause of "the problem" discussed in section 1. Further investigation into the structural engineering approach would be unavailing.

2.3 Mechanics of Materials Approach to Composites

The mechanics of materials approach to composites is fundamentally different from the structure's approach discussed previously. This approach is based on the mix ratio (volume fraction) between the fiber and cementitious materials. The mechanics of materials approach is often referred to as the rule of mixtures for composites. The goal of this theory is to determine the "effective" elastic material properties: Young's modulus (E_1 and E_2), shear modulus (G_{12}), and Poisson's ratio (ν_{12}) from the material properties of the fiber and cementitious material. Numerous examples for the mechanics of materials approach can be found in the literature,[9,10] and the method is explained in detail in section 4. The literature is unanimous[2,9,10] in declaring this method accurate for determining the effective material property E_1, provided the fibers are continuous and aligned in the direction of the load. The remaining material properties, E_2, G_{12}, and ν_{12}, may not be accurately predicted by the rule of mixtures. Although Jones[10] provides detailed and convincing derivations for these material properties, he points out several assumptions in the theory that would lead to errors in the calculation of the values. In addition, Jones[10] strongly points to the need for experimental data to verify the results. Balaguru[4] provides the equations to determine the value of E_1; however, he chose not to address the remaining properties. The literature contains numerous variations on the rule of mixtures theory. These variations attempt to correct the deficiencies in the theory.

Halpin-Tsai,[9,11] for example, made significant contributions to the rule of mixture methods by developing the Halpin-Tsai equations:

$$E_1 \cong E_{\text{fiber}} V_{\text{fiber}} + E_{\text{matrix}} V_{\text{matrix}} \tag{12}$$

$$\nu_{12} \cong \nu_{\text{fiber}} V_{\text{fiber}} + \nu_{\text{matrix}} V_{\text{matrix}} \tag{13}$$

$$\frac{E_2}{E_{\text{matrix}}} = \frac{\left(1 + \varsigma \eta V_{\text{fiber}}\right)}{\left(1 - \eta V_{\text{fiber}}\right)}, \text{ where } \eta = \left(\frac{E_{\text{fiber}}}{E_{\text{matrix}}} - 1\right)\left(\frac{E_{\text{fiber}}}{E_{\text{matrix}}} + \varsigma\right) \tag{14}$$

$$\frac{G_{12}}{G_{\text{matrix}}} = \frac{\left(1+\varsigma\eta V_{\text{fiber}}\right)}{\left(1-\eta V_{\text{fiber}}\right)}, \quad \text{where } \eta = \left(\frac{G_{\text{fiber}}}{G_{\text{matrix}}} - 1\right)\left(\frac{G_{\text{fiber}}}{G_{\text{matrix}}} + \varsigma\right) . \tag{15}$$

The measure of reinforcement (ς) depends on the boundary conditions within the composite and is an empirically derived value for the specific composite. Jones[10] provided sufficient evidence that these equations are accurate, provided ς is available for the composite being considered. However, no data were available for graphite-reinforced cementitious composites.

Another promising variation on the rule of mixtures method is provided by Krenchel.[3] Krenchel used an equilibrium approach that considered reinforcements in both the *x* and *y* directions. The methods provided by Krenchel were applied to the composite considered here. The ply angles ψ_1 and ψ_2 are measured from the direction of the load. The β term represents the volume fraction for the fiber. The *k* term is given by $k = 1 - \beta/(1 - \nu^2_{\text{composite}})$, and must be estimated since $\nu_{\text{composite}}$ is not known. The following equations are then solved simultaneously to determine $E_{\text{composite}}$:

- Stress in direction of force –*x*:

$$E_{\text{composite}}\varepsilon_x = E_{\text{matrix}}k\left(\varepsilon_x + \nu_{\text{matrix}}\varepsilon_y\right) + \left[E_{\text{fiber}}\beta\cos\left(\psi_1\right)^2\left(\varepsilon_x\cos\left(\psi_1\right)^2 + \varepsilon_y\sin\left(\psi_1\right)^2\right)\right]$$

$$+\left[E_{\text{fiber}}\beta\cos\left(\psi_2\right)^2\left(\varepsilon_x\cos\left(\psi_2\right)^2 + \varepsilon_y\sin\left(\psi_2\right)^2\right)\right] \tag{16}$$

- Stress in transverse direction –*y*:

$$0 = E_{\text{matrix}}k\left(\nu_{\text{matrix}}\varepsilon_x + \varepsilon_y\right) + \left[E_{\text{fiber}}\beta\sin\left(\psi_1\right)^2\left(\varepsilon_x\cos\left(\psi_1\right)^2 + \varepsilon_y\sin\left(\psi_1\right)^2\right)\right]$$

$$+\left[E_{\text{fiber}}\beta\cos\left(\psi_2\right)^2\left(\varepsilon_x\cos\left(\psi_2\right)^2 + \varepsilon_y\sin\left(\psi_2\right)^2\right)\right] \tag{17}$$

- Poisson's ratio:

$$\nu_{\text{composite}} = \frac{-\varepsilon_y}{\varepsilon_x} . \tag{18}$$

The Krenchel approach provides significant promise because it considers the loads and forces in both directions. His equations were solved for the example considered in section 4.6 and returned correct values for E_1 and E_2 (app. A). However, the shear modulus (G_{12}) returned the same value as the previous methods. Additionally, Krenchel had no verification data for the shear modulus calculations.

In summary, it can be said that the mechanics of materials approach will provide a set of effective material properties for a fiber-reinforced composite. Balaguru[4] and Krenchel[3] applied the method for fiber-reinforced cementious materials. Krenchel's methods can be manipulated to provide E_1 and E_2 for a composite. However, the literature indicates that estimates of the shear modulus and Poisson's ratio were questionable. Researchers were unanimous in their endorsement of establishing an experimental database for any composite being characterized for the first time.

2.4 Experimental Methods

The literature search for experimental methods concentrated on the standard test methods published by the American Society for Testing and Materials (ASTM). Two ASTM standards described the possible geometry of a tensile test specimen. ASTM Standard D 3039[5] recommended a tensile test specimen with bonded tabs while ASTM Standard E8[12] established the dogbone geometry. The purpose of both configurations is to provide a strong grip area, causing the specimen to strain and break in the center. Bonding grip tabs to the cementitious specimens were found to be difficult and impractical. The grips used on the tensile test machine limited the thickness of the tabs. One specimen with tab ends was successfully tested. However, the machined dogbone specimens (sec. 3.3) were much easier to produce and worked well. The ASTM recommendation to use extensometers to measure the strain was a significant impact to the tensile test. The extensometers were found to be unreliable because the knife blades would not grip the test article properly. Strain gauges provided a much more reliable method for strain measurement (sec. 3.5). Strain gauge installation was achieved by following the recommendations of Measurement Group Bulletin 309D.[13] In addition, Measurement Group Tech Tip TT–611[14] was reviewed for applicable information. Tech Tip TT–611[14] appears more suitable for large concrete structures.

Several experimental procedures for determining the shear modulus were offered by Jones.[10] The most compelling was producing a specimen with the fibers running at a 45° angle, and testing the specimen as a tensile test. Jones[10] provides the necessary equations to determine the shear modulus. However, ASTM standard D 5379–93[15] recommended an Iosipescu shear test for determining the shear modulus. On further investigations, it was found that the ASTM standard also had problems. Conant and Odom[16] identified numerous problems with the ASTM/Wyoming Iosipescu test fixture. The most significant was the tendency for the specimen to twist during testing. They made improvements to the design and termed it the Idaho shear test fixture. Ifju[17] describes a serious inadequacy in the instrumentation recommended in the ASTM standard.[15] Ifju[18] demonstrated that by using a strain gauge rosette, which covered the entire shear area, the accuracy of the test could be ensured. In addition, Ifju showed that by placing these gauges on each side of the specimen, the effects of twisting could be removed.

It was concluded from the literature search that the ASTM standard tensile[5,12] and shear test[15] for a composite material were the most desirable methods for determining the material properties

for a composite material. Interestingly, no reference was found to these tests being applied to graphite-based cementitious composites.

2.5 Laminated Plate Theory

Halpin, Jones, and Tsai[9–11] each considered the determination of the composite material properties as an intermediate step in the analysis of a composite. The next logical step is to use these effective material properties to develop a laminated composite plate. Gurdal[19] pointed out that a significant advantage of a composite material is the ability to optimize the geometry of the fibers for a given loading condition. Krenchel's[3] equations provided a crude means to rotate fibers in a cementitious matrix. However, his work was limited in that it assumes each layer will have the same geometry. The literature search failed to find an example of the laminated composite plate theory being applied to a fiber-reinforced cementitious composite.

The laminated plate theories provided by Jones[10] et al.[9,11,20] each contained similar derivations and arrived at the same equations for determining the effective material properties of a laminated plate. However, these authors each chose different methods to solve this complex system of equations. As a result, there is a significant difference in the final effective properties determined by the authors. Because of these conflicting results, the laminated plate theory is investigated. The equations are arranged in such a way as to allow an exact solution to be determined. In addition, Jones et al. developed separate solutions, depending on whether the laminated plate was symmetric or nonsymmetric in nature. It is not necessary to make that distinction for the equations developed here. As shown by Nettles,[20] the laminated composite plate theory can be used to determine the deflections, stresses, and strains for the multilayered composite plates. However, for complex loads or geometry, these methods are difficult to apply. The finite element methods offer an opportunity to analyze complex layups and geometry.

2.6 Finite Element Modeling

Matthews[21] illustrated that finite element analysis is applicable to composite materials, provided the user adequately represents the properties and layup of the plates. MSC/Nastran[22] was chosen as the finite element code because of the layered composite element capabilities. The example problem provided by Nettles[20] was analyzed using the finite element model. MSC/Nastran defined the required material input and the equations from laminated plate theory were used to generate the input data for the finite element model. Although the literature contains references to finite element modeling of fiber-reinforced cementitious beams, there was no reference for a multilayered plate.

3. MATERIAL PROPERTIES TESTING

The process of preparing and testing the tensile and shear specimens is described in section 3, along with details of mixing and placing the cementitious materials. The specimen geometry is briefly discussed and presented. The process of producing a graphite-reinforced composite plate is then described, followed by a unique method of machining the plates into tensile and shear specimens. The use of several types of extensometers and strain gauges is demonstrated for the tensile test specimens. A specialized Iosipescu strain gauge is described for the shear test. The tensile test procedure and the results from six test specimens are provided. The shear test procedure and the results for two shear test specimens are also included.

3.1 Mixing and Placing Cementitious Composites

Mixing and placing the cementitious matrix material is a very important aspect of specimen development. The cementitious mix used in this investigation was developed for use in the American Society of Civil Engineers' concrete canoe competition. The mix development is not a part of this investigation. Table 3 defines the mix used in all specimens.

Table 3. Ingredients of the cementitious mixture.

Cementitious Mixture	Grams
K–25 Microbubbles	218
Portland cement	558
Latex	310
Fortifier	150
Denatured water	~620

The constituents of the mix were each weighed prior to the mixing process (fig. 8). The K–25 microbubbles were then added to the cement in small amounts and stirred by hand. Care was taken not to break the microbubbles. The mixing process was judged complete by its color. The latex, fortifier, and half of the water were then poured together repeatedly to ensure a thorough mixing of the liquid ingredients—a very important step. It was found that the consistency of the cementitious matrix was smooth and creamy when the latex and fortifier were mixed with water before they were added to the dry ingredients. If the latex and fortifier are added separately, the consistency of the mixture is lumpy and coarse.

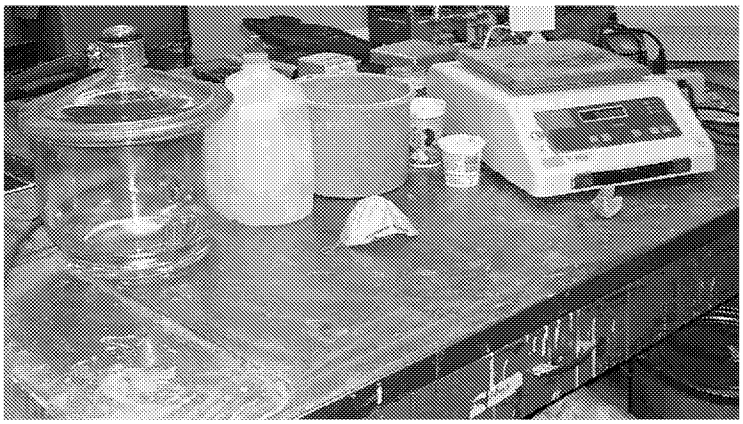

Figure 8. Tools used for mixing and weighing ingredients.

The liquid ingredients are then mixed with the cement and microbubbles. The remaining denatured water (≈50 percent of the original weight) is added until the mixture reaches the proper consistency. The cementitious mixture should be smooth and creamy with the consistency of warm butter (fig. 9). A mixture with too much water will leak out of the mold, leaving voids in the specimen. A mixture that is too dry will not "flow" around the graphite mesh, weakening the bond between the matrix and the reinforcement. In addition, a dry mixture will tend to displace the graphite as the mixture is pushed through the mesh.

Figure 9. Cementitious mixture with proper consistency.

Numerous attempts were made to remove air from the final mix before it was poured. Air in the mix was apparent by the high porosity seen in some of the specimens during finishing and sanding (fig. 10). The mix was placed in a vacuum bottle with a small vacuum applied (fig. 8). This process should be considered marginally successful. Too much vacuum pressure caused the mix to splatter and spill in the vacuum bottle. Reducing the vacuum to levels that eliminated the splatter had little effect on the amount of air in the mix. The mix was placed on vibrating and shaking tables, causing air bubbles to rise to the top of the mix. However, it tended to separate the mix (liquids came to the top) such that some remixing was necessary before placement.

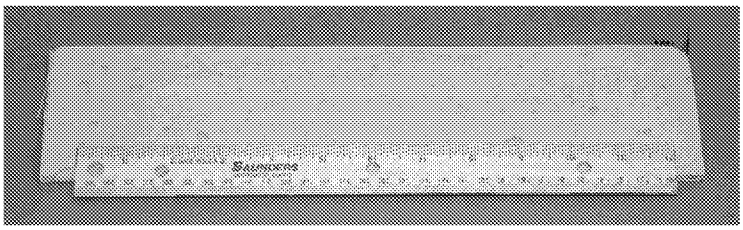

Figure 10. Specimen with high porosity.

Experience indicated that the best opportunity for reducing the specimen porosity was during the placement process. The cementitious mix was added to the mold in small amounts. The thin layers of cementitious mix were slowly "worked" into the molds and graphite mesh. Working or floating the cementitious mix caused the air bubbles to rise to the top, and porosity was eventually reduced to acceptable levels.

3.2 Tensile and Shear Specimens

Tensile testing is used to determine the composite material properties E_1, E_2, and ν_{12}. These properties are needed to complete the compliance matrix (sec. 5.3) for an orthotropic material:

$$S = \begin{bmatrix} \frac{1}{E_1} & \frac{-\nu_{12}}{E_1} & 0 \\ \frac{-\nu_{21}}{E_2} & \frac{1}{E_2} & 0 \\ 0 & 0 & \frac{1}{G_{12}} \end{bmatrix}. \tag{19}$$

The first step in the process is to determine the size and shape of a tensile test specimen for an orthotropic composite material. The ASTM provides standards for tensile testing for a wide variety of materials. A search of the ASTM database[12] provided a number of testing standards for materials similar to the considered composite. The mutual goal of these test methods is to develop a test specimen that provides tensile strain data, modulus of elasticity, and Poisson's ratio. ASTM Standard E8–99, "Standard Test Methods for Tension Testing of Metallic Materials,"[12] establishes the dogbone configuration for the tensile test specimen, as shown in figure 11.

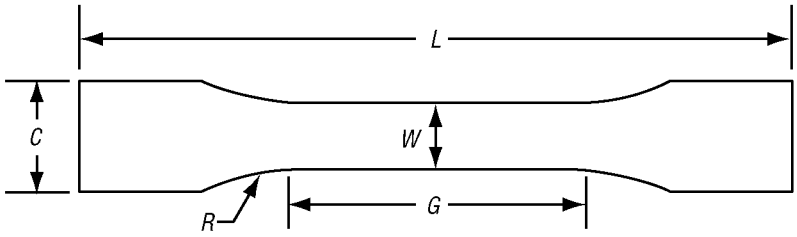

Figure 11. Dogbone configuration.

This test method employs small specimens that have a reduced cross section at the center of their length to avoid failure in the grip area. The transition from the full width of specimen to a reduced section at the center is gradual to minimize stress concentrations. ASTM Standard D 638–99, "Standard Test Method for Tensile Properties of Plastics,"[5] demonstrates the use of the dogbone specimen for reinforced composites, including orthotropic laminates. A unique characteristic of this composite is the relatively wide spacing of the graphite tows. The mesh contains eight yarns per inch in both axial and transverse directions (8 in. by 8 in. weave). Reducing the width of the gauge section limits the number of graphite yarns in the tensile test. A decision to hold the gauge width to 1 in. made the specimen geometry dimensions similar to the type III specimen of ASTM Standard D 638. In each specimen geometry, the configuration is determined by the desire to produce failure in the gauge section without inducing stress concentrations in the gauge section. The specimen length is substantially longer than the width to minimize the bending stresses due to minor grip eccentricities. The final specimen configuration is analogous to the specimens described in the ASTM standards,[5,12] with the exception that the gauge width was 1 in.

The geometry of the shear specimen is established in ASTM D 5379–93, "Standard Test Method for Shear Properties of Composite Materials by the V-Notched Beam Methods."[15] This test is often referred to as the Iosipescu shear test. Figure 12 illustrates the geometry of the shear test specimen.

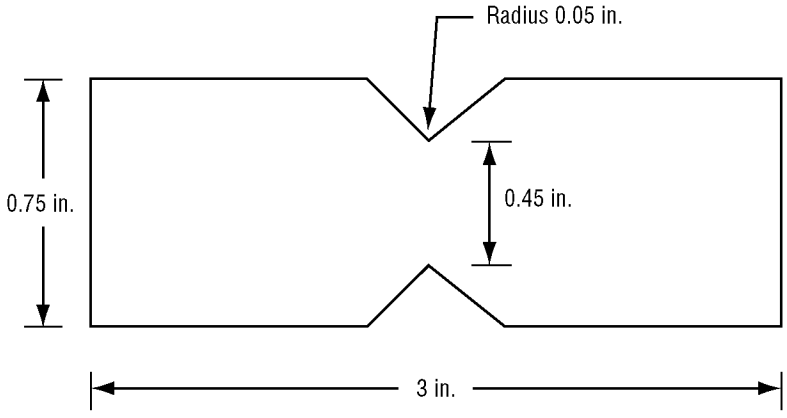

Figure 12. Shear test specimen.

3.3 Tensile Specimen Production

Specimens were made in a plexiglass mold designed to place the graphite mesh at the center of the laminated composite. As shown in figure 13, the graphite was placed in tension to prevent the weight of the cementitious mixture from pushing the graphite toward the bottom of the mold.

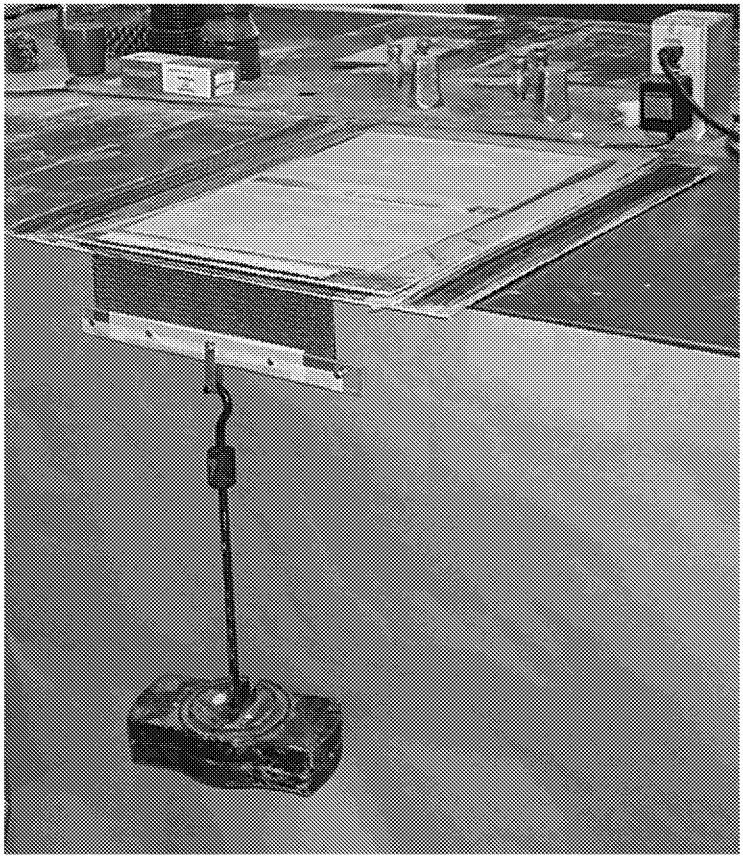

Figure 13. Plexiglas mold with graphite tensioning device.

The cementitious mix was floated to the top level of the bottom spacer and a sheet of graphite mesh was placed over the bottom spacer. The graphite tensioning device was then installed. The top spacer was added and cementitious mix was floated to the top of the spacer. The tensioned graphite mesh was trapped between two layers of the cementitious mix. The composite was allowed to cure at room temperature for at least 21 days before the mold and tensioning device was removed. Even though mold release agents were used, it was necessary to twist and flex the plexiglass to remove the specimens without breaking them. After the specimens were removed from the molds, the graphite was trimmed. The plexiglass side of the specimen had a smooth finish, while the top of each specimen had a coarser texture. A bandsaw was then used to cut the "cookie-sheet" specimen into 2-in. by 14-in. strips for machining.

An undesirable aspect of the dogbone geometry is that it requires machining of the composite laminate. Laminated composites can be difficult to machine;[2] delaminations, notches, and uneven surfaces can result from inappropriate machining methods. In an effort to fix edges damaged by a milling machine, it was found that a bandsaw could be used to cut the cementitious and graphite composite. The cuts were smooth and notch free. A dogbone specimen was then cut out using the bandsaw. Taking the machining process further, it was found that a router would cut a smooth radius on the specimen (fig. 14).

Figure 14. Router used to machine dogbone specimens.

The router left the edges smooth and notch free. On further investigation, it was learned that a template, shown in figure 15, used with a table-mounted router, provided an excellent method of machining the dogbone specimens. A specimen configured with this template is shown in figure 16. The specimen has a 5-in. gauge length, a 1-in. gauge section width, and a 14-in. length.

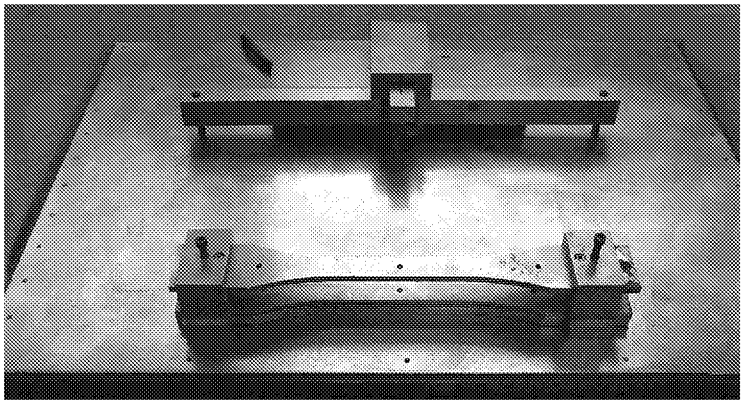

Figure 15. Template used for machining specimens.

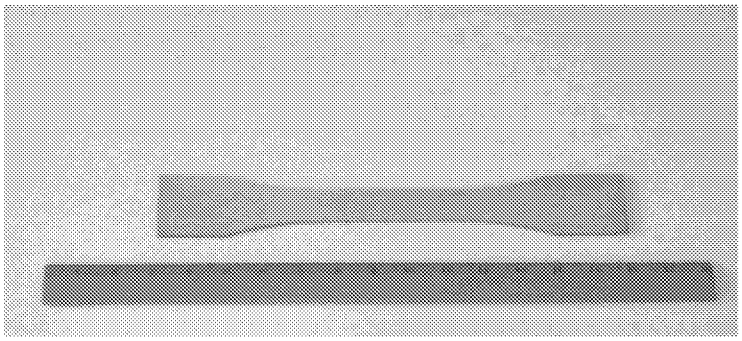

Figure 16. Machined dogbone specimen.

As previously mentioned, the top side of the specimen had a coarse texture. The textured surface made it difficult to attach instrumentation. A flat backing plate equipped with fine grit sandpaper, shown in figure 17, was used to finish the top surface of the specimen. This process was also used to ensure that the graphite mesh was in the geometric center of the specimen. Occasionally, finishing the top surface of the specimen resulted in the top layer being thinner than the bottom. In such a case, the bottom layer was sanded to the same thickness as the top. Using shimming material as a guide ensured that the top and bottom layers were the same thickness (fig. 18).

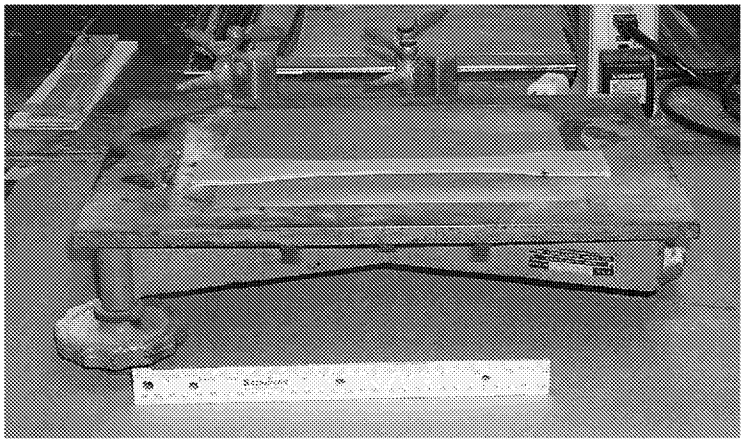

Figure 17. Flat plate used to polish surface.

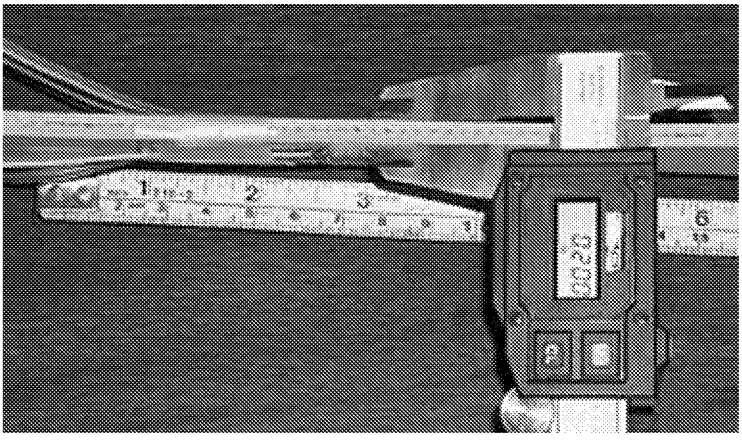

Figure 18. Edge view of finished specimen.

3.4 Shear Specimen Production

The geometry of the shear specimen was difficult to machine because of the small radius at the base of the notch. Designing a router blade with a cutting diameter of 0.05 in. solved the problem. A router template was then machined to the dimensions specified in the ASTM standard[15] (fig. 19). Shear test specimens could then be machined using a router and table (fig. 20) in the same manner as the tension test specimens.

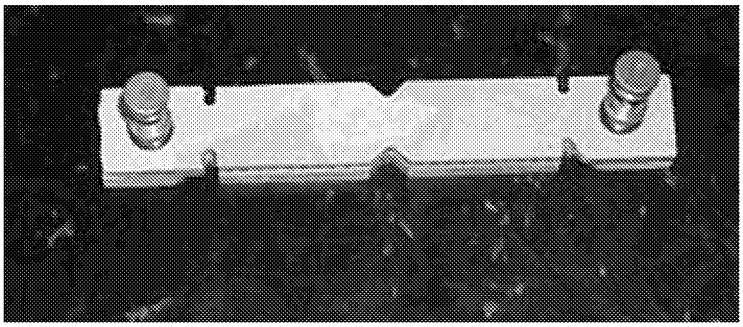

Figure 19. Shear specimen router template.

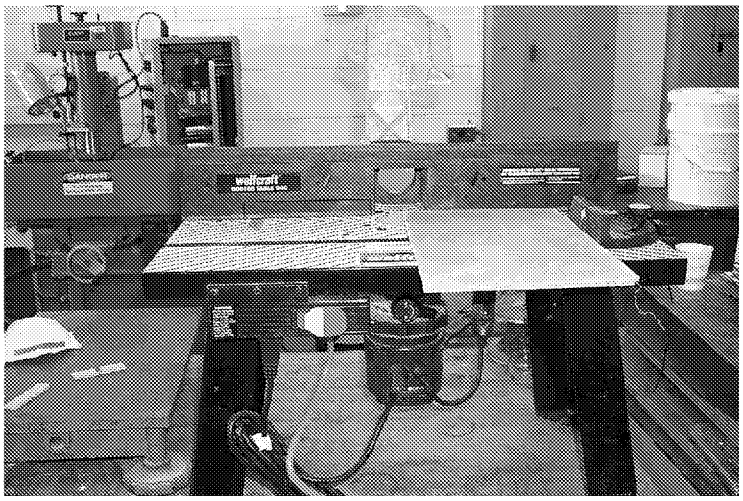

Figure 20. Shear specimen router table.

The router machines the shear specimen, leaving the edges smooth and the dimensions within specification (fig. 21). The top surface of the specimen requires sanding for a smooth finish and allows adjustment of the thickness if required.

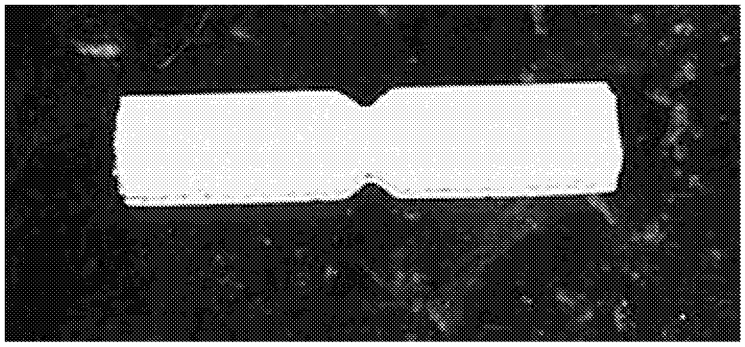

Figure 21. Shear test specimen.

3.5 Tensile Specimen Instrumentation

The instrumentation for the tensile test specimen must simultaneously measure the longitudinal and transverse strain. The ASTM standards recommend using extensometers,[5] noting that strain gauges provide a viable alternative. However, proper techniques for mounting strain gauges are crucial to obtaining accurate data.[13]

Instrumentation of the specimens became a significant challenge to successful testing. Three types of extensometers were available during testing. The 2-in. gauge length was used for axial strain measurement (fig. 22).

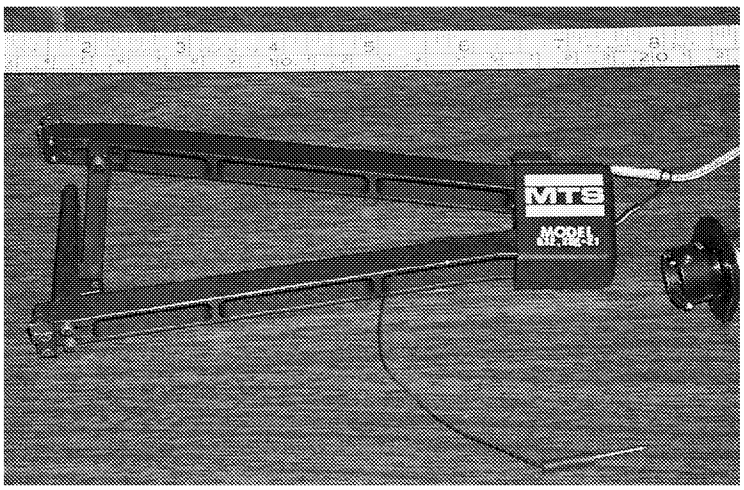

Figure 22. Extensometer with a 2-in. gauge length.

The extensometer was attached to the edge of the test specimen. The data were compared to the axial strain gauge data. Plots of the strain gauge and extensometer data for the axial direction were in good agreement (fig. 23), indicating that the strain gauge application methods were acceptable. The 1-in. gauge length was intended for transverse strain measurement (fig. 24). This extensometer was attached to the face of the test specimen. However, the thin specimen did not have adequate stiffness to support the weight of the extensometer. The instrument appeared to deflect the specimen, causing the knife edges of the extensometer to lose contact with the specimen surface. As a result, the data from the transverse extensometer did not correspond to the data from the transverse strain gauge (fig. 25).

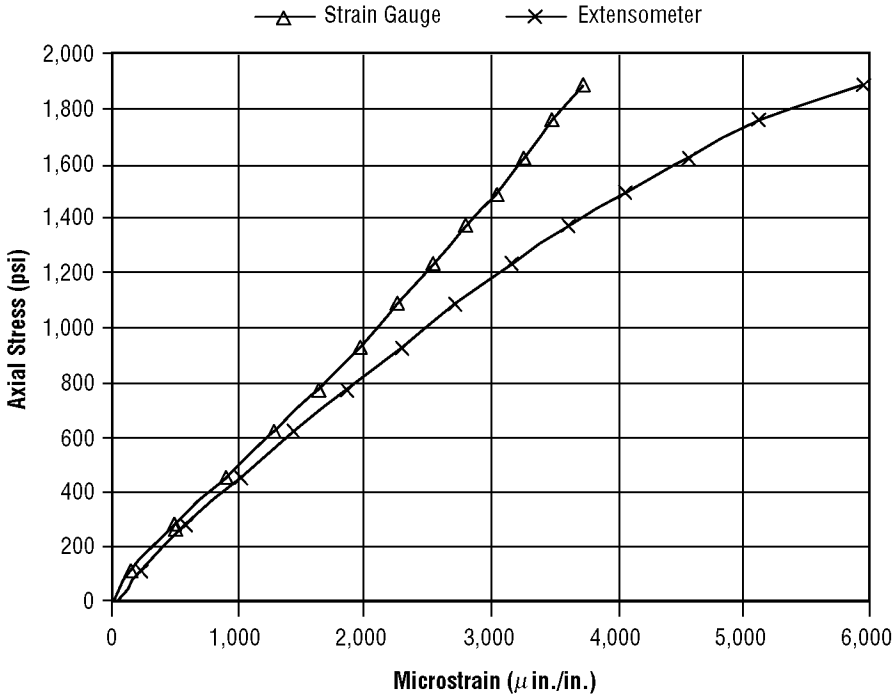

Figure 23. Axial strain gauge and extensometer.

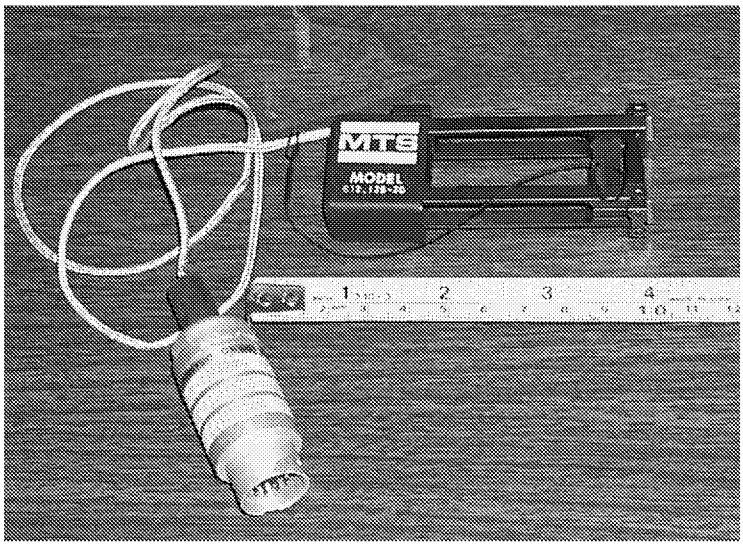

Figure 24. Extensometer with a 1-in. gauge length.

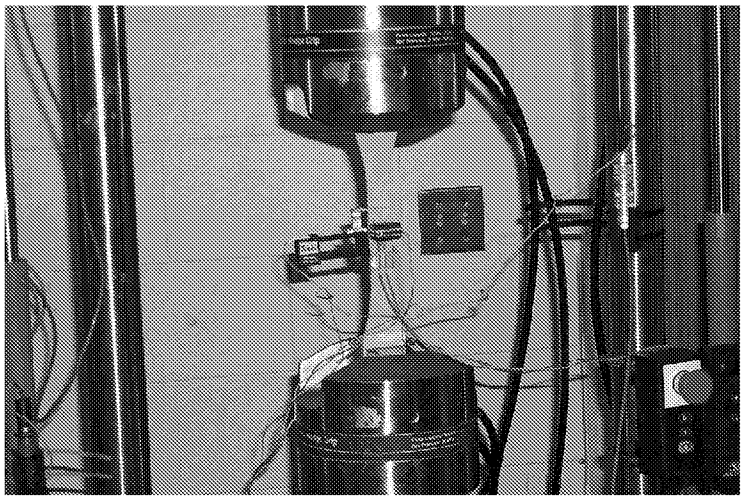

Figure 25. Extensometer mounted on test specimen.

The biaxial extensometer, as shown in figure 26, was also considered. However, the instrument weight deformed the specimen unacceptably. Efforts were made to support the weight of the instrument. Unfortunately, the instrument relies on its weight to maintain contact between the knife edges and the specimen. It was too difficult to reduce the deformation in the specimen and maintain adequate weight on the knife edges of the instrument. The biaxial extensometer was abandoned in place of the previously mentioned extensometers and strain gauges. Strain gauges were attached to both sides of the specimen (fig. 27). The strain gauges were 90° Tee rosettes, model CEA–06–125UT–120, manufactured by Micro-Measurements. The gauges were oriented in the axial and transverse directions.

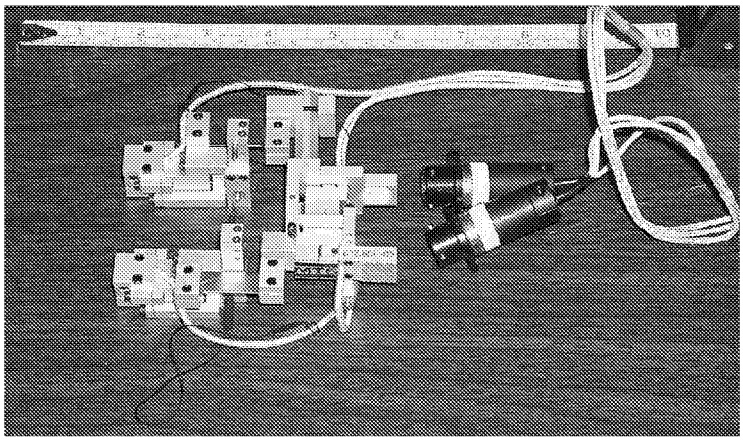

Figure 26. Biaxial extensometer.

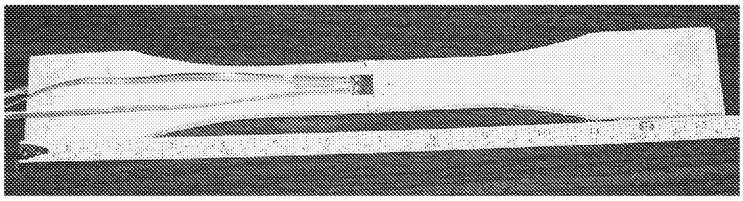

Figure 27. Specimen with strain gauge installed.

All the strain measurements were made at room temperature (≈75 °F). The strain gauge installation was completed by the strain gauge manufacturer's recommendation (fig. 28).[13]

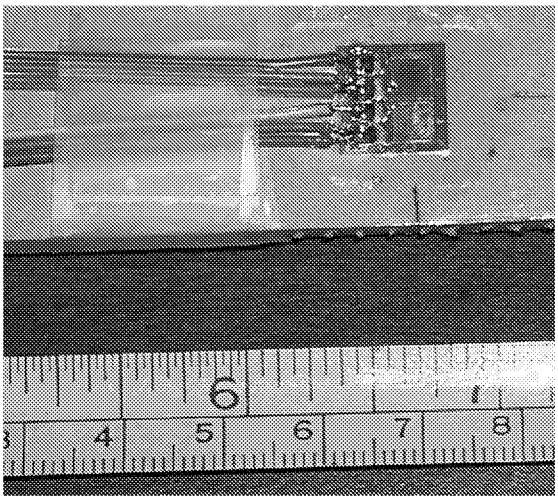

Figure 28. Strain gauge installation.

The specimen was smoothed using fine-grit sandpaper and was free from irregularities and contaminates. An acidic cleaner, Prep Conditioner A, was applied to the gauge region. M–Prep Neutralizer 5A followed the acid cleaner. Micro-Measurements M–Bond 200 and a catalyst were used to bond the gauges to the specimen. The four strain gauges provided axial and transverse strain data for each side of the specimen. This allowed the data to be corrected for any bending.

The strain gauge installation method worked well providing no porosity or surface "grit" was present. As mentioned earlier, the order in which the ingredients are mixed and the manner in which the molds are poured significantly affected specimen porosity and texture. Specimens with high porosity or a texture that could not be sanded smooth were discarded.

3.6 Shear Specimen Instrumentation

ASTM D 537993 defines the instrumentation for the shear test article.[15] This standard specifies a strain gauge rosette with two 45° strain gauges be placed in the center of the specimen. The gauges are oriented at ±45° to the loading axis (fig. 29).

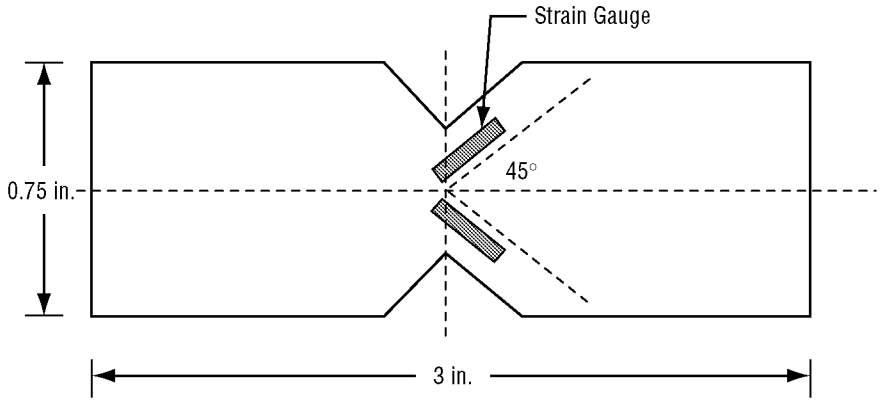

Figure 29. Strain gauge location for shear specimen.

The recommended strain gauge configuration requires the use of correction factors to account for the gradient of strain between the notches. Ifju[18] developed a special strain gauge that overcomes many of the problems associated with the ASTM recommended strain gauges. Micro-Measurements offers this strain gauge configuration as N2A–08–C032A.[18] It is a two-gauge rosette with the gauges at 45° and –45° and records the average strain between the notches. These strain gauges were recommended in the Micro-Measurements catalog as being specifically made for Iosipescu shear testing (fig. 30).[23] The strain gauge outputs the shear strain directly, avoiding the need for correction factors. The strain gauge installation was the same as used for the tensile test specimens.

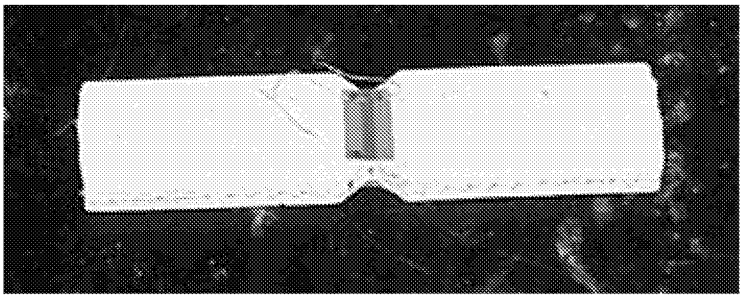

Figure 30. Shear specimen with strain gauges.

The gauges are mounted on each side of the test specimen[18] in order to remove the effects of twisting from the specimen. The strain gauges were connected into a full-bridge circuit as recommended.[18,23] This configuration of four strain gauges, two on each side of the specimen, results in a strain reading that is twice the desired reading. A metallic "pathfinder" specimen was used to verify the Iosipescu test fixture and instrumentation (fig. 31). The pathfinder specimen had a known shear modulus value of 10.8×10^6 lbf/in.^{2} The percentage of error is shown in the following calculation:

$$\text{Error}\% = \frac{10.8 - 10.93}{10.8} \times 100\% = -1.2\% \quad . \tag{20}$$

The test data compared very well to the actual value for the shear modulus.

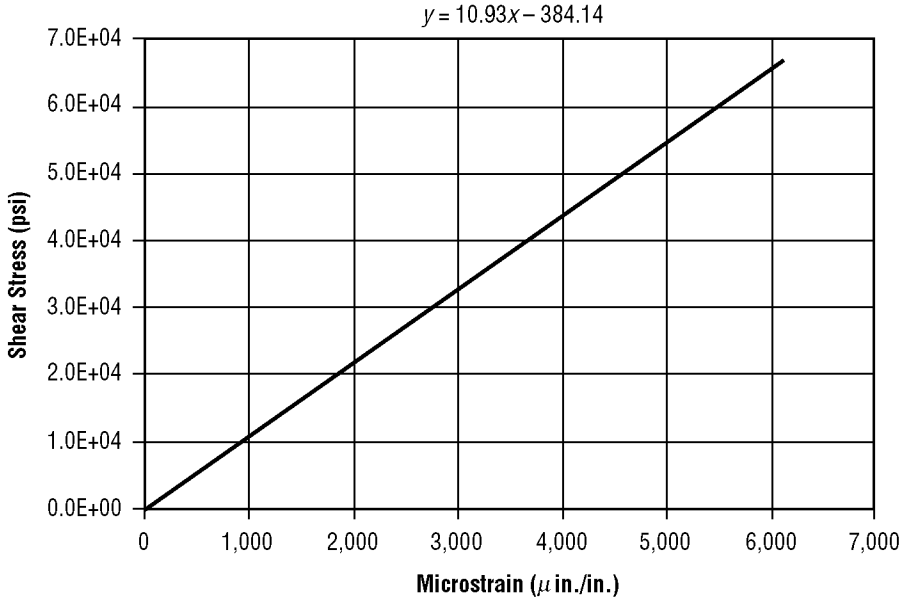

Figure 31. Iosipescu pathfinder specimen.

3.7 Tensile Test Procedure

The tensile test was run using an MTS 20-kip test machine with a numerical control system (fig. 32). The strain gauge and extensometer data were recorded with a digital data acquisition system. The load was applied at a rate of 0.05 in. per minute and data were recorded every 0.5 sec. Load was applied until an auditable "snap" marked the initial failure point of the cementitious material; strain data beyond that point were unreliable.

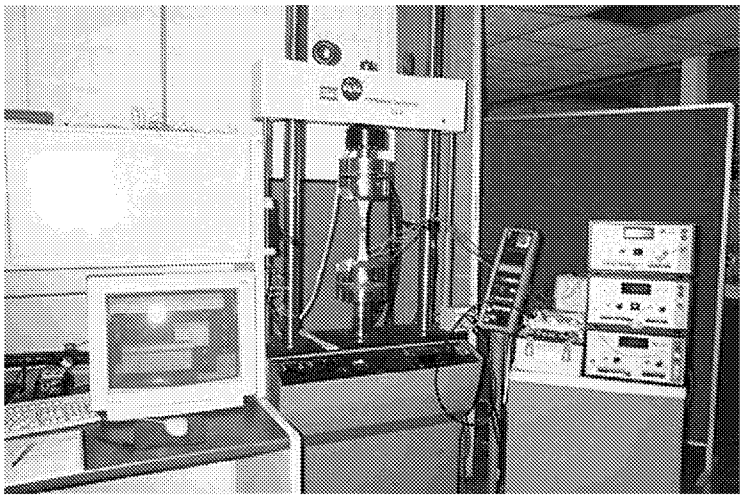

Figure 32. Tensile test machine.

As discussed in section 3.5, extensometers and strain gauges were initially used for strain measurement. The axial extensometer and the strain gauge data were in fairly good agreement (fig. 23). However, the extensometers could not be attached to both sides of the test specimens. In addition, the knife edges of the transverse extensometers slipped and lost contact with the specimen easily. Therefore, the extensometers were replaced with strain gauges.

Each tensile test specimen had four strain gauges, one axial and one transverse gauge on each side. The strain gauges were located back to back on each specimen; this allowed the strain data to be corrected for any bending caused by misalignment of the test articles. The data were corrected for bending by taking the average of the two strain gauges (fig. 33).

The strain gauges in the axial direction provided consistent and reliable data throughout the test program. However, the strain gauges in the transverse direction proved to be less trustworthy. The data illustrated in figure 34 are typical of the transverse data recorded for most of the tensile specimens. The strain data appear to be constant for a number of loads; then the strain suddenly increases. This pattern repeats itself, forming a curve that resembles a step function. A linear best-fit line through the data will be used to approximate the curve.

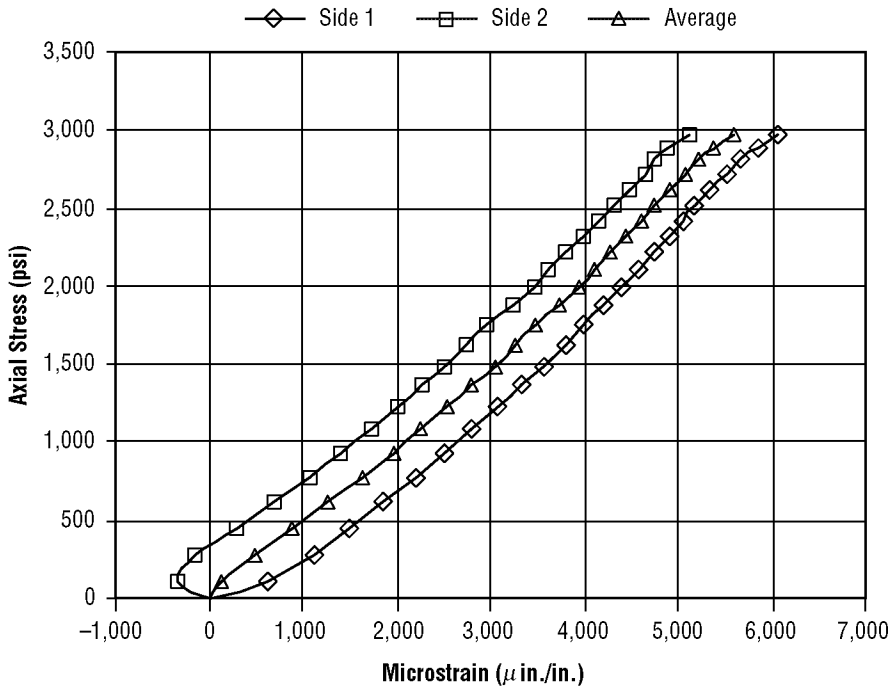

Figure 33. Sample axial strain gauge readings.

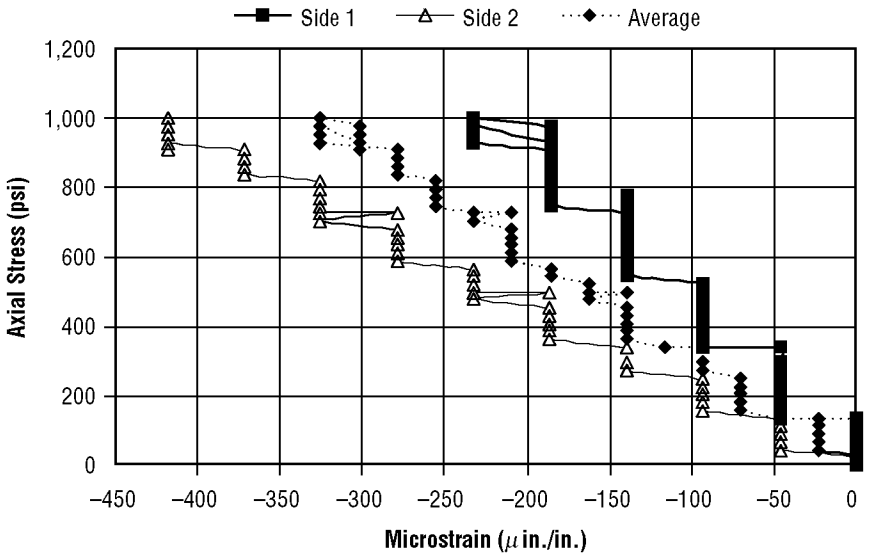

Figure 34. Sample transverse strain gauge readings.

3.8 Axial Properties From Tensile Test Data

Numerous tensile test specimens were produced and tested while developing the testing procedures described in this TM. While this trial-and-error procedure was time consuming and labor intensive, it eventually produced an acceptable test specimen and procedure. A final set of tensile test specimens was produced using the lessons learned from previous experience.

The test specimens were each tested using the same procedure. Data from four strain gauges and the machine load were recorded. The data acquisition system stored the load and strain data in a spreadsheet for analysis and plotting. The stress values are calculated from the area of the test specimen and applied load:

$$\sigma = \frac{\text{Load}}{(\text{Width})(\text{Thickness})} \frac{\text{lbf}}{\text{in.}^2} \tag{21}$$

As previously discussed, the strain values are the average from the back-to-back gauges:

$$\varepsilon_{\text{axial}} = \frac{\left(\varepsilon_{\text{axial}}^{\text{side 1}} + \varepsilon_{\text{axial}}^{\text{side 2}}\right)}{2} \; . \tag{22}$$

The data were then plotted to produce a stress-strain curve (fig. 35) for each specimen.

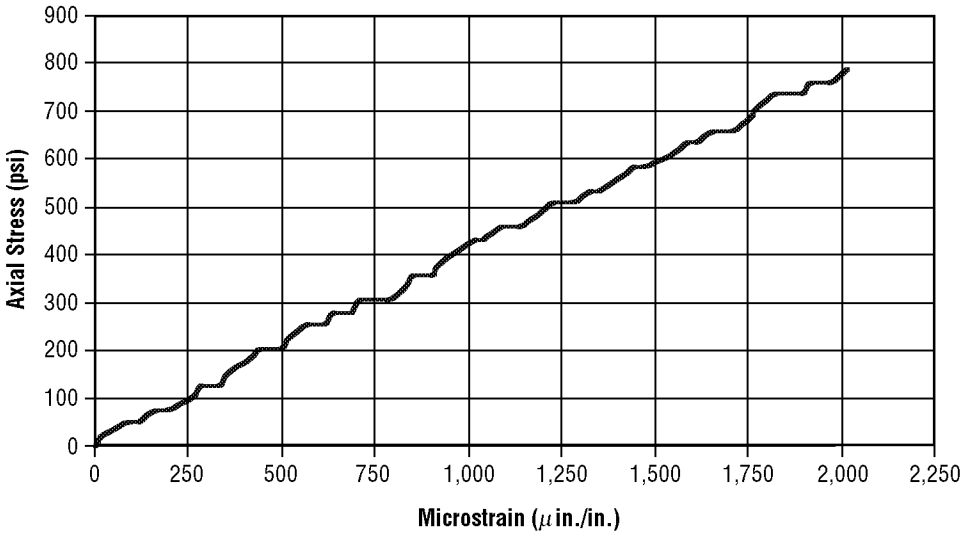

Figure 35. Typical stress-strain curve for each specimen.

Young's modulus is defined as the slope of the linear portion of the stress-strain curve.[6] The value can be determined by placing a best-fit line through the data points. The slope of the line is then taken as Young's modulus for the specimen (fig. 36). This procedure was repeated for six test specimens. A summary of tensile test data indicates consistent results (fig. 37). Appendix B contains the complete set of data plots for the tensile test specimens.

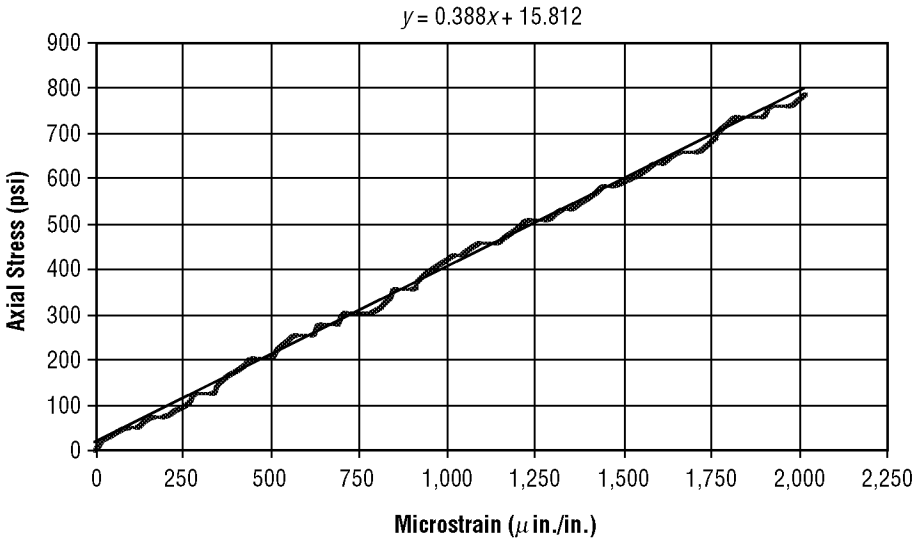

Figure 36. Calculation of Young's modulus for each specimen.

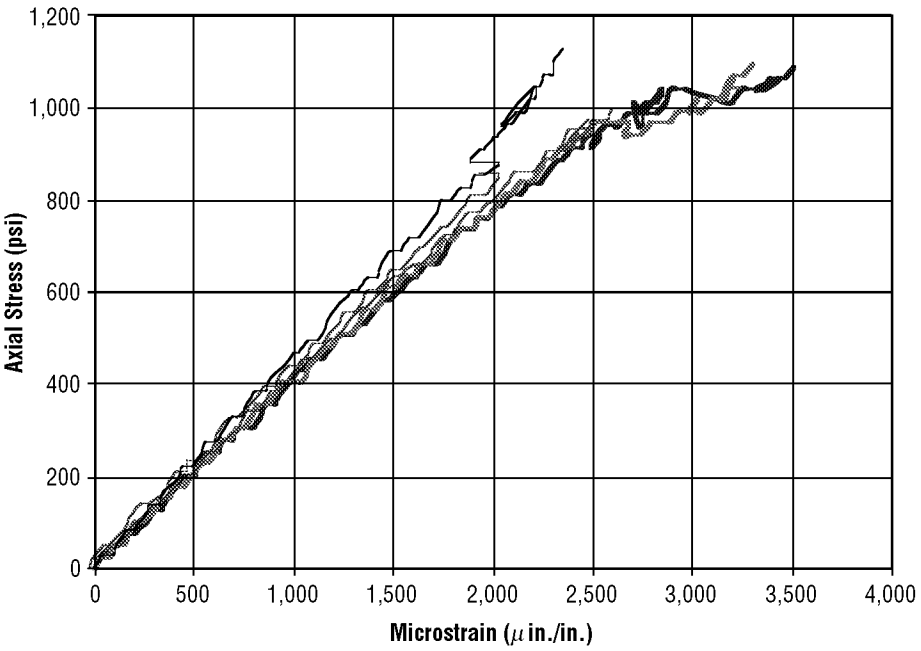

Figure 37. Summary of tensile test specimens.

Young's modulus values from the six tensile test specimens are summarized in table 4. The "pathfinder" specimen CG–SG4 was made thinner than the other specimens. Several of the thinner specimens were damaged during the sanding process, so a thicker mold and specimen were later produced. The remaining five specimens were made from the thicker mold and are represented in figure 37. The average Young's modulus value for the five specimens is 4.04×10^5 lbf/in.^{2}, with a standard deviation of 0.20×10^5 lbf/in.^{2}

Table 4. Young's modulus from tensile test.

Specimen	Width (in.)	Thickness (in.)	Young's Modulus Test Results (lbf/in.^{2})
CG–SG4	1.004	0.120	5.00×10^5
Dec_28-4	1.016	0.190	3.88×10^5
Dec_28-5	1.006	0.196	3.91×10^5
Dec_28-6	1.000	0.216	4.07×10^5
Dec_28-7	1.003	0.210	3.98×10^5
Dec_28-8	1.000	0.180	4.40×10^5

3.9 Poisson's Ratio From Transverse Test Data

The transverse strain values can be used to determine the Poisson's ratio for the composite material. By definition, Poisson's ratio is given by the equation $\nu_{12} = -\varepsilon_2/\varepsilon_1$, assuming a uniaxial stress.[6] The transverse strain data from each of the five test specimens is presented in detail in appendix B. As mentioned in section 3.7, the transverse strain data presented here are the average of two back-to-back strain gauges (fig. 38). In addition, a best-fit line is drawn through the data points. The data were fairly consistent from one test article to another (fig. 39); the same "step function" pattern was present in all the test articles (sec. 3.7).

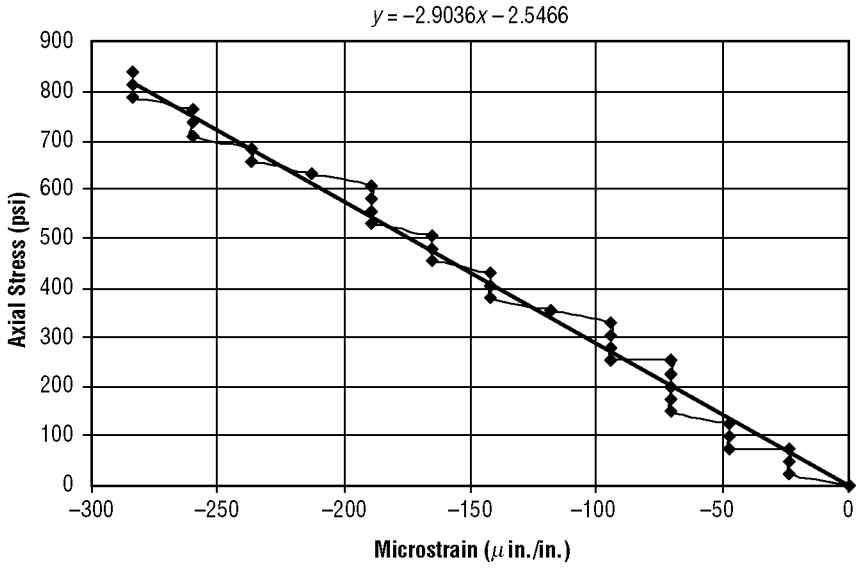

Figure 38. Typical transverse strain curve.

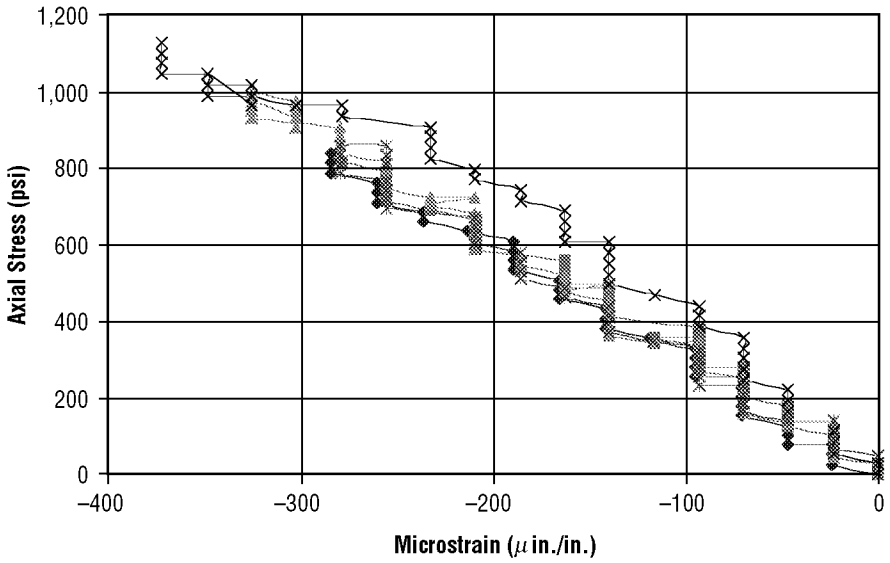

Figure 39. Summary of transverse strain data.

The Poisson's ratio calculations were made from the following straight-line approximation:

$$\sigma = 0.388\varepsilon_{\text{axial}} + 15.812 \tag{23}$$

and

$$\sigma = -2.9036\varepsilon_{\text{trans}} - 2.5466\,. \tag{24}$$

Solving the equations for the strain,

$$\varepsilon_{\text{axial}} = \frac{(\sigma - 15.812)}{0.388} \tag{25}$$

and

$$\varepsilon_{\text{trans}} = \frac{(\sigma + 2.5466)}{-2.9036}\,. \tag{26}$$

Substituting into the equation for Poisson's ratio,

$$\nu = -\frac{\varepsilon_{\text{trans}}}{\varepsilon_{\text{axial}}}\,, \tag{27}$$

then

$$\nu = \frac{\left[\frac{(\sigma + 2.5466)}{-2.9036}\right]}{\left[\frac{(\sigma - 15.812)}{0.388}\right]} . \tag{28}$$

Poisson's ratio can now be calculated for each of the five test specimens (table 5).

Table 5. Poisson's ratio.

Specimen	Experimental
Dec_28-4	0.136
Dec_28-5	0.135
Dec_28-6	0.142
Dec_28-7	0.131
Dec_28-8	0.144

The average Poisson's ratio is 0.137 with a standard deviation of 0.00532. The small standard deviation provides confidence that the data are reasonable.

3.10 Shear Test Procedure

ASTM standard D 5379–93[15,16] documents the standard shear test for determining the shear properties of composite materials. This test uses a specimen referred to as the V-notched beam (fig. 40). This test is often referred to as the Iosipescu shear test, in honor of its developer. The test specimen is placed in a massive test fixture referred to as an Iosipescu shear test fixture (fig. 41). The test fixture is described in detail in the ASTM standards.

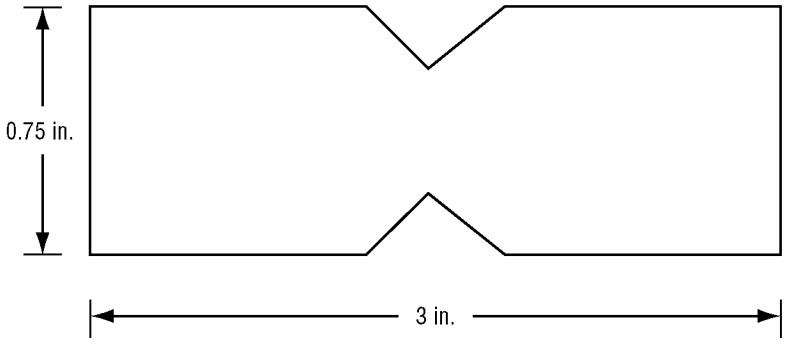

Figure 40. V-notched shear specimen.

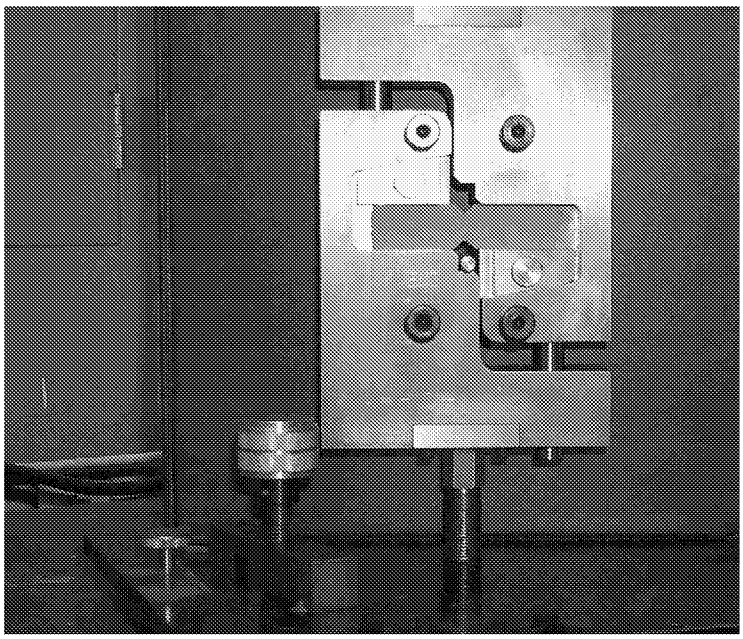

Figure 41. Iosipescu shear test fixture.

The specimen is inserted into the fixture with the notches aligned with the center of the test fixture. The two halves of the test fixture are compressed by the MTS testing machine while monitoring load. The relative displacement between the two halves of the fixture loads the notched specimen. Strain gauges are placed in the center of the specimen to measure the shear strain response during loading.[18,23]

3.11 Shear Properties From Iosipescu Shear Testing

The cost and availability of the strain gauges used on the test specimens limited the number of Iosipescu shear tests. As a result, only six instrumented test specimens were available. The first test specimen was a metallic pathfinder specimen that was used to verify that the test procedure, instrumentation, and fixture could be used to determine the shear modulus for a well-characterized material (sec. 3.5). The results from the pathfinder specimen were in excellent agreement with the known values for the material. However, of the remaining five composite specimens, only two specimens were successfully tested. The data from the first composite specimen were not usable due to a problem with the data acquisition system. The increment for the load data was not properly set during the test. The strain gauges on the third and fifth test articles failed to provide usable data during the test. The gauges apparently debonded from the test specimens. The debonds were most likely caused by poor surface preparation during the strain gauge installation. It should be emphasized that the Iosipescu shear fixture and test specimens performed well during testing. The results from the two successful tests confirm this observation (fig. 42). The strain gauge on specimen 4 failed at ≈3,000 μ; however, the test article continued to take load. The strain gauge on specimen 2 continued to provide strain data until the article failed.

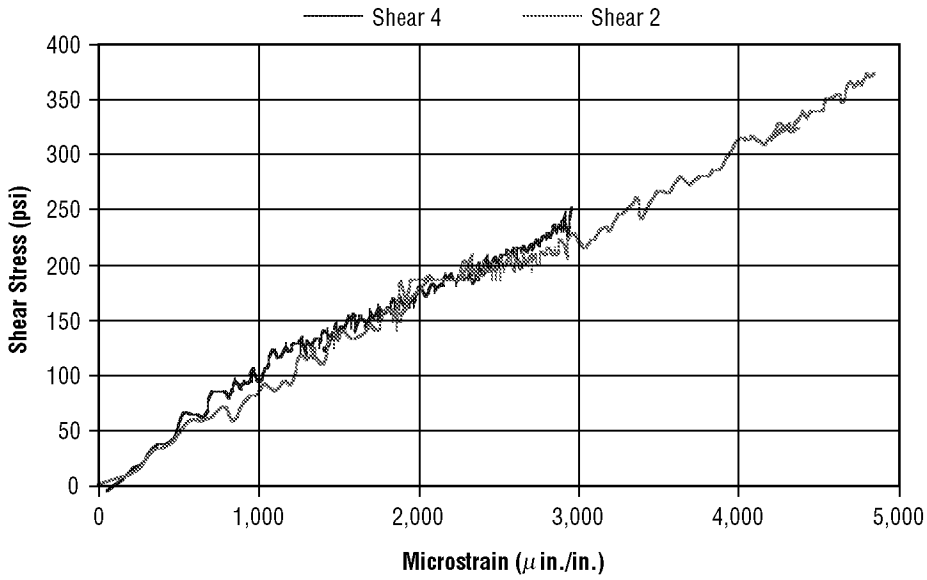

Figure 42. Iosipescu shear test results.

The shear modulus is defined as the slope of the linear portion of the shear stress-shear strain curve.[6,15] The value can be determined by placing a best-fit line through the datapoints. The slope of the line is then taken as the shear modulus for the specimen (fig. 43). This procedure was repeated for two test specimens. A summary of shear test data indicates consistent results (table 6). Appendix B contains the complete set of data plots for the shear test specimens.

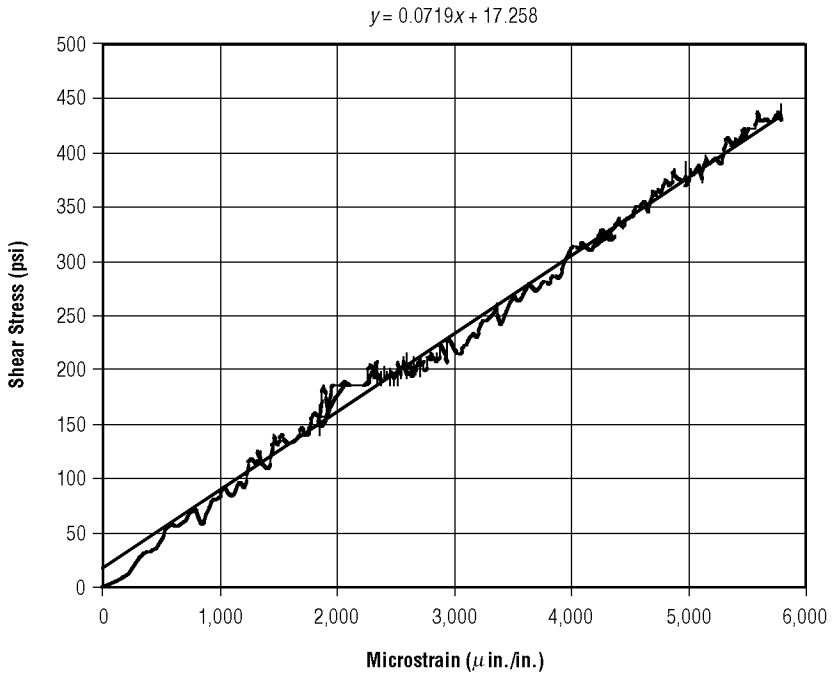

Figure 43. Iosipescu shear test article 2.

Table 6. Shear modulus summary.

Specimen	Width (in.)	Thickness (in.)	Shear Modulus (lbf/in.^{2})
Shear 2	0.458	0.180	7.2×10^4
Shear 4	0.457	0.186	7.8×10^4
Average	–	–	7.5×10^4

A best-fit line is drawn through the datapoints to provide a means of accurately calculating the shear modulus (fig. 43). The shear modulus is given by the slope of the straight line:[19]

$$G_{\text{Article 2}} = \frac{(305 \frac{\text{lbf}}{\text{in.}^2} - 89 \frac{\text{lbf}}{\text{in.}^2})}{(4{,}000\,\mu - 1{,}000\,\mu)} = 7.2 \times 10^4 \frac{\text{lbf}}{\text{in.}^2} \tag{29}$$

$$G_{\text{Article 4}} = \frac{(209 \frac{\text{lbf}}{\text{in.}^2} - 91 \frac{\text{lbf}}{\text{in.}^2})}{(2{,}500\mu - 1{,}000\mu)} = 7.8 \times 10^4 \frac{\text{lbf}}{\text{in.}^2} \tag{30}$$

As shown in table 6, the average shear modulus is 7.5×10^4 lbf/in.^{2}, with a standard deviation of 0.42×10^4 lbf/in.^{2} The percentage of possible error is determined by the following:

$$7.5 \times 10^4 \frac{\text{lbf}}{\text{in.}^2} + 0.42 \times 10^4 \frac{\text{lbf}}{\text{in.}^2} = 7.92 \times 10^4 \frac{\text{lbf}}{\text{in.}^2} \tag{31}$$

and

$$\text{Error\%} = \frac{7.92 \times 10^4 \frac{\text{lbf}}{\text{in.}^2} - 7.5 \times 10^4 \frac{\text{lbf}}{\text{in.}^2}}{7.5 \times 10^4 \frac{\text{lbf}}{\text{in.}^2}} = 5.6\% \ . \tag{32}$$

3.12 Summary of Composite Material Properties

The material properties for this graphite-reinforced cementitious composite material were successfully determined from standard test methods. It was found that the constituent materials can be mixed and placed to form laminated composite plates. The plates were cured at room temperature and without a vacuum bag. The composite material can be machined into various shapes using standard machining tools such as a router. Strain gauges can be applied to the surface of the composite using M–Bond 200 and following the standard methods of installation. The results of the material testing were consistent and repeatable for both tensile and shear testing.

The materials property data can now be used as a basis for comparison to theoretically derived values. In addition, these values will be used to develop the analytical tools needed to predict the response of multilayered beams made from graphite-reinforced cementitious materials.

4. RULE OF MIXTURES FOR A COMPOSITE MATERIAL

The rule of mixtures is investigated as a method to predict the material properties of graphite-reinforced cementitious composites. The equations for the effective material properties are derived using the assumptions associated with the rule of mixtures. These material properties are then compared to the results of the material properties testing. Several derivations are then made to illustrate that these material properties can be used with the elastic curve equations to determine the deflection of simple beams. Deflection results from a finite element model and a static test are compared to the analysis using the elastic curve equations. The results illustrate the deflections can be predicted by using the material property data from the rule of mixtures method. However, several deficiencies and limitations are encountered. The conclusion is made that the rule of mixtures can provide a reasonable value for Young's modulus in the axial direction. However, the theory cannot provide accurate values for Poisson's ratio, the shear modulus, or Young's modulus transverse to the direction of the fibers and load.

4.1 Material Properties in the Axial Direction

The rule of mixtures is a method for determining the effective properties of a composite material based on the contributions of the individual constituents.[10] The properties of the composite are related to the quantity of the fibers in the matrix. The fiber volume fraction (V_{fiber}) and the matrix volume fraction (V_{matrix}) are used to measure the amount of fiber or matrix in a given volume of material. E in the direction of the fiber, E_1, can be determined by assuming the strains in the fiber direction are the same in the fibers as in the matrix; i.e., $\varepsilon_{fiber} = \varepsilon_{matrix}$. Since the strain in the fiber is the same as the strain in the matrix, the sections normal to the fiber direction remain plane after stressing (fig. 44).

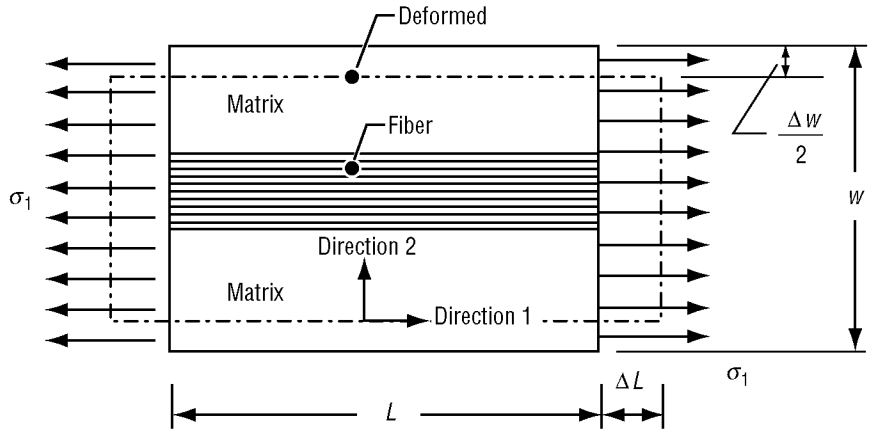

Figure 44. Loading in axial direction.

The strain in direction 1, the fiber direction, is given by the deflection divided by the original length, $\varepsilon_1 = \Delta L/L$. Applying Hooke's law and assuming both the fiber and the matrix are linear, then $\sigma_{fiber} = E_{fiber}\varepsilon_1$ and $\sigma_{matrix} = E_{matrix}\varepsilon_1$. This relationship can be compared to two springs acting in parallel (fig. 45). The total load (P) is carried by the load in the fiber (P_{fiber}) and the load in the matrix (P_{matrix}).

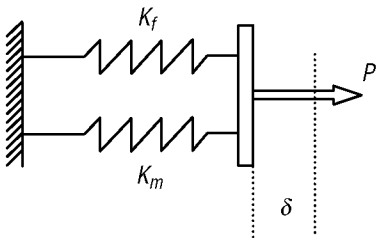

Figure 45. Spring in parallel.

The applied force (P), $P = P_{fiber} + P_{matrix}$, acts on the total cross-sectional area (A). The fiber stress (σ_{fiber}) acts on the cross-sectional area of the fiber (A_{fiber}). The matrix stress (σ_{matrix}) acts on the matrix area (A_{matrix}). The force equation can then be written in terms of the stress and area, $\sigma_1 A_1 = \sigma_{fiber}A_{fiber} + \sigma_{matrix}A_{matrix}$. Now by substituting the Hooke's law equations for the stress terms, the force equation may be written in terms of strain and Young's modulus as $E_1\varepsilon_1 A_1 = E_{fiber}\varepsilon_1 A_{fiber} + E_{matrix}\varepsilon_1 A_{matrix}$. Simplifying the equation results in an expression for Young's modulus in terms of the ratio of the areas:

$$E_1 = \frac{E_{fiber}A_{fiber}}{A_1} + \frac{E_{matrix}A_{matrix}}{A_1} \quad . \tag{33}$$

V_{fiber} and V_{matrix} can be defined as $V_{fiber} = A_{fiber}/A_1$ and $V_{matrix} = A_{matrix}/A_1$.

By definition, the volume fractions must satisfy the equation $V_{fiber} + V_{matrix} = 1$. Thus, the expression for the effective Young's modulus in direction 1 can be written in terms of the volume fractions:

$$E_1 = V_{fiber}E_{fiber} + V_{matrix}E_{matrix} \quad . \tag{34}$$

4.2 Material Properties in the Transverse Direction

The effective property in the matrix direction, perpendicular to the fiber direction, can be determined by assuming equivalent stress in the fiber and the matrix (fig. 46).

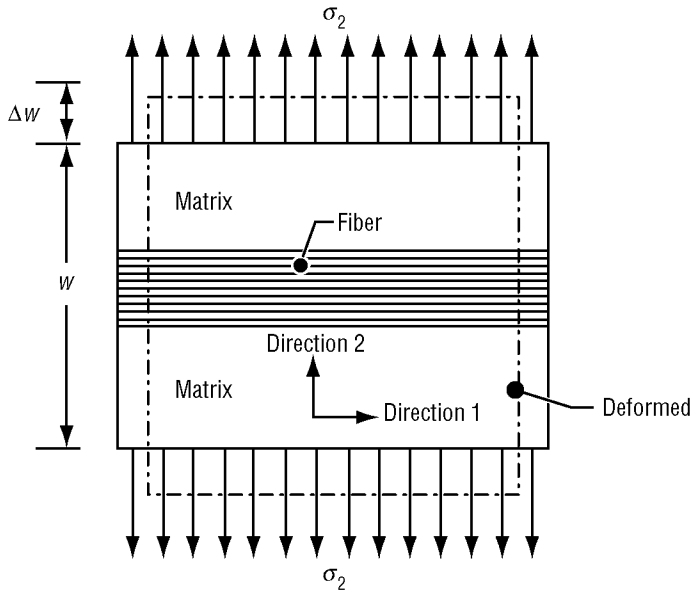

Figure 46. Loading in transverse direction.

In the transverse direction, the cross-sectional areas are equal and the load is constant across the area; therefore, σ is equal for the fiber and the matrix. Then the strains in the fiber and matrix can be written in terms of the stress, $\varepsilon_{fiber} = \sigma_2/\varepsilon_{fiber}$ and $\varepsilon_{matrix} = \sigma_2/\varepsilon_{matrix}$. The fiber and matrix transverse strains are not assumed to be equal. Now consider figure 46. The total transverse deflection (Δw) is the sum of the fiber deflection (Δw_{fiber}) and matrix deflection (Δw_{matrix}): $\Delta w = \Delta w_{fiber} + \Delta w_{matrix}$. Defining the strains in terms of the fiber deflection, $\varepsilon_{fiber} = \Delta w_{fiber}/L_{fiber}$ and the deflection of the matrix, $\varepsilon_{matrix} = \Delta w_{matrix}/L_{matrix}$. The transverse dimension over which the fiber and matrix strains act can be written in terms of V_{fiber}: $L_{fiber} = V_{fiber}w$ and $L_{matrix} = V_{matrix}w$. The deflection equation can now be defined in terms of strain: $\varepsilon_2 w = \varepsilon_{fiber}(V_{fiber}w) + \varepsilon_{matrix}(V_{matrix}w)$. Now the w factor vanishes from both sides of the equation. Hooke's law equations can be substituted for the strains, $\sigma_2/E_2 = V_{fiber}\,\sigma_2/E_{fiber} + V_{matrix}\,\sigma_2/E_{matrix}$. The stress term now vanishes from both sides, $1/E_2 = V_{fiber}/E_{fiber} + V_{matrix}/E_{matrix}$. Solving the above equation for the E_2 term gives an equation for the Young's modulus in the transverse direction as

$$E_2 = \frac{E_{fiber}E_{matrix}}{V_{matrix}E_{fiber} + V_{fiber}E_{matrix}} \quad . \tag{35}$$

4.3 Determination of Poisson's Ratio

Poisson's ratio (ν) is defined as the ratio of the transverse strain over the strain in the fiber direction when stress in the fiber direction is present and all other stress is zero, $\nu_{12} = -\varepsilon_2/\varepsilon_1$. In such a case, the following definitions can be made: $\nu_{matrix} = \varepsilon_{matrix}/\varepsilon_1$ and $\nu_{fiber} = \varepsilon_{fiber}/\varepsilon_1$. Recalling that the deflection equation was previously defined as $\varepsilon_2 w = \varepsilon_{fiber}(V_{fiber}w) + \varepsilon_{matrix}(V_{matrix}w)$, the latter can be divided by ε_1 and simplified to the equation $\varepsilon_2/\varepsilon_1 = \varepsilon_{fiber}/\varepsilon_1(V_{fiber}) + \varepsilon_{matrix}/\varepsilon_1(V_{matrix})$. Substituting the Poisson's ratio (ν_{12}) as defined above in the equations results in the following expression:

$$\nu_{12} = \nu_{fiber}V_{fiber} + \nu_{matrix}V_{matrix} \quad . \tag{36}$$

4.4 Determination of the Shear Modulus

To determine the shear modulus (G_{12}), one assumes that shear stress (τ) on the fiber and the matrix are equal. As illustrated in figure 47, the shear for the composite plate is defined as $\gamma_{12} = \tau/G_{12}$.

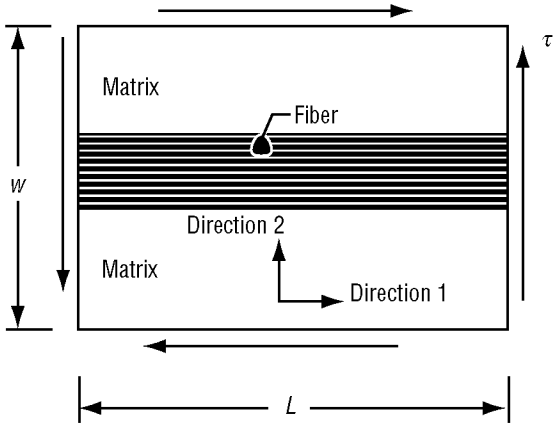

Figure 47. Shear loading.

This assumption means that the shear deformation for the matrix and the fiber can be written as $\gamma_{matrix} = \tau/G_{matrix}$ and $\gamma_{fiber} = \tau/G_{fiber}$. As shown in figure 48, the shear deflection (Δ) is a function of the shear strain and the width (w): $\Delta = \gamma w$. In addition, Δ is the sum of the fiber deflection plus the matrix deflection: $\Delta = \Delta_{fiber} + \Delta_{matrix}$.

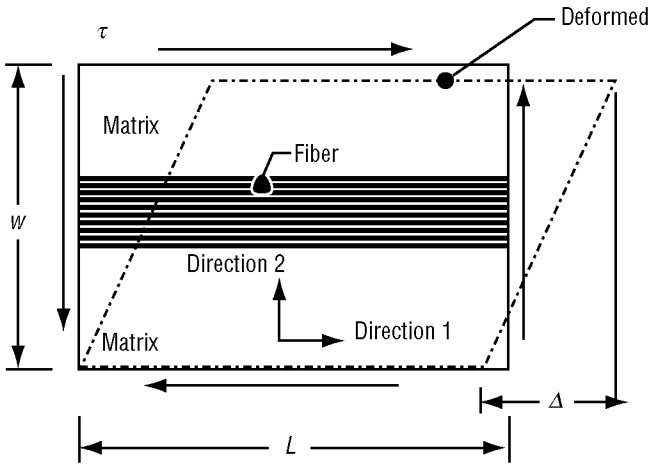

Figure 48. Shear deformations.

As previously shown, the deflection for the matrix and fiber can be stated in terms of the volume fractions, V_{fiber} and V_{matrix}: $\Delta_{matrix} = \gamma_{matrix}(V_{matrix}w)$ and $\Delta_{fiber} = \gamma_{fiber}(V_{fiber}w)$. Substituting into the deflection equations and allowing the w factor to vanish results in the equation for shear strain: $\gamma = \gamma_{matrix}V_{matrix} + \gamma_{fiber}V_{fiber}$. Finally, one can substitute the Hooke's law equations for shear strain to obtain $\tau/G_{12} = V_{matrix}\tau/G_{matrix} + V_{fiber}\tau/G_{fiber}$. This equation can be simplified by allowing the shear stress term to vanish and solving for G_{12}:

$$G_{12} = \frac{G_{matrix}G_{fiber}}{V_{matrix}G_{fiber} + V_{fiber}G_{matrix}} . \tag{37}$$

4.5 Calculation of the Effective Material Properties

Equations (34)–(37) can now be used to calculate the effective material properties of a graphite-reinforced cementitious composite. The material properties for the matrix were obtained from the manufacturer of the graphite mesh. The properties for the matrix were obtained from previous research[1] and confirmed with tensile tests (app. B). The material properties for the fiber and the matrix are defined as follows:

$E_{fiber} = 33.5 \times 10^6$ lbf/in.^{2}
$E_{matrix} = 115.1 \times 10^3$ lbf/in.^{2}
$\nu_{fiber} = 0.3$
$\nu_{matrix} = 0.27$
$\rho_{fiber} = 0.064$ lbf/in.^{3}
$\rho_{matrix} = 0.35$ lbf/in.^{3}
$G_{fiber} = E_{fiber}/2(1 + \nu_{fiber})$
$G_{matrix} = E_{matrix}/2(1 + \nu_{matrix})$.

The fiber area in the composite must be determined from the properties of the graphite. Data provided with the graphite define the area in one graphite yarn (A_{yarn}). The number of yarns (N_{yarn}) is determined for the test specimen and the total area of the graphite (A_{fiber}) is determined: $A_{yarn} = 0.000175$ in.^{2}, $N_{yarn} = 8$, and $A_{fiber} = N_{yarn}A_{yarn}$.

The total area of the specimen (A_1) is determined from the thickness and width of the specimen. For the example presented here, the test article is labeled CG–SG4, and $t = 0.12$ in., $w = 1.004$ in., and $A_1 = 0.012$ in.^{2} The fiber and matrix volumes, respectively, can be calculated as follows: $V_{fiber} = A_{fiber}/A_1$ and $V_{fiber} = 0.012$; $V_{matrix} = 1 - V_{fiber}$ and $V_{matrix} = 0.988$.

Thus, the values for the effective material properties can be calculated as follows:

- Young's modulus (direction 1):

$$E_1 = V_{\text{fiber}} E_{\text{fiber}} + V_{\text{matrix}} E_{\text{matrix}}$$

$$E_1 = 5.045 \times 10^5 \text{ lbf/in.}^2 \tag{38}$$

- Young's modulus (direction 2):

$$E_2 = \frac{E_{\text{fiber}} E_{\text{matrix}}}{V_{\text{matrix}} E_{\text{fiber}} + V_{\text{fiber}} E_{\text{matrix}}}$$

$$E_2 = 1.164 \times 10^5 \text{ lbf/in.}^2 \tag{39}$$

- Poisson's ratio:

$$\nu_{12} = \nu_{\text{fiber}} V_{\text{fiber}} + \nu_{\text{matrix}} V_{\text{matrix}}$$

$$\nu_{12} = 0.27 \tag{40}$$

- Shear modulus:

$$G_{12} = \frac{G_{\text{fiber}} G_{\text{matrix}}}{V_{\text{matrix}} G_{\text{fiber}} + V_{\text{fiber}} G_{\text{matrix}}}$$

$$G_{12} = 4.62 \times 10^4 \text{ lbf/in.}^2 \tag{41}$$

4.6 Comparison of Rule of Mixtures Properties to Test Data

Prior to each tensile test, the width and thickness of each specimen was recorded. Specimen CG–SG_4 was the pathfinder specimen and was made thinner than the other specimens. The hand-polishing of the specimen surface resulted in a variation in specimen thickness for the remaining five specimens (table 7). These dimensions were used with the Mathcad® solution sheet for the rule of mixtures to predict the Young's modulus in the axial direction. The results of the analysis are presented in table 7. The results from the rule of mixtures can be compared to the results from tensile testing. Figure 49 is a stress-strain curve for specimen CG–SG_4.

Table 7. Young's modulus predicted from the rule of mixtures.

Specimen	Width (in.)	Thickness (in.)	Young's Modulus Rule of Mixtures (lbf/in.^{2})
CG–SG4	1.004	0.120	5.05×10^5
Dec_28-4	1.016	0.190	3.58×10^5
Dec_28-5	1.006	0.196	3.52×10^5
Dec_28-6	1.000	0.216	3.31×10^5
Dec_28-7	1.003	0.210	3.37×10^5
Dec_28-8	1.000	0.180	3.75×10^5

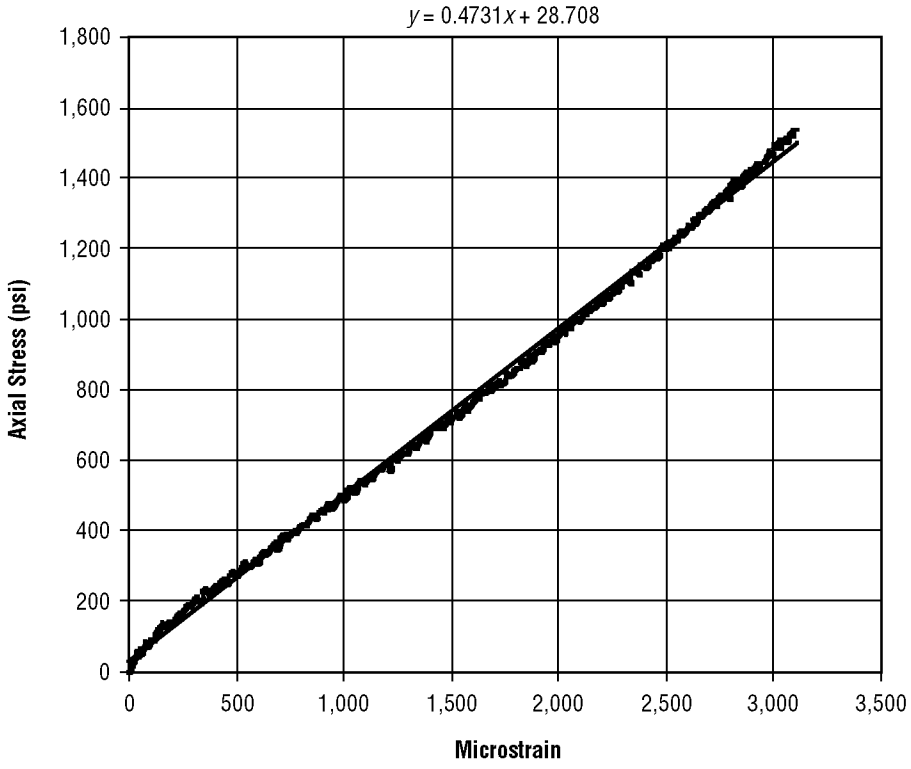

Figure 49. Composite stress-strain curve (SG_4).

The testing of this type of specimen is discussed in detail in section 3. The data are presented here to provide a comparison between the material properties calculated from the rule of mixtures and the test data. Young's modulus from the tensile test is calculated by taking the slope of the stress-strain curve:

$$E_{\text{test}} = \frac{(1,500 - 500)\,\frac{\text{lbf}}{\text{in.}^2}}{(3,000 - 1,000)\times 10^{-6}} \qquad E_{\text{test}} = 5\times 10^5\,\frac{\text{lbf}}{\text{in.}^2}$$

$$\Delta_{\text{error}} = \left|\frac{E_{\text{test}} - E_1}{E_{\text{test}}}\right| \times 100\% \qquad \Delta_{\text{error}} = 0.898\% \ . \tag{42}$$

The analysis is repeated for each of the tensile test specimens. Comparing the Young's modulus data to predicted values provides insight into the accuracy of the rule of mixtures method (table 8).

Table 8. Comparison of predicted Young's modulus with test results.

Specimen	Young's Modulus Rule of Mixtures (lbf/in.^{2})	Young's Modulus Test Results (lbf/in.^{2})	Measurement of Error (%)
CG–SG4	5.05×10^5	5.00×10^5	0.89
Dec_28-4	3.58×10^5	3.88×10^5	7.70
Dec_28-5	3.52×10^5	3.91×10^5	10.00
Dec_28-6	3.31×10^5	4.07×10^5	18.60
Dec_28-7	3.37×10^5	3.98×10^5	15.30
Dec_28-8	3.75×10^5	4.40×10^5	14.80

The errors range from 0.89 to 18.6 percent; averaging the six test specimens yields an average error of 11.23 percent with a standard deviation of 6.4 percent. In each case, the rule of mixtures underestimates the test value, suggesting that the predictions may be modified[9,10] to more closely match the test values. Empirical modifications to the rule of mixtures would require a considerable test program to generate a large enough database from which to derive an accurate factor. It is sufficient for this TM to recognize that the rule of mixtures provides a reasonable estimate of the composite material properties. The comparison establishes the fact that the rule of mixtures is applicable to a cementitious-based composite and suggests that employing empirical modifications can increase the accuracy.

Young's modulus in direction 2 was not accurately determined from the rule of mixtures. This composite is made from a graphite mesh, which results in fibers running in both directions 1 and 2. Since the composite has the same material composition in both directions, it is intuitively obvious that the Young's modulus in directions 1 and 2 would be equal. The rule of mixtures calculates the E_2 value well below test results. This is not unexpected, since this theory considers only fibers in direction 1.[2,10] However, the equations developed by Krenchel[3] can be used to transform the fiber direction and load to accurately predict E_2. Krenchel's transformation equations depend on the orientation of the fibers to the load. These equations are based on the same principles as presented in section 4.2. However, the properties in direction 2 can be calculated by mathematically rotating the load 90° (app. A). Regardless of the apparent inadequate results in direction 2, the rule of mixtures can still provide the necessary data for the analysis of simple beams.

4.7 Comparison of Poisson's Ratio From Tensile Test Data

Poisson's ratio from the transverse data is presented in section 3.8. Poisson's ratio for the five test specimens presented in table 4 is calculated using the rule of mixtures equation (40), $\nu_{12} = \nu_{fiber}V_{fiber} + \nu_{matrix}V_{matrix}$. The results of the calculations are presented in table 9.

Table 9. Comparison of predicted Poisson's with test results.

Specimen	Experimental	Rule of Mixtures	Error (%)
Dec_28-4	0.136	0.262	48.0
Dec_28-5	0.135	0.262	48.5
Dec_28-6	0.142	0.262	45.8
Dec_28-7	0.131	0.262	50.0
Dec_28-8	0.144	0.262	45.0

The error in the Poisson's ratio calculation is substantial. However, it is not entirely unexpected (sec. 3.5).[2,10] The derivation for the rule of mixtures assumes the reinforcement fibers are present in the axial direction only. The theory cannot account for fibers running in the transverse direction, emphasizing the need to develop a solution based on the laminated plate theory for composites.

4.8 Comparison of Shear Modulus Values

The shear modulus (sec. 4.4) of the matrix and the fiber can be obtained knowing the Young's modulus and Poisson's ratio as follows:[6]

$$G_{matrix} = \frac{E_{matrix}}{2(1+\nu_{matrix})} = 4.5\times10^4 \frac{lbf}{in.^2}$$

$$G_{fiber} = \frac{E_{fiber}}{2(1+\nu_{fiber})} = 12.8\times10^6 \frac{lbf}{in.^2} \tag{43}$$

The shear modulus of the composite is determined from the shear moduli of the constituents and the volume fractions of the composite. Applying equation (41),

$$G_{12} = \frac{G_{matrix}G_{fiber}}{V_{matrix}G_{fiber} + V_{fiber}G_{matrix}} = 4.6\times10^4 \frac{lbf}{in.^4} \tag{44}$$

It is apparent from the G_{12} value that the graphite fiber does not significantly increase the shear modulus of this composite. However, the results of the shear testing do not support this observation (fig. 40).

Comparing the predicted value and the value from the test article (table 10),

$$\text{Error}\% = \frac{\left(4.6\times10^4 - 7.2\times10^4\right)}{7.2\times10^4}\times100\% = 36.1\% \ . \tag{45}$$

Table 10. Comparison of predicted shear modulus with test results.

Specimen	Shear Modulus Rule of Mixtures (lbf/in.^{2})	Shear Modulus Test Results (lbf/in.^{2})	Measurement of Error (%)
Shear 2	4.6×10^4	7.2×10^4	–36.1
Shear 4	4.6×10^4	7.8×10^4	–41.0

The average percent of error, 38.6 percent, indicates that the rule of mixtures significantly underpredicts the shear modulus for this composite. The test results indicated the shear modulus is greater for the composite than for the cementitious material.

4.9 Summary of Material Properties

In the axial direction, Young's modulus can be determined from the rule of mixtures. The rule of mixtures prediction is on average 11 percent less than the value obtained from tensile test data. As expected, the rule of mixtures did not predict the Young's modulus in the transverse direction. For the composite considered here, $E_{\text{axial}} = E_{\text{transverse}}$. In addition, the rule of mixtures did not predict the Poisson's ratio for the composite material. The material property testing indicated a Poisson's ratio value ≈50 percent less than the value predicted by the rule of mixtures. The results of the shear test determined a shear modulus that is on average 39 percent higher than the value predicted by the rule of mixtures. Although only two shear test specimens were available, the good correlation in the two test specimens gives credibility to the test data.

The limitations of the rule of mixtures are obvious from the review of these results. This observation leads to the conclusion that additional analytical methods must be investigated to determine all the material properties for the composite. However, before pursing these additional analytical methods, it should be recognized that many analytical problems could be solved using the information provided by the rule of mixtures.

4.10 Calculation of the Deflection for a Beam in Pure Bending

The rule of mixtures method for calculating the effective material properties for a composite beam has been compared to material test data. The results indicated that the rule of mixtures could be used to predict the Young's modulus in the direction of the fiber and load, E_1 or $E_{\text{effective}}$. The next logical step is to combine this material property with an analytical method that can be used to predict the behavior of a composite structure. As noted earlier, the transform section method was not accurate for

this composite because the Young's modulus ratio was extremely high. However, using the effective materials property data, the Young's modulus ratio ($\eta = E_{effective}/E_{matrix}$) is now <20 and in the acceptable range. The Biszick beam[1] can now be analyzed by using the effective material property data and the transform section theory. The results will be compared to static test results to give an indication of the accuracy of the methods employed.

The cross section of a composite beam, fabricated of the same graphite and matrix materials used throughout this research, is illustrated in figure 50. An assumption is made that the beam is composed of two materials; the "graphite section" is composed of graphite and matrix material. The h_g dimension of this section is the same thickness as the tensile test articles used to verify the effective material properties for the composite material. The transform section analysis method will assume the graphite-reinforced section has the effective material properties calculated by the rule of mixture method. The geometry of the test specimen is used to determine the dimensions of the graphite strands and the thickness of the graphite section:

$w_g = 1.20$ in.
$h_g = 0.115$ in.

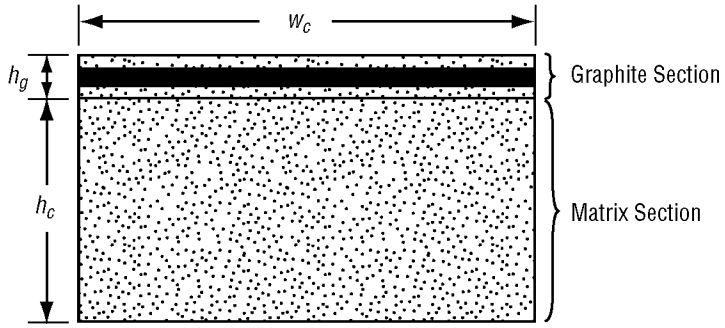

Figure 50. Cross section of beam.

The remaining dimensions of the composite section are calculated as follows:

$h_c = 0.361$ in. $- h_g$
$w_c = 1.20$ in.
$h_c = 2.46 \times 10^{-1}$ in.

This test specimen has nine yarns across the width. The fiber volume can be determined from the geometry of the test specimen:

$A_{yarn} = 0.000175$ in.^{2}
$N_{yarn} = 9$
$A_{fiber} = N_{yarn} A_{yarn}$
$A_1 = (0.115$ in.$)(1.20$ in.$)$
$V_{fiber} = A_{fiber}/A_1$
$V_{fiber} = 1.141 \times 10^{-2}$.

The matrix volume is then calculated from the rule of mixtures:

$$V_{\text{matrix}} = 1 - V_{\text{fiber}}$$
$$V_{\text{matrix}} = 9.886 \times 10^{-1}.$$

The material properties of the graphite and matrix are the same as previously defined:

$$E_{\text{fiber}} = 33.5 \times 10^{6} \text{ lbf/in.}^2$$
$$E_{\text{matrix}} = 115 \times 10^{3} \text{ lbf/in.}^2$$

The effective material properties for the composite section of the beam can be calculated.

- Young's modulus in direction 1:

$$E_1 = V_{\text{fiber}} E_{\text{fiber}} + V_{\text{matrix}} E_{\text{matrix}} \qquad E_1 = 4.9602 \times 10^5 \frac{\text{lbf}}{\text{in.}^2} \tag{46}$$

The moment of inertia for the beam can now be calculated using the transform section method. The Young's modulus ratio for the transform section is calculated from the effective material properties and the matrix material properties:

$$\eta = \frac{E_1}{E_{\text{matrix}}} \qquad \eta = 4.313 \ . \tag{47}$$

The beam geometry is transformed by multiplying the width of the graphite section by η:

$$w_g = \eta w_g \qquad w_g = 5.176 \text{ in.} \tag{48}$$

The centroid and the area of the graphite section are given by

$$y_g = h_c + \left(\frac{h_g}{2}\right) \qquad A_g = h_g w_g \ , \tag{49}$$

while the centroid and the area of the matrix material is

$$y_c = \frac{h_c}{2} \qquad A_c = h_c w_c \ . \tag{50}$$

The centroid of the transform section is given by

$$Y_{\text{bar}} = \frac{A_g y_g + A_C y_C}{A_g + A_C} \qquad Y_{\text{bar}} = 2.4366 \times 10^{-1}\text{in.} \tag{51}$$

The cross section of the composite is symmetric in the *X* direction; thus, the *X* location of the centroid is the center of the beam:

$$X_{\text{bar}} = \frac{w_C}{2} \qquad X_{\text{bar}} = 0.6\text{ in.} \tag{52}$$

The moment of inertia for the graphite-reinforced section of the beam can be calculated by using the parallel axis theorem, $I = I_g + A_g d^2$. The base of the top section is transformed by η and the height of the graphite-reinforced section is given by $h = h_g$. The moment of inertia of the graphite-reinforced section with respect to its centroid is given by the equation

$$I_g = \frac{bh^3}{12} \ . \tag{53}$$

The area of the graphite-reinforced section is the base multiplied by the height:

$$A_g = bh \ . \tag{54}$$

The distance from the center top section to the centroid of the section is

$$d = Y_{\text{bar}} - \left(h_C + \frac{h_g}{2} \right) . \tag{55}$$

Applying the parallel axis theorem,

$$I_{g\_\text{total}} = I_g + A_g d^2 \qquad I_{g\_\text{total}} = 2.7875 \times 10^{-3}\text{in.}^4 \tag{56}$$

The moment of inertia for the matrix (bottom) section of the beam can be calculated using the same method. The base and the height of the matrix section are

$$b = w_C \qquad h = h_C \ . \tag{57}$$

The moment of inertia of the matrix section with respect to its centroid and the areas are

$$I_c = \frac{bh^3}{12} \qquad A_c = bh \ . \tag{58}$$

The distance from the center of the matrix section to the centroid of the section is

$$d = Y_{\text{bar}} - \left(\frac{h_c}{2}\right). \tag{59}$$

The moment of inertia for the matrix with respect to the centroid of the composite beam can be calculated as follows:

$$I_{c\_\text{total}} = I_c + A_c d^2 \qquad I_{c\_\text{total}} = 5.7864 \times 10^{-3}\text{in.}^4 \tag{60}$$

The total moment of inertia for the transform section is the sum of the moment of inertia for each section:

$$I_{\text{total}} = I_{c\_\text{total}} + I_{g\_\text{total}} \qquad I_{\text{total}} = 8.5739 \times 10^{-3}\text{in.}^4 \tag{61}$$

The beam was subjected to a three-section bending test. A rigorous deflection analysis of the beam test was performed to establish a base of comparison to finite element modeling and test data. The comparisons provide insight into the accuracy of the methods used for the analysis.

The equation for the elastic curve of this beam will be derived as part of this analysis. Although a solution to this beam problem is available in the literature, it was important to develop the solution in this TM because of variations in the boundary conditions. Laboratory testing strives to duplicate the exact boundary conditions; however, it is sometimes impractical. The equations aided in determining which boundary conditions had significant effects on the results being recorded. These equations were solved for a variety of boundary conditions using a Mathcad[12] solution sheet (app. C). It should be noted that with the aid of these equations and WD-40® lubricant, the test fixture eventually duplicated the proper boundary conditions.

In general, the elastic equation for a curve is given by $EI(d^2/dx^2)y = M(x)$. The moment in each section of the beam (fig. 51) can be derived by passing a section through that location. In section 1 ($x < a$), for example, the moment at x is computed from the free-body diagram shown in figure 52 as Px.

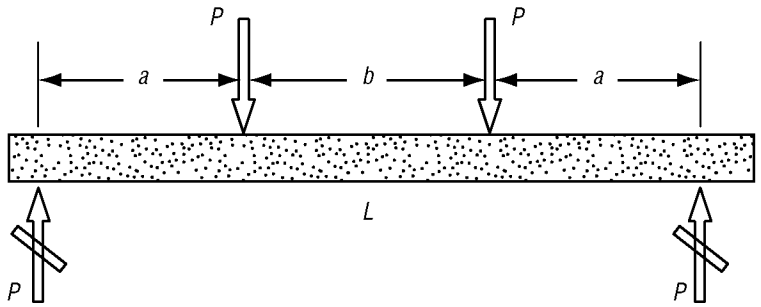

Figure 51. Free-body diagram of the beam.

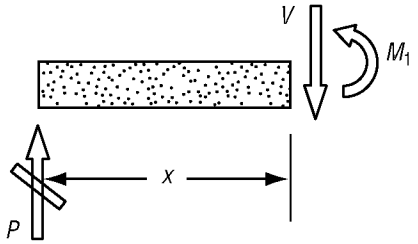

Figure 52. Free-body diagram of section 1.

Substituting the later into the governing equation for section 1, $x < a$:

$$EI\frac{d^2}{dx^2}y_1 = Px \quad . \tag{62}$$

Integrating once,

$$EI\frac{d}{dx}y_1 = \frac{Px^2}{2} + C_1 \quad . \tag{63}$$

Integrating again,

$$EIy_1 = \frac{Px^3}{6} + C_1x + C_2 \quad . \tag{64}$$

Similarly, for section 2, figure 53, $x > a$ but $x < b$:

$$EI\frac{d^2}{dx^2}y_2 = Pa \tag{65}$$

$$EI\frac{d}{dx}y_2 = Pax + C_3 \tag{66}$$

$$EIy_2 = \frac{P}{2}ax^2 + C_3x + C_4 \ . \tag{67}$$

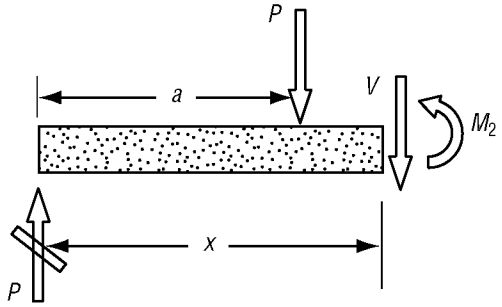

Figure 53. Free-body diagram of section 2.

Finally, for section 3, figure 54, $x > (a + b)$,

$$EI\frac{d^2}{dx^2}y_3 = 2Pa + Pb - Px \tag{68}$$

$$EI\frac{d}{dx}y_3 = 2Pax + Pbx - \frac{Px^2}{2} + C_5 \tag{69}$$

$$EIy_3 = Pax^3 + \frac{Pbx^2}{2} - \frac{Px^3}{6} + C_5x + C_6 \ . \tag{70}$$

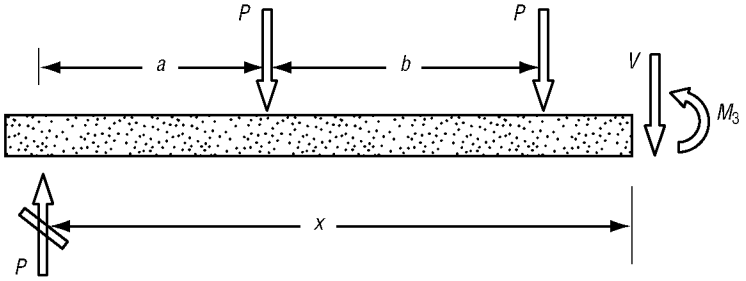

Figure 54. Free-body diagram of section 3.

Summarizing the equations and replacing the derivative with θ,

$$EI\theta_1 y_1 = \frac{Px^2}{2} + C_1 \ , \tag{71}$$

$$EI\theta_2 y_2 = Pax + C_3 \ , \tag{72}$$

$$EI\theta_3 y_3 = 2Pax + Pbx - \frac{Px^2}{2} + C_5 \ , \tag{73}$$

$$EIy_1 = \frac{Px^3}{6} + C_1 x + C_2 \ , \tag{74}$$

$$EIy_2 = \frac{P}{2} ax^2 + C_3 x + C_4 \ , \tag{75}$$

and

$$EIy_3 = Pax^3 + \frac{Pbx^2}{2} - \frac{Px^3}{6} + C_5 x + C_6 \ . \tag{76}$$

The equations must satisfy the boundary conditions. For example, at $x = 0$, $y_1 = 0$, equation (74) can be written

$$0 = \frac{P}{6} x_o^3 + C_1 x_o + C_2 \ . \tag{77}$$

At $x = a$, equation (74) must equal equation (75); therefore,

$$\frac{P}{6} x_1^3 + C_1 x_1 + C_2 = \frac{P}{2} ax_1^2 + C_3 x_1 + C_4 \ . \tag{78}$$

In addition, at $x = a$, $y_1 = y_2$, and $\theta_1 = \theta_2$. Equation (71) must equal equation (72):

$$\frac{Px_1^2}{2} + C_1 = Pax_1 + C_3 \ . \tag{79}$$

For the boundary condition $x = (a + b)$, equation (75) equals equation (76):

$$\frac{P}{2}ax_2^2 + C_3x_2 + C_4 = Pax_2^2 + \frac{Pbx_2^2}{2} - \frac{Px_2^3}{6} + C_5x_2 + C_6 \quad . \tag{80}$$

Continuing in the same manner, at $x = (a + b)$, $y_2 = y_3$, and $\theta_2 = \theta_3$, then equation (72) equals equation (73):

$$Pax_2 + C_3 = 2Pax_2 + Pbx_2 - \frac{Px_2^2}{2} + C_5 \quad . \tag{81}$$

Finally, for the boundary condition $x = L$, equation (76) must equal zero:

$$0 = Pax_3^2 + \frac{Pbx_3^2}{2} - \frac{Px_3^3}{6} + C_5x_3 + C_6 \quad . \tag{82}$$

Equations (71)–(76), with the given boundary conditions, represent a system of equations which can be solved simultaneously for the constants C_1 through C_6. A Mathcad® solution was developed to perform the calculations (app. C). Appendix C contains typical values for these constants. The elastic curve equations may be restated as a function of x:

In section 1, $x < a$:

$$y_1(x) = \frac{1}{EI}\left(\frac{Px^3}{6} + C_1x + C_2\right) \tag{83}$$

and

$$\theta_1(x) = \frac{1}{EI}\left(\frac{Px^2}{2} + C_1\right) . \tag{84}$$

The value for the moment of inertia is set to the value calculated from the rule of mixtures and the transform section method. The Young's modulus in the equation is set equal to that of the matrix; i.e.,

$$I = I_{\text{total}} \qquad I = 8.574 \times 10^{-3}\text{in.}^4$$

$$E = E_{\text{matrix}} \qquad E = 1.15 \times 10^5 \frac{\text{lbf}}{\text{in.}^2} \tag{85}$$

In section 2, $x > a < a + b$:

$$y_2(x) = \frac{1}{EI}\left(Pax^2 + C_3x + C_4\right) \tag{86}$$

and

$$\theta_2(x) = \frac{1}{EI}\left(Pax + C_3\right) \cdot \tag{87}$$

Finally, in section 3, $x > a + b$:

$$y_3(x) = \frac{1}{EI}\left(Pax^2 + \frac{Pbx^2}{2} - \frac{Px^3}{6} + C_5x + C_6\right) \tag{88}$$

and

$$\theta_3(x) = \frac{1}{EI}\left(2Pax + Pbx - \frac{Px^2}{2} + C_5\right) . \tag{89}$$

The composite beam was then subjected to the three-section bending test (fig. 55). Deflection data were recorded at the center of the 9-in. beam.

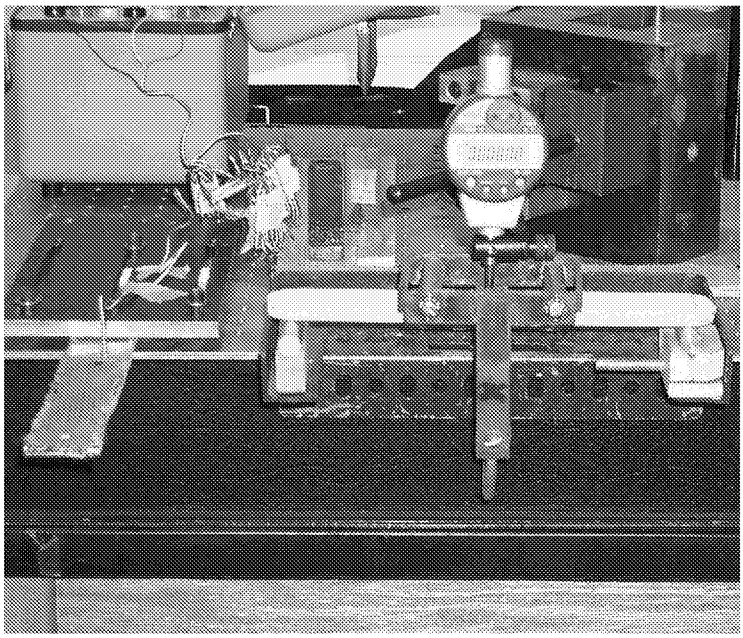

Figure 55. Three-section bending test fixture.

The elastic beam analysis was repeated for each of the load steps used in the three-section beam test. The load and deflection results are listed in the following matrices:

$$\text{Load} = \begin{bmatrix} 0 \\ 3.43 \\ 5.64 \\ 7.41 \\ 9.62 \\ 11.84 \\ 14.05 \\ 16.26 \\ 17.81 \end{bmatrix} \text{lbf}, \quad y_{\text{test}} = \begin{bmatrix} 0 \\ -0.0445 \\ -0.0729 \\ -0.0940 \\ -0.1197 \\ -0.1420 \\ -0.1670 \\ -0.1920 \\ -0.2090 \end{bmatrix} \text{in.}, \quad y_{\text{cal}} = \begin{bmatrix} 0 \\ -0.0420 \\ -0.0690 \\ -0.0910 \\ -0.1180 \\ -0.1450 \\ -0.1720 \\ -0.1990 \\ -0.2180 \end{bmatrix} \text{in.} \tag{90}$$

Figure 56 illustrates that the test results and the analytical data are in very good agreement. Error bars on the analytical data represent the 6.4-percent standard deviation associated in determining Young's modulus (table 8). This indicates that the transform section method of analysis can be used to predict the deflections. However, the rule of mixtures must be applied to determine the effective Young's modulus.

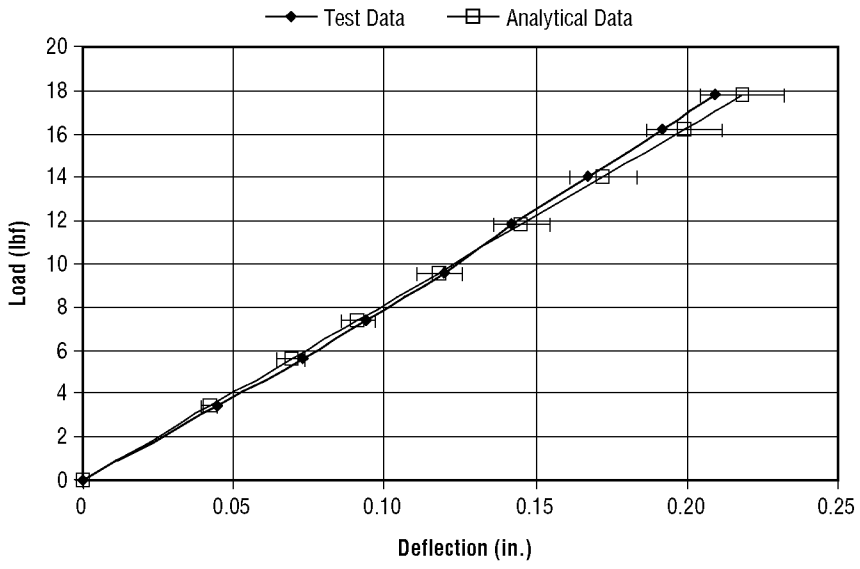

Figure 56. Transform section versus test results.

4.11 Development of a Finite Element Model

An additional point of comparison was obtained by developing a finite element model of the three-section beam test (fig. 57). The finite element model was developed for two reasons: (1) To confirm that the elastic beam analysis was correct and (2) to gain insight into modeling composite structures using finite element codes. The finite element model was executed for each of the static test loads.

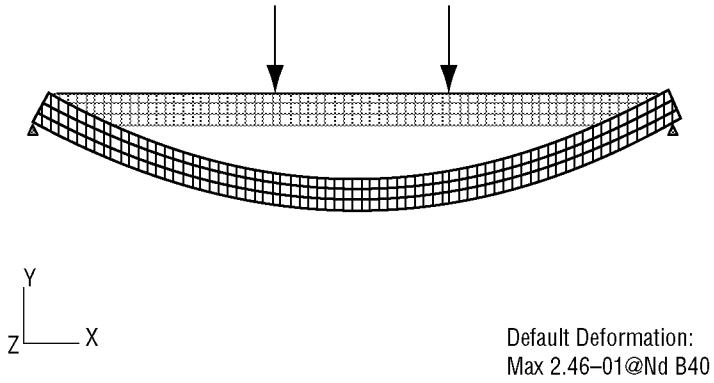

Figure 57. Finite element model.

The deflection results from the finite element model "specimen1" are as follows:

$$y_{\text{fem}} = \begin{bmatrix} 0 \\ -0.0420 \\ -0.0690 \\ -0.0910 \\ -0.1180 \\ -0.1450 \\ -0.1720 \\ -0.1990 \\ -0.2180 \end{bmatrix} \text{in.} \tag{91}$$

The deflection results for both the elastic beam equation and the finite element model were plotted with the deflections from the three-section bending test.

It is significant that the transform section method of analysis returns the same deflections as the finite element solution. This leads to the conclusion that the transform section method of analysis can be used for the analysis of a composite in which the Young's modulus ratio is high, provided the effective material property data are included in the calculations. Figure 57 indicates that both of the analytical methods satisfactorily predict the results of the bending test (fig. 58). The error between the elastic beam equations and the test data is relatively small:

$$\Delta_{error} = \frac{y_{test\_step} - y_2(4.5\text{ in.})}{y_{test\_step}} \times 100\%$$

$$\Delta_{error} = -4.52\% \quad . \tag{92}$$

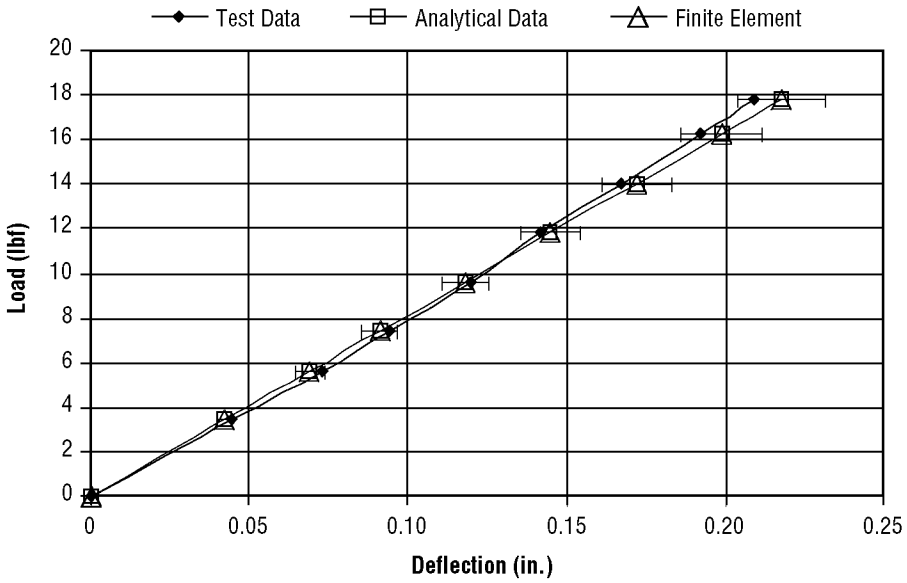

Figure 58. Transform section, finite element, and test results.

4.12 Calculate the Deflection for a Five-Layer Plate in Pure Bending

Section 4.2 demonstrates the analysis of a composite beam made from the graphite-reinforced cementitious material. The University of Alabama in Huntsville (UAH) concrete canoe team produced a large plate that is similar to the layups used in canoe construction. A test article 5 in. wide and 15 in. long was cut from the composite plate. The challenge is to determine the deflections of the plate using the information gained from the material properties of the constituents, the rule and mixtures, and the transform section method of analysis. These are the tools and information that are available to the

students at the time they are designing these competitive canoes. The beam is a buildup of five layers as shown in figure 59.

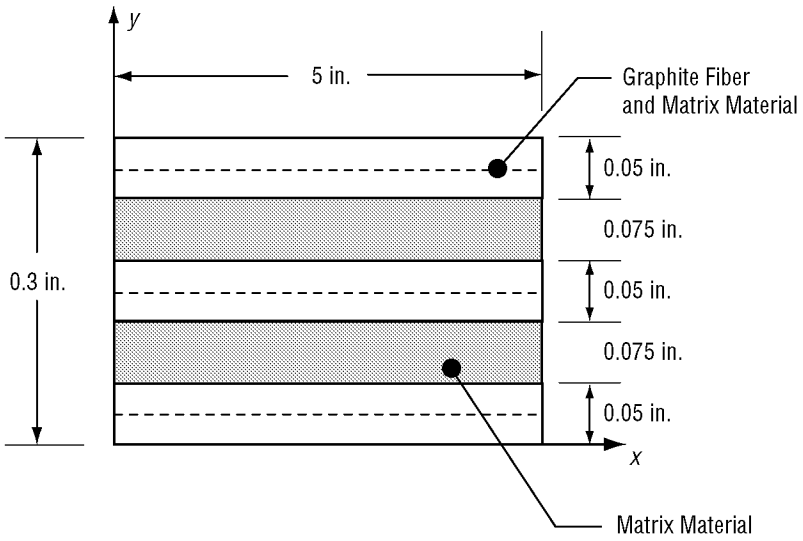

Figure 59. Cross section of multilayered composite beam.

The properties of the beam can be calculated by using the transform section method and the effective material properties as determined from the rule mixtures. The effective Young's modulus for the three graphite and matrix sections is

$$E_2 = 5.04 \times 10^5 \frac{\text{lbf}}{\text{in.}^2} \tag{93}$$

The Young's modulus for the matrix material, E_1, is determined from tensile testing of the cementitious material (app. B):

$$E_1 = 115 \times 10^3 \frac{\text{lbf}}{\text{in.}^2} \tag{94}$$

It was previously established that the Young's modulus ratio must be <20 for the transform section method to be accurate. Using the values established here, the Young's modulus ratio is calculated and is within acceptable limits:

$$\eta = \frac{E_2}{E_1} \qquad \eta = 4.383\,. \tag{95}$$

The dimension of the graphite sections is transformed by multiplying the width of the sections by η. A Mathcad solution sheet (app. C) was used to perform the calculations for determining the moment of inertia for the beam. These calculations are also described in section 4.10. The moment of inertia for this cross section was calculated to be

$$I_{\text{total}} = 38.2 \times 10^{-3} \text{ in.}^4 \tag{96}$$

In general, the procedure for determining the properties of multilayer beams is the same as that for a single-layer beam. It is interesting to note that the graphite section in the middle of the beam does not contribute significantly to the bending strength. The beam is placed in a three-section bending test with the specimen supported over a 15-in. span and loaded at two points, each located at a distance of 2.25 in. from the center of the span. Members of the UAH canoe team performed the testing during the 1999–2000 school year. This test was typical of those used by the team to evaluate the composite designs considered for the canoe.

The elastic beam equation for this problem was provided previously. The deflection of the center of the beam was calculated for the same loads used in the beam tests. Equations (86) and (87) are used for the deflection calculations:

$$y_2(x) = \frac{1}{EI}\left(Pax^2 + C_3 x + C_4\right) \tag{97}$$

and

$$\theta_2(x) = \frac{1}{EI}\left(Pax + C_3\right) \ . \tag{98}$$

The calculations were made using the Mathcad solution sheet (app. C). The derivation for the beam equation is described in detail in section 4.10. Young's modulus used in the equation is from the matrix material: $E_1 = 115 \times 10^3$ lbf/in.^{2}

The results of this analysis are compared to the results from the bending test. As shown in figure 60, they compare well at deflections <0.25 in., then diverge as the deflections reach higher values. The test results also appear to be slightly nonlinear. The nonlinear behavior of the displacements suggests that the material properties are nonlinear.

The stress-strain curve for the test specimen can be established from the flexure formula and the moment in the beam. The strain is calculated from the stress and based on the Young's modulus of the matrix as follows:

$$\sigma(x) = \frac{M(x)c}{I} \qquad c = \frac{t}{2} \qquad \varepsilon(x) = \frac{\sigma(x)}{E_{\text{matrix}}} \ . \tag{99}$$

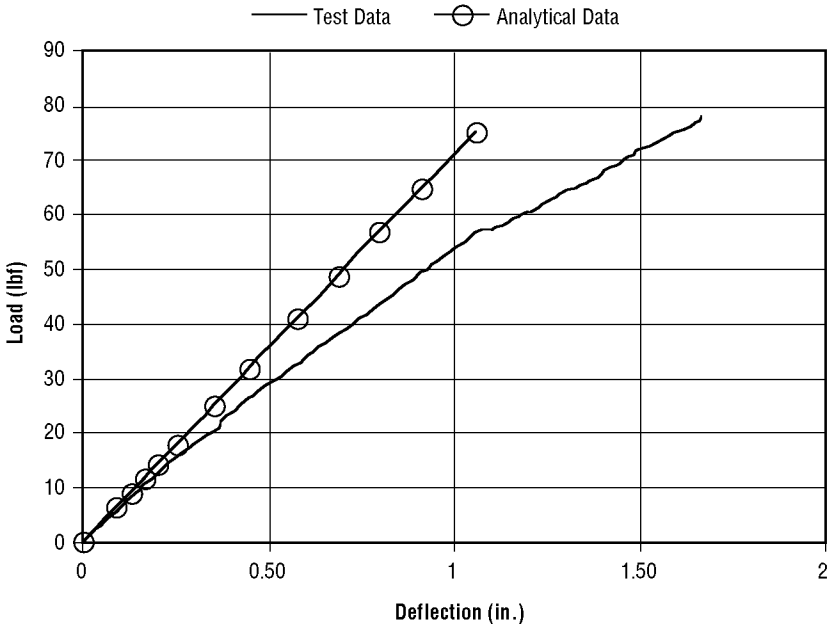

Figure 60. Deflection of multilayer beam versus test data (linear).

These calculations are presented in detail in the Mathcad solution sheet (app. C). The stress-strain curve from the test specimen can now be compared to the stress-strain curve for the matrix material. Figure 61 shows the stress-strain curve for the beam and the matrix material.

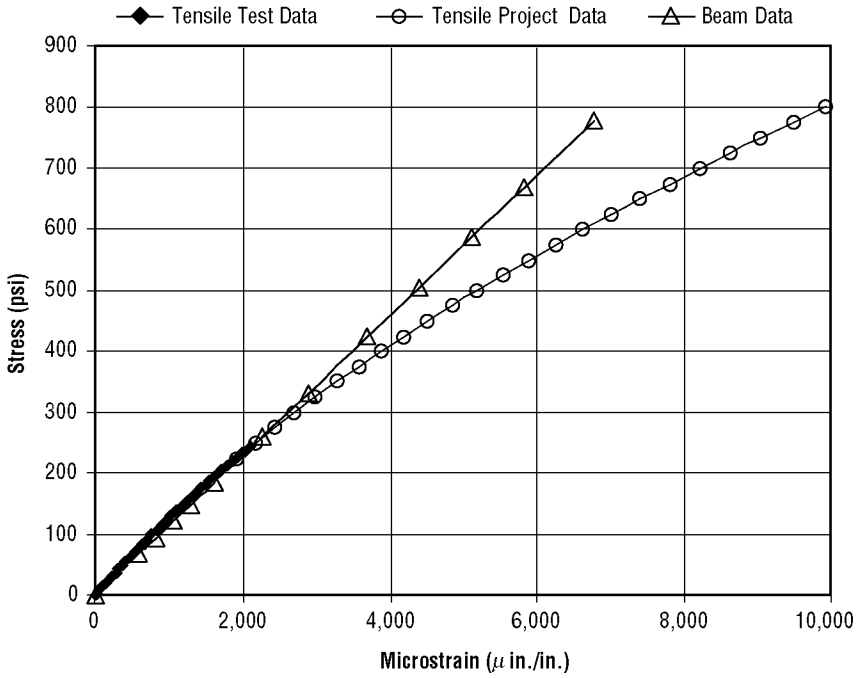

Figure 61. Stress-strain curve for matrix material.

The experimental curve in figure 61 is derived from a combination of test and analysis. The first section of the curve is from tensile testing using extensometers in the axial direction; the tensile test specimens failed at ~2,000 microstrain. The stress-strain curve beyond that point is derived from the tensile test data using a least-squares method to determine an equation for the curve.[2]

$$b_0 n + b_1 \sum_{i=1}^{n} \sigma_{\text{matrix}_i} + b_2 \sum_{i=1}^{n} \left(\sigma_{\text{matrix}_i}\right)^2 = \sum_{i=1}^{n} \varepsilon_{\text{matrix}_i}$$

$$b_0 \sum_{i=1}^{n} \sigma_{\text{matrix}_i} + b_1 \sum_{i=1}^{n} \left(\sigma_{\text{matrix}_i}\right)^2 + b_2 \sum_{i=1}^{n} \left(\sigma_{\text{matrix}_i}\right)^3 = \sum_{i=1}^{n} \left(\sigma_{\text{matrix}_i}\right)\left(\varepsilon_{\text{matrix}_i}\right)$$

$$b_0 \sum_{i=1}^{n} \left(\sigma_{\text{matrix}_i}\right)^2 + b_1 \sum_{i=1}^{n} \left(\sigma_{\text{matrix}_i}\right)^3 + b_2 \sum_{i=1}^{n} \left(\sigma_{\text{matrix}_i}\right)^4 = \sum_{i=1}^{n} \left(\sigma_{\text{matrix}_i}\right)^2 \left(\varepsilon_{\text{matrix}_i}\right) \quad . \tag{100}$$

These equations are solved for the minimum values of b_0, b_1, and b_2:

$$\Psi = b_0 + b_1 \sigma_{\text{matrix}} + b_2 \left(\sigma_{\text{matrix}}\right)^2 \quad . \tag{101}$$

Equation (101) is the resulting stress-strain relationship used to extend the data for the tensile test. The resulting curve is an approximation that does not represent actual material properties and is only used to facilitate the analysis. This analytical method was developed by Balaguru[2] for the nonlinear analysis of ferrocement in bending.

The question arises as to whether the tension or compression properties of the matrix are determining the nonlinear behavior of the plate. Therefore, the compression properties of the matrix must also be considered.[2] Figure 62 compares the analytical curve for tensile properties with the compression properties from the compression test. The data for the tensile (analytical) and compression (test) properties are in good agreement up to 6,000 microstrain. Furthermore, both curves indicate nonlinear behavior beyond the 2,000 microstrain level.

Since Young's modulus is in the nonlinear region, it must be recalculated as the load increases beyond 2,000 microstrain. The elastic beam equation is then used with the nonlinear Young's modulus to calculate the deflections at the higher load levels. These calculations are illustrated in the Mathcad solution sheet (app. C). The results are compared to the test data from the three-section bending test. The error bars on the analytical data represent the 6.4-percent standard deviation associated in determining Young's modulus. As illustrated in figure 63, the data compares fairly well to the test results, even in the nonlinear region of the curve.

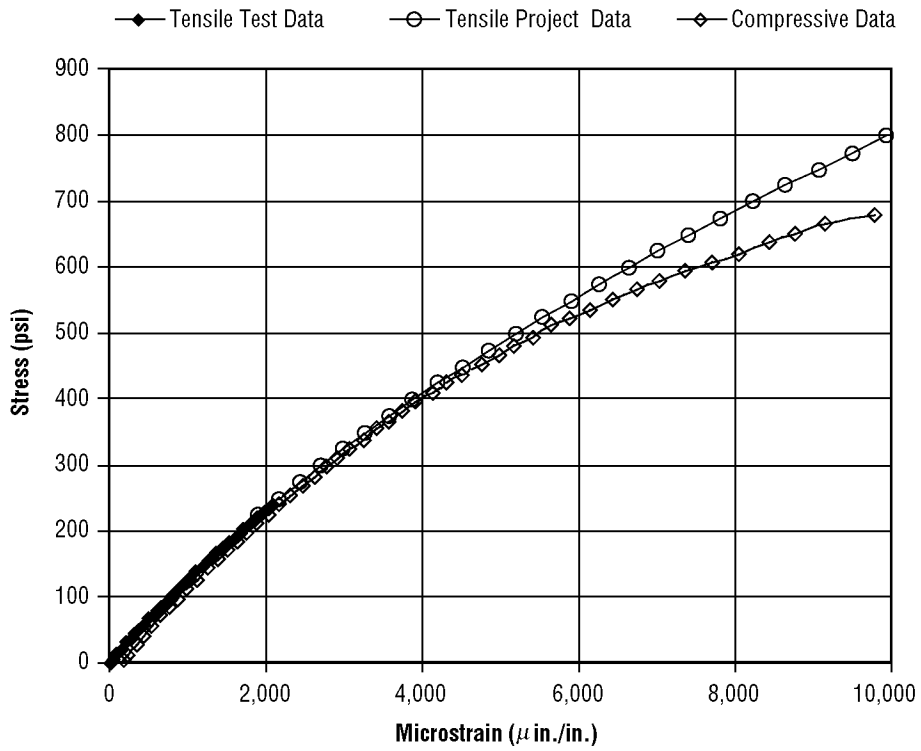

Figure 62. Tension versus compression properties for matrix material.

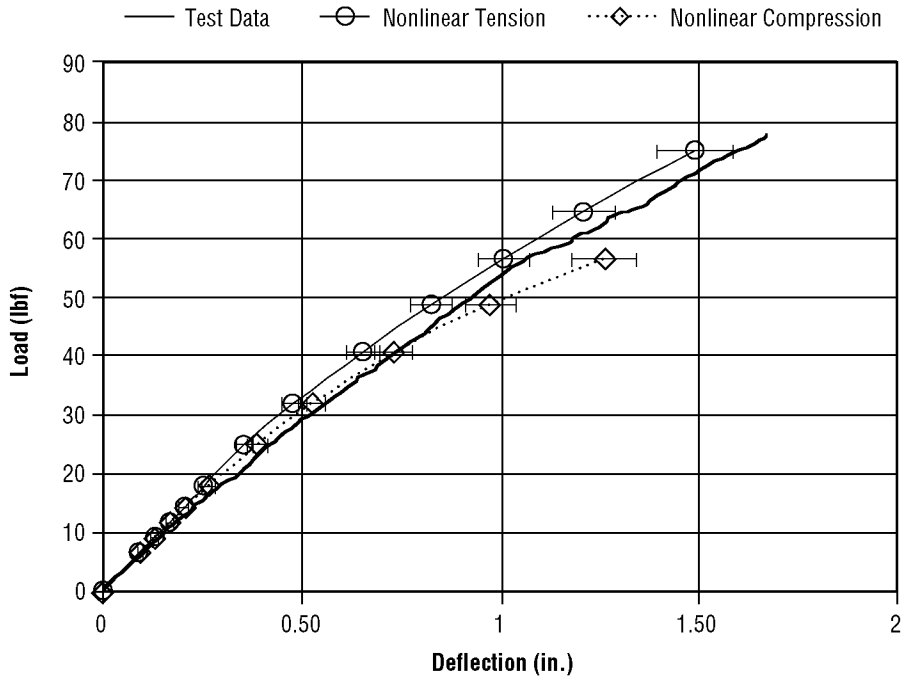

Figure 63. Comparison of test results with nonlinear transform section results.

The preceding analysis indicates that the combination of effective material properties and the transform section method can be used to determine the deflection of multilayered composite beams. This is similar to the work presented by Balaguru[2] for the nonlinear behavior of ferrocement. These data also indicate that as the matrix material becomes nonlinear, the deflection curve follows the same trend, indicating that the bond between the fiber material and the matrix material may be slipping. However, it should be noted that the beam did not fail even when the tension strain levels were far above the maximum tension strain found when testing the matrix material.

It must be pointed out that several deficiencies exist in the preceding analysis. The first is recognizing that the Young's modulus ratio is constantly changing as the matrix material becomes nonlinear. This implies that the moment of inertia for the beam is also changing. These changes are not considered in the analysis. In addition, this method of analysis does not provide a means to determine the strains or stresses in each layer of the composite beam.

4.13 Summary of the Rule of Mixtures Analysis

The rule of mixtures provides a method of calculating the effective material properties of the composite from the volume fraction and material properties of the constituents. Comparing the effective material properties with the data from the tensile and shear tests provided a measure of accuracy for this method. Young's modulus in the axial direction (E_1) was 11 percent lower than the value found in the tensile test. However, Young's modulus in the transverse direction (E_2) and Poisson's ratio (ν_{12}) did not agree with the test data. The poor comparison for E_2 and ν_{12} was not unexpected, since the composite under consideration has fibers running in the transverse direction. These fibers are not considered in the rule of mixtures theory. The shear modulus G_{12} was 39 percent lower than the value found in two test specimens.

Although the information derived from the rule of mixtures is limited, it was used successfully to predict the deflection of single and multilayer composite beams. The analysis used the transform section method and the elastic beam equation to demonstrate that the effective Young's modulus (E_1) could be used to predict deflections for a beam in pure bending. The analysis was verified by comparison to test data and finite element models, and the analysis was extended to predict the nonlinear behavior of composite material.

The fact remains, however, that these derivations are limited to the case in which the fibers are running in the axial direction. This limitation can be overcome by applying the laminated plate theory of composites to the cementitious composite in question.[10]

5. LAMINATED PLATE THEORY OF COMPOSITES

The rule of mixtures is limited by the assumption that the fibers are aligned in the direction of the load.[4,10] Laminated plate theory for composites offers a more complete analytical tool, provided this class of material is compatible with the assumptions and derivations involved with the theory. Beginning with laminated plate theory, the laminated composite plate equations will be derived. The derivations will be programmed into a Mathcad[24] solution sheet (app. D) to provide an automated method for solving the equations. The equations will be arranged to form a system of simultaneous equations from which an exact solution can be found. The solution includes all elements of the stiffness matrix and can be used for symmetric or nonsymmetric laminated plates. The program is used to analyze a composite plate for which the results are well known. Comparisons are made with other programs to demonstrate an increase in accuracy. A finite element model is generated to provide a verification of the methods and establish the procedures for modeling composite beams.

5.1 Plate Theory

Figure 64 shows a load-free plate where the midplane point A coincides with the x-y plane. The deflection in the z direction is zero for all points on the plate. The deflection components at a point in the x, y, and z directions are given by u, v, and w, respectively.

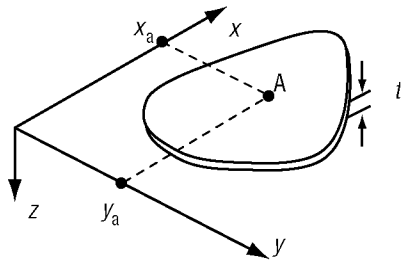

Figure 64. Load-free plate.

The fundamental assumptions of the small deflection theory of bending for isotropic, homogeneous, elastic thin plates are based on their geometry. These assumptions are known as the Kirchhoff hypotheses and can be stated as follows:[10]

- The midsurface deflection is small compared with the plate thickness. The slope of the deflected surface is very small and the square of slope is negligible.

- The midplane remains unstrained subsequent to bending.

- Plane sections initially normal to the midsurface remain plane and normal to surface after the bending.

- The stress normal to the midplane (σ_z) is small compared to the other stress components and may be neglected.

A plate can be deformed by normal, shear, and bending loads. The displacements in the *x, y, z* directions are defined as *u*, *v*, *w*, respectfully. Figure 65 shows a plate experiencing normal stresses.[20]

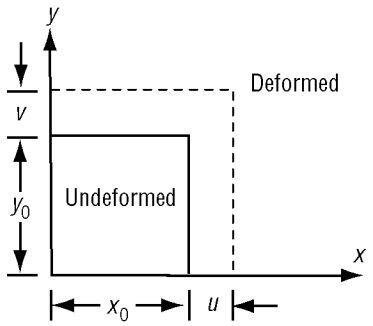

Figure 65. Plate with normal displacements.

The strains for this displacement state in the *x* and *y* directions are defined by

$$\varepsilon_x = \frac{d}{dx}u \tag{102}$$

and

$$\varepsilon_y = \frac{d}{dy}v \ , \tag{103}$$

respectively.

Figure 66, on the other hand, shows that when shear stresses are applied to a plate, they produce strains that are a function of both *u* and *v* displacements.[20]

The equation for the in-plane shear strain is

$$\gamma_{xy} = \frac{d}{dy}u + \frac{d}{dx}v \ . \tag{104}$$

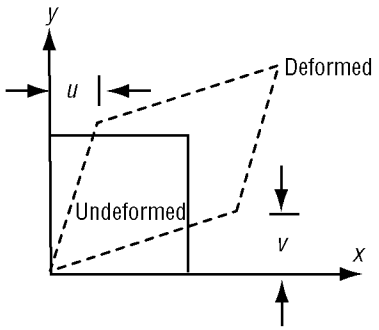

Figure 66. Shear displacement of plate.

The total in-plane displacement at any point in a plate is the sum of the normal displacements plus the displacements induced by bending. Figure 67 shows the geometry associated with a plate in bending.[9]

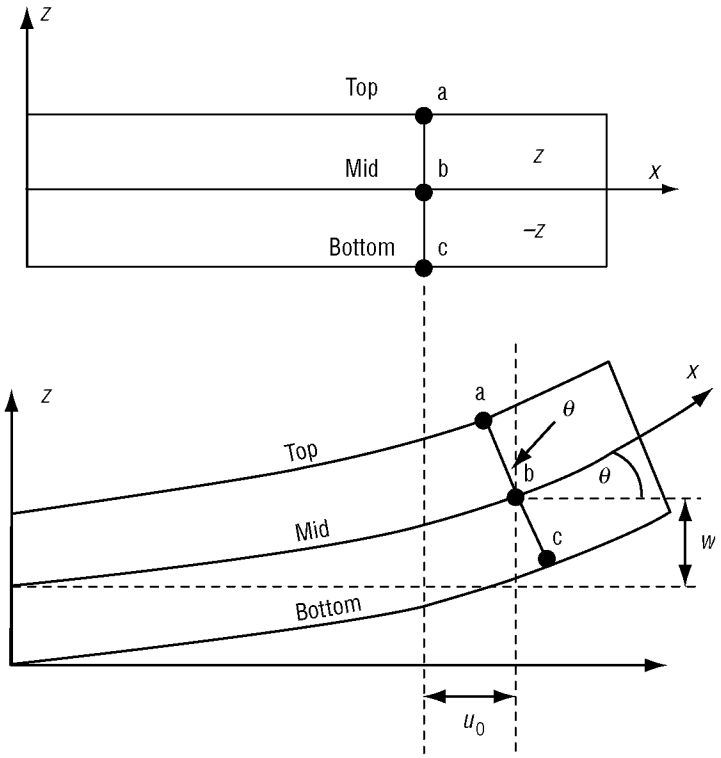

Figure 67. Bending displacement.

The displacement along the z direction due to bending is $z \times \sin(\theta)$. Since θ is small, $\sin(\theta) = \theta$, and the displacement is $z\theta$. In addition, from the geometry, it is clear that θ is the slope of the plate, $d/dx \times w$.

The displacements of the midplane of the plate in the x and y directions are defined as u_0 and v_0, respectively. Then the displacement in the x direction can be defined in terms of the midplane displacement, the slope of the plate, and the location from the midplane as

$$u = u_0 - z\frac{d}{dx}w_0 \,. \tag{105}$$

Similarly, the displacement in the y direction is

$$v = v_0 - z\frac{d}{dy}w_0 \,. \tag{106}$$

The Kirchoff hypotheses state that plane sections remain plane. This implies that there is no strain in the z direction. According to Kirchoff, the normal and shear strains in the z direction may be written as

$$\varepsilon_z = \frac{d}{dz}w \qquad \varepsilon_z = 0 \tag{107}$$

$$\gamma_{xz} = \frac{d}{dx}w + \frac{d}{dz}u \qquad \gamma_{xz} = 0 \tag{108}$$

$$\gamma_{yz} = \frac{d}{dy}w + \frac{d}{dz}v \qquad \gamma_{yz} = 0 \,. \tag{109}$$

.

When the displacements in equations (105) and (106) are substituted into equations (102)–(104), the strain equation accounts for the midplane displacements and the bending displacements and is written as

$$\varepsilon_x = \frac{d}{dx}u_0 - z\frac{d^2}{dx^2}w_0 \tag{110}$$

$$\varepsilon_y = \frac{d}{dy}v_0 - z\frac{d^2}{dy^2}w_0 \tag{111}$$

$$\gamma_{xy} = \frac{\partial}{\partial y}u_0 + \frac{\partial}{\partial x}v_0 - 2z\frac{d}{dx}\frac{d}{dy}w_0 \,. \tag{112}$$

These equations can be further simplified by defining the midplane strains as

$$\varepsilon_{0x} = \frac{d}{dx} u_0 \tag{113}$$

$$\varepsilon_{0y} = \frac{d}{dy} v_0 \tag{114}$$

$$\gamma_{0xy} = \frac{d}{dy} u_0 + \frac{d}{dx} v_0 \ . \tag{115}$$

Substituting equations (113)–(115) into equations (110)–(112) results in the strain equations written in terms of the midplane strains:[10]

$$\varepsilon_x = \frac{d}{dx} u_0 - z \frac{d^2}{dx^2} w_0 \tag{116}$$

$$\varepsilon_x = \varepsilon_{0x} - z \frac{d^2}{dx^2} w_0 \tag{117}$$

$$\varepsilon_y = \frac{d}{dy} v_0 - z \frac{d^2}{dy^2} w_0 \tag{118}$$

$$\varepsilon_y = \varepsilon_{0y} - z \frac{d^2}{dy^2} w_0 \tag{119}$$

$$\gamma_{xy} = \frac{\partial}{\partial y} u_0 + \frac{\partial}{\partial x} v_0 - 2z \frac{d}{dx} \frac{d}{dy} w_0 \tag{120}$$

$$\gamma_{xy} = \gamma_{0xy} - 2z \frac{d}{dx} \frac{d}{dy} w_0 \ . \tag{121}$$

The midplane surface curvatures are now defined as follows:[10]

$$K_x = \frac{d^2}{dx^2} w_0 \tag{122}$$

$$K_y = \frac{d^2}{dy^2} w_0 \tag{123}$$

$$K_{xy} = 2\frac{d}{dx}\frac{d}{dy}w_0 \ . \tag{124}$$

Finally, the strain equations may be stated in matrix form:

$$\begin{bmatrix} \varepsilon_x \\ \varepsilon_y \\ \gamma_{xy} \end{bmatrix} = \begin{bmatrix} \varepsilon_{0x} \\ \varepsilon_{0y} \\ \gamma_{0xy} \end{bmatrix} - z \begin{bmatrix} K_x \\ K_y \\ K_{xy} \end{bmatrix} . \tag{125}$$

5.2 Generalized Hooke's Law for Nonisotropic Materials

For isotropic materials (properties are the same in any direction), the relationship between stress and strain is independent of the direction of the force. Young's modulus is the only elastic constant required to describe the stress-strain relationship for a uniaxial force.

For a nonisotropic material, at least two elastic constants are needed to describe the stress-strain behavior of the material. Consider, for example, the case of a nonisotropic plate made of a fiber-reinforced material (fig. 68). The fibers are in direction 1, resulting in the direction 1 properties being much higher than the direction 2 properties.

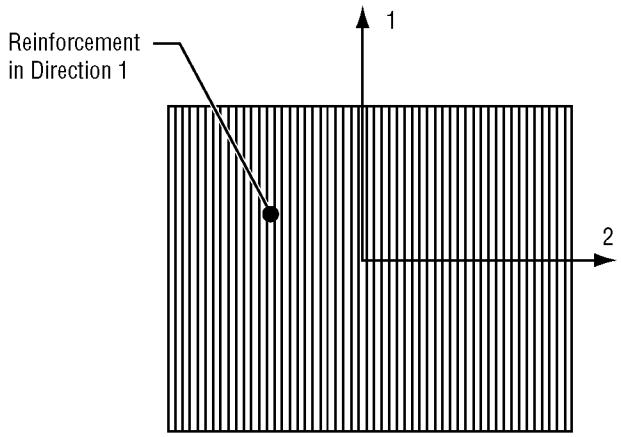

Figure 68. Nonisotropic plate with fiber reinforcement.

A special case of anisotropy is the existence of two perpendicular planes of symmetry in material properties. Such materials are referred to as orthotropic. This configuration is characteristic of a laminated composite that may have different material properties in the perpendicular planes. In general, the properties of the material are direction specific.

The analysis of an orthotropic system must take into account the direction of the material properties. For such a system, the stress can be expressed for each direction as

$$\sigma_1 = E_1 \varepsilon_1 \tag{126}$$

and

$$\sigma_2 = E_2 \varepsilon_2 \ . \tag{127}$$

Consider the case shown in figure 69; an applied load acts parallel to the fibers.

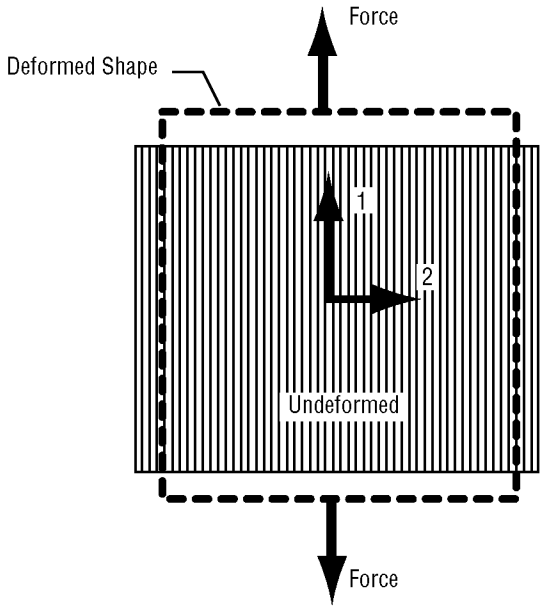

Figure 69. Applied load parallel to fibers.

This type of loading produces stress in more than one direction within the plate and is referred to as plane stress. The plate is elongated in direction 1 and contracted in direction 2. This illustrates the Poisson's effect, which may be defined as

$$\nu_{12} = \frac{-\varepsilon_2}{\varepsilon_1} \ . \tag{128}$$

The total strain in the orthotropic material must consider the Poisson's ratio effect for each direction. The strain in the plate is now a function of several material properties:

$$\varepsilon_2 = \frac{\sigma_2}{E_2} - \nu_{12}\varepsilon_1 \tag{129}$$

and

$$\varepsilon_1 = \frac{\sigma_1}{E_1} - \nu_{21}\varepsilon_2 \,. \tag{130}$$

Shear forces must also be considered in the plate analysis. Shear stress is related to the shear strain by a material constant called the shear modulus (G). As with the normal stress, the shear stress (τ) must be defined in terms of the direction of the material as follows:

$$\tau_{12} = \gamma_{12} G_{12} \,. \tag{131}$$

In general, the equations for strains can be expressed in terms of stress and the orthotropic material properties (Young's modulus, Poisson ratio, and the shear modulus) as

$$\varepsilon_1 = \frac{\sigma_1}{E_1} - \nu_{21}\frac{\sigma_2}{E_2} \tag{132}$$

$$\varepsilon_2 = \frac{\sigma_2}{E_2} - \nu_{12}\frac{\sigma_1}{E_1} \tag{133}$$

$$\gamma_{12} = \frac{\tau_{12}}{G_{12}} \,. \tag{134}$$

These equations can be expressed in matrix form as follows:

$$\begin{bmatrix} \varepsilon_1 \\ \varepsilon_2 \\ \gamma_{12} \end{bmatrix} = \begin{bmatrix} \frac{1}{E_1} & -\frac{\nu_{21}}{E_2} & 0 \\ -\frac{\nu_{12}}{E_1} & \frac{1}{E_2} & 0 \\ 0 & 0 & \frac{1}{G_{12}} \end{bmatrix} \begin{bmatrix} \sigma_1 \\ \sigma_2 \\ \tau_{12} \end{bmatrix} . \tag{135}$$

The 3×3 matrix in equation (135) is made up entirely of material properties for the orthotropic material. This matrix is called the compliance matrix (S):

$$S = \begin{bmatrix} \frac{1}{E_1} & -\frac{\nu_{21}}{E_2} & 0 \\ -\frac{\nu_{12}}{E_1} & \frac{1}{E_2} & 0 \\ 0 & 0 & \frac{1}{G_{12}} \end{bmatrix}. \tag{136}$$

Equation (135) may be rewritten to form an equation for the stress:

$$\begin{bmatrix} \sigma_1 \\ \sigma_2 \\ \tau_{12} \end{bmatrix} = [S]^{-1} \begin{bmatrix} \varepsilon_1 \\ \varepsilon_2 \\ \gamma_{12} \end{bmatrix}. \tag{137}$$

Furthermore, $\nu_{12}/E_1 = \nu_{21}/E_2$, then the stiffness matrix (Q) can now be defined as the inverse of the compliance matrix *(S)* as follows:

$$Q = [S]^{-1} = \begin{bmatrix} E_1 \frac{-E_2}{(-E_2 + \nu_{12}\nu_{21}E_1)} & -\nu_{21}E_1 \frac{E_2}{(-E_2 + \nu_{12}\nu_{21}E_1} & 0 \\ -\nu_{12}E_1 \frac{E_2}{(-E_2 + \nu_{12}\nu_{21}E_1} & E_2^2 \frac{-1}{(-E_2 + \nu_{12}\nu_{21}E_1)} & 0 \\ 0 & 0 & G_{12} \end{bmatrix}. \tag{138}$$

Finally, the stress equation can be expressed as a function of the stiffness matrix (Q) to further simplify the equation:

$$\begin{bmatrix} \sigma_1 \\ \sigma_2 \\ \tau_{12} \end{bmatrix} = Q \begin{bmatrix} \varepsilon_1 \\ \varepsilon_2 \\ \gamma_{12} \end{bmatrix}. \tag{139}$$

5.3 Plane Stress for Generally Orthotropic Plates

The previous discussion was limited to the case in which the load is either parallel or perpendicular to the principal material directions of the lamina; i.e., reinforcement fibers. In general, the loading is not in the principal material direction. The equations for the generally orthotropic plates transform the stress and strain into coordinates that coincide with the principal material directions. Figure 70 is a free-body diagram of a composite laminate; it indicates the directions of the stress in relation to the direction of the reinforcement fiber. Direction 1 is the direction of the fiber and direction 2 is perpendicular to the fiber.

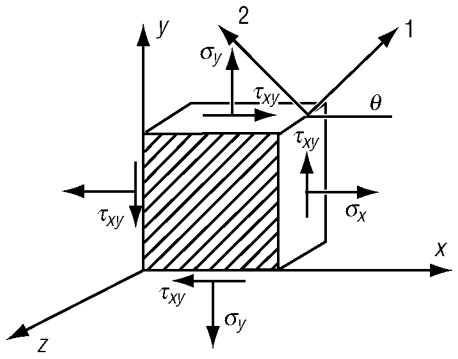

Figure 70. Direction of stress.

The transformation of plane stress is a fundamental part of mechanics of materials. In the case of composite materials, the idea is to transform the stress from the direction of the load to the principal material direction. As shown in figure 71, the element is cut to produce an area, ΔA. A free-body diagram is used to sum the forces in direction 1.

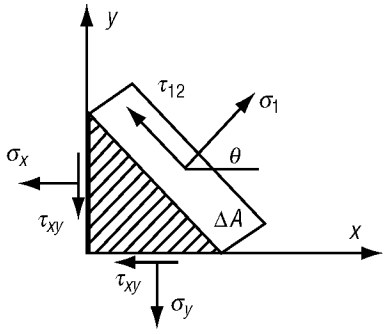

Figure 71. Sum force in direction 1.

The sum of the forces in direction 1, for example, results in the following equation for σ_1:

$$0 = \sigma_1 \Delta A - \sigma_x (\Delta A \cos\theta)\cos\theta - \sigma_y (\Delta A \sin\theta)\sin\theta + -\tau_{xy}(\Delta A \cos\theta)\sin\theta - \tau_{xy}(\Delta A \sin\theta)\cos\theta \quad . \tag{140}$$

From the free-body diagram of figure 72, the sum of the forces in direction 2 results in an equation for σ_2:

$$0 = \sigma_2 \Delta A - \sigma_x (\Delta A \sin\theta)\sin\theta - \sigma_y (\Delta A \cos\theta)\cos\theta + \tau_{xy}(\Delta A \cos\theta)\sin\theta + \tau_{xy}(\Delta A \sin\theta)\cos\theta \quad . \tag{141}$$

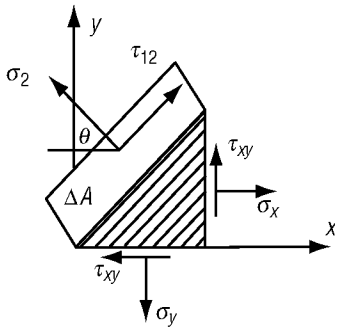

Figure 72. Sum force in direction 2.

Using figure 72, sum the forces in direction 1 to obtain an equation for τ_{12}:

$$0 = \tau_{12}\Delta A + \sigma_x \Delta A \sin\theta\cos\theta - \left(\sigma_y \Delta A \cos\theta\sin\theta\right) + \left(-\tau_{xy}\Delta A \cos\theta\cos\theta\right) + \tau_{xy}\Delta A \sin\theta\sin\theta \quad . \tag{142}$$

Simplifying equations (140)–(142) and solving for the stresses in the direction of the principal material direction yields the stress transformation equations:

$$\sigma_1 = \sigma_x \cos\theta^2 + \sigma_y \cos\theta^2 + 2\tau_{xy}\sin\theta\cos\theta \tag{143}$$

$$\sigma_2 = \sigma_x \sin\theta^2 + \sigma_y \cos\theta^2 - 2\tau_{xy}\sin\theta\cos\theta \tag{144}$$

$$\tau_{12} = -\sigma_x \sin\theta\cos\theta + \sigma_y \sin\theta\cos\theta + \tau_{xy}\left(\cos\theta^2 - \sin\theta^2\right) \quad . \tag{145}$$

Equations (140)–(142) can now be written in matrix form:

$$\begin{bmatrix} \sigma_1 \\ \sigma_2 \\ \tau_{12} \end{bmatrix} = \begin{bmatrix} \cos\theta^2 & \sin\theta^2 & 2\sin\theta\cos\theta \\ \sin\theta^2 & \cos\theta^2 & -2\sin\theta\cos\theta \\ -\sin\theta\cos\theta & \sin\theta\cos\theta & \cos\theta^2 - \sin\theta^2 \end{bmatrix} \begin{bmatrix} \sigma_x \\ \sigma_y \\ \tau_{xy} \end{bmatrix}. \tag{146}$$

The 3×3 matrix is known as the transformation matrix (T):

$$T = \begin{bmatrix} \cos\theta^2 & \sin\theta^2 & 2\sin\theta\cos\theta \\ \sin\theta^2 & \cos\theta^2 & -2\sin\theta\cos\theta \\ -\sin\theta\cos\theta & \sin\theta\cos\theta & \cos\theta^2 - \sin\theta^2 \end{bmatrix}. \tag{147}$$

Thus, the stress transformation equation (146) may be written in terms of *(T)* as follows:

$$\begin{bmatrix} \sigma_1 \\ \sigma_2 \\ \tau_{12} \end{bmatrix} = T \begin{bmatrix} \sigma_x \\ \sigma_y \\ \tau_{xy} \end{bmatrix}. \tag{148}$$

Similarly, to transform from the 1-2 coordinate system to the *x-y* coordinate system, use the inverse of the transformation matrix:

$$\begin{bmatrix} \sigma_x \\ \sigma_y \\ \tau_{xy} \end{bmatrix} = T^{-1} \begin{bmatrix} \sigma_1 \\ \sigma_2 \\ \tau_{12} \end{bmatrix}. \tag{149}$$

The strains can be transformed in the same manner as the stresses. Equations (150) and (151) represent the transformation of strain:

$$\begin{bmatrix} \varepsilon_1 \\ \varepsilon_2 \\ \frac{\gamma_{12}}{2} \end{bmatrix} = T \begin{bmatrix} \varepsilon_x \\ \varepsilon_y \\ \frac{\gamma_{xy}}{2} \end{bmatrix} \tag{150}$$

$$\begin{bmatrix} \varepsilon_x \\ \varepsilon_y \\ \dfrac{\gamma_{xy}}{2} \end{bmatrix} = T^{-1} \begin{bmatrix} \varepsilon_1 \\ \varepsilon_2 \\ \dfrac{\gamma_{12}}{2} \end{bmatrix} . \tag{151}$$

However, the strain transformation equation (151) creates a numerical problem. The shear strain term ($\gamma_{12}/2$) is not compatible with the shear strain term from equation (139), γ_{12}. To overcome this problem, a factor of 2 is introduced into the matrix equations as follows:

$$\begin{bmatrix} \varepsilon_x \\ \varepsilon_y \\ \gamma_{xy} \end{bmatrix} = \begin{bmatrix} 1 & 0 & 0 \\ 0 & 1 & 0 \\ 0 & 0 & 2 \end{bmatrix} \begin{bmatrix} \varepsilon_x \\ \varepsilon_y \\ \dfrac{\gamma_{xy}}{2} \end{bmatrix} . \tag{152}$$

The resulting matrix is called Reuter's matrix (R):

$$R = \begin{bmatrix} 1 & 0 & 0 \\ 0 & 1 & 0 \\ 0 & 0 & 2 \end{bmatrix} . \tag{153}$$

The shear strain values can be multiplied as needed to combine the transformation equations (148)–(151) with the compliance equation (139). These derivations are provided in the Mathcad program listed in appendix D. The resulting equation is as follows:

$$\begin{bmatrix} \sigma_x \\ \sigma_y \\ \tau_{xy} \end{bmatrix} = T^{-1} Q R T R^{-1} \begin{bmatrix} \varepsilon_x \\ \varepsilon_y \\ \gamma_{xy} \end{bmatrix} . \tag{154}$$

Equation (154) illustrates the transformed stiffness relationship between the stresses and strains for an orthotropic plate. This equation provides the stress-strain relationship in the x-y direction.

Equation (154) is difficult to work with because of the number of matrices involved. However, the equation can be simplified to three matrices by defining the transformed reduced stiffness matrix ($\overline{Q}$):

$$\overline{Q} = T^{-1}QRTR^{-1} \quad . \tag{155}$$

Finally, equation (154) may be written in terms of $\overline{Q}$:

$$\begin{bmatrix} \sigma_x \\ \sigma_y \\ \tau_{xy} \end{bmatrix} = \overline{Q} \begin{bmatrix} \varepsilon_x \\ \varepsilon_y \\ \gamma_{xy} \end{bmatrix} . \tag{156}$$

The $\overline{Q}$ matrix is a 3×3 matrix that represents the transformation of the stiffness matrix (Q). The terms in the matrix contain four independent material properties and the angle between the reinforcement fibers and the load.

5.4 Mechanics of Laminated Composite Plates

The strain equations for a plate in bending must now be related to a plate made from several layers or lamina. Solving equation (156) for the strain values results in the following:

$$\begin{bmatrix} \varepsilon_x \\ \varepsilon_y \\ \gamma_{xy} \end{bmatrix} = \overline{Q}^{-1} \begin{bmatrix} \sigma_x \\ \sigma_y \\ \tau_{xy} \end{bmatrix} . \tag{157}$$

The midplane strains and the curvatures can now be equated to the stress values by combining equations (125) and (157),

$$\overline{Q}^{-1} \begin{bmatrix} \sigma_x \\ \sigma_y \\ \tau_{xy} \end{bmatrix} = \begin{bmatrix} \varepsilon_{0x} \\ \varepsilon_{0y} \\ \gamma_{0xy} \end{bmatrix} - z \begin{bmatrix} K_x \\ K_y \\ K_{xy} \end{bmatrix} . \tag{158}$$

Simplifying equation (158) and solving for the stress matrix results in an equation for the stress in terms of the midplane strains and curvatures:

$$\begin{bmatrix} \sigma_x \\ \sigma_y \\ \tau_{xy} \end{bmatrix} = \overline{Q} \begin{bmatrix} \varepsilon_{0x} \\ \varepsilon_{0y} \\ \gamma_{0xy} \end{bmatrix} - z\overline{Q} \begin{bmatrix} K_x \\ K_y \\ K_{xy} \end{bmatrix}. \tag{159}$$

Equation (159) represents the stress in each ply of the laminate for an orthotropic plate.

5.5 Determination of Force and Moment Resultants

The resultant forces and moments acting on a laminate are a function of the stresses on each layer through the thickness of the plate. The force and moment resultants are important for the analysis of composite plates because the stress in the plate varies from top to bottom. The force and the moment act at the midplane of the plate in the same direction as the stresses.

Figure 73 illustrates the normal and shear forces that act on a plate. The resultant force can be found by the summation of the stress multiplied by the area. The sum of the forces can also be found by integration of the stress multiplied over the thickness (t) of the plate, then multiplied by the area. Figure 74 represents a cross section of a plate. The width (w) times an incremental thickness (dz) represents the area over which the force is acting.

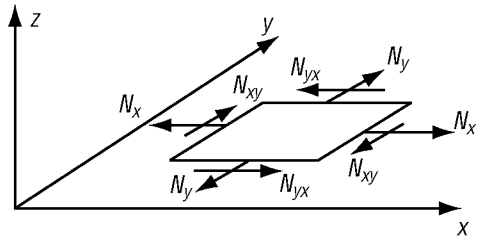

Figure 73. Resultant forces.

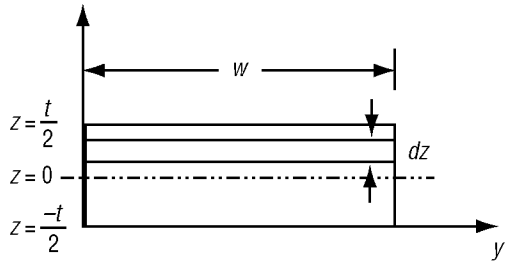

Figure 74. Integration over width of plate.

Equation (160) represents the forces acting on the plate:

$$\sum_{n} \sigma_x w \, dz = \int_{\frac{-t}{2}}^{\frac{t}{2}} \sigma_x w \, dz \quad . \tag{160}$$

The width (w) of the plate occurs on both sides of the equation and cancels. This allows the resultant force to be defined in units of force per unit length. The resultant force per unit length at the midplane of the plate is defined as

$$N_x = \int_{\frac{-t}{2}}^{\frac{t}{2}} \sigma_x dz \quad . \tag{161}$$

Similarly, for the remaining directions of stress,

$$N_y = \int_{\frac{-t}{2}}^{\frac{t}{2}} \sigma_y dz \tag{162}$$

and

$$N_{xy} = \int_{\frac{-t}{2}}^{\frac{t}{2}} \tau_{xy} dz \quad . \tag{163}$$

In matrix form, these equations can be written as

$$\begin{bmatrix} N_x \\ N_y \\ N_{xy} \end{bmatrix} = \int_{\frac{-t}{2}}^{\frac{t}{2}} \begin{bmatrix} \sigma_x \\ \sigma_y \\ \tau_{xy} \end{bmatrix} dz \quad . \tag{164}$$

Figure 75 illustrates the moments acting on a plate. The resultant moments for the midplane of each plate can also be calculated from the stresses. The moments are defined as the sum of the stress multiplied by the area, multiplied by the moment arm with respect to the midplane. The moments are also defined in terms of unit lengths. The moment equations are as follows:

$$M_x = \int_{-\frac{t}{2}}^{\frac{t}{2}} \sigma_x z \, dz \tag{165}$$

$$M_y = \int_{-\frac{t}{2}}^{\frac{t}{2}} \sigma_y z \, dz \tag{166}$$

$$M_{xy} = \int_{-\frac{t}{2}}^{\frac{t}{2}} \tau_{xy} z \, dz \ . \tag{167}$$

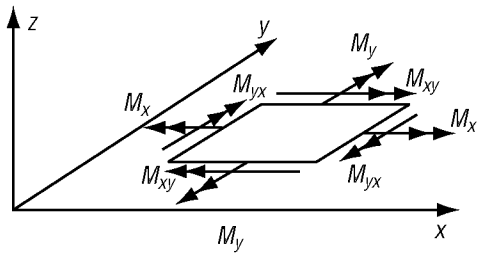

Figure 75. Resultant moments on plate.

In the same manner as the forces, the moments can be stated in a matrix equation:

$$\begin{bmatrix} M_x \\ M_y \\ M_{xy} \end{bmatrix} = \int_{\frac{-t}{2}}^{\frac{t}{2}} \begin{bmatrix} \sigma_x \\ \sigma_y \\ \tau_{xy} \end{bmatrix} z \, dz \ . \tag{168}$$

5.6 Laminate Constitutive Equations

Equations (164) and (168) define the forces and moments acting on the midplane of the plate in terms of the plate stresses. Equation (159) defines the stresses acting on any layer in the plate in terms of the midplane strains and plate curvatures. The midplane strains are functions of the midplane displacements and the midplane curvatures are functions of the displacement (w). Equations (159), (164), and (168) are the plate constitutive equations.

Equations (164) and (168) must be modified to define the midplane forces and moments for each layer in the plate. This can be done by recognizing that the stress resultants can be expressed as the sum of the stress resultant for each layer. Letting n represent the number of layers in the plate, the equation for the forces becomes

$$\begin{bmatrix} N_x \\ N_y \\ N_{xy} \end{bmatrix} = \sum_{k=1}^{n} \int_{h(k-1)}^{h_k} \begin{bmatrix} \sigma_x \\ \sigma_y \\ \tau_{xy} \end{bmatrix} dz \ . \tag{169}$$

Similarly, the equations for moments are written as

$$\begin{bmatrix} M_x \\ M_y \\ M_{xy} \end{bmatrix} = \sum_{k=1}^{n} \int_{h(k-1)}^{h_k} \begin{bmatrix} \sigma_x \\ \sigma_y \\ \tau_{xy} \end{bmatrix} z \, dz \ . \tag{170}$$

The integration parameters have now changed from the thickness of the plate to the location of the top and bottom of each layer. Figure 76 illustrates the integration terms.

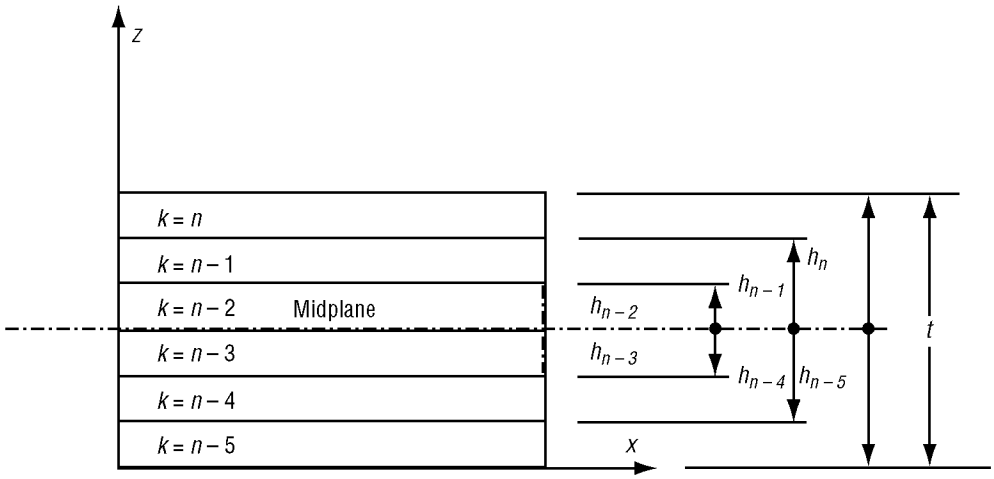

Figure 76. Layer location.

The equation for the transformed stress, equation (159), can be substituted into the equations for the midplane forces and moments. The resulting equations (171) and (172) state the forces and moments in terms of the strain and curvatures:

$$\begin{bmatrix} N_x \\ N_y \\ N_{xy} \end{bmatrix} = \sum_{k=1}^{n} \int_{h(k-1)}^{h_k} \left[\overline{Q} \begin{bmatrix} \varepsilon_{0x} \\ \varepsilon_{0y} \\ \gamma_{0xy} \end{bmatrix} + z\overline{Q} \begin{bmatrix} K_x \\ K_y \\ K_{xy} \end{bmatrix} \right] dz \tag{171}$$

$$\begin{bmatrix} M_x \\ M_y \\ M_{xy} \end{bmatrix} = \sum_{k=1}^{n} \int_{h(k-1)}^{h_k} \left[\overline{Q} \begin{bmatrix} \varepsilon_{0x} \\ \varepsilon_{0y} \\ \gamma_{0xy} \end{bmatrix} + z\overline{Q} \begin{bmatrix} K_x \\ K_y \\ K_{xy} \end{bmatrix} \right] z\, dz \ . \tag{172}$$

Integrating these equations is relatively simple because the matrices ε_0 and K are not functions of z and are not included in the integration. The plate stiffness matrix ($\overline{Q}$) is constant over the thickness of any layer; equation (172) can be written as

$$\begin{bmatrix} N_x \\ N_y \\ N_{xy} \end{bmatrix} = \sum_{k=1}^{n} \left[\left[\overline{Q} \begin{bmatrix} \varepsilon_{0x} \\ \varepsilon_{0y} \\ \gamma_{0xy} \end{bmatrix} \int_{h_{(k-1)}}^{h_k} 1\, dz \right] + \left[\overline{Q} \begin{bmatrix} K_x \\ K_y \\ K_{xy} \end{bmatrix} \int_{h_{(k-1)}}^{h_k} z\, dz \right] \right] . \tag{173}$$

Performing the integration results in the following equation:

$$\begin{bmatrix} N_x \\ N_y \\ N_{xy} \end{bmatrix} = \sum_{k=1}^{n} \left[\left[\overline{Q} \begin{bmatrix} \varepsilon_{0x} \\ \varepsilon_{0y} \\ \gamma_{0xy} \end{bmatrix} \left(h_k - h_{k-1} \right) \right] + \left[\overline{Q} \begin{bmatrix} K_x \\ K_y \\ K_{xy} \end{bmatrix} \frac{h_k^2 - h_{k-1}^2}{2} \right] \right] . \tag{174}$$

The moment equation can also be simplified as

$$\begin{bmatrix} M_x \\ M_y \\ M_{xy} \end{bmatrix} = \sum_{k=1}^{n} \int_{h(k-1)}^{h_k} \left[\overline{Q} \begin{bmatrix} \varepsilon_{0x} \\ \varepsilon_{0y} \\ \gamma_{0xy} \end{bmatrix} + z\overline{Q} \begin{bmatrix} K_x \\ K_y \\ K_{xy} \end{bmatrix} \right] z \, dz \tag{175}$$

$$\begin{bmatrix} M_x \\ M_y \\ M_{xy} \end{bmatrix} = \sum_{k=1}^{n} \left[\left[\overline{Q} \begin{bmatrix} \varepsilon_{0x} \\ \varepsilon_{0y} \\ \gamma_{0xy} \end{bmatrix} \frac{h_k^2 - h_{k-1}^2}{2} \right] + \left[\overline{Q} \begin{bmatrix} K_x \\ K_y \\ K_{xy} \end{bmatrix} \frac{h_k^3 - h_{k-1}^3}{3} \right] \right] . \tag{176}$$

Note that the midsurface strains (ε_0) and the curvatures (K) are not part of the summations.

The stiffness ($\overline{Q}$) and the h_k terms can be summed outside equations (174) and (176) to form new matrices, and the equations become

$$\begin{bmatrix} N_x \\ N_y \\ N_{xy} \end{bmatrix} = A \begin{bmatrix} \varepsilon_{0x} \\ \varepsilon_{0y} \\ \gamma_{0xy} \end{bmatrix} + B \begin{bmatrix} K_x \\ K_y \\ K_{xy} \end{bmatrix} \tag{177}$$

and

$$\begin{bmatrix} M_x \\ M_y \\ M_{xy} \end{bmatrix} = B \begin{bmatrix} \varepsilon_{0x} \\ \varepsilon_{0y} \\ \gamma_{0xy} \end{bmatrix} + D \begin{bmatrix} K_x \\ K_y \\ K_{xy} \end{bmatrix} . \tag{178}$$

In equation (177), matrix A is called the extensional stiffness matrix. This matrix relates the normal stress and strains similar to the modulus of elasticity. However, if the matrix terms A_{13} and A_{23} are nonzero and the plate has a shear load applied to it, normal stresses will be produced:

$$A = \sum_{k=1}^{n} \left[\overline{Q}_{k,1} \left(h_k - h_{k-1} \right) \right] . \tag{179}$$

The thickness of the kth layer can be defined as t_k, where $t_k = h_k - h_{k-1}$. Then equation (179) can be written as a function of the thickness of the layer:

$$A = \sum_{k=1}^{n} \left[\overline{Q}_{k,1}(t_k) \right] \ . \tag{180}$$

The B matrix in equations (177) and (178) is called the coupling stiffness matrix. The B matrix relates bending strains with normal stresses:

$$B = \sum_{k=1}^{n} \overline{Q}_{k,1} \left[\frac{h_k^2 - h_{k-1}^2}{2} \right] \ . \tag{181}$$

This equation can also be stated as a function of the layer thickness (z_k) and the distance from the layer midplane to the center of the kth layer. Defining z_k with the following equation,

$$z_k = \frac{h_k + h_{k-1}}{2} \ . \tag{182}$$

The equation for the coupling matrix B may be stated as

$$B = \sum_{k=1}^{n} \overline{Q}_{k,1} \, t_k \, z_k \ . \tag{183}$$

The coupling stiffness matrix has substantial influence on a laminated composite plate. A non-zero B matrix implies that an axial load will cause the plate to bend and/or twist. Also, any moment applied to the plate will cause extension of the plate midplane. This coupling between bending and extension is key to understanding composite plates, and neglecting the effects of the B matrix could be catastrophic to a composite structure.

The D matrix in equation (178) is called the bending stiffness matrix. This matrix relates the plate curvatures with the bending moments:

$$D = \sum_{k=1}^{n} \overline{Q}_{k,1} \left[\frac{h_k^3 - h_{k-1}^3}{3} \right] \ . \tag{184}$$

The equations for D can also be written in terms of t_k and z_k:

$$D = \sum_{k=1}^{n} \overline{Q}_{k,1} \left(\frac{t_k^3}{12} + t_k \, z_k^2 \right) \ . \tag{185}$$

5.7 Effective Engineering Properties for Laminated Composite Plates

The effective engineering properties are determined from the A, B, and D matrices. The concept is to determine the longitudinal Young's modulus (E_x), transverse Young's modulus (E_y), shear modulus G_{xy}, and longitudinal Poisson ratio (ν_{xy}) of the laminate (plate) from the E_1, E_2, G_{12}, and ν_{12} material properties of one of the layers. A plate can be designed and optimized by varying the angles of the reinforcement fibers in each layer.

Recalling Hooke's law for an isotropic plate, $E_x = \sigma_x/\varepsilon_x$. Similarly, the relationship developed for laminates relates the midplane force to the axial strain:

$$E_x = \frac{N_x}{h\varepsilon_x} , \tag{186}$$

where h is the laminate thickness.

Equations (177) and (178) may be combined to form a linear system of equations. The force and moment equation may be written as follows:

$$\begin{bmatrix} N_x \\ N_y \\ N_{xy} \\ M_x \\ M_y \\ M_{xy} \end{bmatrix} = \begin{bmatrix} A_{11} & A_{12} & A_{13} & B_{11} & B_{12} & B_{13} \\ A_{21} & A_{22} & A_{23} & B_{21} & B_{22} & B_{23} \\ A_{31} & A_{32} & A_{33} & B_{31} & B_{32} & B_{33} \\ B_{11} & B_{12} & B_{13} & D_{11} & D_{12} & D_{13} \\ B_{21} & B_{22} & B_{23} & D_{21} & D_{22} & D_{23} \\ B_{31} & B_{32} & B_{33} & D_{31} & D_{32} & D_{33} \end{bmatrix} \begin{bmatrix} \varepsilon_{0x} \\ \varepsilon_{0y} \\ \gamma_{0xy} \\ K_x \\ K_y \\ K_{xy} \end{bmatrix} . \tag{187}$$

This relationship is a system of six equations and six unknowns. The midplane strains and curvatures are the unknowns. The A, B, and D matrices are constants.

The force and moment matrix can be defined to determine the effective material properties for the composite. In the symmetric case, the layers above the midplane are identical to the layers below the midplane, resulting in zero values for the B matrix. This greatly reduces the size and complexity of the solution. For this analysis, however, the case of nonsymmetric plates is considered.

5.8 Calculation of Effective Material Properties

The solution to the system of equations (187) is best demonstrated through an example problem. A Mathcad solution sheet (app. D) contains the calculations used in this example. Consider,

for example, a plate that is made up of four fiber-reinforced layers as shown in figure 77. The angles of the reinforcements are 0° and 45° and each layer is 0.005 in. thick.

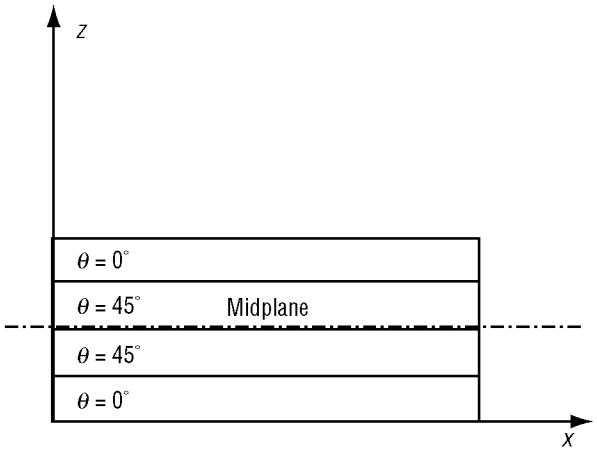

Figure 77. Angle of fiber reinforcement.

The following material constants are assumed for an arbitrary composite material:

- Young's modulus in the principal material direction 1: $E_1 = 20.01 \times 10^6$ lbf/in.^{2}
- Young's modulus in the principal material direction 2: $E_2 = 1.301 \times 10^6$ lbf/in.^{2}
- Shear modulus in the principal material direction 1–2: $G_{12} = 1.001 \times 10^6$ lbf/in.^{2}
- Poisson's ratio in direction 1–2: $\nu_{12} = 0.30$
- Poisson's ratio in direction 2–1: $\nu_{21} = \nu_{12}E_2/E_1$.

The compliance matrix is determined as follows from equation (137):

$$S = \begin{bmatrix} \frac{1}{E_1} & \frac{-\nu_{12}}{E_2} & 0 \\ \frac{-\nu_{21}}{E_2} & \frac{1}{E_2} & 0 \\ 0 & 0 & \frac{1}{G_{12}} \end{bmatrix} = \begin{bmatrix} 4.998\times10^{-8} & -1.499\times10^{-8} & 0\times10^{0} \\ -1.499\times10^{-8} & 7.686\times10^{-7} & 0\times10^{0} \\ 0\times10^{0} & 0\times10^{0} & 9.99\times10^{-7} \end{bmatrix} \frac{\text{lbf}}{\text{in.}^2} \tag{188}$$

The stiffness matrix, inverse of the compliance matrix, is calculated from equation (138):

$$Q = S^{-1} = \begin{bmatrix} 2.013\times10^{7} & 3.926\times10^{5} & 0 \\ 3.926\times10^{5} & 1.309\times10^{6} & 0 \\ 0 & 0 & 1.001\times10^{6} \end{bmatrix} \frac{\text{lbf}}{\text{in.}^2} \tag{189}$$

The geometry of the layup is then used to determine the transformation matrix. These data are presented in detail in the Mathcad solution sheet (app. D). The transformation matrix is derived from the stress transformation equation. The matrix is solved for each ply angle:

$$T_n = \begin{bmatrix} \cos\theta_n^2 & \sin\theta_n^2 & 2\sin\theta_n\cos\theta_n \\ \sin\theta_n^2 & \cos\theta_n^2 & -2\sin\theta_n\cos\theta_n \\ -\sin\theta_n\cos\theta_n & \sin\theta_n\cos\theta_n & \cos\theta_n^2 - \sin\theta_n^2 \end{bmatrix} \tag{190}$$

$$\text{Ply 1: } T_1 = \begin{bmatrix} 1 & 0 & 0 \\ 0 & 1 & 0 \\ 0 & 0 & 1 \end{bmatrix} \quad \text{Ply 2: } T_2 = \begin{bmatrix} 0.5 & 0.5 & 1 \\ 0.5 & 0.5 & -1 \\ -0.5 & 0.5 & 0 \end{bmatrix}$$

$$\text{Ply 3: } T_1 = \begin{bmatrix} 0.5 & 0.5 & 1 \\ 0.5 & 0.5 & -1 \\ -0.5 & 0.5 & 0 \end{bmatrix} \quad \text{Ply 4: } T_1 = \begin{bmatrix} 1 & 0 & 0 \\ 0 & 1 & 0 \\ 0 & 0 & 1 \end{bmatrix}. \tag{191}$$

As previously described, Reuter's matrix (R) is used to condition the $\overline{Q}$ matrix:

$$R = \begin{bmatrix} 1 & 0 & 0 \\ 0 & 1 & 0 \\ 0 & 0 & 2 \end{bmatrix}. \tag{192}$$

The $\overline{Q}$ matrix represents the stiffness and transform matrix; the $\overline{Q}$ matrix is calculated for each ply using equation (193):

$$\overline{Q} = T_n^{-1} Q R T_n R^{-1}. \tag{193}$$

$$\overline{Q}_1 = \begin{bmatrix} 2.01\times10^{7} & 3.93\times10^{5} & 0 \\ 3.93\times10^{5} & 1.31\times10^{6} & 0 \\ 0 & 0 & 1\times10^{6} \end{bmatrix} \frac{\text{lbf}}{\text{in.}^2} \tag{194}$$

$$\overline{Q}_2 = \begin{bmatrix} 6.56\times10^{6} & 4.55\times10^{5} & 4.7\times10^{6} \\ 4.55\times10^{5} & 6.56\times10^{6} & 4.7\times10^{6} \\ 4.7\times10^{6} & 4.7\times10^{6} & 5.16\times10^{6} \end{bmatrix} \frac{\text{lbf}}{\text{in.}^2} \tag{195}$$

$$\overline{Q}_3 = \begin{bmatrix} 6.56\times10^6 & 4.55\times10^6 & 4.7\times10^6 \\ 4.55\times10^5 & 6.56\times10^6 & 4.7\times10^6 \\ 4.7\times10^6 & 4.7\times10^6 & 5.16\times10^6 \end{bmatrix} \frac{\text{lbf}}{\text{in.}^2} \tag{196}$$

$$\overline{Q}_4 = \begin{bmatrix} 2.01\times10^7 & 3.93\times10^5 & 0\times10^0 \\ 3.93\times10^5 & 1.31\times10^6 & 0\times10^0 \\ 0\times10^0 & 0\times10^0 & 1\times10^6 \end{bmatrix} \frac{\text{lbf}}{\text{in.}^2} \tag{197}$$

As expected, the plies with the same angles are equivalent.

The *A* matrix, or the extensional stiffness matrix, is calculated using equation (180):

$$A = \sum_{k=1}^{\text{plies}} \overline{Q}_k t_k = \begin{bmatrix} 2.67\times10^5 & 4.95\times10^4 & 4.7\times10^4 \\ 4.95\times10^4 & 7.87\times10^4 & 4.7\times10^4 \\ 4.7\times10^4 & 4.7\times10^4 & 6.16\times10^4 \end{bmatrix} \frac{\text{lbf}}{\text{in.}} \tag{198}$$

The *B* matrix, or the coupling stiffness matrix, is calculated using equation (183). In the case of a symmetric plate, the *B* matrix is zero:

$$B = \sum_{k=1}^{\text{plies}} \overline{Q}_k t_k z_k = \begin{bmatrix} 0 & -0 & 0 \\ -0 & -0 & 0 \\ 0 & 0 & 0 \end{bmatrix} \frac{\text{lbf}}{\text{in.}} \tag{199}$$

The *D* matrix, or the bending stiffness matrix, is calculated using equation (185). These values indicate how the bending moments will affect the plate curvatures:

$$D = \sum_{k=1}^{\text{plies}} \overline{Q}_k \left(\frac{t_k^3}{12} + t_k z_k^2 \right) = \begin{bmatrix} 1.23\times10^1 & 6.09\times10^{-1} & 3.92\times10^{-1} \\ 6.09\times10^{-1} & 1.31\times10^0 & 3.92\times10^{-1} \\ 3.92\times10^{-1} & 3.92\times10^{-1} & 1.01\times10^0 \end{bmatrix} \text{lbf in.} \tag{200}$$

Since the *A*, *B*, and *D* matrices are defined, equation (187) can be solved for the strains and curvatures. However, the loads must first be defined. In the Mathcad solution sheet, the load matrix is created to represent the forces and moments at the midplane of the laminate. The load matrix is from equation (187). In the first case, a uniaxial load is applied in the *x* direction:

$$\begin{bmatrix} N_x \\ N_y \\ N_{xy} \\ M_x \\ M_y \\ M_{xy} \end{bmatrix} = \begin{bmatrix} 1 \\ 0 \\ 0 \\ 0 \\ 0 \\ 0 \end{bmatrix} \frac{\text{lbf}}{\text{in.}} \tag{201}$$

A global matrix that represents the stiffness matrix in equation (187) is constructed from the *A*, *B*, and *D* matrices. Equation (187) may now be written in terms of the loads and the global stiffness matrix:

$$\begin{bmatrix} 1 \\ 0 \\ 0 \\ 0 \\ 0 \\ 0 \end{bmatrix} \frac{\text{lbf}}{\text{in.}} = \begin{bmatrix} 266841.87 & 49470.05 & 47047.8 & 0 & -0 & 0 \\ 49470.05 & 78650.66 & 47047.8 & -0 & -0 & 0 \\ 47047.8 & 47047.8 & 61638.11 & 0 & 0 & 0 \\ 0 & -0 & 0 & 12.29 & 0.61 & 0.39 \\ -0 & -0 & 0 & 0.61 & 1.31 & 0.39 \\ 0 & 0 & 0 & 0.39 & 0.39 & 1.01 \end{bmatrix} \begin{bmatrix} \varepsilon_{0x} \\ \varepsilon_{0y} \\ \gamma_{0xy} \\ K_x \\ K_y \\ K_{xy} \end{bmatrix} . \tag{202}$$

This system of equations represents a plate with a uniaxial load applied in the *x* direction. There are six equations and six unknown strain and curvature values. A Mathcad subroutine, lsolve, is used to find a solution to the system of equations. The lsolve function returns values for strains and curvatures. Hooke's law can then be applied to determine Young's modulus and Poisson's ratio:

- Young's modulus in *x*:

$$E_x = \frac{N_x}{h\varepsilon_{0x}} = 1.13 \times 10^7 \frac{\text{lbf}}{\text{in.}^2} \tag{203}$$

- Poisson's ratio:

$$\nu_{xy} = \frac{-\varepsilon_{0y}}{\varepsilon_{0x}} = 3.17 \times 10^{-1} \ . \tag{204}$$

The effective modulus in the *y* direction is found by assuming a unit force in the *y* direction and setting all other forces and moments to zero. The system of equations is now solved with the boundary conditions for a uniaxial load in the *y* direction. Then based on Hooke's Law, Young's modulus and Poisson's ratio can be calculated:

- Young's modulus in x:

$$E_y = \frac{N_y}{h\varepsilon_{0y}} = 2.0972 \times 10^6 \frac{\text{lbf}}{\text{in.}^2} \tag{205}$$

- Poisson's ratio:

$$\nu_{yx} = \frac{-\varepsilon_{0x}}{\varepsilon_{0y}} = 5.87 \times 10^{-2} \quad . \tag{206}$$

The effective shear modulus is found by assuming a unit force in the x-y direction and setting all other forces and moments to zero. The shear modulus (G_{xy}) is a function of the shear load and the shear strain:

- Shear modulus:

$$G_{xy} = \frac{N_{xy}}{h\gamma_{0xy}} = 3.22 \times 10^6 \frac{\text{lbf}}{\text{in.}^2} \tag{207}$$

5.9 Comparison of Results for the Symmetric Solution

The engineering properties for a symmetric laminate can be compared to solutions from a number of sources. This comparison illustrates that the method used for finding a solution to the constitutive equation (187) significantly affects the accuracy of the calculations. For example, Halpin[9] reduces the constitutive equations by assuming the $A_{1,3}$ and $A_{2,3}$ terms in the A matrix are zero. This results in the following equations for the material properties:

$$E_{x\_\text{Halpin}} = \frac{A_{1,1}A_{2,2} - \left(A_{1,2}\right)^2}{A_{2,2}h} \quad , \tag{208}$$

$$E_{y\_\text{Halpin}} = \frac{A_{1,1}A_{2,2} - \left(A_{1,2}\right)^2}{A_{1,1}h} \quad , \tag{209}$$

and

$$G_{xy\_\text{Halpin}} = \frac{A_{3,3}}{h} \quad . \tag{210}$$

Nettles,[20] on the other hand, includes all the terms in the A matrix and is able to develop the following equations for the materials properties:

$$E_{x\_\text{Nettles}} = \left[\frac{A_{1,1}}{h} + \frac{A_{1,2}}{h}\left[\frac{A_{2,3}A_{1,3} - A_{1,2}A_{3,3}}{A_{2,2}A_{3,3} - \left(A_{2,3}\right)^2}\right]\right] + \frac{A_{1,3}}{h}\left[\frac{-A_{1,3}}{A_{3,3}} + \frac{A_{2,3}A_{1,2}A_{3,3} - \left(A_{2,3}\right)^2 A_{1,3}}{A_{2,2}\left(A_{3,3}\right)^2 - \left(A_{2,3}\right)^2 A_{3,3}}\right], \quad (211)$$

$$E_{y\_\text{Nettles}} = \left[\frac{A_{2,2}}{h} + \frac{A_{1,2}}{h}\left[\frac{A_{2,3}A_{1,3} - A_{1,2}A_{3,3}}{A_{1,1}A_{3,3} - \left(A_{1,3}\right)^2}\right]\right] + \frac{A_{2,3}}{h}\left[\frac{-A_{2,3}}{A_{3,3}} + \frac{A_{1,3}A_{1,2}A_{3,3} - \left(A_{1,3}\right)^2 A_{2,3}}{A_{1,1}\left(A_{3,3}\right)^2 - \left(A_{1,3}\right)^2 A_{3,3}}\right], \quad (212)$$

and

$$G_{xy\_\text{Nettles}} = \left[\frac{A_{3,3}}{h} - \frac{\left(A_{2,3}\right)^2}{hA_{2,2}} + \frac{2A_{1,3}A_{1,2}A_{2,2}A_{2,3} - \left(A_{1,2}\right)^2\left(A_{2,3}\right)^2 - \left(A_{1,3}\right)^2\left(A_{2,2}\right)^2}{h\left[A_{1,1}\left(A_{2,2}\right)^2 - \left(A_{1,2}\right)^2 A_{2,2}\right]}\right]. \quad (213)$$

Although Nettles' method is an improvement over the Halpin method, these equations do not apply to the nonsymmetric case. When the $A_{1,3}$ and $A_{2,3}$ terms are set equal to zero, the Nettles[20] equations reduce to the Halpin[9] equations.

Table 11 is a comparison of results obtained from several commercially available computer programs for laminated composite plate analysis.

Table 11. Results from different laminated plate solution techniques.

	E_x	E_y	G_{xy}
Exact	1.13×10^7	2.1×10^6	3.22×10^6
Nettles	1.13×10^7	2.1×10^6	3.22×10^6
Halpin	1.18×10^7	3.47×10^6	3.08×10^6
Inplane	1.18×10^7	3.48×10^6	3.08×10^6
Patran	1.18×10^7	3.48×10^6	3.08×10^6

As expected, the Nettles equations provide the same solution as the exact solution. However, these equations do not work for the nonsymmetric case. The Halpin, Inplane, and Patran solutions overestimate the stiffness of the composite in the transverse direction and underestimate the torsional stiffness for the composite.

It is difficult to determine the specific effects this type of inaccuracy could produce. It is the intent of this study to indicate that these inaccuracies can be avoided by using the solution techniques developed in the previous sections.

5.10 Determination of Strain

Section 5.9 determined the effective material properties of the laminated composite plate. It is also desirable to determine the stress and strain in each layer of the plate. This is accomplished by using constitutive equations (177) and (178) to determine the midplane strains and curvatures. The total strain in each ply or layer is then found by using equation (125). The resulting strains are then transformed by equation (150) to the principal material direction. As shown previously, the constitutive equation can be solved for the midplane strains and curvatures.

For example, assume the laminated plate in the first example is loaded with 1,000 lbf in the x direction. The plate is 5 in. wide. The x direction is parallel to the 0° plies. The calculations for this example are contained in the Mathcad solution sheet (app. D).

As stated in the problem definition, a force is applied in the x direction. The plate is 5 in. wide so N_x would be calculated as follows:

$$N_x = \frac{1{,}000 \text{ lbf}}{5 \text{ in.}} \tag{214}$$

The load matrix in equation (187) will contain the following values:

$$\begin{bmatrix} N_x \\ N_y \\ N_{xy} \\ M_x \\ M_y \\ M_{xy} \end{bmatrix} = \begin{bmatrix} 2\times10^2 \\ 0\times10^0 \\ 0\times10^0 \\ 0\times10^0 \\ 0\times10^0 \\ 0\times10^0 \end{bmatrix} \frac{\text{lbf}}{\text{in.}} \tag{215}$$

The midplane strains and curvatures can be determined in the same manner as demonstrated in section 5.9. The solution indicates that the midplane strain includes axial, transverse, and shear strains, while curvatures are zero:

Midplane Strains:	Midplane Curvatures:
$\varepsilon_{0x} = 8.82\times10^{-4}$	$K_x = 0\times10^0$
$\varepsilon_{0y} = -2.8\times10^{-4}$	$K_y = 0\times10^0$
$\gamma_{0xy} = -4.6\times10^{-4}$	$K_{xy} = 0\times10^0$.

Equation (125) can be used to transform the midplane strains and curvatures into the strains in each ply. To determine the strains in the first 45° ply, define z_{ply} as the distance from the midplane to the center of the ply: $z_{\text{ply}} = 2.5 \times 10^{-3}$ in.

The strains in the first 45° ply in the x-y coordinate system are calculated from the midplane strain and curvatures (eq. (125)). The values are then transformed into the principal material directions for the 45° ply with equation (150). The details of the calculation can be found in the Mathcad solution sheet (app. D). The resulting matrix is the strain in the principal material direction:

$$\begin{bmatrix} \varepsilon_1 \\ \varepsilon_2 \\ \gamma_{12} \end{bmatrix} = \begin{bmatrix} 7.13\times10^{-5} \\ 5.31\times10^{-4} \\ -1.16\times10^{-3} \end{bmatrix}. \tag{216}$$

5.11 Determination of Stress

The stress values can be calculated from the strain by applying equation (155) to determine the $\overline{Q}$ matrix for the given ply. The $\overline{Q}$ value for the 45° ply is as follows:

$$\overline{Q}_n = \begin{bmatrix} 6.56\times10^6 & 4.55\times10^6 & 4.7\times10^6 \\ 4.55\times10^6 & 6.56\times10^6 & 4.7\times10^6 \\ 4.7\times10^6 & 4.7\times10^6 & 5.16\times10^6 \end{bmatrix} \frac{\text{lbf}}{\text{in.}^2} \tag{217}$$

The strain in the 45° ply for layer 2 is determined from equation (125). Equation (156) is then used to determine the stresses in the ply:

$$\begin{bmatrix} \sigma_x \\ \sigma_y \\ \tau_{xy} \end{bmatrix} = \overline{Q}_n \begin{bmatrix} \varepsilon_x \\ \varepsilon_y \\ \gamma_{xy} \end{bmatrix} = \begin{bmatrix} 2.35\times10^3 \\ 1.99\times10^1 \\ 4.6\times10^2 \end{bmatrix} \frac{\text{lbf}}{\text{in.}^2} \tag{218}$$

Now use equation (148) to transform the ply stress into the principle material direction:

$$\begin{bmatrix} \sigma_1 \\ \sigma_2 \\ \tau_{12} \end{bmatrix} = T_n \begin{bmatrix} \sigma_x \\ \sigma_y \\ \tau_{xy} \end{bmatrix} = \begin{bmatrix} 1.64\times10^3 \\ 7.23\times10^2 \\ -1.16\times10^3 \end{bmatrix} \frac{\text{lbf}}{\text{in.}^2} \tag{219}$$

5.12 Determination of Displacement

The deflection of the plate is found from the midplane strains and the curvatures of the plates. Since these values are known, the deflections can be found by integration:

$$\Delta x = \int_{x_1}^{x_2} \varepsilon_{0x} dx - z_n \int_{x_1}^{x_2} \left(\int_{x_1}^{x_2} -K_x dx \right) dx \ . \tag{220}$$

The limits of integration are along the edge of the plate. In the example, the plate is symmetric. As a result, the coupling stiffness matrix and the curvatures are zero. The Mathcad solution sheet (app. D) includes the calculations; the curvature values are included for the nonsymmetric case. In the example problem, the deflection in the x direction is calculated as

$$\Delta x = 8.82 \times 10^{-3} \text{in.} \tag{221}$$

5.13 Determination of Neutral Axis

The neutral axis is the plane of zero strain for any direction in an unsymmetrical plate. The location of the plane may be determined from equations (125) and (187). For pure bending in the x direction, the force and moment matrix is zero except for the moment about the x axis:

$$\begin{bmatrix} 0 \\ 0 \\ 0 \\ M_x \\ 0 \\ 0 \end{bmatrix} = \begin{bmatrix} A_{11} & A_{12} & A_{13} & B_{11} & B_{12} & B_{13} \\ A_{21} & A_{22} & A_{23} & B_{21} & B_{22} & B_{23} \\ A_{31} & A_{32} & A_{33} & B_{31} & B_{32} & B_{33} \\ B_{11} & B_{12} & B_{13} & D_{11} & D_{12} & D_{13} \\ B_{21} & B_{22} & B_{23} & D_{21} & D_{22} & D_{23} \\ B_{31} & B_{32} & B_{33} & D_{31} & D_{32} & D_{33} \end{bmatrix} \begin{bmatrix} \varepsilon_{0x} \\ \varepsilon_{0y} \\ \gamma_{0xy} \\ K_x \\ K_y \\ K_{xy} \end{bmatrix} . \tag{222}$$

Solving for the midplane strains and curvatures and then reducing the matrix equation yields the following expression:

$$\begin{bmatrix} \varepsilon_{0x} \\ \varepsilon_{0y} \\ \gamma_{0xy} \\ K_x \\ K_y \\ K_{xy} \end{bmatrix} = \begin{bmatrix} B_{11} \\ B_{21} \\ B_{31} \\ D_{11} \\ D_{21} \\ D_{31} \end{bmatrix}^{-1} M_x \ . \tag{223}$$

The above equation can then be separated to form an expression for the midplane strains and curvatures. Equation (125) can then be used to find the location of the neutral axis. These derivations are contained in the Mathcad solution sheet (app. D).

5.14 Comparison of Results to a Finite Element Model

A finite element model of a simple plate is developed to verify the previous set of equations. The plate is 10 in. long and 5 in. wide. As in the previous example, the plate has four layers oriented 0°, 45°, 45°, and 0°. As shown in figure 78, the plate is clamped at the left end with a load of 1,000 lbf applied at the right. The model uses MSC/Nastran as the finite element code.

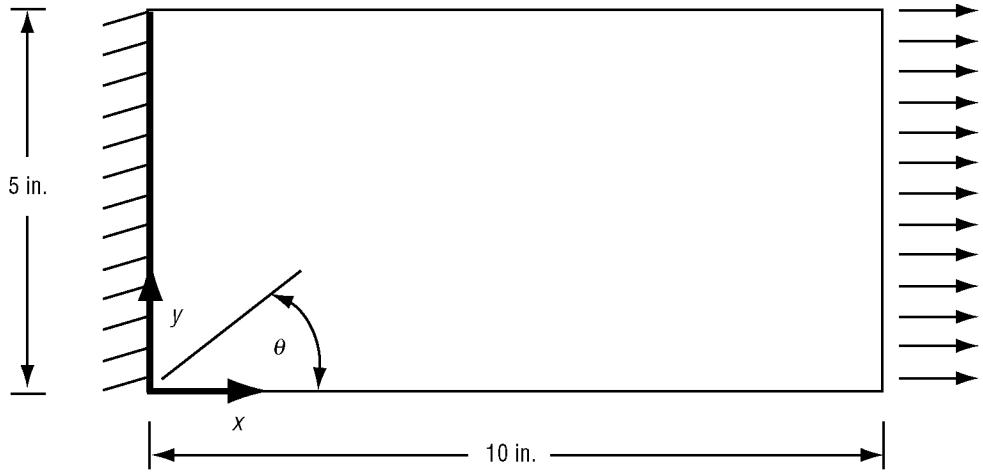

Figure 78. Boundary conditions on finite element model.

The input for the composite material properties was calculated using equation (187). The effective material properties from equation (187) for the model were defined in the MSC/Nastran format by using a MAT2 card. The input for the MAT2 card is represented by the following matrix equation:

$$\begin{bmatrix} \sigma_1 \\ \sigma_2 \\ \tau_{12} \end{bmatrix} = \begin{bmatrix} G_{11} & G_{12} & G_{13} \\ G_{21} & G_{22} & G_{23} \\ G_{31} & G_{32} & G_{33} \end{bmatrix} \begin{bmatrix} \varepsilon_1 \\ \varepsilon_2 \\ \gamma_{12} \end{bmatrix} - \left(T - T_O\right) \begin{bmatrix} \alpha_1 \\ \alpha_2 \\ \alpha_3 \end{bmatrix} . \tag{224}$$

For the purpose of this example, the thermal effects are neglected. The above equation becomes the stress-strain relationship of equation (139). As previously discussed, Q is the stiffness matrix where

$$Q = \begin{bmatrix} \frac{1}{E_1} & \frac{-\nu_{21}}{E_2} & 0 \\ \frac{-\nu_{21}}{E_1} & \frac{1}{E_2} & 0 \\ 0 & 0 & \frac{1}{G_{12}} \end{bmatrix}^{-1} . \tag{225}$$

The material property data for the finite element code are calculated using equation (225). The MAT2 input card is written to reflect the following Q:

$$Q = \begin{bmatrix} G_{11} & G_{12} & G_{13} \\ G_{21} & G_{22} & G_{23} \\ G_{31} & G_{32} & G_{33} \end{bmatrix} = \begin{bmatrix} 2.013\times10^{7} & 3.926\times10^{5} & 0 \\ 3.926\times10^{5} & 1.309\times10^{6} & 0 \\ 0 & 0 & 1.001\times10^{6} \end{bmatrix} \frac{\text{lbf}}{\text{in.}^2} \tag{226}$$

The properties of the composite plate are defined by the PCOMP command. This input is unique to the MSC/Nastran code and requires no calculations. The input is listed for completeness as follows:

```
PCOMP, 1, , , 10000.0, STRN,
+, 1, .005, 0.0, YES, 1, .005, 45.0, YES,
+, 1, .005, 45.0, YES, 1, .005, 0.0, YES  .
```

The ply stress and strain in the principal material directions are calculated using the Mathcad solution sheet with the geometry and loading from the example problem. The results are provided and compared to the results of the finite element model below.

These results are the ply strains in the principal material direction for the 45° ply:

- Laminated plate theory results:

$$\begin{bmatrix} \varepsilon_1 \\ \varepsilon_2 \\ \gamma_{12} \end{bmatrix} = \begin{bmatrix} 7.08\times10^{-5} \\ 5.283\times10^{-4} \\ -1.166\times10^{-3} \end{bmatrix} \tag{227}$$

- Finite element model results:

$$\begin{bmatrix} \varepsilon_1 \\ \varepsilon_2 \\ \gamma_{12} \end{bmatrix} = \begin{bmatrix} 7.13\times10^{-5} \\ 5.31\times10^{-4} \\ -1.16\times10^{-3} \end{bmatrix}. \tag{228}$$

These results are the ply stress in the principal material direction for the 45° ply:

- Laminated plate theory results:

$$\begin{bmatrix} \sigma_1 \\ \sigma_2 \\ \tau_{12} \end{bmatrix} = \begin{bmatrix} 1.633\times10^{3} \\ 7.194\times10^{2} \\ -1.1673\times10^{3} \end{bmatrix} \tag{229}$$

- Finite element model results:

$$\begin{bmatrix} \sigma_1 \\ \sigma_2 \\ \tau_{12} \end{bmatrix} = \begin{bmatrix} 1.64 \times 10^3 \\ 7.23 \times 10^2 \\ -1.16 \times 10^3 \end{bmatrix} . \tag{230}$$

The deflection of the plate in the direction of the load (x) compared very well with the finite element model:

- Laminated plate theory results:

$$\Delta x = 8.8 \times 10^{-3} \tag{231}$$

- Finite element model results:

$$\Delta x = 8.8 \times 10^{-3} \ . \tag{232}$$

The comparison of the results shows that the finite element model agrees perfectly with the Mathcad solution for the plate under uniaxial load.

5.15 Conclusions From Laminated Plate Theory

As stated previously, the purpose of the laminated plate derivations and the development of the Mathcad and finite element solutions is to create methods for the analysis of complex multilayered, graphite-reinforced cementitious composite structures. The development of the Mathcad solution sheet proved that there is no numerical constraint to the laminated plate theory as found in the transform section theory (sec. 1.4). In addition, it has been determined that the material property data developed previously are adequate for the analysis of any conceivable combination of layers and graphite orientations. An improvement has also been made to the accuracy of the solution method used to solve the laminated plate equations.

6. ANALYSIS OF MULTILAYERED SYMMETRIC AND NONSYMMETRIC GRAPHITE-REINFORCED CEMENTITIOUS BEAMS

Section 6 demonstrates that cementitious composite material can be analyzed using the laminated composite plate theory. Section 5 verified the laminated plate equations for an arbitrary composite by comparison to the results of a finite element model. The equations will now be applied to the analysis of three graphite-reinforced cementitious beams subjected to pure bending.

The rule of mixtures is used to determine the effective E_1 and E_2 values. The shear modulus and Poisson's ratio values are taken from the results of the material properties tests. The laminated plate theory is then used to determine the effective material properties for each of the beams. These properties are used with the elastic beam equation to predict the deflection of each beam. The results from the analysis are compared to the results from the test. In addition, the laminated plate equations are used to derive a set of material constants for a finite element model. The results from the model are also compared to the test results.

6.1 Introduction

As shown in figure 79, each beam will consist of two graphite-reinforced layers. The graphite mesh in the first beam will not be rotated. In the second beam, both layers of the graphite mesh are rotated 45°. In the third beam, the bottom layer of graphite is rotated 45° while the top layer will not be rotated, producing a nonsymmetric laminated section.

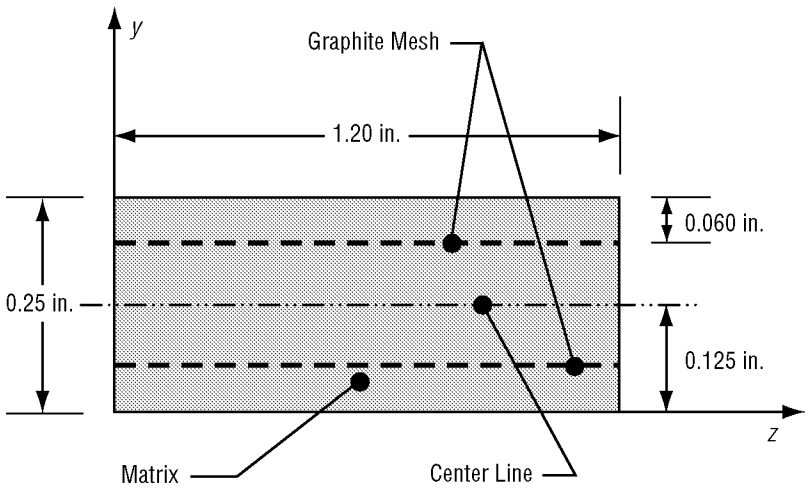

Figure 79. Cross section of multilayered composite beam.

In each case, the laminated plate equations are used to determine the effective material constants. Elastic beam equations, developed in section 4.11, are used to determine the deflection at the center of each beam. The analysis is repeated for several load increments to produce a load versus deflection plot.

A finite element model is developed for each beam consistent with the methodology developed in section 4.12. The MSC/Nastran finite element program is given the data for each layer in the form of MAT2 and PCOMP input commands. The finite element model computes the deflection at the center of the beam, and the model is run with incrementing loads to produce the load versus deflection plot.

Finally, a comparison is made between the analytical data and the test data, and conclusions are drawn based on these results.

6.2 Three-Section (Pure Bending) Testing

The beam is placed in a three-section bending test with the specimen supported over an 8.75-in. span and loaded at two points, each located 1.375 in. from the center of the span. This is the same three-section bending test that is described in section 4.10.

The deflections were measured at the center of each beam using a digital deflection gauge (fig. 80). A cup was hung from the loading hook of the fixture. Loading was achieved by incrementally placing a measured amount of lead pellets in the cup. The time between load increments was not controlled but could be estimated at ≈30 sec. The displacement was recorded at each load increment. Each beam was tested by the same method and with the same loading increment.

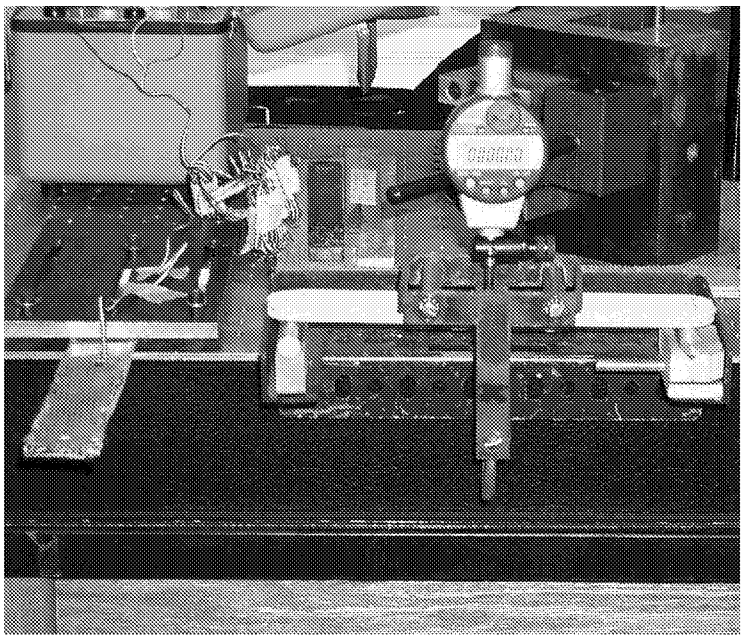

Figure 80. Three-section bending test.

The results of the beam tests, illustrated in figure 81, show that beam 1 [90,90] is much stiffer than beam 2 [45,45]. As expected, beam 3 [45,90] has a stiffness value between beams 1 and 2. The 45° layer is on the tension side of the pure bending test, which may explain why the beam behavior is close to beam 2.

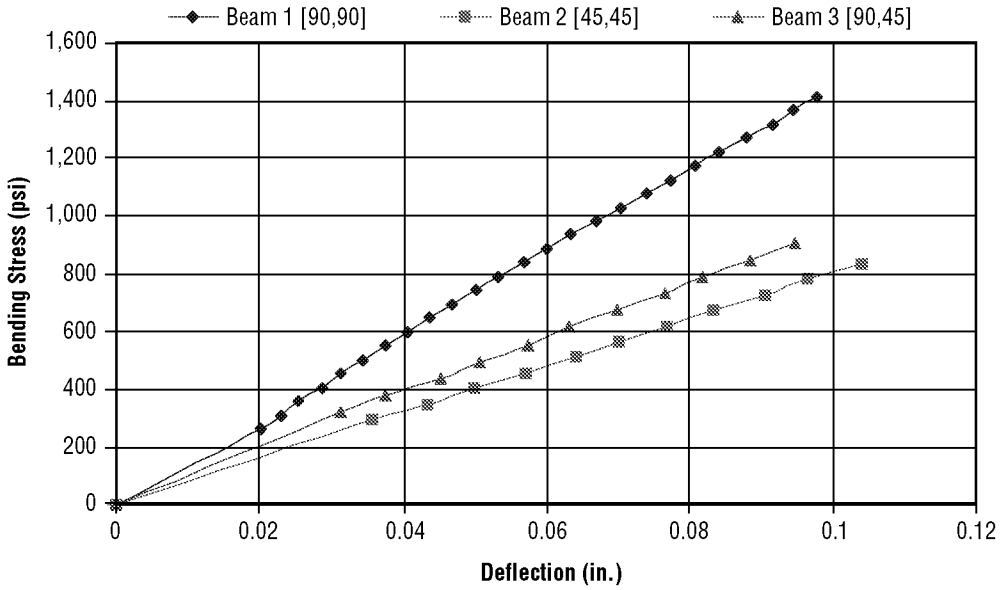

Figure 81. Deflection plot of multilayered beams.

6.3 Calculation of the Deflection Using Elastic Beam Equations

The deflection of the center of the beam was calculated for the same loads used in the three-section bending tests. The elastic beam equation for this problem was provided in section 4.10. The moment of inertia is calculated by $I = bh^3/12$. The Young's modulus is calculated from the laminated plate theory. The Mathcad solution sheet (app. C) is used to perform the calculation to determine the deflection at each load increment.

6.4 Determination of Effective Material Properties

The material properties for each layer of the composite are determined from the rule of mixtures and the laminated composite plate theory. For example, using the equations developed in section 4.11, the material properties of the fiber and matrix are as follows:

$$E_{\text{fiber}} = 33.5 \times 10^6 \text{ lbf/in.}^2$$

$$E_{\text{matrix}} = 115.1 \times 10^3 \text{ lbf/in.}^2 \tag{233}$$

The area of the graphite material is calculated from the manufacturer's data as

$$A_{\text{yarn}} = 0.000175 \text{ in.}^2 \qquad N_{\text{yarn}} = 8$$

$$A_{\text{fiber}} = N_{\text{yarn}} A_{\text{yarn}} \ . \tag{234}$$

The area of each layer is the thickness multiplied by the width $A_1 = 0.120 \text{ in.} \times 1 \text{ in.}$:

$$V_{\text{fiber}} = \frac{A_{\text{fiber}}}{A_1} = 0.012$$

$$V_{\text{matrix}} = 1 - V_{\text{fiber}} = 0.988 \ . \tag{235}$$

Thus, the values for the effective material properties can be calculated for each layer:

- Young's modulus (direction 1):

$$E_1 = V_{\text{fiber}} E_{\text{fiber}} + V_{\text{matrix}} E_{\text{matrix}}$$

$$E_1 = 5.045 \times 10^5 \text{ lbf/in.}^2 \tag{236}$$

This procedure is used to determine the effective Young's modulus for each layer in the composite beam.

The shear modulus and Poisson's ratio values are determined from the material test results (sec. 4.14). These effective properties are used with the laminate composite plate equations to determine the effective material properties for the composite beam.

The Mathcad solution sheet (app. D) was set up for a two-ply plate consistent with the procedure for determining the effective properties of a multilayer composite plate, described in detail in section 5.9. The bottom entry in each property array corresponds to the bottom ply of the plate and the geometric center of the beam is considered zero:

$$E_1 = \begin{bmatrix} 5.0 \times 10^5 \\ 5.0 \times 10^5 \end{bmatrix} \frac{\text{lbf}}{\text{in.}^2} \qquad E_2 = \begin{bmatrix} 5.0 \times 10^5 \\ 5.0 \times 10^5 \end{bmatrix} \frac{\text{lbf}}{\text{in.}^2} \qquad G_{12} = \begin{bmatrix} 7.5 \times 10^4 \\ 7.5 \times 10^4 \end{bmatrix} \frac{\text{lbf}}{\text{in.}^2} \qquad \nu_{12} = \begin{bmatrix} 0.15 \\ 0.15 \end{bmatrix} . \tag{237}$$

The orientation, thickness, and centroid of each ply are as follows:

$$t = \begin{bmatrix} 0.125 \\ 0.125 \end{bmatrix} \text{in.} \quad \text{thickness} \qquad z = \begin{bmatrix} .0625 \\ -.0625 \end{bmatrix} \text{in.} \quad \text{centroid} \qquad \theta = \frac{\pi}{180} \begin{bmatrix} 90 \\ 45 \end{bmatrix} \quad \text{ply angles} \cdot \tag{238}$$

The thickness of each layer is one half the beam thickness. It should be noted the exact thickness of each beam varies (0.24 to 0.27 in.) due to imperfections in making the beams. The centroid of each layer is measured from the geometric center of the beam.

The compliance matrix is then calculated for each layer in the composite. The stiffness matrix (Q_n) is then formed from the inverse of the compliance matrix:

$$S_n = \begin{bmatrix} \frac{1}{E_{1_n}} & \frac{-\nu_{21_n}}{E_{2_n}} & 0 \\ \frac{-\nu_{12_n}}{E_{1_n}} & \frac{1}{E_{2_n}} & 0 \\ 0 & 0 & \frac{1}{G_{12_n}} \end{bmatrix}$$

$$Q_n = [S_n]^{-1} \ . \tag{239}$$

The subscript n refers to the layer number.

A stress transformation matrix is calculated from the angles given in the θ_n array:

$$T_n = \begin{bmatrix} \cos\theta_n^2 & \sin\theta_n^2 & 2\sin\theta_n\cos\theta_n \\ \sin\theta_n^2 & \cos\theta_n^2 & -2\sin\theta_n\cos\theta_n \\ -\sin\theta_n\cos\theta_n & \sin\theta_n\cos\theta_n & \cos\theta_n^2 - \sin\theta_n^2 \end{bmatrix} . \tag{240}$$

The $\overline{Q}$ matrix can then be calculated from equation (241):

$$\overline{Q}_n = T_n^{-1} Q_n R T_n R^{-1} \cdot \tag{241}$$

The extensional matrix A can now be calculated from equation (242):

$$A = \sum_{k=1}^{\text{plies}} \overline{Q}_k t_k = \begin{bmatrix} 1.10\times10^5 & 3.70\times10^4 & 0 \\ 3.70\times10^4 & 1.10\times10^5 & 0 \\ 0 & 0 & 3.65\times10^4 \end{bmatrix} \frac{\text{lbf}}{\text{in.}} \tag{242}$$

The coupling stiffness matrix B, for a nonsymmetric matrix, can also be calculated from equation (243):

$$B = \sum_{k=1}^{\text{plies}} \overline{Q}_k t_k z_k = \begin{bmatrix} 1.11\times10^3 & -1.11\times10^3 & 0 \\ -1.11\times10^3 & 1.11\times10^3 & 0 \\ 0 & 0 & -1.11\times10^3 \end{bmatrix} \frac{\text{lbf}}{\text{in.}} \tag{243}$$

The bending stiffness matrix D, equation (244), completes the calculations of the stiffness terms:

$$D = \sum_{k=1}^{\text{plies}} \overline{Q}_k \left(\frac{t_k^3}{12} + t_k z_k^2 \right) = \begin{bmatrix} 5.73\times10^2 & 1.93\times10^2 & 0 \\ 1.93\times10^2 & 5.73\times10^2 & 0 \\ 0 & 0 & 1.9\times10^2 \end{bmatrix} \frac{\text{lbf}}{\text{in.}} \tag{244}$$

The global stiffness matrix from equation (246) can then be determined by combining the A, B, and D matrices:

$$\text{Global} = \begin{bmatrix} 1.10\times10^5 & 3.70\times10^4 & 0 & 1.11\times10^3 & -1.11\times10^3 & 0 \\ 3.70\times10^4 & 1.10\times10^5 & 0 & -1.11\times10^3 & 1.11\times10^3 & 0 \\ 0 & 0 & 3.65\times10^4 & 0 & 0 & -1.11\times10^3 \\ 1.11\times10^3 & -1.11\times10^3 & 0 & 5.73\times10^2 & 1.93\times10^2 & 0 \\ -1.11\times10^3 & 1.11\times10^3 & 0 & 1.93\times10^2 & 5.73\times10^2 & 0 \\ 0 & 0 & -1.11\times10^3 & 0 & 0 & 1.9\times10^2 \end{bmatrix}. \tag{245}$$

Equation (246) is written in terms of the global stiffness matrix as

$$\begin{bmatrix} N_x \\ N_y \\ N_{xy} \\ M_x \\ M_y \\ M_{xy} \end{bmatrix} = [\text{Global}] \begin{bmatrix} \varepsilon_{0x} \\ \varepsilon_{0y} \\ \gamma_{0xy} \\ K_x \\ K_y \\ K_{xy} \end{bmatrix}. \tag{246}$$

Additionally, equation (246) can be solved to determine the effective material properties of the composite beam:

$$E_x = \frac{N_x}{h\varepsilon_{0x}} = 3.41\times10^5 \frac{\text{lbf}}{\text{in.}^2} \qquad \nu_{xy} = \frac{-\varepsilon_{0y}}{\varepsilon_{0x}} = 0.42$$

$$E_y = \frac{N_y}{h\varepsilon_{0y}} = 3.41\times10^5 \frac{\text{lbf}}{\text{in.}^2} \qquad \nu_{yx} = \frac{-\varepsilon_{0x}}{\varepsilon_{0y}} = 0.42 \ .$$

$$G_{xy} = \frac{N_{xy}}{h\gamma_{oxy}} = 1.20\times10^5 \frac{\text{lbf}}{\text{in.}^2} \tag{247}$$

The analysis was repeated for each of the three composite beams. Table 12 contains the effective material properties for each beam.

Table 12. Effective material properties.

	θ	E_x (lbf/in.^{2})	E_y (lbf/in.^{2})	G_{xy} (lbf/in.^{2})
Beam 1	[90,90]	4.12×10^5	4.12×10^5	7.50×10^4
Beam 2	[45,45]	2.40×10^5	2.40×10^5	1.88×10^5
Beam 3	[90,45]	3.20×10^5	3.20×10^5	1.15×10^5

6.5 Comparison of Test Data to Analytical Predictions

The effective material properties can now be used with the elastic beam equation (124) to calculate the deflections in the beam. To illustrate the steps in the analysis, the results obtained for beam 1 at a typical load increment follow:

$$y_2(x) = \frac{1}{EI}\left(Pax^2 + C_3x + C_4\right) \tag{248}$$

$$E = 4.12 \times 10^5 \frac{\text{lbf}}{\text{in.}^2} \tag{249}$$

$$I = \frac{bh^3}{12} = \frac{(1.189\ \text{in.})(0.265\ \text{in.})^3}{12} = 0.00184\ \text{in.}^4 \tag{250}$$

$$x = 4.375\ \text{in.} \tag{251}$$

$$C_3 = -25.39\ \text{lbf/in.}^2 \tag{252}$$

$$C_4 = 8.707\ \text{lbf/in.}^3 \tag{253}$$

$$y_2 = \frac{1}{\left(4.12 \times 10^5 \frac{\text{lbf}}{\text{in.}^2}\right)(0.00184\ \text{in.}^4)} \left[\begin{array}{l} \left[(1.94\ \text{lbf})(3\ \text{in.})(4.375\ \text{in.})^2\right] \\ \\ +\left(-25.39 \frac{\text{lbf}}{\text{in.}^2}\right)(4.375\ \text{in.}) + \left(8.707 \frac{\text{lbf}}{\text{in.}^3}\right) \end{array} \right] \tag{254}$$

$$y_2 = -0.062\ \text{in.} \tag{255}$$

The above analysis is repeated at incremental loads to generate a load versus deflection curve for each beam.

The results of the three-section bending test can now be compared to the results calculated using the elastic beam equation with the effective material properties derived from the rule of mixtures and the laminated composite plate theory. A measure of the possible error associated with these calculations is determined as follows:

- Error from Young's modulus test = 6.4 percent
- Error from shear modulus test = 5.6 percent
- Error % $= \sqrt{(6.4\%)^2 + (5.6\%)^2} = 8.5\%$.

Error bars on figures 82–84 will reflect this measure of error.

As shown in figure 82, the predicted deflections for beam 1 [90,90] are in good agreement with the test results, indicating that the effective Young's modulus used in the predictions, $E_x = 4.12 \times 10^5$ lbf/in.^{2}, adequately predicts the behavior of this two-layer composite.

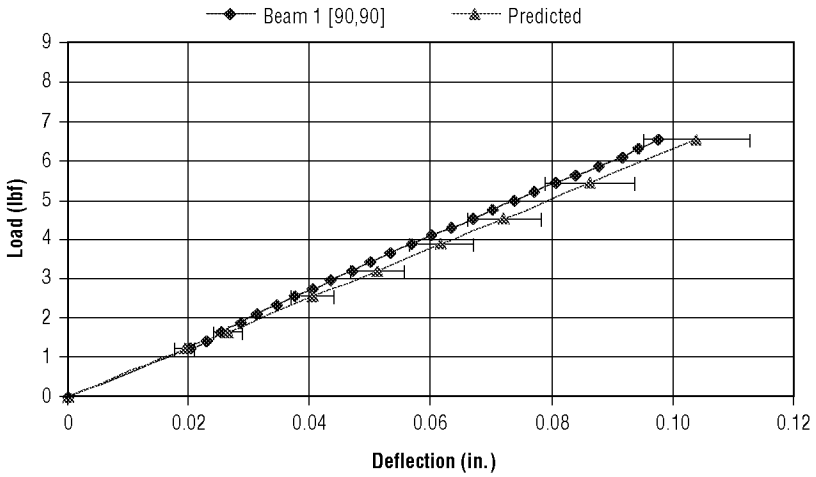

Figure 82. Beam 1 comparison of predicted versus test deflections.

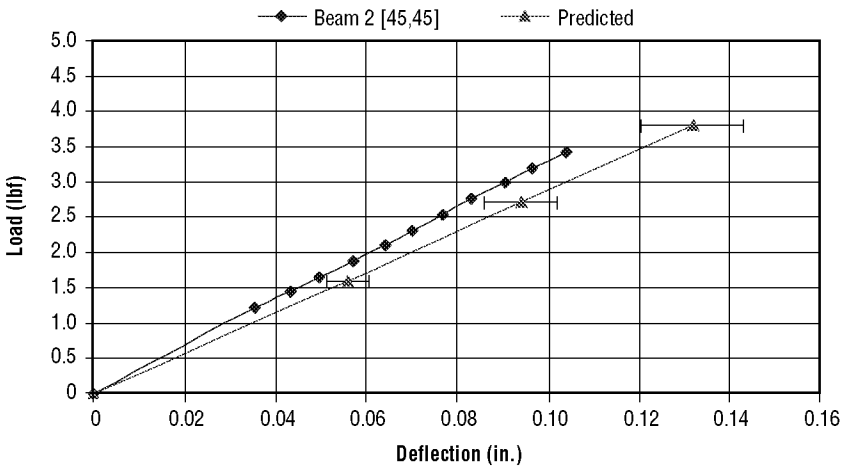

Figure 83. Beam 2 comparison of predicted versus test deflections.

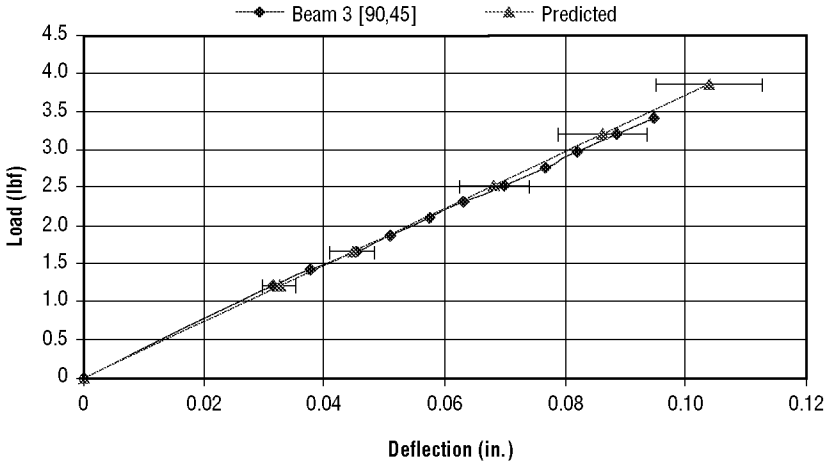

Figure 84. Beam 3 comparison of predicted versus test deflections.

Figure 83 compares the predicted deflections for beam 2 [45,45] with test results. The data compare reasonably well with the test results, indicating that the effective Young's modulus used in the predictions, $E_x = 2.31 \times 10^5$ lbf/in.^{2}, also adequately predicts the behavior of this two-layer composite.

Figure 84 illustrates the results for the nonsymmetric beam 3 [90,45]. The test data for beam 3 [90,45] compare very well with the test results. The effective Young's modulus calculated for this beam, $E_x = 3.2 \times 10^5$ lbf/in.^{2}, was calculated using the same methods as the previous symmetric beams.

Based on these results, it can be concluded that the solution to the constitutive equations presented can be used to accurately determine the effective material properties for a symmetric or a nonsymmetric multilayered laminated composite.

6.6 Analysis of Beams Using Finite Element Methods

The analysis of simple composite structures such as beams can be achieved using the methods described in this TM. However, when the geometry or loading of the structure becomes more complex, this method of analysis may be too difficult to apply. For that reason, it is important to extend the verification process to include finite element modeling.

The input for the MSC/Nastran program is calculated from the equation for the stiffness matrix, equation (257), $Q_n = [S_n]^{-1}$. The MAT2 input for beam 1 can be taken from the Q_n matrix. For example, the stiffness matrix for layer one of beam 1 [90,90] is calculated and given:

$$Q_1 = \begin{bmatrix} 4.30\times10^5 & 6.45\times10^4 & 0 \\ 6.45\times10^4 & 4.30\times10^5 & 0 \\ 0 & 0 & 7.50\times10^4 \end{bmatrix}. \tag{257}$$

Incorporating these values into the MAT2 results in the following:

```
$ Description of Matrix Material:
MAT2,1,4.30+5,6.45+4,0.0,4.30+5,0.0,7.50+4,
0.,      0.,      0.,      0.,      0.
```

The orientation of each layer is described in the PCOMP command. An example of the PCOMP command for beam 1 is provided below for reference:

```
$
PCOMP, 1, , , 10000.0, STRN,
+, 1, .1325, 90.0, YES, 1,.1325, 90.0, YES
$
```

The finite element model is generated in the same procedures as those verified in section 4.12.

Figures 85–87 show that the results of the finite element models for each of the three beams are in agreement with both the test data and the analytical solution from the elastic beam equation (86).

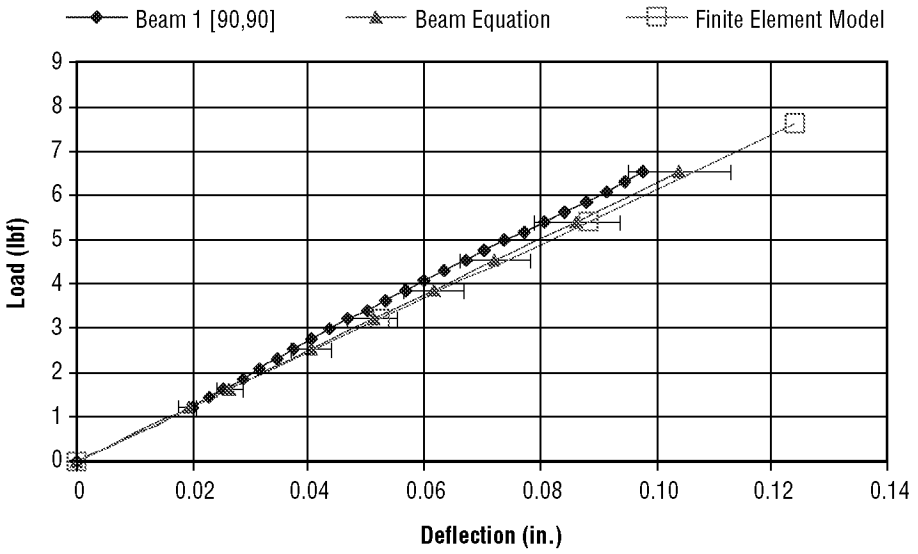

Figure 85. Beam 1 comparison of finite element versus test deflections.

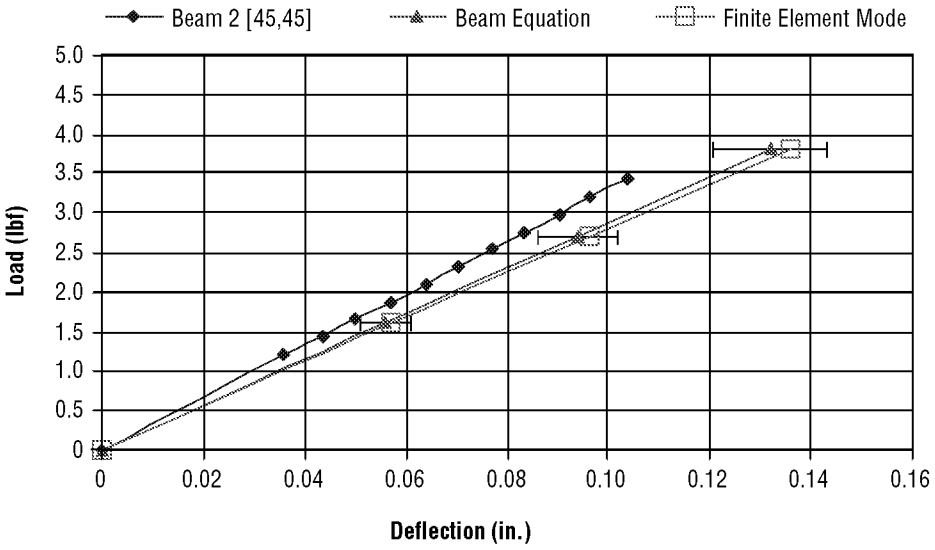

Figure 86. Beam 2 comparison of finite element versus test deflections.

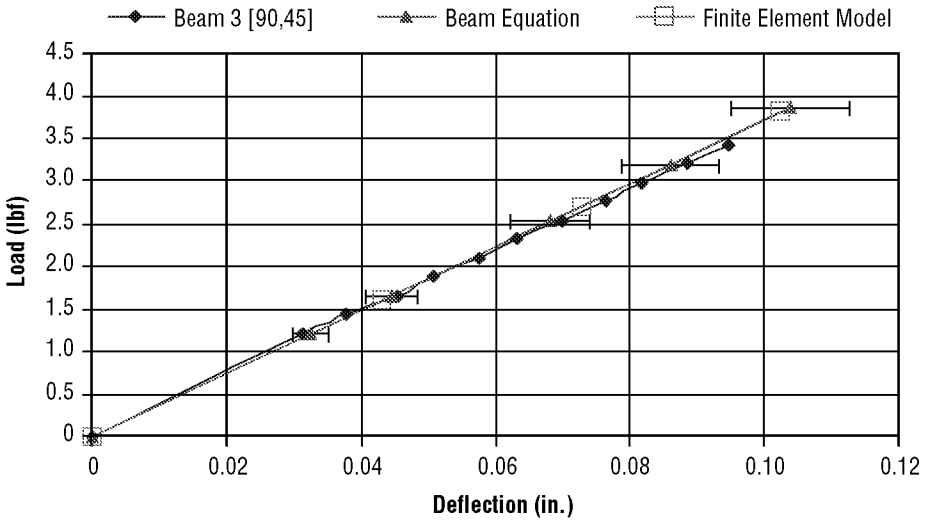

Figure 87. Beam 3 comparison of finite element versus test deflections.

6.7 Summary and Conclusions

The preceding results indicate that cementitious composites can be analyzed using the laminated composite plate theory. This is a significant improvement over the methods based on the rule of mixtures and the transform section methods. The composite plate theory has no limitations on the orientation of the fibers or the geometry of the layup. As a result, the designer can strategically place and orient the reinforcement fibers to optimize the design.

7. CONCLUSIONS AND RECOMMENDATIONS

7.1 Conclusions

This research establishes the procedures for producing, instrumenting, and testing graphite-reinforced cementitious specimens to determine the material characteristics. Tensile tests are used to successfully determine Young's modulus and Poisson's ratio. Iosipescu shear tests are used to determine the shear modulus. Comparisons are then made to the material properties calculated from the mechanics of materials approach for composite analysis; i.e., rule of mixtures. Consistent with the literature,[2,9,10] it is determined that the rule of mixtures is accurate for determining the effective material property, E_1, provided the fibers are continuous and aligned in the direction of the load. However, the remaining material properties, E_2, v_{12}, and G_{12} may not be accurately predicted by the rule of mixtures.

A modified transform section approach is used with the E_1 value from the rule of mixtures to accurately predict the deflection of a beam in pure bending with a single layer of graphite reinforcement. A similar approach is used for a multilayered beam in pure bending. The beam analysis is extended to include nonlinear material properties. The results compare well to test data.

Laminated composite plate theory is investigated as a means for analyzing even more complex composites, consisting of multiple graphite layers oriented in different directions. Equations for the effective material properties are derived based on the laminated composite plate theory. The equations are arranged to form a system of simultaneous equations from which an exact solution can be found. A Mathcad solution sheet is developed to make the calculations. An increase in accuracy is demonstrated when this solution method is compared to other solution methods. The results of the Mathcad solution sheet are verified with an example problem. A composite plate with known material properties is analyzed using the Mathcad solution sheet. The plate is then analyzed using a finite element model. The results compare very well, demonstrating the accuracy of the solution method.

The analytical methods developed in this TM are demonstrated with the analysis and test of three beams with various ply angles and layups. The effective material property for each beam is determined by using laminated plate equations and the Mathcad solution program. In addition, a finite element model is developed for each beam. The results of three-section bending tests are then compared to the analytical results to determine the accuracy of the methods developed in this TM. The analytical results compare very well to the test results.

The research presented establishes a methodology that can be used to determine the deflections and stresses in graphite-reinforced laminated composites. In addition, it demonstrates methods of determining the appropriate material properties necessary for the analysis.

APPENDIX A—MATHCAD SOLUTION SHEET: RULE OF MIXTURES

Note: This program is provided as an example only. The content of this file is similar to that found in the text. However, this program is subject to modification and may not match the previous text.

A.1 Rule of Mixtures for a Composite Material

The rule of mixtures is a method for determining the effective properties of a composite material based on the contributions of the individual constituents. This method assumes that the strains in the fiber direction of a composite are the same in the fibers as in the matrix. Since the strain in the fiber is the same as the strain in the matrix, the sections normal to the fiber direction remain plane after stressing:

- Determination of E_1

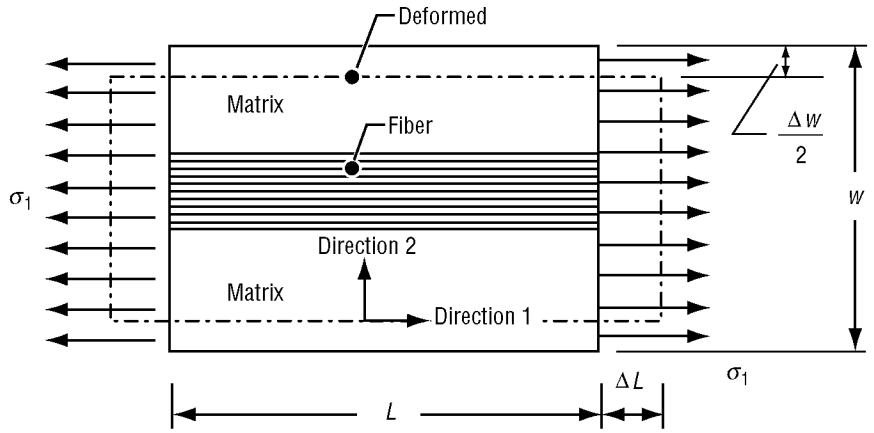

The strain in direction 1, the fiber direction, is given by

$$\varepsilon_1 := \frac{\Delta L}{L}.$$

The strain in the fiber direction is same for the fiber and the matrix:

$$\sigma_{fiber} := E_{fiber}\,\varepsilon_1.$$

Applying Hooke's law and assuming both the fiber and the matrix are linear:

$$\sigma_{matrix} := E_{matrix}\,\varepsilon_1.$$

This relationship is similar to two springs acting in parallel. The total load (P) is carried by the load in fiber (P_f) and the load in the matrix (P_m):

$$P := P_f + P_m \blacksquare .$$

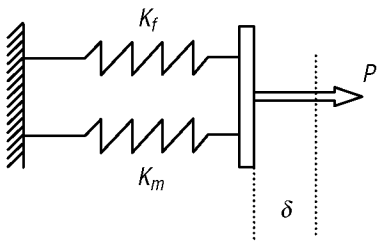

The force equation can then be written in terms of the stress and area:

$$\sigma_1 \cdot A_1 := \sigma_{fiber} \cdot A_{fiber} + \sigma_{matrix} \cdot A_{matrix} \blacksquare .$$

Now substitute the Hooke's law equations for the stress terms to relate the force equation in terms of strain and Young's modulus:

$$E_1 \cdot \varepsilon_1 \cdot A_1 := E_{fiber} \cdot \varepsilon_1 \cdot A_{fiber} + E_{matrix} \cdot \varepsilon_1 \cdot A_{matrix} \blacksquare .$$

Simplifying the equation,

$$E_1 := \frac{E_{fiber} \cdot A_{fiber}}{A_1} + \frac{E_{matrix} \cdot A_{matrix}}{A_1} \blacksquare .$$

The fiber volume fraction (V_{fiber}) and the matrix volume fraction (V_{matrix}) can be defined as

$$V_{matrix} := \frac{A_{matrix}}{A_1} \blacksquare$$

$$V_{fiber} := \frac{A_{fiber}}{A_1} \blacksquare .$$

In addition, the fiber volume fractions must satisfy the equation:

$$V_{fiber} + V_{matrix} := 1 \blacksquare .$$

Thus the expression for the effective Young's modulus in direction 1 is as follows:

$$E_1 := V_{fiber} E_{fiber} + V_{matrix} E_{matrix}.$$

Determine the effective property in direction 2, perpendicular to the fiber direction,

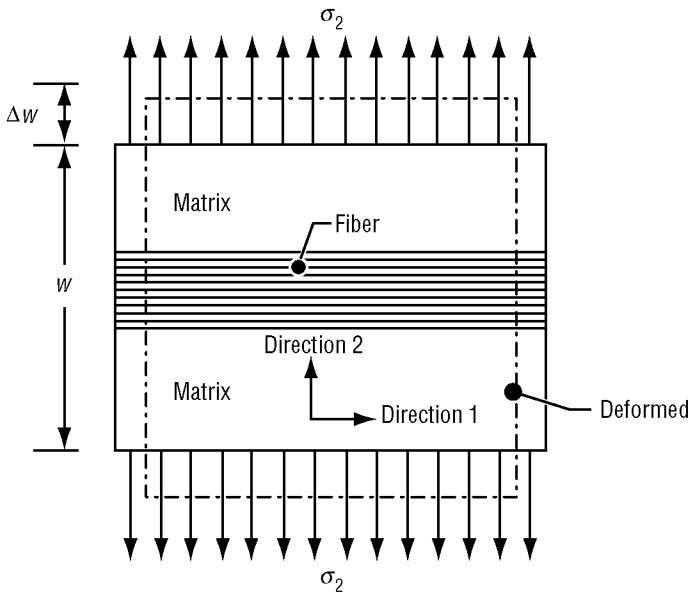

The fiber and matrix transverse strains are not assumed to be equal. However, in the transverse direction, the cross-sectional areas are equal and the load is constant across the area; therefore, the stress is equal for the fiber and the matrix. Then the strains in the fiber and matrix can be written in terms of the stress:

$$\varepsilon_{fiber} := \frac{\sigma 2}{E_{fiber}},$$

$$\varepsilon_2 := \frac{\sigma 2}{E_2},$$

and

$$\varepsilon_{matrix} := \frac{\sigma 2}{E_{matrix}}.$$

The total transverse deflection is the sum of the fiber deflection and matrix deflection:

$$\Delta w := \Delta w_{fiber} + \Delta w_{matrix}.$$

Defining the strains in terms of the deflection:

$$\varepsilon_2 := \frac{\Delta w}{w},$$

$$\varepsilon_{fiber} := \frac{\Delta w_{fiber}}{L_{fiber}},$$

and

$$\varepsilon_{matrix} := \frac{\Delta w_{matrix}}{L_{matrix}}.$$

The transverse dimension over which the fiber and matrix strains act can be written in terms of the fiber volume:

$$L_{fiber} := V_{fiber} \cdot w$$

and

$$L_{matrix} := V_{matrix} \cdot w.$$

The deflection equation can now be defined in terms of strain:

$$\varepsilon_2 \cdot w := \varepsilon_{fiber} \cdot (V_{fiber} \cdot w) + \varepsilon_{matrix} \cdot (V_{matrix} \cdot w).$$

Now the *w* term vanishes from both sides of the equation. Hooke's law equations can be substituted for the strains:

$$\frac{\sigma 2}{E_2} := V_{fiber} \cdot \frac{\sigma 2}{E_{fiber}} + V_{matrix} \cdot \frac{\sigma 2}{E_{matrix}}.$$

The stress term now vanishes from both sides:

$$\frac{1}{E_2} := \frac{V_{fiber}}{E_{fiber}} + \frac{V_{matrix}}{E_{matrix}}.$$

Solving the above equation for the E_2 term,

$$E_2 := \frac{E_{fiber} \cdot E_{matrix}}{V_{matrix} \cdot E_{fiber} + V_{fiber} \cdot E_{matrix}}.$$

Determination of the Poisson's ratio between the transverse and the fiber directions:

$$\nu_{12} := \frac{-\varepsilon_2}{\varepsilon_1}.$$

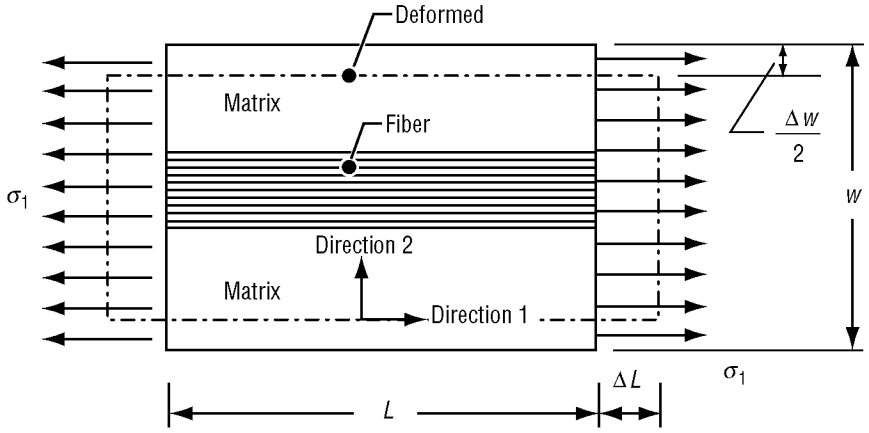

As shown above, the deflection equation can now be defined in terms of strain:

$$\nu_{matrix} := \frac{\varepsilon_{matrix}}{\varepsilon_1},$$

$$\nu_{fiber} := \frac{\varepsilon_{fiber}}{\varepsilon_1},$$

and

$$\varepsilon_2 \cdot w := \varepsilon_{fiber} \cdot \left(V_{fiber} \cdot w\right) + \varepsilon_{matrix} \cdot \left(V_{matrix} \cdot w\right).$$

Now simplify,

$$\frac{\varepsilon_2}{\varepsilon_1} := \frac{\varepsilon_{fiber}}{\varepsilon_1} \cdot \left(V_{fiber}\right) + \frac{\varepsilon_{matrix}}{\varepsilon_1} \cdot \left(V_{matrix}\right).$$

Substitute in the equations for the Poisson's ratio:

$$\nu_{12} := \nu_{fiber} \cdot V_{fiber} + \nu_{matrix} \cdot V_{matrix}.$$

Determine the shear modulus (G_{12}) by assuming the shearing stress on the fiber and the matrix is the same. This assumption means that the shear deformation can be written as

$$\gamma_{matrix} := \frac{\tau}{G_{matrix}}.$$

- Shear strain in the matrix:

$$\gamma_{fiber} := \frac{\tau}{G_{fiber}}.$$

- Shear strain in the fiber:

$$\gamma_{12} := \frac{\tau}{G_{12}}.$$

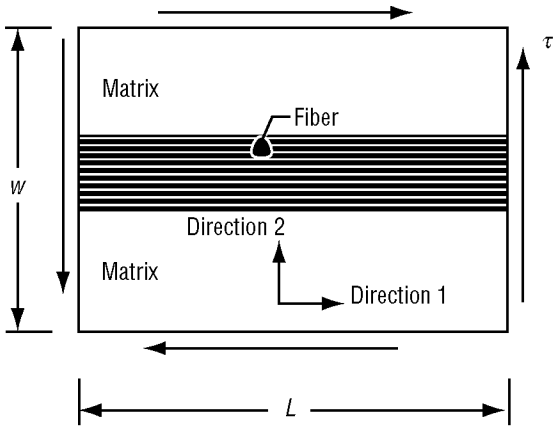

Shear strain in the fiber and transverse direction.

The shear deflection is a function of the shear strain and the width (w):

$$\Delta := \gamma \cdot w$$

and

$$\Delta := \Delta_{fiber} + \Delta_{matrix}.$$

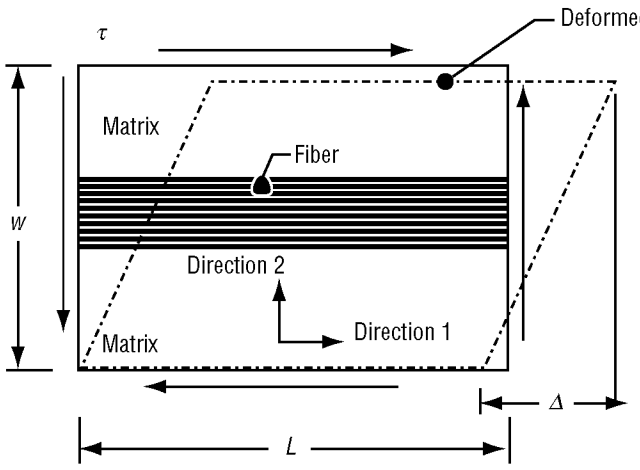

As shown in the previous equations, the deflection for the matrix and fiber can be stated in terms of the volume fractions, V_{fiber} and V_{matrix}:

$$\Delta_{matrix} := \gamma_{matrix} \cdot (V_{matrix} \cdot w) \blacksquare$$

and

$$\Delta_{fiber} := \gamma_{fiber} \cdot (V_{fiber} \cdot w) \blacksquare .$$

Then, substituting into the deflection equation and allowing the w term to vanish:

$$\gamma := \gamma_{matrix} \cdot V_{matrix} + \gamma_{fiber} \cdot V_{fiber} \blacksquare .$$

Finally, substitute the Hooke's law equations for shear strain and allow the shear stress:

$$\frac{\tau}{G_{12}} := V_{matrix} \cdot \frac{\tau}{G_{matrix}} + V_{fiber} \cdot \frac{\tau}{G_{fiber}} \blacksquare .$$

Now, this equation can be simplified by allowing the shear stress term to vanish and solving for G_{12}:

$$G_{12} := \frac{G_{matrix} \cdot G_{fiber}}{V_{matrix} \cdot G_{fiber} + V_{fiber} \cdot G_{matrix}} \blacksquare .$$

Calculate the effective material properties of a cementitious composite:

- Material properties:

$$E_{matrix} := 115 \cdot 10^3 \cdot \frac{lbf}{in^2} \qquad E_{fiber} := 33.5 \cdot 10^6 \cdot \frac{lbf}{in^2}$$

$$\nu_{matrix} := 0.27 \qquad \nu_{fiber} := 0.30$$

$$\rho_{matrix} := 35 \cdot \frac{lbf}{in^3} \qquad \rho_{fiber} := .064 \cdot \frac{lbf}{in^3}$$

$$G_{matrix} := \frac{E_{matrix}}{2 \cdot (1 + \nu_{matrix})} \qquad G_{fiber} := \frac{E_{fiber}}{2 \cdot (1 + \nu_{fiber})}$$

$$G_{matrix} = 4.528 \times 10^4 \frac{lbf}{in^2} \qquad G_{fiber} = 1.288 \times 10^7 \frac{lbf}{in^2} \quad .$$

- Fiber area in a graphite yarn:

$$A_{yarn} := .000175 \cdot in^2 \qquad N_{yarn} := 8$$

$$A_{fiber} := N_{yarn} \cdot A_{yarn} \qquad A_1 := .12 \cdot in^2$$

$$V_{fiber} := \frac{A_{fiber}}{A_1} \qquad V_{matrix} := 1 - V_{fiber}$$

$$V_{fiber} = 0.012 \qquad V_{matrix} = 0.988 \quad .$$

Thus, the expressions for the effective material properties can be calculated:

- Young's modulus in direction 1:

$$E_1 := V_{fiber} \cdot E_{fiber} + V_{matrix} \cdot E_{matrix}$$

and

$$E_1 = 5.045 \times 10^5 \frac{lbf}{in^2} \quad .$$

- Young's modulus in direction 2:

$$E_2 := \frac{E_{fiber} \cdot E_{matrix}}{V_{matrix} \cdot E_{fiber} + V_{fiber} \cdot E_{matrix}}$$

and

$$E_2 = 1.164 \times 10^5 \frac{lbf}{in^2} .$$

- Poisson's ratio:

$$\nu_{12} := \nu_{fiber} \cdot V_{fiber} + \nu_{matrix} \cdot V_{matrix}$$

and

$$\nu_{12} = 0.27 .$$

- Shear modulus:

$$G_{12} := \frac{G_{matrix} \cdot G_{fiber}}{V_{matrix} \cdot G_{fiber} + V_{fiber} \cdot G_{matrix}}$$

and

$$G_{12} = 4.581 \times 10^4 \frac{lbf}{in^2} .$$

- Composite Density

$$\rho_{composite} := \rho_{fiber} \cdot V_{fiber} + \rho_{matrix} \cdot V_{matrix}$$

and

$$\rho_{composite} = 34.592 \frac{lbf}{in^3} .$$

Now compare the results from the rule of mixtures to the results of tensile testing.

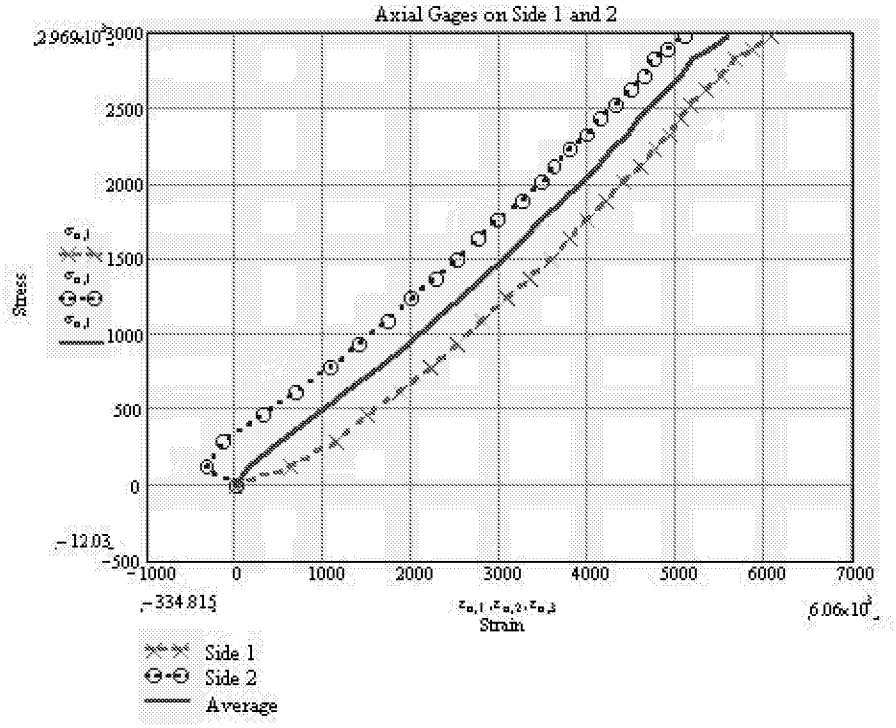

- Young's modulus from the tensile test:

$$E_{test} := \frac{(1500 - 500)\cdot \frac{lbf}{in^2}}{(3000 - 1000)\cdot 10^{-6}} ,$$

$$E_{test} = 5 \times 10^{5} \frac{lbf}{in^2} ,$$

$$\Delta error := \left| \frac{E_{test} - E_1}{E_{test}} \right| \cdot 100 ,$$

and

$$\Delta error = 0.898 .$$

Krenchel methods:

- Calculate the effective material properties of a cementitious composite:

$$E_{fiber} := 33.5 \cdot 10^6 \cdot \frac{lbf}{in^2} \qquad E_{matrix} := 115 \cdot 10^3 \cdot \frac{lbf}{in^2}$$

$$\nu_{matrix} := 0.27 \qquad \nu_{fiber} := 0.30$$

$$\rho_{fiber} := .064 \cdot \frac{lbf}{in^3} \qquad \rho_{matrix} := 35 \cdot \frac{lbf}{in^3}$$

$$G_{fiber} := \frac{E_{fiber}}{2 \cdot (1 + \nu_{fiber})} \qquad G_{matrix} := \frac{E_{matrix}}{2 \cdot (1 + \nu_{matrix})}$$

$$G_{fiber} = 1.28846 \times 10^7 \frac{lbf}{in^2} \qquad G_{matrix} = 4.52756 \times 10^4 \frac{lbf}{in^2} \quad .$$

- Fiber area in a graphite yarn:

$$A_{yarn} := .000175 \cdot in^2 \qquad N_{yarn} := 8$$

$$A_{fiber} := N_{yarn} \cdot A_{yarn} \qquad t_{ply} := \frac{0.241 \cdot in}{2}$$

$$w_{beam} := 1.163 \cdot in \qquad A_1 := t_{ply} \cdot w_{beam}$$

$$A_1 = 1.40141 \times 10^{-1} in^2 \qquad V_{fiber} := \frac{A_{fiber}}{A_1}$$

$$V_{matrix} := 1 - V_{fiber} \qquad V_{fiber} = 9.9899 \times 10^{-3} \qquad V_{matrix} = 9.9001 \times 10^{-1} \quad .$$

Thus, the expressions for the effective material properties can be calculated:

$$E_1 := V_{fiber} \cdot E_{fiber} + V_{matrix} \cdot E_{matrix}.$$

- Young's modulus in direction 1:

$$E_1 = 4.48513 \times 10^5 \frac{lbf}{in^2} .$$

- Young's modulus in direction 2:

$$E_2 := \frac{E_{fiber} \cdot E_{matrix}}{V_{matrix} \cdot E_{fiber} + V_{fiber} \cdot E_{matrix}}$$

and

$$E_2 = 1.16156 \times 10^5 \frac{lbf}{in^2} .$$

- Poisson's ratio:

$$\nu_{12} := \nu_{fiber} \cdot V_{fiber} + \nu_{matrix} \cdot V_{matrix}$$

and

$$\nu_{12} = 2.703 \times 10^{-1} .$$

- Shear modulus:

$$G_{12} := \frac{G_{matrix} \cdot G_{fiber}}{V_{matrix} \cdot G_{fiber} + V_{fiber} \cdot G_{matrix}}$$

and

$$G_{12} = 4.57308 \times 10^4 \frac{lbf}{in^2} .$$

- Composite density:

$$\rho_{composite} := \rho_{fiber} \cdot V_{fiber} + \rho_{matrix} \cdot V_{matrix}$$

and

$$\rho_{composite} = 3.4651 \times 10^1 \frac{lbf}{in^3} .$$

Now refer to Krenchel, p. 29:

$$\psi := 45$$

$$Factor := \left(\sin\left(\frac{\pi}{180}\cdot\psi\right)\right)^2\cdot\left(\cos\left(\frac{\pi}{180}\cdot\psi\right)^2\right)$$

$$Factor = 2.5\times10^{-1}$$

$$G_{fc} := \left(V_{matrix}\cdot G_{matrix}\right) + \left[V_{fiber}\cdot E_{fiber}\left(\sin\left(\frac{\pi}{180}\cdot\psi\right)\right)^2\cdot\left(\cos\left(\frac{\pi}{180}\cdot\psi\right)^2\right)\right]$$

$$G_{fc} = 1.28489\times10^{5}\,\frac{lbf}{in^2}\quad .$$

- Krenchel case 2a

$$a_1 := 1 \qquad a_2 := 1 \qquad n := 1 \qquad \beta := V_{fiber}$$

$$k := \frac{1-\beta}{1-\nu_{matrix}^2} \qquad k = 1.06786\times10^{0}$$

$$\nu_{composite} := \frac{k\cdot\nu_{matrix}}{\left[k+\left(a_2\cdot n\cdot\beta\right)\right]} \qquad \nu_{composite} = 2.67498\times10^{-1}$$

$$\omega_2 := \left(k + a_1\cdot n\cdot\beta\right) - \left(k\cdot\nu_{matrix}\cdot\nu_{composite}\right) \qquad \omega_2 = 1.00072\times10^{0}$$

$$E_{fc} := \omega_2\cdot E_{matrix}$$

$$E_{fc} = 1.15083\times10^{5}\,\frac{lbf}{in^2}\quad .$$

- Krenchel case 1a

$$E_{fc} := \left[E_{matrix}\cdot k\cdot\left(1-\nu_{matrix}^2\right)\right] + E_{fiber}\cdot\beta$$

$$E_{fc} = 4.48513\times10^{5}\,\frac{lbf}{in^2}\quad .$$

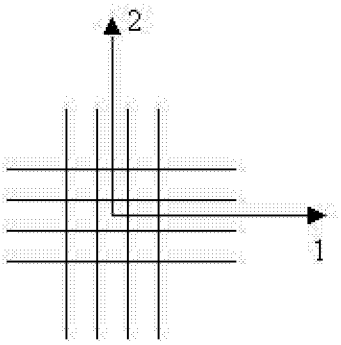

Direction of the Load

- Krenchel case 2b

$$\psi_1 := \frac{\pi}{180} \cdot 0$$

$$\psi_2 := \frac{\pi}{180} \cdot 90 \quad .$$

These angles describe the load in relation to the fibers (see Krenchel[3], pp. 17 and 26).

The *n* represents the number of groups of fibers; in this case, two groups:

$$n := 2 \quad .$$

This represents the proportion fibers in each group; half of the fibers are in group 1 and the other half are in group 2:

$$a_1 := 0.5 \qquad a_2 := 0.5$$

- Efficiency factor:

$$\eta := a_1 \cdot \cos(\psi_1)^4 + a_2 \cdot \cos(\psi_2)^4$$

$$\eta = 5 \times 10^{-1} \quad .$$

- Makes the derivations easier (p. 27):

$$k := \frac{1 - \beta}{1 - \nu_{matrix}^2} \quad .$$

- Page 34 equations:

$$\nu_{composite} := \frac{k \cdot \nu_{matrix} + (\eta \cdot a_1 \cdot n \cdot \beta)}{[k + (\eta \cdot a_2 \cdot n \cdot \beta)]}$$

$$\nu_{composite} = 2.73399 \times 10^{-1} \quad .$$

- Volume fraction for the fiber:

$$\beta := V_{fiber}$$

$$\beta = 9.9899 \times 10^{-3} \quad .$$

- Guess values to make the program solve:

$$\varepsilon_x := 1 \cdot 10^{-1}$$

$$\varepsilon_y := 1 \cdot 10^{-1}$$

$$E_{composite} := 1.0 \cdot 10^{5} \cdot \frac{lbf}{in^2} \quad .$$

Equations (28) and (32) from p. 27:

$$E_{composite} = \frac{E_{matrix} \cdot k \cdot (\varepsilon_x + \nu_{matrix} \cdot \varepsilon_y) + \left[\begin{array}{l} E_{fiber} \cdot \beta \cdot \cos(\psi_1)^2 \cdot \left[(\varepsilon_x) \cdot \cos(\psi_1)^2 + \varepsilon_y \cdot \sin(\psi_1)^2 \right] \ldots \\ + E_{fiber} \cdot \beta \cdot \cos(\psi_2)^2 \cdot \left[(\varepsilon_x) \cdot \cos(\psi_2)^2 + \varepsilon_y \cdot \sin(\psi_2)^2 \right] \end{array} \right]}{\varepsilon_x} \quad .$$

Equations (29) and (33) from p. 27:

$$0.0 = \left[E_{matrix} \cdot k \cdot (\nu_{matrix} \cdot \varepsilon_x + \varepsilon_y) \right] + \left[\begin{array}{l} E_{fiber} \cdot \beta \cdot \sin(\psi_1)^2 \cdot \left[(\varepsilon_x) \cdot \cos(\psi_1)^2 + \varepsilon_y \cdot \sin(\psi_1)^2 \right] \ldots \\ + E_{fiber} \cdot \beta \cdot \cos(\psi_2)^2 \cdot \left[(\varepsilon_x) \cdot \cos(\psi_2)^2 + \varepsilon_y \cdot \sin(\psi_2)^2 \right] \end{array} \right] \quad .$$

Equation (34) from p. 27:

$$-\varepsilon_y = \nu_{composite} \cdot \varepsilon_x \quad .$$

Solve three equations with three unknowns:

$$\begin{pmatrix} E_{composite} \\ \varepsilon_y \\ \varepsilon_x \end{pmatrix} := Find(E_{composite}, \varepsilon_y, \varepsilon_x)$$

$$E_{composite} = 4.48513 \times 10^5 \frac{lbf}{in^2} \quad .$$

Now use equation (39) to calculate shear modulus, p. 29:

$$G_{composite} := (1 - \beta) \cdot G_{matrix} + \left[\beta \cdot E_{fiber} \left(a_1 \cdot \sin(\psi_1)^2 \cdot \cos(\psi_1)^2 + a_2 \cdot \sin(\psi_2)^2 \cdot \cos(\psi_2)^2 \right) \right]$$

$$G_{composite} = 4.48233 \times 10^4 \frac{lbf}{in^2} \quad .$$

APPENDIX B—MATERIAL PROPERTIES DATA

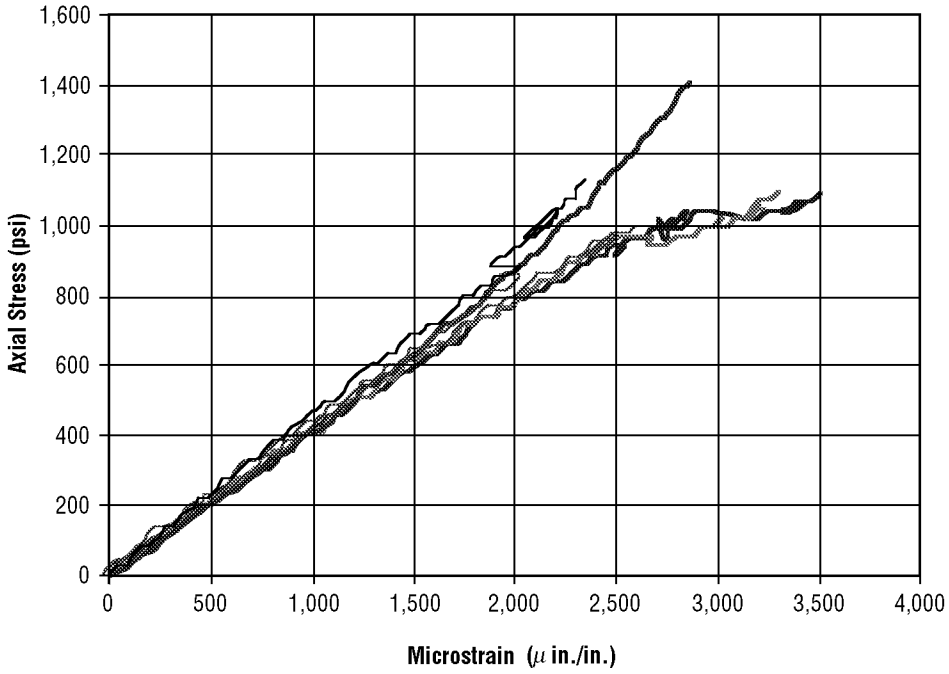

Figure B.1. Tensile test summary—six test articles.

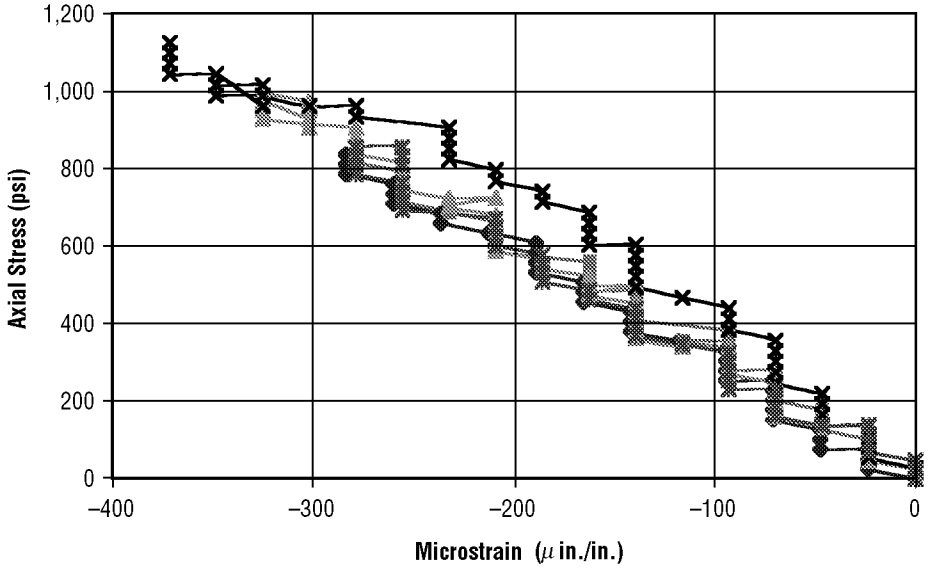

Figure B.2. Average transverse strain—five test articles.

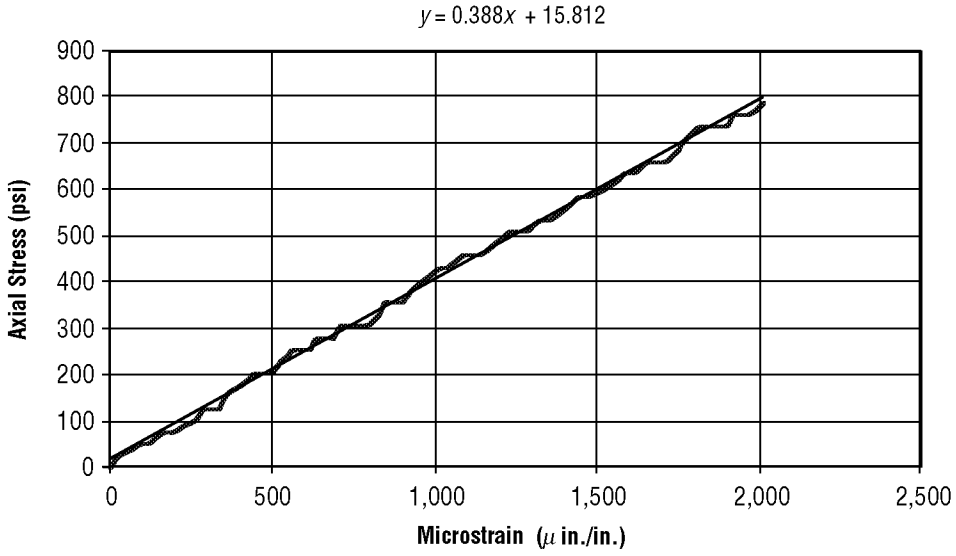

Figure B.3. Average tensile strain Dec_28_4.

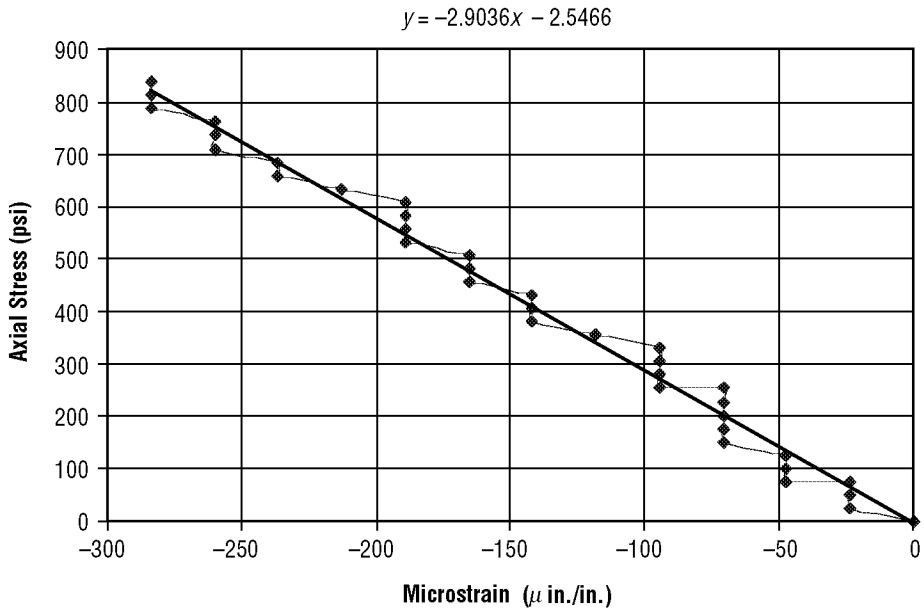

Figure B.4. Average transverse strain Dec_28_4.

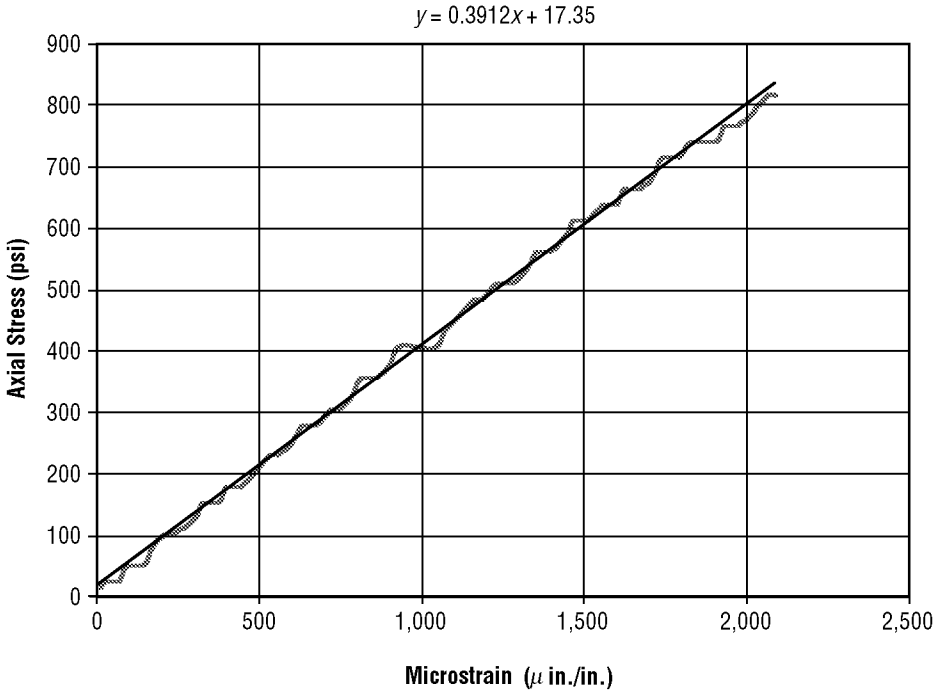

Figure B.5. Average tensile strain Dec_28_5.

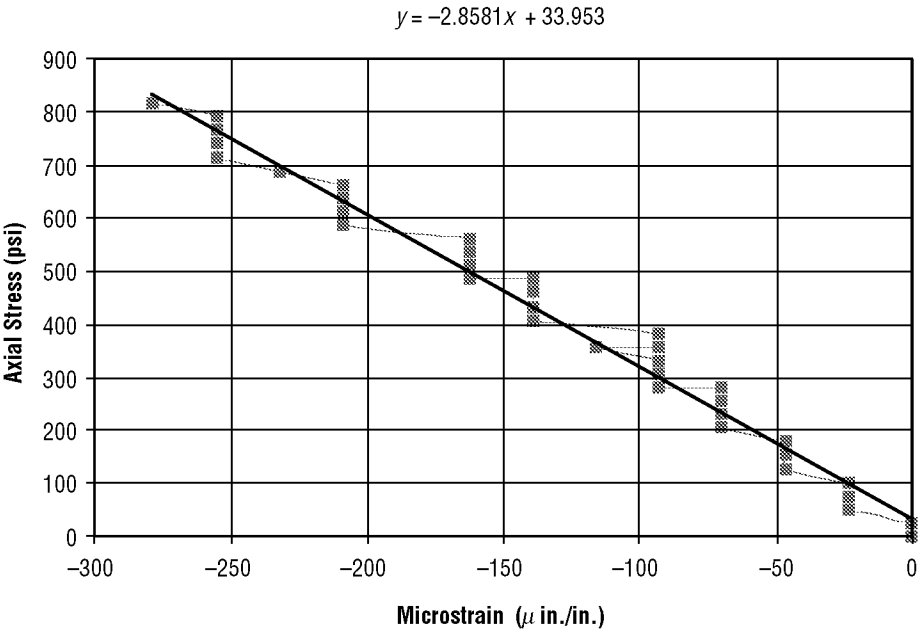

Figure B.6. Average transverse strain Dec_28_5.

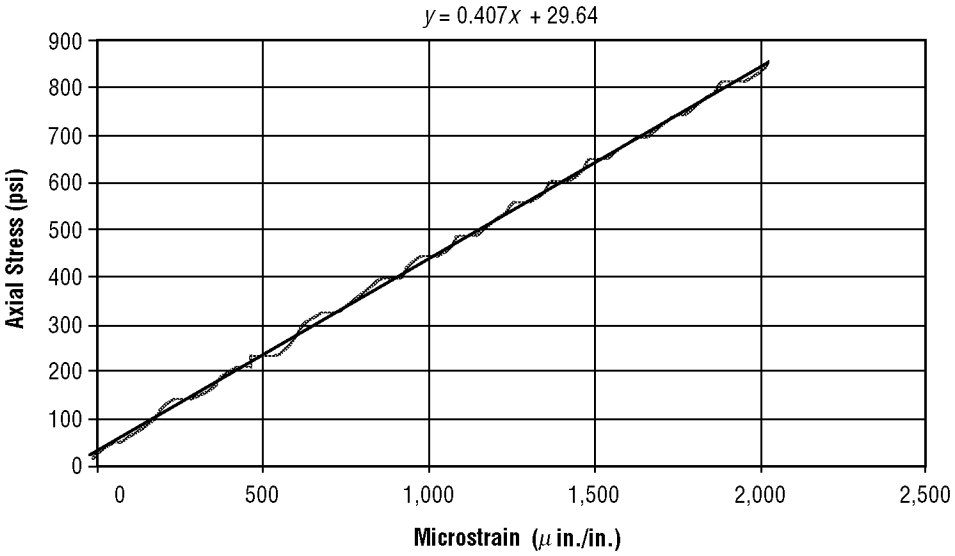

Figure B.7. Average tensile strain Dec_28_6.

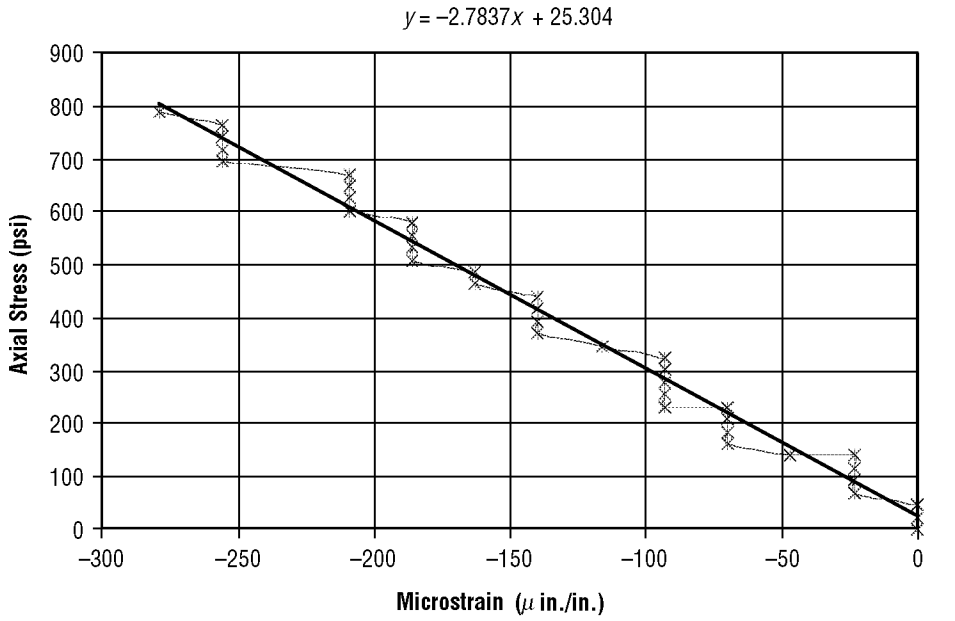

Figure B.8. Average transverse strain Dec_28_6.

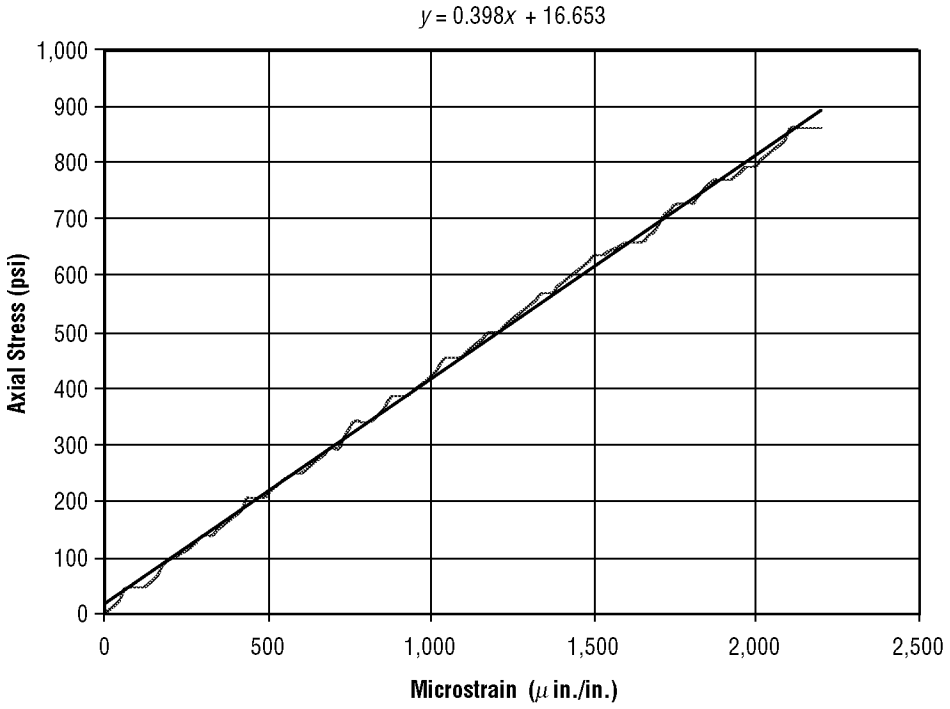

Figure B.9. Average tensile strain Dec_28_7.

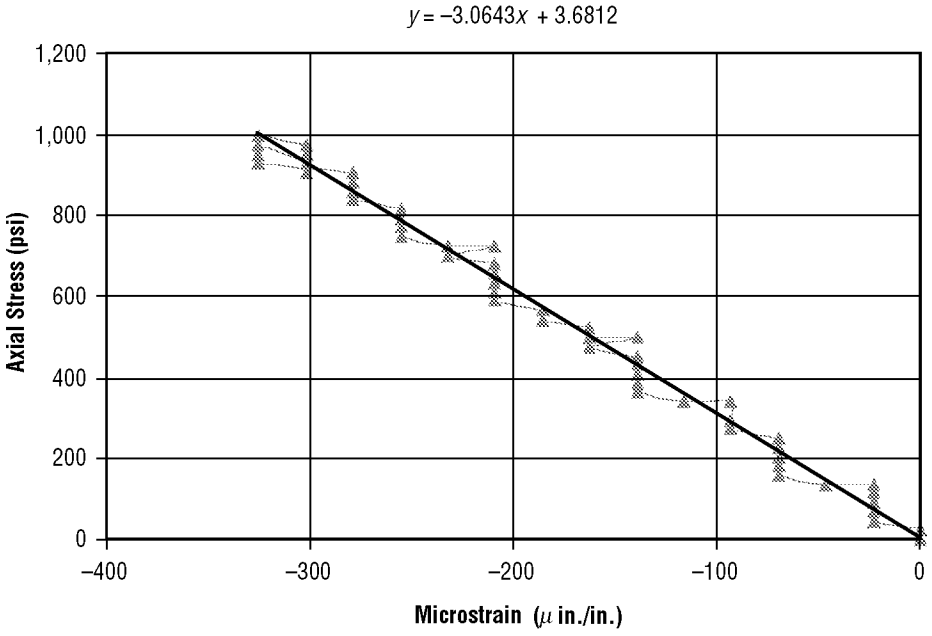

Figure B.10. Average transverse strain Dec_28_7.

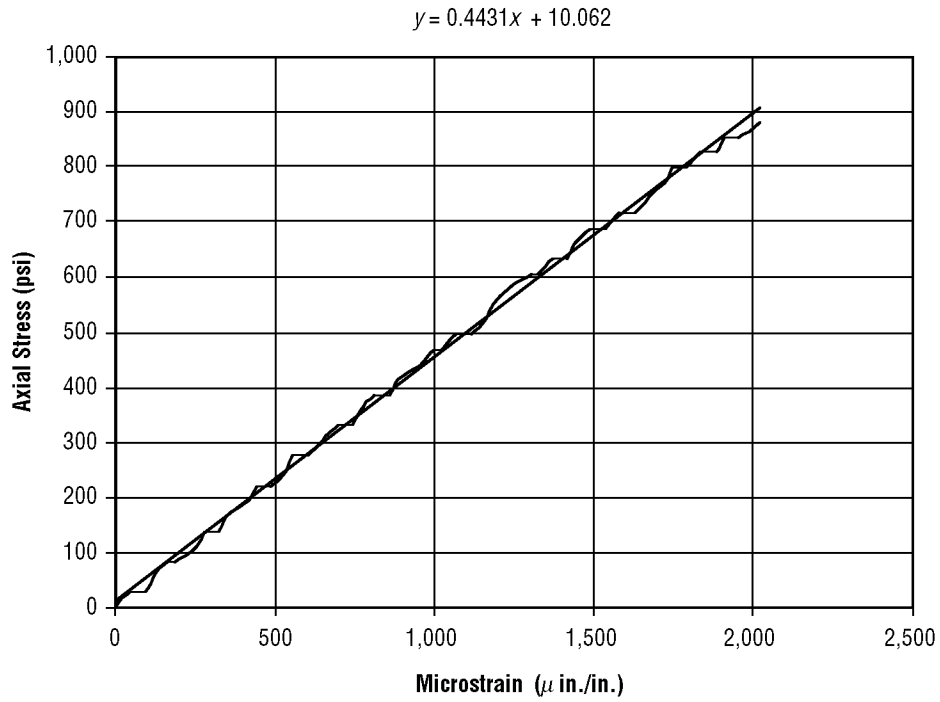

Figure B.11. Average tensile strain Dec_28_8.

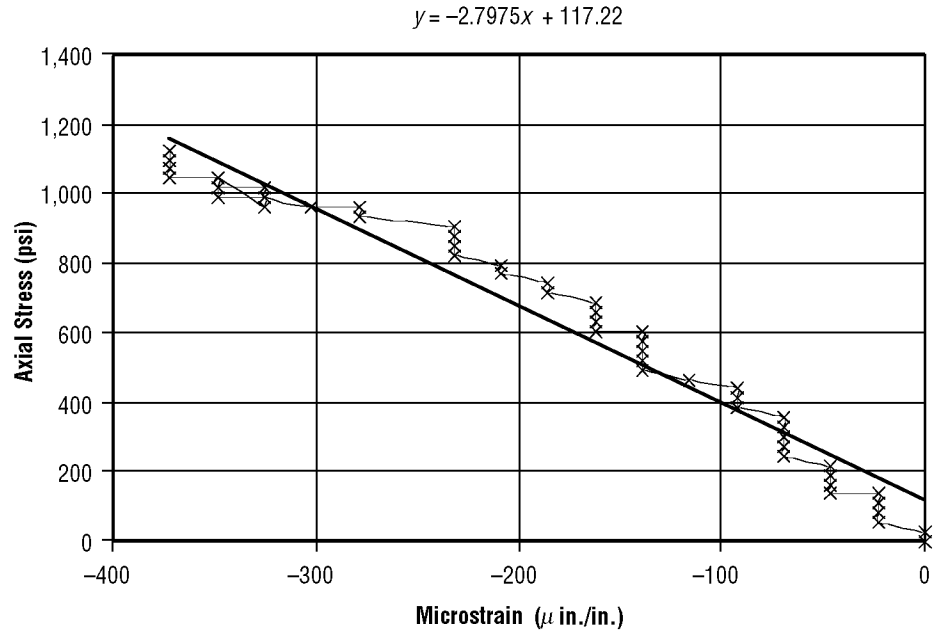

Figure B.12. Average transverse strain Dec_28_8.

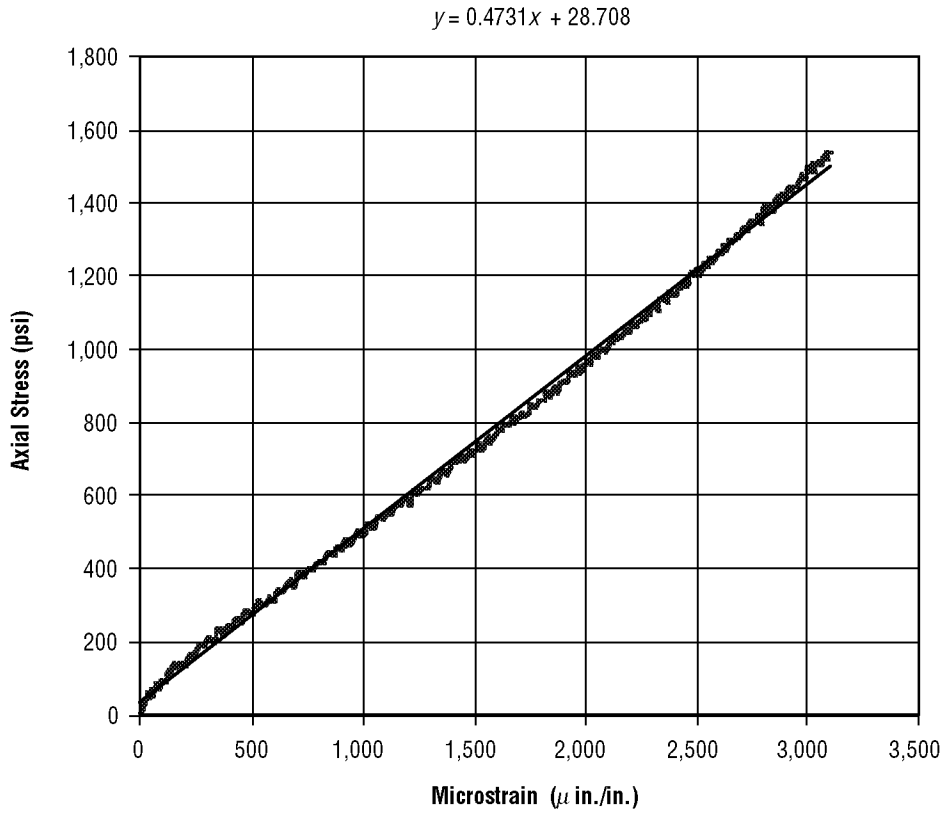

Figure B.13. Average tensile strain article SG4.

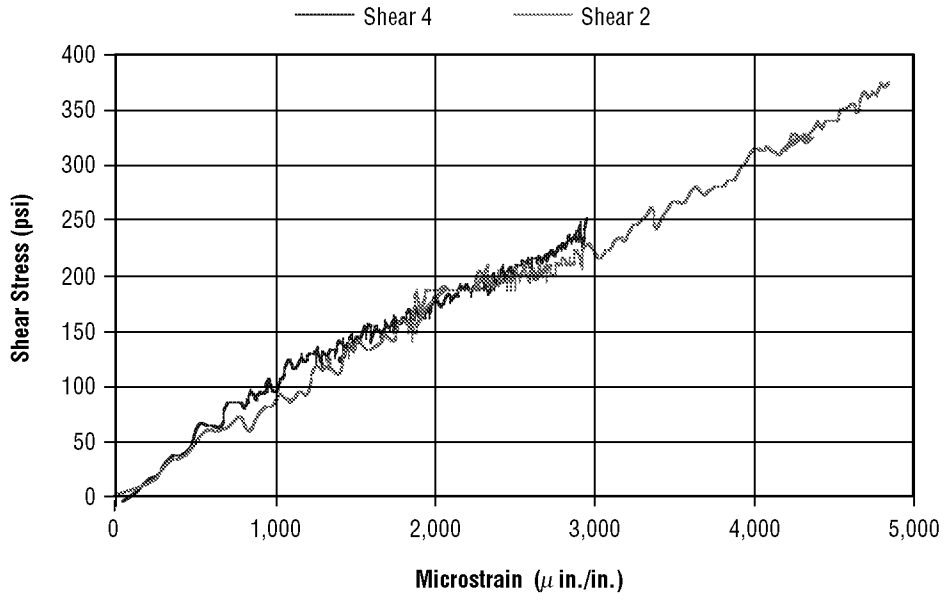

Figure B.14. Iosipescu shear test articles.

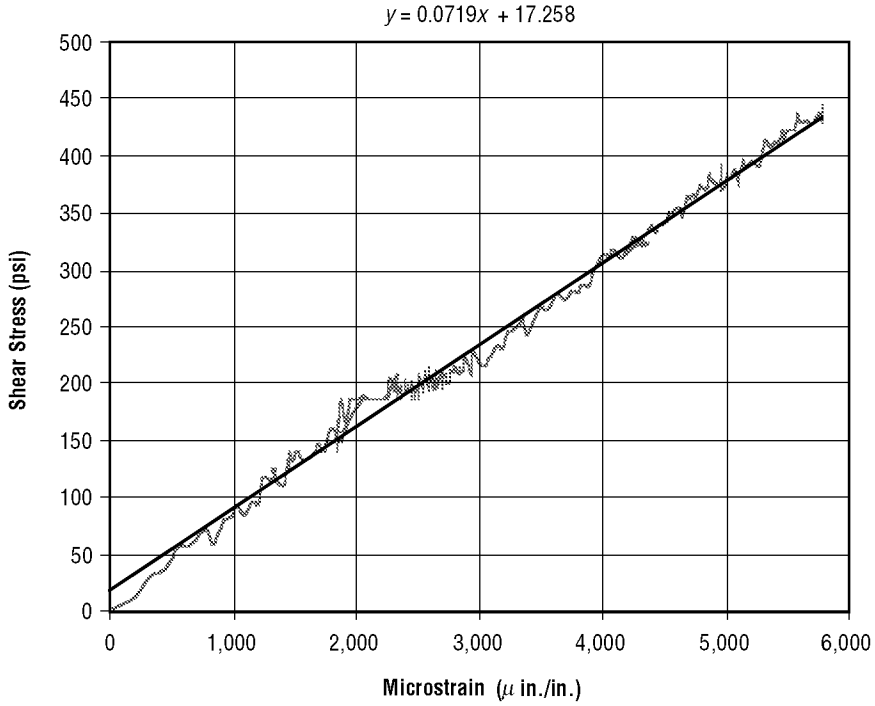

Figure B.15. Iosipescu shear test—article 2.

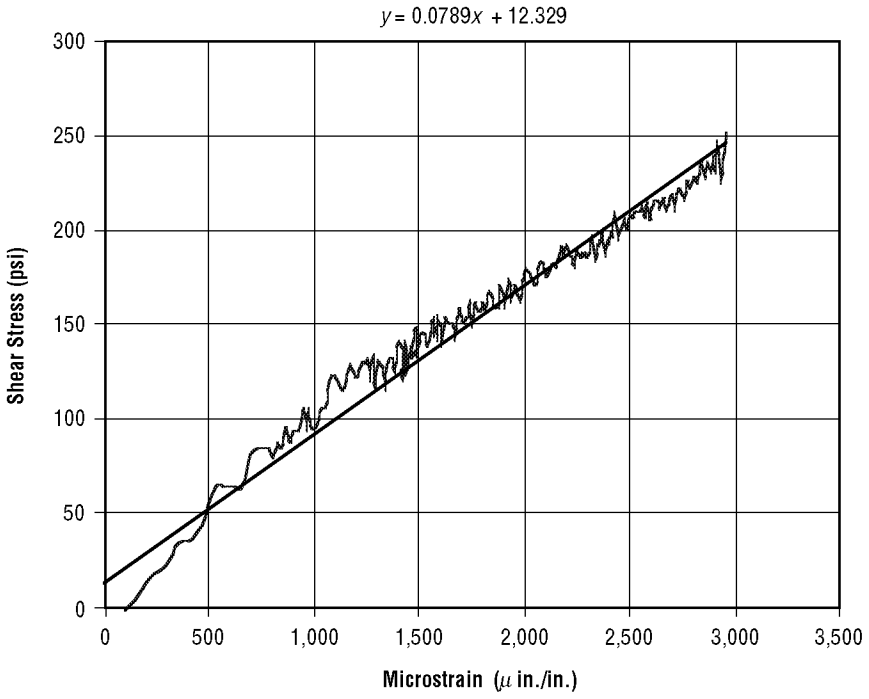

Figure B.16. Iosipescu shear test—article 4.

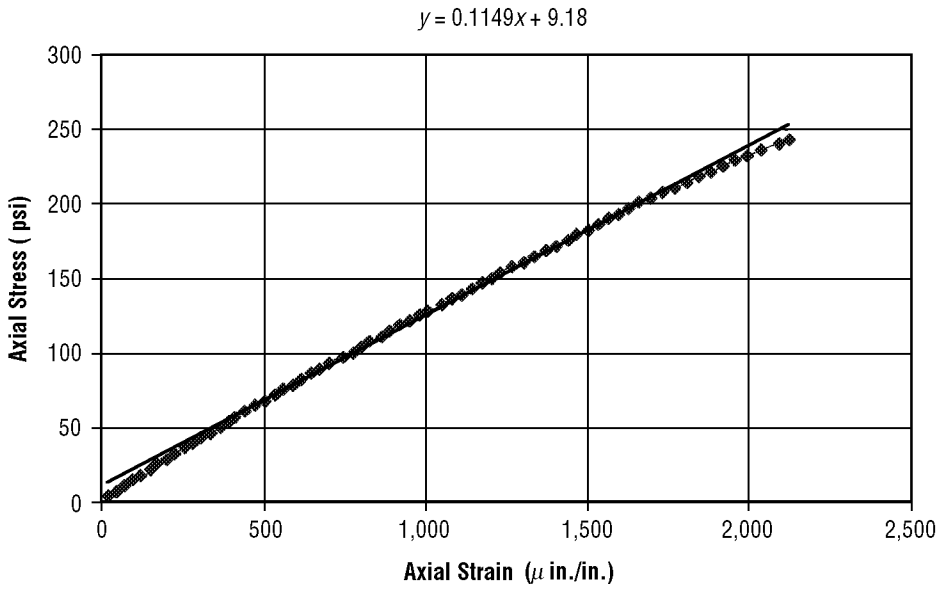

Figure B.17. Cementitious material tensile strain.

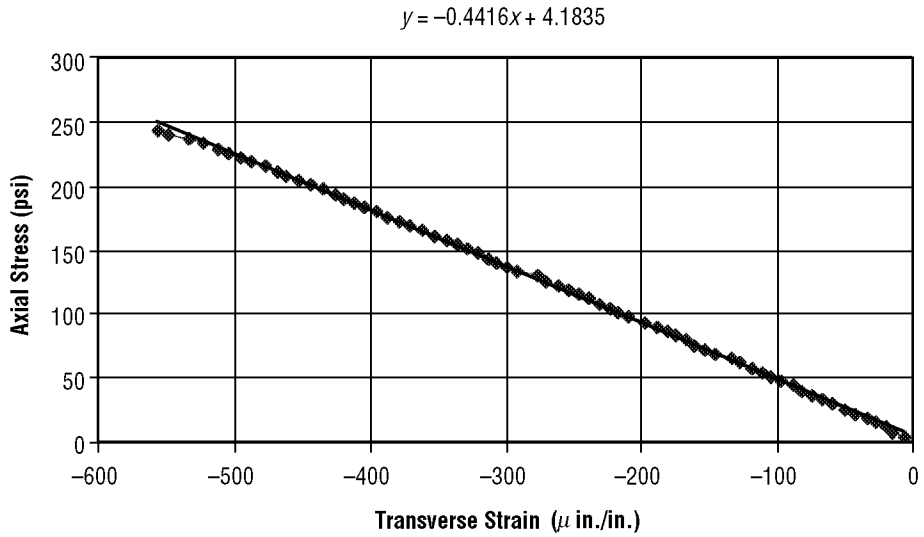

Figure B.18. Cementitious material transverse strain.

APPENDIX C—MATHCAD PROGRAM FOR COMPOSITE BEAM IN BENDING

Note: This program is provided as an example only. The content of this file is similar to that found in the text. However, this program is subject to modification and may not match the previous text.

C.1 Mathcad Solution Sheet: Calculate Deflection for Three-Section Bending Test—One Graphite-Reinforced Section on Top With Linear Material Properties

C.1.1 Calculate the Deflection for a Beam in Pure Bending

The rule of mixtures method for calculating the effective material properties for a composite beam will be verified by comparison to test data. A composite beam was made to the following dimensions:

- Graphite strands:

$$w_g := 1.20 \cdot in \qquad h_g := .115 \cdot in \ .$$

- Composite section:

$$h_c := .361 \cdot in - h_g \qquad w_c := 1.20 \cdot in \qquad h_c = 2.46 \times 10^{-1}\, in \ .$$

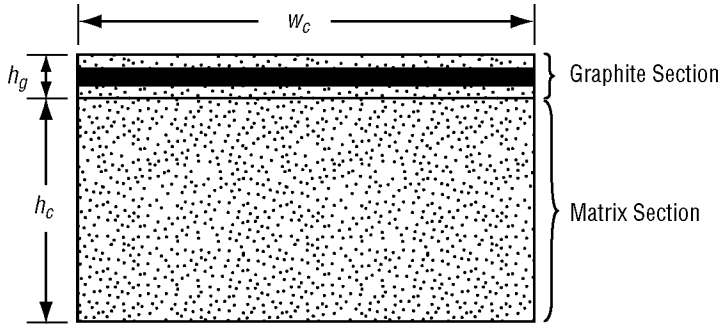

The fiber volume can be determined from the geometry of the test specimen. This test specimen has nine yarns across the width:

$$A_{yarn} := .000175 \cdot in^2 \qquad N_{yarn} := 9 \qquad A_{fiber} := N_{yarn} \cdot A_{yarn}$$

$$A_1 := .115 \cdot in \cdot 1.20 \cdot in \qquad V_{fiber} := \frac{A_{fiber}}{A_1} \qquad V_{fiber} = 1.141 \times 10^{-2} \ .$$

The volume fraction for the matrix:

$$V_{matrix} := 1 - V_{fiber} \qquad V_{matrix} = 9.886 \times 10^{-1} \ .$$

The material properties of the graphite and matrix are the same as previously defined:

$$E_{matrix} := 115 \cdot 10^3 \cdot \frac{lbf}{in^2} \qquad E_{fiber} := 33.5 \cdot 10^6 \cdot \frac{lbf}{in^2}$$

$$\nu_{matrix} := 0.27 \qquad \nu_{fiber} := 0.30$$

$$\rho_{matrix} := 35 \cdot \frac{lbf}{in^3} \qquad \rho_{fiber} := .064 \cdot \frac{lbf}{in^3}$$

$$G_{matrix} := \frac{E_{matrix}}{2 \cdot (1 + \nu_{matrix})} \qquad G_{fiber} := \frac{E_{fiber}}{2 \cdot (1 + \nu_{fiber})}$$

$$G_{matrix} = 4.528 \times 10^4 \frac{lbf}{in^2} \qquad G_{fiber} = 1.288 \times 10^7 \frac{lbf}{in^2} \ .$$

The effective material properties for the composite section of the beam can be calculated:

- Young's modulus in direction 1:

$$E_1 := V_{fiber} \cdot E_{fiber} + V_{matrix} \cdot E_{matrix}$$

$$E_1 = 4.9602 \times 10^5 \frac{lbf}{in^2} \ .$$

- Young's modulus in direction 2:

$$E_2 := \frac{E_{fiber} \cdot E_{matrix}}{V_{matrix} \cdot E_{fiber} + V_{fiber} \cdot E_{matrix}}$$

$$E_2 = 1.163 \times 10^5 \frac{lbf}{in^2} \ .$$

- Poisson's ratio:

$$\nu_{12} := \nu_{fiber} \cdot V_{fiber} + \nu_{matrix} \cdot V_{matrix}$$

$$\nu_{12} = 2.703 \times 10^{-1} \ .$$

- Shear modulus:

$$G_{12} := \frac{G_{matrix} \cdot G_{fiber}}{V_{matrix} \cdot G_{fiber} + V_{fiber} \cdot G_{matrix}}$$

$$G_{12} = 4.58 \times 10^{4} \frac{lbf}{in^2} .$$

- Composite density:

$$\rho_{composite} := \rho_{fiber} \cdot V_{fiber} + \rho_{matrix} \cdot V_{matrix}$$

$$\rho_{composite} = 3.46 \times 10^{1} \frac{lbf}{in^3} .$$

Now consider the composite beam composed of two homogenous materials. The top section of the beam is made from a material whose properties are calculated from the rule of mixtures. The remainder of the beam is made from the matrix material. The moment of inertia for the beam can now be calculated using the transform section method:

$$\eta := \frac{E_1}{E_{matrix}} .$$

- Ratio for transform section:

$$\eta = 4.313 .$$

- Transform section by multiplying the width of the graphite sections by η:

$$w_g := \eta \cdot w_g$$

$$w_g = 5.176\,in .$$

- Now calculate the centroid of the transformed section:

$$A_g := h_g \cdot w_g .$$

- Calculate the area of the top section:

$$y_g := h_c + \left(\frac{h_g}{2}\right) .$$

- Locate the centroid of the top section:

$$A_c := h_c \cdot w_c.$$

- Calculate the area of the matrix:

$$y_c := \frac{h_c}{2}.$$

- Calculate the centroid of the matrix:

$$Y_{bar} := \frac{A_g \cdot y_g + A_c \cdot y_c}{A_g + A_c}.$$

- Equation to find the centroid of the transform section:

$$Y_{bar} = 2.4366 \times 10^{-1}\,in \ .$$

C.1.2 The Centroid of the Transform Section

The cross section of the composite is symmetric in the *x* direction. The *x* location of the centroid is the center of the beam:

$$X_{bar} := \frac{w_c}{2} \qquad X_{bar} = 0.6\,in \ .$$

- Calculate the moment of inertia for the top section of the beam by using the parallel axis theorem:

$$b := w_g \quad \text{and} \quad h := h_g \ .$$

- Moment of inertia of the top section in respect to its centroid:

$$I_g := \frac{1}{12} \cdot b \cdot h^3 \ .$$

- Area of the top section:

$$A_g := b \cdot h \ .$$

- Distance from the center top section to the centroid of the section:

$$d := Y_{bar} - \left(h_c + \frac{h_g}{2}\right) .$$

- Applying the parallel axis theorem:

$$I_{g\_total} := I_g + A_g \cdot d^2 .$$

- Total moment of inertia for the top section with respect to the centroid of the entire beam:

$$I_{g\_total} = 2.7874 \times 10^{-3}\ in^4 .$$

Now, using the same methods, calculate the moment of inertia for the matrix (bottom) section of the beam:

$$b := w_c$$

and

$$h := h_c, \qquad I_c := \frac{1}{12} \cdot b \cdot h^3 .$$

- Area of the matrix:

$$A_c := b \cdot h .$$

- Distance from the center of the matrix section to the centroid of the section:

$$d := Y_{bar} - \left(\frac{h_c}{2}\right) .$$

- Moment of inertia for the matrix with respect to the centroid of the beam:

$$I_{c\_total} := I_c + A_c \cdot d^2$$

$$I_{c\_total} = 5.7864 \times 10^{-3}\ in^4 .$$

- Total moment of inertia for the transform section:

$$I_{total} := I_{c\_total} + I_{g\_total}$$

$$I_{total} = 8.5739 \times 10^{-3}\ in^4 .$$

The beam was then subjected to a three-section bending test. A rigorous analysis of the beam test was performed to establish a base of comparison to finite element modeling and test data. The comparison will provide insight into the accuracy of the methods used for the analysis.

- Free-body diagram of the beam:

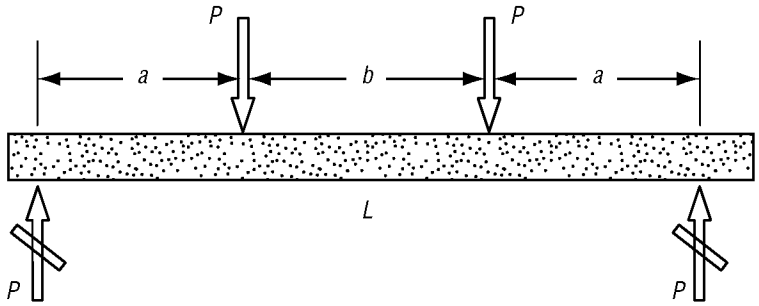

Derive the equation for the elastic curve from sum of the moment at x:

- Section 1, $x < a$:

$$E \cdot I \cdot \frac{d^2}{dx^2} y_1 = P \cdot x$$

$$E \cdot I \cdot \frac{d}{dx} y_1 = \frac{P}{2} \cdot x^2 + C_1$$

$$E \cdot I \cdot y_1 = \frac{P}{6} \cdot x^3 + C_1 \cdot x + C_2 \quad .$$

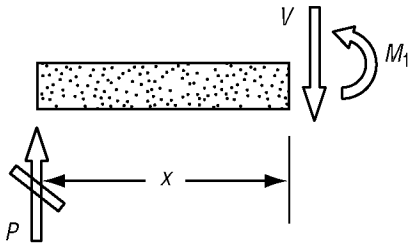

- Section 2, $x > a$ but $x < b$:

$$E \cdot I \cdot \frac{d^2}{dx^2} y_2 = P \cdot a$$

$$E \cdot I \cdot \frac{d}{dx} y_2 = P \cdot a \cdot x + C_3$$

$$E \cdot I \cdot y_2 = \frac{P}{2} \cdot a \cdot x^2 + C_3 \cdot x + C_4 \quad .$$

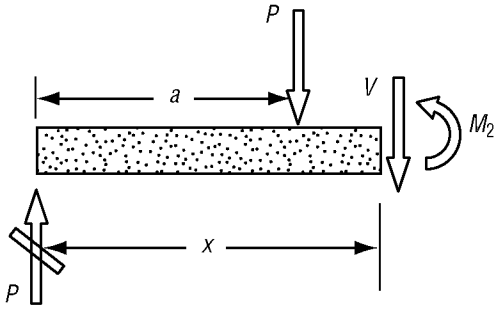

- Section 3, $x > (a + b)$:

$$E \cdot I \cdot \frac{d^2}{dx^2} y_3 = 2 \cdot P \cdot a + P \cdot b - P \cdot x$$

$$E \cdot I \cdot \frac{d}{dx} y_3 = 2 \cdot P \cdot a \cdot x + P \cdot b \cdot x - \frac{P}{2} \cdot x^2 + C_5$$

$$E \cdot I \cdot y_3 = P \cdot a \cdot x^2 + \frac{P}{2} \cdot b \cdot x^2 - \frac{P}{6} \cdot x^3 + C_5 \cdot x + C_6 \quad .$$

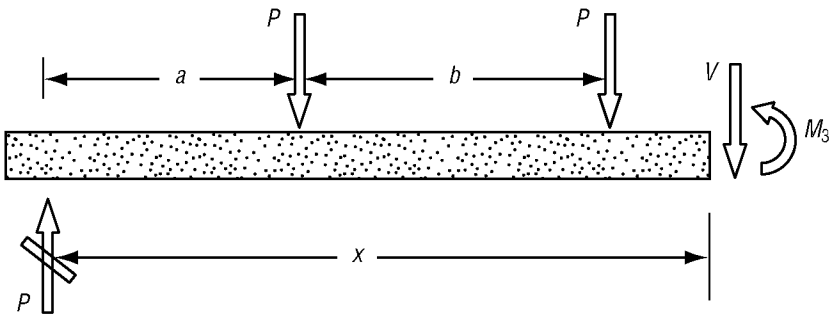

Summarize the equations. Replace the derivative with θ:

$$E \cdot I \cdot \theta_1 = \frac{P}{2} \cdot x^2 + C_1$$

$$E \cdot I \cdot \theta_2 = P \cdot a \cdot x + C_3$$

$$E \cdot I \cdot y_1 = \frac{P}{6} \cdot x^3 + C_1 \cdot x + C_2$$

$$E \cdot I \cdot y_2 = \frac{P}{2} \cdot a \cdot x^2 + C_3 \cdot x + C_4$$

$$E \cdot I \cdot \theta_3 = 2 \cdot P \cdot a \cdot x + P \cdot b \cdot x - \frac{P}{2} \cdot x^2 + C_5$$

$$E \cdot I \cdot y_3 = P \cdot a \cdot x^2 + \frac{P}{2} \cdot b \cdot x^2 - \frac{P}{6} \cdot x^3 + C_5 \cdot x + C_6 \quad .$$

Values from the test fixture and the test loads:

- Maximum load from 5/2/00 test:

$$Load := 50 \qquad P := .2207 \cdot lbf \cdot \frac{Load}{2} \quad .$$

- Geometry of the test fixture:

$$a := 3.0 \cdot in \qquad b := 2.75 \cdot in \qquad L := 8.75 \cdot in \quad .$$

- Input values to represent the boundary conditions:

$$x_1 := a \qquad x_2 := (a + b) \qquad x_3 := L$$

$$x_0 := 0.0 \cdot in \qquad x_1 = 3 \times 10^0\ in \qquad x_2 = 5.75 \times 10^0\ in \qquad x_3 = 8.75 \times 10^0\ in \quad .$$

- Guess values to start the program to solve for the constants:

$$C_1 := 1.0 \cdot lbf \cdot in^2 \qquad C_2 := 1.0 \cdot lbf \cdot in^3 \qquad C_3 := 1.0 \cdot lbf \cdot in^2$$

$$C_4 := 1.0 \cdot lbf \cdot in^3 \qquad C_5 := 1.0 \cdot lbf \cdot in^2 \qquad C_6 := 1.0 \cdot lbf \cdot in^3 \quad .$$

The elastic curve equations written to satisfy the boundary conditions:

- For the boundary condition $x = 0$, at $x = 0$, $y_1 = 0$:

$$0.0 \cdot lbf \cdot in^3 = \frac{P}{6} \cdot x_0^3 + C_1 \cdot x_0 + C_2 \quad .$$

- For the boundary condition $x = a$, at $x = a$ $y_1 = y_2$:

$$\frac{P}{6} \cdot x_1^3 + C_1 \cdot x_1 + C_2 = \frac{P}{2} \cdot a \cdot x_1^2 + C_3 \cdot x_1 + C_4$$

$$\frac{P}{2} \cdot x_1^2 + C_1 = P \cdot a \cdot x_1 + C_3 \quad .$$

- For the boundary condition $x = (a + b)$, at $x = a + b$ $y_2 = y_3$:

$$\frac{P}{2} \cdot a \cdot x_2^2 + C_3 \cdot x_2 + C_4 = P \cdot a \cdot x_2^2 + \frac{P}{2} \cdot b \cdot x_2^2 - \frac{P}{6} \cdot x_2^3 + C_5 \cdot x_2 + C_6$$

$$P \cdot a \cdot x_2 + C_3 = 2 \cdot P \cdot a \cdot x_2 + P \cdot b \cdot x_2 - \frac{P}{2} \cdot x_2^2 + C_5 \quad .$$

- For the boundary condition $x = L$, at $x = L$, $y_3 = 0$:

$$0.0 \cdot lbf \cdot in^3 = P \cdot a \cdot x_3^2 + \frac{P}{2} \cdot b \cdot x_3^2 - \frac{P}{6} \cdot x_3^3 + C_5 \cdot x_3 + C_6 \quad .$$

Find constants to solve the above equations simultaneously:

$$\begin{pmatrix} C_1 \\ C_2 \\ C_3 \\ C_4 \\ C_5 \\ C_6 \end{pmatrix} := \text{Find}(C_1, C_2, C_3, C_4, C_5, C_6) \ .$$

Ends the program loop.

The above equations are solved simultaneously to find the constants. The constants are listed below:

$$C_1 = -7.681 \times 10^{1}\ \text{lbf in}^2 \qquad C_2 = 0 \times 10^{0}\ \text{lbf in}^3 \qquad C_3 = -1.169 \times 10^{2}\ \text{lbf in}^2$$

$$C_5 = -2.641 \times 10^{2}\ \text{lbf in}^2 \qquad C_6 = 3.222 \times 10^{2}\ \text{lbf in}^3 \qquad C_4 = 4.007 \times 10^{1}\ \text{lbf in}^3 \ .$$

The value for the moment of inertia is set to the value calculated from the rule of mixtures and the transform section method. Young's modulus for the matrix is used for the beam equations:

$$I := I_{total} \qquad I = 8.574 \times 10^{-3}\ \text{in}^4$$

$$E := E_{matrix} \qquad E = 1.15 \times 10^{5}\ \frac{\text{lbf}}{\text{in}^2} \ .$$

Restate each elastic curve equation as a function of *x*:

- Section 1: $x < a$:

$$y_1(x) := \frac{1}{E \cdot I} \cdot \left(\frac{P}{6} \cdot x^3 + C_1 \cdot x + C_2 \right)$$

$$\theta_1(x) := \frac{1}{E \cdot I} \cdot \left(\frac{P}{2} \cdot x^2 + C_1 \right) \ .$$

- Section 2: $x > a$ but $< a + b$:

$$y_2(x) := \frac{1}{(E \cdot I)} \cdot \left(\frac{P}{2} \cdot a \cdot x^2 + C_3 \cdot x + C_4 \right)$$

$$\theta_2(x) := \frac{1}{E \cdot I} \left(P \cdot a \cdot x + C_3 \right) .$$

- Section 3, $x > a + b$:

$$\theta_3(x) := \frac{1}{E \cdot I} \cdot \left(2 \cdot P \cdot a \cdot x + P \cdot b \cdot x - \frac{P}{2} \cdot x^2 + C_5 \right)$$

$$y_3(x) := \frac{1}{E \cdot I} \cdot \left(P \cdot a \cdot x^2 + \frac{P}{2} \cdot b \cdot x^2 - \frac{P}{6} \cdot x^3 + C_5 \cdot x + C_6 \right) .$$

Check boundary conditions: $x = 0$ and $y_1 = 0$ and $y_1 = y_2$ at $x = a$:

$y_1(0.0 \cdot in) = 0 \times 10^{0}\ in$ $\quad$ $y_1(a) = -1.93 \times 10^{-1}\ in$ $\quad$ $\theta_1(a) = -3.725 \times 10^{-2}$

$y_2(a) = -1.93 \times 10^{-1}\ in$ $\quad$ $\theta_2(a) = -3.725 \times 10^{-2}$.

- If $x = a + b$, then $y_2 = y_3$:

$y_2(a + b) = -1.93 \times 10^{-1}\ in$ $\quad$ $\theta_2(a + b) = 3.725 \times 10^{-2}$

$y_3(a + b) = -1.93 \times 10^{-1}\ in$ $\quad$ $\theta_3(a + b) = 3.725 \times 10^{-2}$.

- If $x = L$, then $y_3 = 0$:

$$y_3(L) = 0 \times 10^{0}\ in .$$

C.2 Mathcad Solution Sheet: Calculate Deflection for Three-Section Bending Test—Three Graphite-Reinforced Sections With Nonlinear Material Properties

C.2.1 Determination of Transform Section Properties

Cross section of composite beam:

- Number of layers:

$$\psi := 5$$

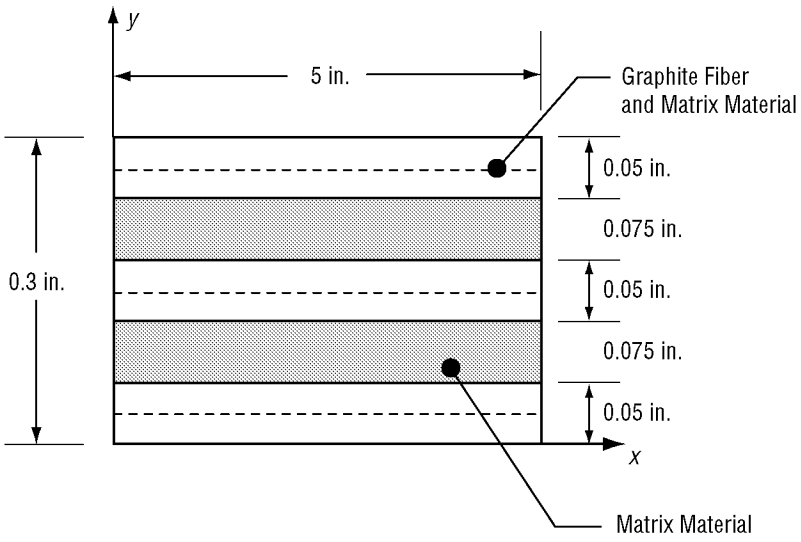

- Depth of each layer (bottom surface is zero):

$$D := \begin{pmatrix} .025 \\ .0875 \\ .150 \\ .2125 \\ .2750 \end{pmatrix} .$$

- Modulus for the graphite:

$$E_2 := 5.04 \cdot 10^5 .$$

- Modulus for the matrix

$$E_1 := 115 \cdot 10^3 .$$

- Ratio for transform section:

$$\eta := \frac{E_2}{E_1} \qquad \eta = 4.383 .$$

- Dimension of the composite section

$$h_c := .075 \qquad w_c := 5.00 \quad .$$

- Dimension of the graphite section:

$$h_g := .050 \qquad w_g := 5.00$$

$$w_g := \eta \cdot w_g \quad .$$

- Calculate the area of the fiber:

$$A_{fiber} := h_g \cdot (w_g) \quad .$$

- Calculate the area of the matrix:

$$A_{matrix} := h_c \cdot w_c \quad .$$

- Equation to find the centroid of the transform section:

$$Y_{bar} := \frac{\sum_{i=1}^{\psi} A_{map_i} \cdot D_i}{\sum_{i=1}^{\psi} A_{map_i}} \qquad A_{map} := \begin{pmatrix} A_{fiber} \\ A_{matrix} \\ A_{fiber} \\ A_{matrix} \\ A_{fiber} \end{pmatrix} \quad .$$

- Centroid of the transform section:

$$Y_{bar} = 1.5 \times 10^{-1} \quad .$$

- Moment of inertia of the transform section using the parallel axis theorem:

$$I := I_g + A_g \cdot d^2 \qquad I_g := \frac{1}{12} \cdot w_g \cdot h_g^3 \qquad I_c := \frac{1}{12} \cdot w_c \cdot h_c^3 \quad .$$

- Determine the distance from the center of the graphite to the centroid of the section:

$$\text{Layer\_d}(\psi) := \left| \begin{array}{l} \text{for } i \in 1..\psi \\ \quad d_i \leftarrow Y_{bar} - D_i \\ d \end{array} \right.$$

$$d := \text{Layer\_d}(\psi)$$

$$d = \begin{pmatrix} 0.125 \\ 0.063 \\ 0 \\ -0.063 \\ -0.125 \end{pmatrix} .$$

- Moment of inertia for each section:

$$I := I_g + A_g \cdot d^2$$

$$\text{Layer\_I} := \left| \begin{array}{l} \text{for } i \in 1,3,5 \\ \quad I_i \leftarrow I_g + A_{map_i} \cdot (d_i)^2 \\ \text{for } j \in 2,4 \\ \quad I_j \leftarrow I_c + A_{map_j} \cdot (d_j)^2 \\ I \end{array} \right.$$

$$I_{layer} := \text{Layer\_I}$$

$$I_{layer} = \begin{pmatrix} 0.017 \\ 0.002 \\ 0 \\ 0.002 \\ 0.017 \end{pmatrix} \qquad I_{total} := \sum_{i=1}^{\psi} I_{layer_i} .$$

- Moment of inertia of the five-layer composite:

$$I_{total} = 0.038 .$$

C.2.2 Calculate the Deflection for a Beam in Pure Bending—Consider the Nonlinear Nature of the Material Properties

Beam is in pure bending (no shear) in section b. Free-body diagram of the beam:

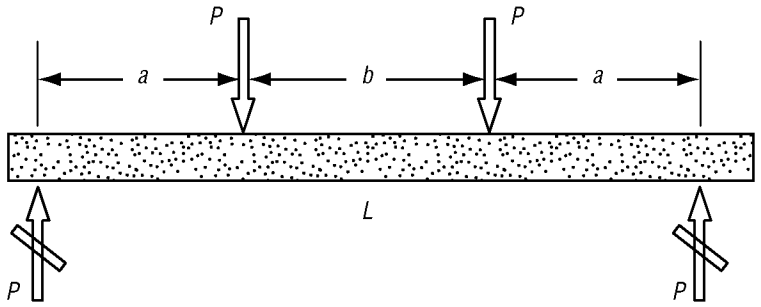

- Sample values from the test fixture and the test loads:

$t := 0.30 \cdot in$ Thickness of the beam

$P := \frac{Yload_{ln} \cdot lbf}{2}$ Load applied to beam .

- Geometry of the test fixture:

$a := 5.25 \cdot in \qquad b := 4.5 \cdot in \qquad L := 15.0 \cdot in$.

- Input values to represent the boundary conditions:

$x_1 := a \qquad x_2 := (a + b) \qquad x_3 := L$

$x_0 := 0.0 \cdot in \qquad x_1 = 5.25 \times 10^{0}\ in \qquad x_2 = 9.75 \times 10^{0}\ in \qquad x_3 = 1.5 \times 10^{1}\ in$.

- Guess values to start the program to solve for the constants:

$C_1 := 1.0 \cdot lbf \cdot in^2 \qquad C_2 := 1.0 \cdot lbf \cdot in^3 \qquad C_3 := 1.0 \cdot lbf \cdot in^2$

$C_4 := 1.0 \cdot lbf \cdot in^3 \qquad C_5 := 1.0 \cdot lbf \cdot in^2 \qquad C_6 := 1.0 \cdot lbf \cdot in^3$.

Following are the elastic curve equations written to satisfy the boundary conditions:

- For the boundary condition $x = 0$ and $y_1 = 0$,

$$0.0 \cdot lbf \cdot in^3 = \frac{P}{6} \cdot x_0^3 + C_1 \cdot x_0 + C_2 \ .$$

- For the boundary condition $x = a$; $y_1 = y_2$ and $\theta_1 = \theta_2$:

$$\frac{P}{6} \cdot x_1^3 + C_1 \cdot x_1 + C_2 = \frac{P}{2} \cdot a \cdot x_1^2 + C_3 \cdot x_1 + C_4$$

$$\frac{P}{2} \cdot x_1^2 + C_1 = P \cdot a \cdot x_1 + C_3 \ .$$

- For the boundary condition $x = (a + b)$; $y_2 = y_3$ and $\theta_1 = \theta_2$:

$$\frac{P}{2} \cdot a \cdot x_2^2 + C_3 \cdot x_2 + C_4 = P \cdot a \cdot x_2^2 + \frac{P}{2} \cdot b \cdot x_2^2 - \frac{P}{6} \cdot x_2^3 + C_5 \cdot x_2 + C_6$$

$$P \cdot a \cdot x_2 + C_3 = 2 \cdot P \cdot a \cdot x_2 + P \cdot b \cdot x_2 - \frac{P}{2} \cdot x_2^2 + C_5 \ .$$

- For the boundary condition $x = L$; $y_3 = 0$:

$$0.0 \cdot lbf \cdot in^3 = P \cdot a \cdot x_3^2 + \frac{P}{2} \cdot b \cdot x_3^2 - \frac{P}{6} \cdot x_3^3 + C_5 \cdot x_3 + C_6 \ .$$

Find constants to solve the above equations simultaneously:

$$\begin{pmatrix} C_1 \\ C_2 \\ C_3 \\ C_4 \\ C_5 \\ C_6 \end{pmatrix} := \text{Find}(C_1, C_2, C_3, C_4, C_5, C_6) \ .$$

Ends the program loop.

Now compare these equations with actual test results:

- Values used in the beam equations:

$$E = 115 \times 10^{3} \frac{lbf}{in^{2}} \qquad I = 3.8 \times 10^{-2} in^{4} \quad .$$

The load is applied by hanging weight centered in the 'b' section:

$$Test\_load := P \cdot 2 \quad .$$

Deflection data at the center of the 15-in. beam (x = 7.5 in.) :

$$y_2(7.5 \cdot in) = -8.01449 \times 10^{-1} in$$

$$Test\_load = 5.67 \times 10^{1} lbf \quad .$$

Now repeat above analysis at each load step. *Y*load is the load data supplied to the elastic beam equation:

$$Yload \equiv \begin{pmatrix} 0 \\ 6.5 \\ 9.1 \\ 11.8 \\ 14.4 \\ 17.9 \\ 25.0 \\ 32.0 \\ 40.9 \\ 48.8 \\ 56.7 \\ 64.6 \\ 75.1 \end{pmatrix} \quad .$$

The deflection calculated by the elastic beam equation is contained in y_{cal}:

$$y_{cal} := \begin{pmatrix} 0 \\ .092 \\ .129 \\ .167 \\ .203 \\ .254 \\ .354 \\ .452 \\ .578 \\ .690 \\ .801 \\ .913 \\ 1.06 \end{pmatrix}$$

This Excel file contains the test data for the five-layer composite beam in bending (the UAH canoe team supplied the test data):

$$k := 2,3..89$$

$$Test\_Data :=$$

Worksheet

The test data is compared to the results of the analysis.

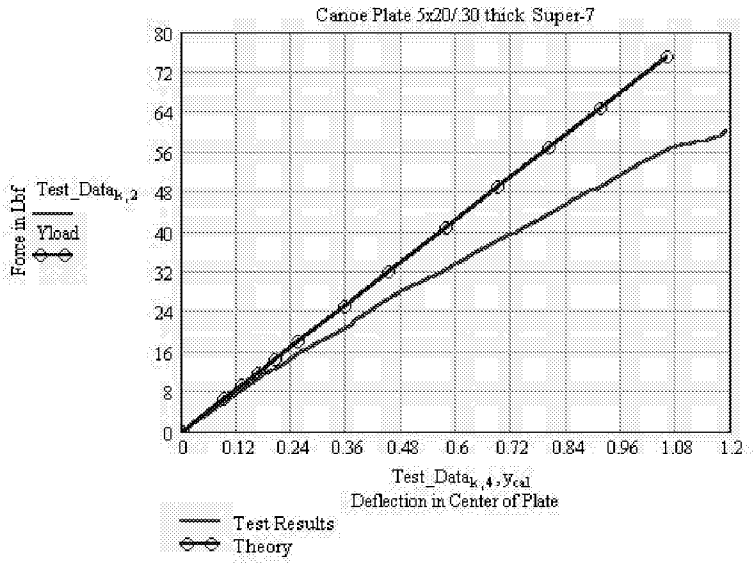

This Excel file contains the results of tensile test specimens. These data will allow the program to consider the nonlinear properties of matrix material (tension).

Test2 :=

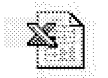

Worksheet

$m := 2,3..69$

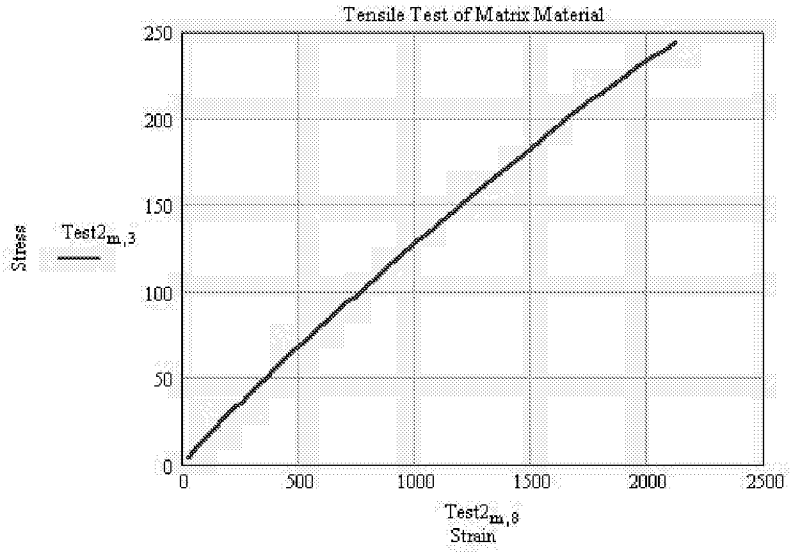

- Assign values to stress and strain data matrix:

$$\sigma_{concrete_m} := Test2_{m,3} \qquad \varepsilon_{concrete_m} := Test2_{m,8} \ .$$

- Guess values to initialize the program:

$$b_0 := 1 \qquad b_1 := 1 \qquad b_2 := 1 \qquad n := 69 \ .$$

Use Balaguru's methods[2] (least-squares methods):

Given

$$b_0 \cdot n + b_1 \cdot \sum_{i=1}^{n} \sigma_{concrete_i} + b_2 \cdot \sum_{i=1}^{n} \left(\sigma_{concrete_i}\right)^2 = \sum_{i=1}^{n} \varepsilon_{concrete_i}$$

$$b_0 \cdot \sum_{i=1}^{n} \sigma_{concrete_i} + b_1 \cdot \sum_{i=1}^{n} \left(\sigma_{concrete_i}\right)^2 + b_2 \cdot \sum_{i=1}^{n} \left(\sigma_{concrete_i}\right)^3 = \sum_{i=1}^{n} \sigma_{concrete_i} \cdot \varepsilon_{concrete_i}$$

$$b_0 \cdot \sum_{i=1}^{n} \left(\sigma_{concrete_i}\right)^2 + b_1 \cdot \sum_{i=1}^{n} \left(\sigma_{concrete_i}\right)^3 + b_2 \cdot \sum_{i=1}^{n} \left(\sigma_{concrete_i}\right)^4 = \sum_{i=1}^{n} \left[\left(\sigma_{concrete_i}\right)^2 \cdot \varepsilon_{concrete_i}\right] .$$

- Find the minimum solution to the simultaneous equations:

$$\begin{pmatrix} b_0 \\ b_1 \\ b_2 \end{pmatrix} := \text{Minerr}(b_0, b_1, b_2) .$$

- The equation for strain from the resulting values:

$$\varphi := b_0 + b_1 \cdot \sigma_{concrete} + b_2 \cdot \sigma_{concrete}^2 .$$

Compare the results of the derivation with the actual test data.

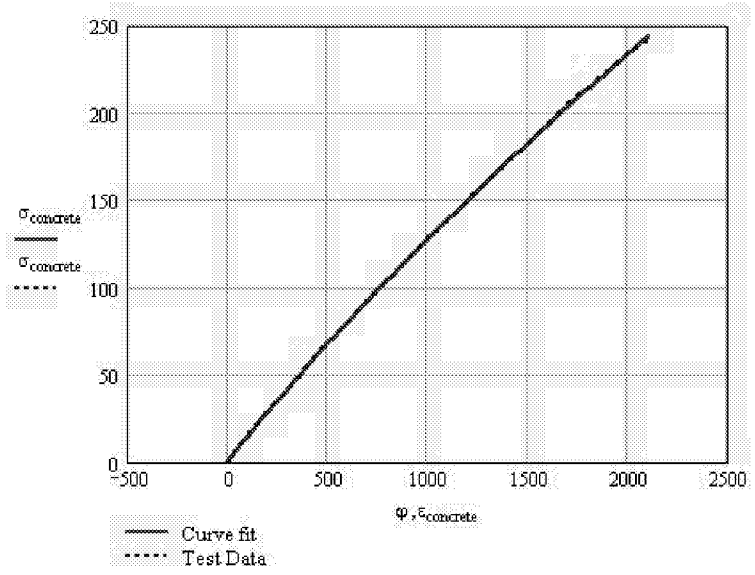

Now, increase the stress to levels exceeding the tension test:

- Stress equation:

$$\sigma(7.5 \cdot \text{in}) = 5.87516 \times 10^{2} \frac{\text{lbf}}{\text{in}^2} \quad .$$

Assume the stress ξ varies from 225 to 800 in increments of 25:

$$\xi := 225, 250 .. 800 \quad .$$

- Equation for the 'simulated' stress values:

$$\varepsilon(\xi) := b_0 + b_1 \cdot \xi + b_2 \cdot \xi^2 \quad .$$

Plot the simulated stress and the results from the tensile test. The simulated stress projects the curve to higher strain values:

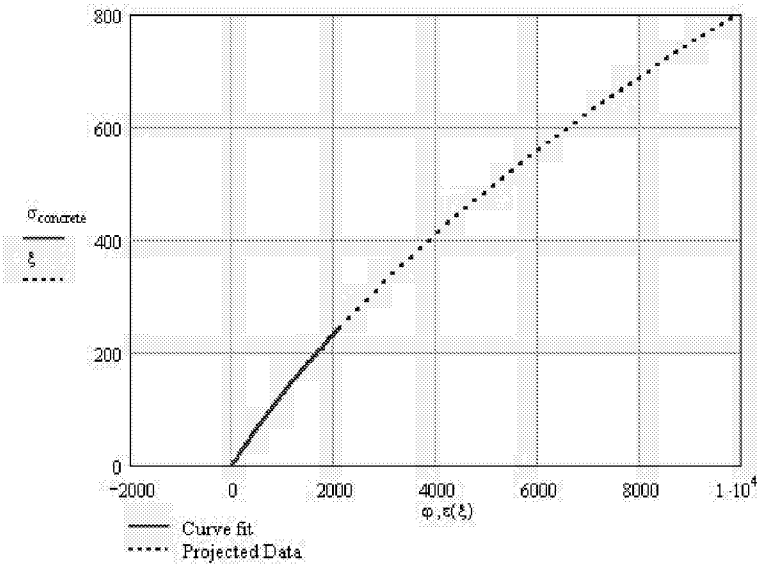

- Young's modulus for the matrix changes from E to E_r as the stress increases to 800:

$$E = 1.15 \times 10^{5} \frac{\text{lbf}}{\text{in}^2} \qquad \Phi := 800 \qquad E_r := \frac{\Phi}{\varepsilon(\Phi) \cdot 10^{-6}} \qquad E_r = 8.07035 \times 10^{4} \quad .$$

- In section 2 for the elastic beam equation, $x > a$ but $< a + b$:

$$Yload_{ln} = 56.7 \qquad x := 7.5 \cdot in \quad .$$

The beam equation has been modified to calculate the deflection at stress levels above the linear range of the material:

$$y2(x,\Phi) := \frac{1}{\left(if\left(\Phi > 250, \frac{\Phi}{\varepsilon(\Phi)\cdot 10^{-6}}, 115000\right)\cdot\frac{lbf}{in^2}\cdot I\right)}\cdot\left(\frac{P}{2}\cdot a\cdot x^2 + C_3\cdot x + C_4\right)$$

$$y2\left(7.5\cdot in, 4.23799\times 10^2\right) = -0.90774\,in \quad .$$

The deflection is calculated at increasing load levels:

$$Ycal\_2 := \begin{pmatrix} 0 \\ 0.092 \\ 0.129 \\ 0.167 \\ 0.203 \\ 0.254 \\ 0.3547 \\ .479 \\ .655 \\ .825 \\ 1.009 \\ 1.21 \\ 1.49 \end{pmatrix} .$$

Compare the results of the analysis with the results of the canoe panel-bending test:

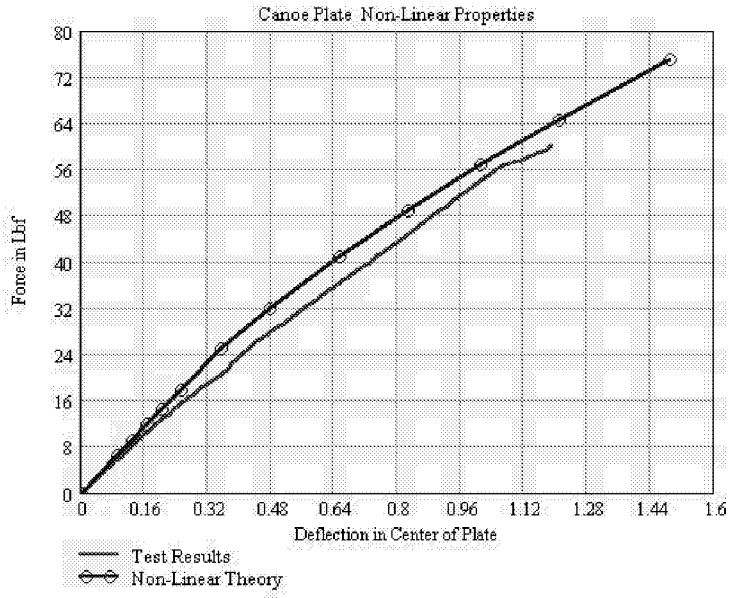

The analysis is repeated for the properties from compression testing of the cementitious material.

This Excel file contains data from compression cylinder testing of the cementitious material:

$$\text{Test\_Comp} :=$$

Worksheet

$$i := 2,3 .. 50$$

- Equation to calculate the compressive Young's modulus:

$$E_{comp} := \frac{\text{Test\_Comp}_{kj,6}}{\text{Test\_Comp}_{kj,5} \cdot 10^{-6}} \quad .$$

- The highest value is at $kj = 44$:

$$E_{comp} = 8.12316 \times 10^{4} \quad .$$

The beam equation has been modified to calculate the deflection at stress levels above the linear range of the material:

$$x := 7.5 \cdot in$$

$$y_2(x, E_{comp}) := \frac{1}{\left(E_{comp} \cdot \frac{lbf}{in^2} \cdot I\right)} \cdot \left(\frac{P}{2} \cdot a \cdot x^2 + C_3 \cdot x + C_4\right) \quad .$$

- Sample calculation at maximum load value:

$$y_2\left(7.5\cdot in, 7.29676\times 10^{4}\right) = -1.26312\,in \quad .$$

The results of the analysis are listed in y_{cal}_3:

$$y_{cal\_3} := \begin{pmatrix} 0 \\ 0.092 \\ 0.129 \\ 0.167 \\ 0.203 \\ .264 \\ .389 \\ .524 \\ .731 \\ .976 \\ 1.26 \end{pmatrix} .$$

The results using the compressive data compare very well to both the canoe panel data and the results from using the projected tensile.

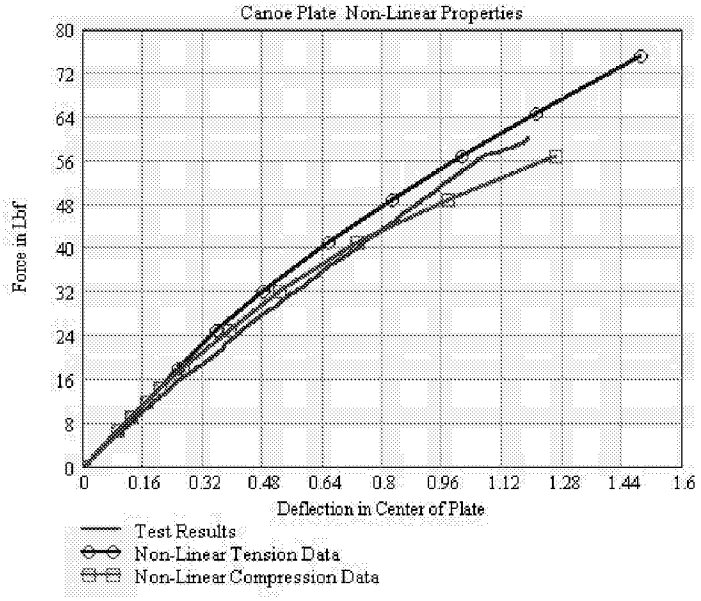

APPENDIX D—MATHCAD SOLUTION SHEET: LAMINATED COMPOSITE PLATES—SYMMETRIC AND NONSYMMETRIC SOLUTIONS

Note: This program is provided as an example only. The content of this file is similar to that found in the text. However, this program is subject to modification and may not match the previous text.

D.1 Calculation of Effective Material Properties

It should be noted that for laminates that are symmetric about the midplane; i.e., the layers above the midplane are identical to the layers below the midplane, the B matrix will be zero. In the case of symmetric laminates, the equations for the effective properties can be greatly reduced. However, for the purposes of this analysis, the case of the nonsymmetric laminates will be considered:

$$\begin{pmatrix} N_x \\ N_y \\ N_{xy} \\ M_x \\ M_y \\ M_{xy} \end{pmatrix} = \begin{pmatrix} A_{11} & A_{12} & A_{13} & B_{11} & B_{12} & B_{13} \\ A_{21} & A_{22} & A_{23} & B_{21} & B_{22} & B_{23} \\ A_{31} & A_{32} & A_{33} & B_{31} & B_{32} & B_{33} \\ B_{11} & B_{12} & B_{13} & D_{11} & D_{12} & D_{13} \\ B_{21} & B_{22} & B_{23} & D_{21} & D_{22} & D_{23} \\ B_{31} & B_{32} & B_{33} & D_{31} & D_{32} & D_{33} \end{pmatrix} \cdot \begin{pmatrix} \varepsilon_{0x} \\ \varepsilon_{0Y} \\ \gamma_{0xy} \\ K_x \\ K_y \\ K_{xy} \end{pmatrix}$$

This relationship is a system of six equations and six unknowns. The midplane strains and curvatures are the unknowns. The A, B, and D terms are derived previously and are now constants. The force and moment matrix can be defined to determine the effective material properties for the composite:

$$\begin{pmatrix} N_x \\ N_y \\ N_{xy} \\ M_x \\ M_y \\ M_{xy} \end{pmatrix} = \begin{pmatrix} A_{11}\cdot\varepsilon_{0x} + A_{12}\cdot\varepsilon_{0Y} + A_{13}\cdot\gamma_{0xy} + B_{11}\cdot K_x + B_{12}\cdot K_y + B_{13}\cdot K_{xy} \\ A_{21}\cdot\varepsilon_{0x} + A_{22}\cdot\varepsilon_{0Y} + A_{23}\cdot\gamma_{0xy} + B_{21}\cdot K_x + B_{22}\cdot K_y + B_{23}\cdot K_{xy} \\ A_{31}\cdot\varepsilon_{0x} + A_{32}\cdot\varepsilon_{0Y} + A_{33}\cdot\gamma_{0xy} + B_{31}\cdot K_x + B_{32}\cdot K_y + B_{33}\cdot K_{xy} \\ B_{11}\cdot\varepsilon_{0x} + B_{12}\cdot\varepsilon_{0Y} + B_{13}\cdot\gamma_{0xy} + D_{11}\cdot K_x + D_{12}\cdot K_y + D_{13}\cdot K_{xy} \\ B_{21}\cdot\varepsilon_{0x} + B_{22}\cdot\varepsilon_{0Y} + B_{23}\cdot\gamma_{0xy} + D_{21}\cdot K_x + D_{22}\cdot K_y + D_{23}\cdot K_{xy} \\ B_{31}\cdot\varepsilon_{0x} + B_{32}\cdot\varepsilon_{0Y} + B_{33}\cdot\gamma_{0xy} + D_{31}\cdot K_x + D_{32}\cdot K_y + D_{33}\cdot K_{xy} \end{pmatrix}$$

The solution to this system of equations can best be demonstrated through an example problem. The calculations for this problem will be made in a Mathcad Pro 2000 program file. Consider a laminated plate made of four layers of fiber-reinforced material. The angle of the reinforcements is 0° and 45° and each layer is 0.005 in. thick.

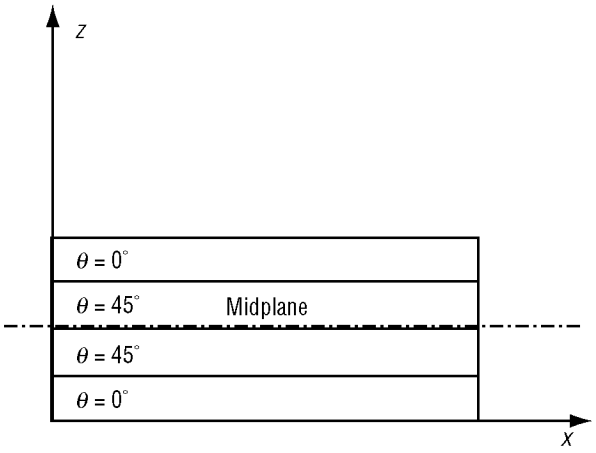

- Material constants are obtained by tensile and shear testing of the material:

$$E_1 := 20.01 \cdot 10^6 \cdot \frac{lbf}{in^2} \quad .$$

- Young's modulus in the principal material direction 1:

$$E_2 := 1.301 \cdot 10^6 \cdot \frac{lbf}{in^2} \quad .$$

- Young's modulus in the principal material direction 2:

$$G_{12} := 1.001 \cdot 10^6 \cdot \frac{lbf}{in^2} \quad .$$

- Shear modulus in the principal material direction 12:

$$\nu_{12} := 0.30 \quad .$$

- Poisson's ratio:

$$\nu_{21} := \frac{\nu_{12} \cdot E_2}{E_1} \quad .$$

These properties are used to determine the compliance matrix:

$$S := \begin{pmatrix} \frac{1}{E_1} & \frac{-\nu 12}{E_1} & 0 \\ \frac{-\nu 21}{E_2} & \frac{1}{E_2} & 0 \\ 0 & 0 & \frac{1}{G_{12}} \end{pmatrix}$$

$$S = \begin{pmatrix} 4.998 \times 10^{-8} & -1.499 \times 10^{-8} & 0 \times 10^{0} \\ -1.499 \times 10^{-8} & 7.686 \times 10^{-7} & 0 \times 10^{0} \\ 0 \times 10^{0} & 0 \times 10^{0} & 9.99 \times 10^{-7} \end{pmatrix} \frac{in^2}{lbf} \quad .$$

The stiffness matrix is formed from the inverse of the compliance matrix:

$$Q := S^{-1}$$

$$Q = \begin{pmatrix} 2.013 \times 10^{7} & 3.926 \times 10^{5} & 0 \\ 3.926 \times 10^{5} & 1.309 \times 10^{6} & 0 \\ 0 & 0 & 1.001 \times 10^{6} \end{pmatrix} \frac{lbf}{in^2} \quad .$$

Geometry of the layup is then used to determine the transformation matrix:

$plys := 4$ $\qquad$ $n := 1..plys$

Ply thickness $\qquad$ Ply angles

$$t := \begin{pmatrix} .005 \\ .005 \\ .005 \\ .005 \end{pmatrix} in \qquad \theta := \frac{\pi}{180} \cdot \begin{pmatrix} 0 \\ 45 \\ 45 \\ 0 \end{pmatrix} .$$

The center of each ply must be located:

$$z := \begin{bmatrix} t_1 + \frac{t_2}{2} \\ \frac{t_1}{2} \\ \frac{-t_3}{2} \\ -\left(t_3 + \frac{t_4}{2}\right) \end{bmatrix}.$$

The transformation matrix is derived from the stress transformation equations:

$$T_n := \begin{pmatrix} \cos(\theta_n)^2 & \sin(\theta_n)^2 & 2\cdot\sin(\theta_n)\cdot\cos(\theta_n) \\ \sin(\theta_n)^2 & \cos(\theta_n)^2 & -2\cdot\sin(\theta_n)\cdot\cos(\theta_n) \\ -\sin(\theta_n)\cdot\cos(\theta_n) & \sin(\theta_n)\cdot\cos(\theta_n) & \cos(\theta_n)^2 - \sin(\theta_n)^2 \end{pmatrix}$$

$$T_1 = \begin{pmatrix} 1\times10^{0} & 0\times10^{0} & 0\times10^{0} \\ 0\times10^{0} & 1\times10^{0} & 0\times10^{0} \\ 0\times10^{0} & 0\times10^{0} & 1\times10^{0} \end{pmatrix}$$

$$T_2 = \begin{pmatrix} 5\times10^{-1} & 5\times10^{-1} & 1\times10^{0} \\ 5\times10^{-1} & 5\times10^{-1} & -1\times10^{0} \\ -5\times10^{-1} & 5\times10^{-1} & 0\times10^{0} \end{pmatrix}$$

$$T_3 = \begin{pmatrix} 5\times10^{-1} & 5\times10^{-1} & 1\times10^{0} \\ 5\times10^{-1} & 5\times10^{-1} & -1\times10^{0} \\ -5\times10^{-1} & 5\times10^{-1} & 0\times10^{0} \end{pmatrix}$$

$$T_4 = \begin{pmatrix} 1 \times 10^0 & 0 \times 10^0 & 0 \times 10^0 \\ 0 \times 10^0 & 1 \times 10^0 & 0 \times 10^0 \\ 0 \times 10^0 & 0 \times 10^0 & 1 \times 10^0 \end{pmatrix} .$$

- Reuter's matrix:

$$R := \begin{pmatrix} 1 & 0 & 0 \\ 0 & 1 & 0 \\ 0 & 0 & 2 \end{pmatrix} .$$

The Qbar matrix represents the stiffness and transform matrix:

$$Qbar_n := \left(T_n\right)^{-1} \cdot Q \cdot R \cdot T_n \cdot R^{-1} .$$

Each ply has a Qbar matrix:

$$Qbar_1 = \begin{pmatrix} 2.01 \times 10^7 & 3.93 \times 10^5 & 0 \\ 3.93 \times 10^5 & 1.31 \times 10^6 & 0 \\ 0 & 0 & 1 \times 10^6 \end{pmatrix} \frac{lbf}{in^2}$$

$$Qbar_2 = \begin{pmatrix} 6.56 \times 10^6 & 4.55 \times 10^6 & 4.7 \times 10^6 \\ 4.55 \times 10^6 & 6.56 \times 10^6 & 4.7 \times 10^6 \\ 4.7 \times 10^6 & 4.7 \times 10^6 & 5.16 \times 10^6 \end{pmatrix} \frac{lbf}{in^2}$$

$$Qbar_3 = \begin{pmatrix} 6.56 \times 10^6 & 4.55 \times 10^6 & 4.7 \times 10^6 \\ 4.55 \times 10^6 & 6.56 \times 10^6 & 4.7 \times 10^6 \\ 4.7 \times 10^6 & 4.7 \times 10^6 & 5.16 \times 10^6 \end{pmatrix} \frac{lbf}{in^2}$$

$$Qbar_4 = \begin{pmatrix} 2.01 \times 10^7 & 3.93 \times 10^5 & 0 \times 10^0 \\ 3.93 \times 10^5 & 1.31 \times 10^6 & 0 \times 10^0 \\ 0 \times 10^0 & 0 \times 10^0 & 1 \times 10^6 \end{pmatrix} \frac{lbf}{in^2} .$$

- Calculate the total thickness of the layup:

$$h := \sum_{n=1}^{plys} t_n \qquad h = 2 \times 10^{-2}\,in \quad .$$

The A matrix or the extensional stiffness matrix is calculated:

$$A := \sum_{k=1}^{plys} Qbar_k \cdot \left(t_k\right)$$

$$A = \begin{pmatrix} 2.67 \times 10^{5} & 4.95 \times 10^{4} & 4.7 \times 10^{4} \\ 4.95 \times 10^{4} & 7.87 \times 10^{4} & 4.7 \times 10^{4} \\ 4.7 \times 10^{4} & 4.7 \times 10^{4} & 6.16 \times 10^{4} \end{pmatrix} \frac{lbf}{in} \quad .$$

The B matrix or the coupling stiffness matrix is now calculated. In the case of a symmetric laminate, the B matrix will be zero:

$$B := \sum_{k=1}^{plys} Qbar_k \cdot \left(t_k\right) \cdot z_k$$

$$B = \begin{pmatrix} 0 & -0 & 0 \\ -0 & -0 & 0 \\ 0 & 0 & 0 \end{pmatrix} lbf \quad .$$

The D matrix or the bending stiffness matrix is calculated:

$$D := \sum_{k=1}^{plys} Qbar_k \cdot \left[\frac{\left(t_k\right)^3}{12} + t_k \left(z_k\right)^2 \right]$$

$$D = \begin{pmatrix} 1.23 \times 10^{1} & 6.09 \times 10^{-1} & 3.92 \times 10^{-1} \\ 6.09 \times 10^{-1} & 1.31 \times 10^{0} & 3.92 \times 10^{-1} \\ 3.92 \times 10^{-1} & 3.92 \times 10^{-1} & 1.01 \times 10^{0} \end{pmatrix} lbf\,in \quad .$$

To find a solution to this system of equations, define a matrix V to represent the forces and moments at the midplane of the plate. Then construct a "Global" matrix that represents the stiffness matrix. A computer subroutine "lsolve" will be used to find the matrix for the strain and curvatures. For the following equations to work in the Mathcad program, the matrices A, B, and D, must be made dimensionless:

$$A := \frac{A}{1 \cdot \frac{lbf}{in}} \qquad B := \frac{B}{1 \cdot lbf} \qquad D := \frac{D}{1 \cdot lbf \cdot in} .$$

Define V as the force and moment matrix. Force and moment matrix will be set to zero initially:

$$V := \begin{pmatrix} N_x \\ N_y \\ N_{xy} \\ M_x \\ M_y \\ M_{xy} \end{pmatrix} \qquad \begin{pmatrix} N_x \\ N_y \\ N_{xy} \\ M_x \\ M_y \\ M_{xy} \end{pmatrix} := \begin{pmatrix} 0 \\ 0 \\ 0 \\ 0 \\ 0 \\ 0 \end{pmatrix} \cdot \frac{lbf}{in} .$$

Create a global matrix to represent the A, B, and D matrices:

$$Global := stack(augment(A, B), augment(B, D))$$

$$Global = \begin{pmatrix} 266841.87 & 49470.05 & 47047.8 & 0 & -0 & 0 \\ 49470.05 & 78650.66 & 47047.8 & -0 & -0 & 0 \\ 47047.8 & 47047.8 & 61638.11 & 0 & 0 & 0 \\ 0 & -0 & 0 & 12.29 & 0.61 & 0.39 \\ -0 & -0 & 0 & 0.61 & 1.31 & 0.39 \\ 0 & 0 & 0 & 0.39 & 0.39 & 1.01 \end{pmatrix} .$$

The global matrix is equivalent to:

$$\begin{pmatrix} A_{11} & A_{12} & A_{13} & B_{11} & B_{12} & B_{13} \\ A_{21} & A_{22} & A_{23} & B_{21} & B_{22} & B_{23} \\ A_{31} & A_{32} & A_{33} & B_{31} & B_{32} & B_{33} \\ B_{11} & B_{12} & B_{13} & D_{11} & D_{12} & D_{13} \\ B_{21} & B_{22} & B_{23} & D_{21} & D_{22} & D_{23} \\ B_{31} & B_{32} & B_{33} & D_{31} & D_{32} & D_{33} \end{pmatrix} .$$

Find the effective modulus in the *x* direction by assuming a unit force in the *x* direction:

$$V = \begin{pmatrix} 1 \\ 0 \\ 0 \\ 0 \\ 0 \\ 0 \end{pmatrix} \frac{lbf}{in} \qquad \begin{pmatrix} N_x \\ N_y \\ N_{xy} \\ M_x \\ M_y \\ M_{xy} \end{pmatrix} := V \cdot \frac{lbf}{in} .$$

The lsolve function can be used to solve a linear system of *n* equations in *n* unknowns:

$$\begin{pmatrix} \varepsilon 0_x \\ \varepsilon 0_y \\ \gamma 0_{xy} \\ K_x \\ K_y \\ K_{xy} \end{pmatrix} := lsolve(Global, V) .$$

The lsolve function returns values for strain and curvature matrix. Young's modulus and Poisson's ratio can be calculated:

$$E_x := \frac{N_x}{h \cdot \varepsilon 0_x} \qquad E_x = 1.13 \times 10^7 \frac{lbf}{in^2} .$$

- Poisson's ratio

$$\nu_{xy} := \frac{-\varepsilon_{0y}}{\varepsilon_{0x}} \qquad \nu_{xy} = 3.17 \times 10^{-1} \ .$$

Now to find the effective modulus in the *y* direction, assume a unit force in the *y* direction:

$$V = \begin{pmatrix} 0 \times 10^{0} \\ 1 \times 10^{0} \\ 0 \times 10^{0} \\ 0 \times 10^{0} \\ 0 \times 10^{0} \\ 0 \times 10^{0} \end{pmatrix} \frac{lbf}{in} \qquad \begin{pmatrix} N_x \\ N_y \\ N_{xy} \\ M_x \\ M_y \\ M_{xy} \end{pmatrix} := V \cdot \frac{lbf}{in} \ .$$

Now solve the system of equations for the strain matrix:

$$\begin{pmatrix} \varepsilon_{0x} \\ \varepsilon_{0y} \\ \gamma_{0xy} \\ K_x \\ K_y \\ K_{xy} \end{pmatrix} := lsolve(Global, V) \ .$$

- Young's modulus in *y* direction:

$$E_y := \frac{N_y}{h \cdot \varepsilon_{0y}} \qquad E_y = 2.0972 \times 10^{6} \frac{lbf}{in^2} \ .$$

- Poisson's ratio:

$$\nu_{yx} := \frac{-\varepsilon_{0x}}{\varepsilon_{0y}} \qquad \nu_{yx} = 5.87 \times 10^{-2} \ .$$

Now to find the effective modulus in the *x* direction, assume a unit force in the *x*-*y* direction:

$$V = \begin{pmatrix} 0 \times 10^{0} \\ 0 \times 10^{0} \\ 1 \times 10^{0} \\ 0 \times 10^{0} \\ 0 \times 10^{0} \\ 0 \times 10^{0} \end{pmatrix} \frac{lbf}{in} \qquad \begin{pmatrix} N_x \\ N_y \\ N_{xy} \\ M_x \\ M_y \\ M_{xy} \end{pmatrix} := V \cdot \frac{lbf}{in} \ .$$

Now solve the system of equations for the strain matrix:

$$\begin{pmatrix} \varepsilon 0_x \\ \varepsilon 0_y \\ \gamma 0_{xy} \\ K_x \\ K_y \\ K_{xy} \end{pmatrix} := lsolve(Global, V) \ .$$

The shear modulus is calculated by:

$$G_{xy} := \frac{N_{xy}}{h \cdot \frac{\gamma 0_{xy}}{2}} \qquad G_{xy} = 3.22 \times 10^{6} \frac{lbf}{in^2} \ .$$

D.2 Determination of Ply Strains

Section D.1 determined the effective material properties of the plate or laminate. It is also desirable to determine the stress and strain of each ply. This is accomplished by using the constitutive equations to determine the midplane strains and curvatures.

For example, assume the laminated plate in the first example is loaded with 1,000 lbf in the *x* direction. The plate is 2 in. wide; the *x* direction is parallel to the 0° plies:

$$N_x := \frac{1000 \cdot lbf}{5 \cdot in} \qquad V_1 := N_x \frac{in}{lbf} \ .$$

The force applied in the x direction, set the first element of the V matrix equal to N_x. The values in the matrix must be unitless:

$$V = \begin{pmatrix} 2 \times 10^{2} \\ 0 \times 10^{0} \\ 0 \times 10^{0} \\ 0 \times 10^{0} \\ 0 \times 10^{0} \\ 0 \times 10^{0} \end{pmatrix} .$$

Now solve the system of equations for the strain matrix:

$$\begin{pmatrix} \varepsilon_{0x} \\ \varepsilon_{0y} \\ \gamma_{0xy} \\ K_x \\ K_y \\ K_{xy} \end{pmatrix} := \text{lsolve}(Global, V) .$$

Strains and curvatures at the midplane are found:

$$\varepsilon_{0x} = 8.82 \times 10^{-4} \qquad \varepsilon_{0y} = -2.8 \times 10^{-4} \qquad \gamma_{0xy} = -4.6 \times 10^{-4}$$

$$K_x = 0 \times 10^{0} \qquad K_y = 0 \times 10^{0} \qquad K_{xy} = 0 \times 10^{0} .$$

Transform the midplane strains and curvatures into the strains in each ply. Now determine the strains in the first 45° ply. z_{ply} is the distance from the midplane to the center of the ply:

$$n := 2 \qquad z_{ply} := z_n \cdot \frac{1}{in} \qquad z_{ply} = 2.5 \times 10^{-3}$$

$$\begin{pmatrix} \varepsilon_x \\ \varepsilon_y \\ \gamma_{xy} \end{pmatrix} := \begin{pmatrix} \varepsilon_{0x} \\ \varepsilon_{0y} \\ \gamma_{0xy} \end{pmatrix} + z_{ply} \begin{pmatrix} K_x \\ K_y \\ K_{xy} \end{pmatrix}$$

$$\begin{pmatrix} \varepsilon_x \\ \varepsilon_y \\ \gamma_{xy} \end{pmatrix} = \begin{pmatrix} 8.82 \times 10^{-4} \\ -2.8 \times 10^{-4} \\ -4.6 \times 10^{-4} \end{pmatrix} .$$

Transform these strains into the principal material directions for the 45° ply:

- Transformation matrix for 45° ply:

$$T_n = \begin{pmatrix} 5 \times 10^{-1} & 5 \times 10^{-1} & 1 \times 10^{0} \\ 5 \times 10^{-1} & 5 \times 10^{-1} & -1 \times 10^{0} \\ -5 \times 10^{-1} & 5 \times 10^{-1} & 0 \times 10^{0} \end{pmatrix} .$$

- Transformation equation:

$$\begin{pmatrix} \varepsilon_1 \\ \varepsilon_2 \\ \varepsilon_{12} \end{pmatrix} := T_n \begin{pmatrix} \varepsilon_x \\ \varepsilon_y \\ \varepsilon_{xy} \end{pmatrix} \qquad \begin{pmatrix} \varepsilon_1 \\ \varepsilon_2 \\ \varepsilon_{12} \end{pmatrix} = \begin{pmatrix} 7.13 \times 10^{-5} \\ 5.31 \times 10^{-4} \\ -5.81 \times 10^{-4} \end{pmatrix} .$$

- Use Reuter's matrix to convert to engineering strain:

$$\begin{pmatrix} \varepsilon_1 \\ \varepsilon_2 \\ \gamma_{12} \end{pmatrix} := R \cdot \begin{pmatrix} \varepsilon_1 \\ \varepsilon_2 \\ \varepsilon_{12} \end{pmatrix} \qquad \begin{pmatrix} \varepsilon_1 \\ \varepsilon_2 \\ \gamma_{12} \end{pmatrix} = \begin{pmatrix} 7.13 \times 10^{-5} \\ 5.31 \times 10^{-4} \\ -1.16 \times 10^{-3} \end{pmatrix} .$$

- Calculate the stresses within each ply. The stress can be calculated from the strain:

$$Qbar_n = \begin{pmatrix} 6.56 \times 10^{6} & 4.55 \times 10^{6} & 4.7 \times 10^{6} \\ 4.55 \times 10^{6} & 6.56 \times 10^{6} & 4.7 \times 10^{6} \\ 4.7 \times 10^{6} & 4.7 \times 10^{6} & 5.16 \times 10^{6} \end{pmatrix} \frac{lbf}{in^2} .$$

- Transformed reduced stiffness matrix for layer $n = 2$:

$$\begin{pmatrix} \varepsilon_x \\ \varepsilon_y \\ \gamma_{xy} \end{pmatrix} = \begin{pmatrix} 8.82 \times 10^{-4} \\ -2.8 \times 10^{-4} \\ -4.6 \times 10^{-4} \end{pmatrix}$$

$$\begin{pmatrix} \sigma_x \\ \sigma_y \\ \tau_{xy} \end{pmatrix} := Qbar_n \cdot \begin{pmatrix} \varepsilon_x \\ \varepsilon_y \\ \gamma_{xy} \end{pmatrix} .$$

- The stress for 45° ply in layer 2:

$$\begin{pmatrix} \sigma_x \\ \sigma_y \\ \tau_{xy} \end{pmatrix} = \begin{pmatrix} 2.35 \times 10^{3} \\ 1.99 \times 10^{1} \\ 4.6 \times 10^{2} \end{pmatrix} \frac{lbf}{in^2} .$$

- Transform the stress into the principal material direction:

$$\begin{pmatrix} \sigma_1 \\ \sigma_2 \\ \tau_{12} \end{pmatrix} := T_n \cdot \begin{pmatrix} \sigma_x \\ \sigma_y \\ \tau_{xy} \end{pmatrix} \qquad \begin{pmatrix} \sigma_1 \\ \sigma_2 \\ \tau_{12} \end{pmatrix} = \begin{pmatrix} 1.64 \times 10^{3} \\ 7.23 \times 10^{2} \\ -1.16 \times 10^{3} \end{pmatrix} \frac{lbf}{in^2} .$$

D.3 Determine the Displacement of the Laminated Plate

The definition of the plate curvatures provides an equation to determine the out-of-plane displacements for the plate. The curvature in the x and y directions is given by the following equations:

$$K_x := -\frac{d^2}{dx^2} w \qquad K_y := -\frac{d^2}{dy^2} w .$$

Since the curvatures are known values; i.e. constants, then *w* can be found by integration:

$$\int_{x_1}^{x_2}\left(\int_{x_1}^{x_2} -K_x\,dx\right) dx \text{ factor} \rightarrow .$$

Example of the integration:

- Limits of integration are along the edge of the plate:

$$x_1 := 0 \qquad x_2 := 0, .5 .. 10$$

$$y_1 := 0 \qquad y_2 := 0, .5 .. 5 .$$

- Example values ONLY!

$$K_x := .1371 \qquad K_y := -.4733 \qquad K_{xy} := 1.5 .$$

- Integrate the *x* curvature along the *x* edge of the plate:

$$w_x(x_1, x_2) := \int_{x_1}^{x_2}\left(\int_{x_1}^{x_2} -K_x\,dx\right) dx .$$

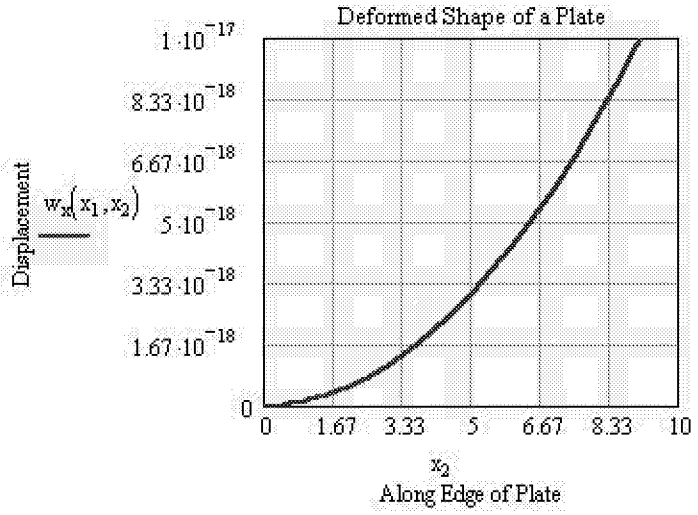

- Integrate the *y* curvature along the *y* edge of the plate:

$$w_y(y_1, y_2) := \int_{y_1}^{y_2} \left(\int_{y_1}^{y_2} -K_y \, dy \right) dy \ .$$

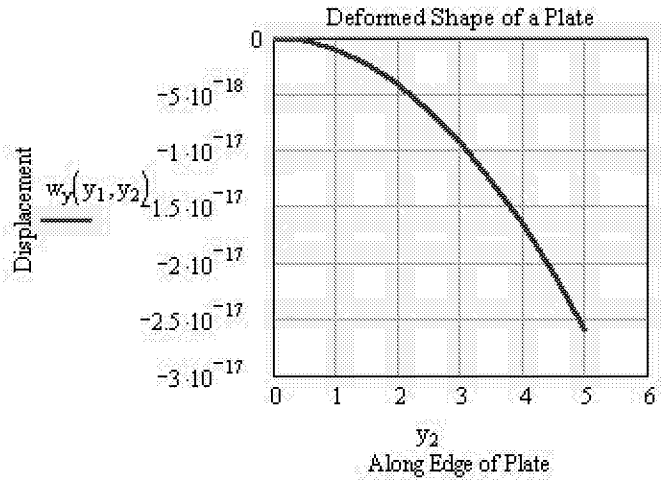

The *x* and *y* deflections can be found from the strains and the curvatures:

$$\varepsilon_x := \frac{d}{dx} u_0 - z \cdot \frac{d^2}{dx^2} w$$

$$\varepsilon_y := \frac{d}{dy} v_0 - z \cdot \frac{d^2}{dy^2} w$$

$$\gamma_{xy} := -2 \cdot z \cdot \frac{d}{dx} w \cdot \frac{d}{dy} w \ .$$

Midplane Strains	Midplane Curvatures
$\varepsilon_{0x} = 8.82 \times 10^{-4}$	$K_x = 0 \times 10^{0}$
$\varepsilon_{0y} = -2.8 \times 10^{-4}$	$K_y = 0 \times 10^{0}$
$\gamma_{0xy} = -4.6 \times 10^{-4}$	$K_{xy} = 0 \times 10^{0}$.

- Remove the units:

$$z := \frac{z}{1 \cdot in} .$$

Now integrating the midplane strains and curvatures over the length *x* and the width *y* of the plate:

$$\Delta x(x_1, x_2) := \int_{x_1}^{x_2} \varepsilon_{0x}\, dx - z_n \int_{x_1}^{x_2} \left(\int_{x_1}^{x_2} -K_x\, dx \right) dx$$

$$\Delta x(0.0, 10.0) = 8.82 \times 10^{-3} .$$

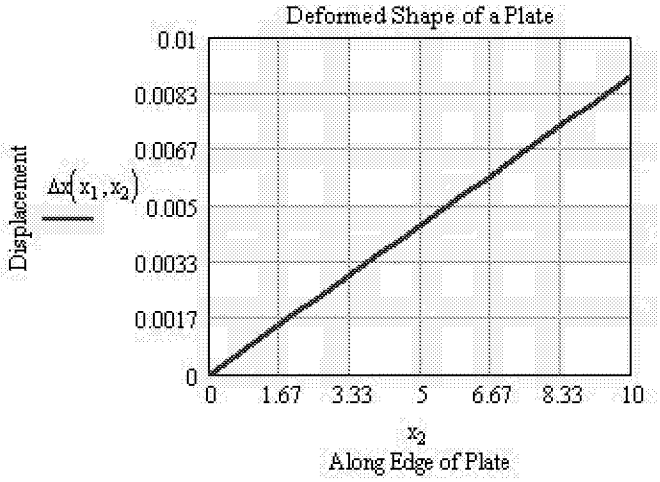

Now integrating the midplane strains and curvatures for the *y* direction:

$$\Delta y(y_1, y_2) := \int_{y_1}^{y_2} \varepsilon_{0y}\, dy - z_n \cdot \int_{y_1}^{y_2} \left(\int_{y_1}^{y_2} -K_y\, dy \right) dy$$

$$\Delta y(0.0, 5.0) = -1.4 \times 10^{-3} \quad .$$

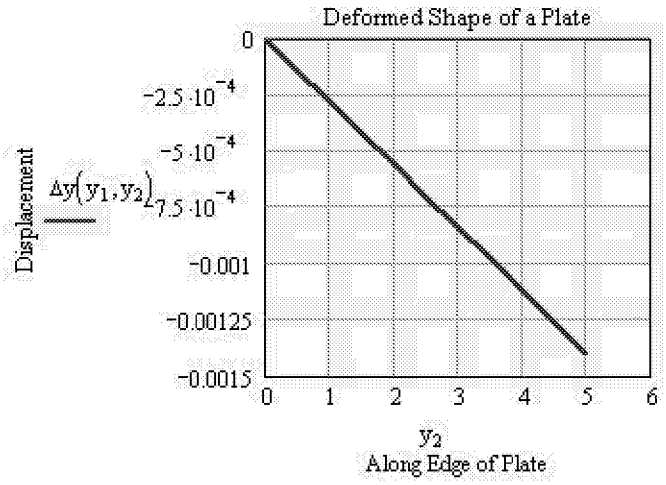

D.4 Determination of the Neutral Axis

The neutral axis is the plane of zero strain for any direction in an unsymmetric laminate:

- Strain equations in matrix form:

$$\begin{pmatrix} \varepsilon_x \\ \varepsilon_y \\ \gamma_{xy} \end{pmatrix} := \begin{pmatrix} \varepsilon_{0x} \\ \varepsilon_{0y} \\ \gamma_{0xy} \end{pmatrix} + z \cdot \begin{pmatrix} K_x \\ K_y \\ K_{xy} \end{pmatrix} \quad .$$

- Pure bending in the *x* direction:

$$\begin{pmatrix} 0 \\ 0 \\ 0 \\ M_x \\ 0 \\ 0 \end{pmatrix} = \begin{pmatrix} A_{11} & A_{12} & A_{13} & B_{11} & B_{12} & B_{13} \\ A_{21} & A_{22} & A_{23} & B_{21} & B_{22} & B_{23} \\ A_{31} & A_{32} & A_{33} & B_{31} & B_{32} & B_{33} \\ B_{11} & B_{12} & B_{13} & D_{11} & D_{12} & D_{13} \\ B_{21} & B_{22} & B_{23} & D_{21} & D_{22} & D_{23} \\ B_{31} & B_{32} & B_{33} & D_{31} & D_{32} & D_{33} \end{pmatrix} \cdot \begin{pmatrix} \varepsilon_{0x} \\ \varepsilon_{0Y} \\ \gamma_{0xy} \\ K_x \\ K_y \\ K_{xy} \end{pmatrix} .$$

- Solving for the midplane strains and curvatures:

$$\begin{pmatrix} \varepsilon_{0x} \\ \varepsilon_{0Y} \\ \gamma_{0xy} \\ K_x \\ K_y \\ K_{xy} \end{pmatrix} = \begin{pmatrix} A_{11} & A_{12} & A_{13} & B_{11} & B_{12} & B_{13} \\ A_{21} & A_{22} & A_{23} & B_{21} & B_{22} & B_{23} \\ A_{31} & A_{32} & A_{33} & B_{31} & B_{32} & B_{33} \\ B_{11} & B_{12} & B_{13} & D_{11} & D_{12} & D_{13} \\ B_{21} & B_{22} & B_{23} & D_{21} & D_{22} & D_{23} \\ B_{31} & B_{32} & B_{33} & D_{31} & D_{32} & D_{33} \end{pmatrix}^{-1} \cdot \begin{pmatrix} 0 \\ 0 \\ 0 \\ M_x \\ 0 \\ 0 \end{pmatrix} .$$

The equation can be reduced to the following:

$$\begin{pmatrix} \varepsilon_{0x} \\ \varepsilon_{0Y} \\ \gamma_{0xy} \\ K_x \\ K_y \\ K_{xy} \end{pmatrix} = \begin{pmatrix} B_{11} \\ B_{21} \\ B_{31} \\ D_{11} \\ D_{21} \\ D_{31} \end{pmatrix}^{-1} \cdot M_x .$$

Invert the B and D matrices; if B is singular, the program will set $B_{invrt} = 0$:

$$D_{invrt} := D^{-1} \qquad B_{invrt} := B \text{ on error } B^{-1} .$$

The above equation can then be separated to form an expression for the midplane strains and curvatures:

$$\begin{pmatrix} \varepsilon_{0x} \\ \varepsilon_{0Y} \\ \gamma_{0xy} \end{pmatrix} = \begin{pmatrix} B_{invrt_{11}} \\ B_{invrt_{21}} \\ B_{invrt_{31}} \end{pmatrix} \cdot M_x \qquad \begin{pmatrix} K_x \\ K_y \\ K_{xy} \end{pmatrix} = \begin{pmatrix} D_{invrt_{11}} \\ D_{invrt_{21}} \\ D_{invrt_{31}} \end{pmatrix} \cdot M_x \quad .$$

These equations are then substituted into the strain equation:

$$\begin{pmatrix} \varepsilon_x \\ \varepsilon_y \\ \gamma_{xy} \end{pmatrix} := \begin{pmatrix} B_{invrt_{1,1}} \\ B_{invrt_{2,1}} \\ B_{invrt_{3,1}} \end{pmatrix} \cdot M_x + z \cdot \left[\begin{pmatrix} D_{invrt_{1,1}} \\ D_{invrt_{2,1}} \\ D_{invrt_{3,1}} \end{pmatrix} \cdot M_x \right] \quad .$$

The general form of the equation to determine the neutral axis is given as guess values:

$$\begin{array}{lll} Z_{neuX} := 1.0 & \varepsilon_x := 0.0 & M_x := 1.0 \\ Z_{neuY} := 1.0 & \varepsilon_y := 0.0 & M_y := 0.0 \\ Z_{neuXY} := 1.0 & \gamma_{xy} := 0.0 & M_{xy} := 0.0 \end{array} \quad .$$

The general form of the equations to determine the neutral axis is given as:

$$\begin{aligned} \varepsilon_x &= B_{invrt_{1,1}} \cdot M_x + B_{invrt_{1,2}} \cdot M_y + B_{invrt_{1,3}} \cdot M_{xy} \ldots \\ &\quad + Z_{neuX} \cdot \left(D_{invrt_{1,1}} \cdot M_x + D_{invrt_{1,2}} \cdot M_y + D_{invrt_{1,3}} \cdot M_{xy} \right) \\ \varepsilon_y &= B_{invrt_{1,2}} \cdot M_x + B_{invrt_{2,2}} \cdot M_y + B_{invrt_{2,3}} \cdot M_{xy} \ldots \\ &\quad + Z_{neuY} \cdot \left(D_{invrt_{1,2}} \cdot M_x + D_{invrt_{2,2}} \cdot M_y + D_{invrt_{2,3}} \cdot M_{xy} \right) \\ \gamma_{xy} &= B_{invrt_{1,3}} \cdot M_x + B_{invrt_{2,3}} \cdot M_y + B_{invrt_{3,3}} \cdot M_{xy} \ldots \\ &\quad + Z_{neuXY} \cdot \left(D_{invrt_{1,3}} \cdot M_x + D_{invrt_{2,3}} \cdot M_y + D_{invrt_{3,3}} \cdot M_{xy} \right) \end{aligned} \quad .$$

The neutral axis is found using the Find command:

$$\begin{pmatrix} Z_{neuX} \\ Z_{neuY} \\ Z_{neuXY} \end{pmatrix} := \text{Find}\left(Z_{neuX}, Z_{neuY}, Z_{neuXY} \right) \quad .$$

The neutral axis for this example is at zero:

$$\begin{pmatrix} Z_{neuX} \\ Z_{neuY} \\ Z_{neuXY} \end{pmatrix} = \begin{pmatrix} 0 \\ -0 \\ 0 \end{pmatrix} \text{in} \quad .$$

Compare these results to the results from other methods:

- Nettles equations:

$$Ex_{Nettles} := \frac{A_{1,1}}{h} + \frac{A_{1,2}}{h}\cdot\left[\frac{A_{2,3}A_{1,3} - A_{1,2}\cdot A_{3,3}}{A_{2,2}\cdot A_{3,3} - (A_{2,3})^2}\right] \ldots + \frac{A_{1,3}}{h}\cdot\left[\frac{-A_{1,3}}{A_{3,3}} + \frac{A_{2,3}\cdot A_{1,2}\cdot A_{3,3} - (A_{2,3})^2\cdot A_{1,3}}{A_{2,2}\cdot(A_{3,3})^2 - (A_{2,3})^2\cdot A_{3,3}}\right]$$

$$Ex_{Nettles} = 1.13 \times 10^7 \frac{lbf}{in^2}$$

$$Ey_{Nettles} := \frac{A_{2,2}}{h} + \frac{A_{1,2}}{h}\cdot\left[\frac{A_{2,3}A_{1,3} - A_{1,2}\cdot A_{3,3}}{A_{1,1}\cdot A_{3,3} - (A_{1,3})^2}\right] \ldots + \frac{A_{2,3}}{h}\cdot\left[\frac{-A_{2,3}}{A_{3,3}} + \frac{A_{1,3}\cdot A_{1,2}\cdot A_{3,3} - (A_{1,3})^2\cdot A_{2,3}}{A_{1,1}\cdot(A_{3,3})^2 - (A_{1,3})^2\cdot A_{3,3}}\right]$$

$$Ey_{Nettles} = 2.1 \times 10^6 \frac{lbf}{in^2}$$

$$Gxy_{Nettles} := 2\cdot\left[\frac{A_{3,3}}{h} - \frac{(A_{2,3})^2}{h\cdot A_{2,2}} + \frac{2\cdot A_{1,3}\cdot A_{1,2}\cdot A_{2,2}\cdot A_{2,3} - (A_{1,2})^2\cdot(A_{2,3})^2 - (A_{1,3})^2\cdot(A_{2,2})^2}{h\cdot\left[(A_{1,1})\cdot(A_{2,2})^2 - (A_{1,2})^2\cdot A_{2,2}\right]}\right]$$

$$Gxy_{Nettles} = 3.22 \times 10^6 \frac{lbf}{in^2}$$

$$\nu_{xyNettles} := \frac{-2\cdot\left(A_{1,2} - \frac{A_{1,3}\cdot A_{2,3}}{A_{3,3}}\right)}{\left[A_{2,2} - \frac{(A_{2,3})^2}{A_{3,3}}\right]}$$

$$\nu_{xyNettles} = -6.34 \times 10^{-1}$$

$$\nu_{yxNettles} := \frac{-\left(\frac{A_{1,3}\cdot A_{2,3}}{A_{3,3}} - A_{1,2}\right)}{\left[\frac{(A_{1,3})^2}{A_{3,3}} - A_{1,1}\right]}$$

$$\nu_{yxNettles} = -5.87 \times 10^{-2} \quad .$$

- Halpin equations:

$$E_{xHalpin} := \frac{A_{1,1}\cdot A_{2,2} - (A_{1,2})^2}{A_{2,2}\cdot h}$$

$$E_{xHalpin} = 1.18 \times 10^{7}\ \frac{lbf}{in^2}$$

$$E_{yHalpin} := \frac{A_{1,1}\cdot A_{2,2} - (A_{1,2})^2}{A_{1,1}\cdot h}$$

$$E_{yHalpin} = 3.47 \times 10^{6}\ \frac{lbf}{in^2}$$

$$G_{xyHalpin} := \frac{A_{3,3}}{h}$$

$$G_{xyHalpin} = 3.08 \times 10^{6} \frac{lbf}{in^2}$$

$$\nu_{xyHalpin} := \frac{A_{1,2}}{A_{2,2}}$$

$$\nu_{xyHalpin} = 6.29 \times 10^{-1} \quad .$$

REFERENCES

1. Biszick, K.R.: "Design of Lightweight, Thin-Walled, Reinforced Concrete Panels for Reverse Bending," *Masters Thesis*, University of Alabama in Huntsville, Huntsville, AL, 1999.

2. Balaguru, P.: *Ferrocement in Bending, Part I: Static Nonlinear Analysis,* National Science Foundation NSF Eng–20829, August 1976.

3. Krenchel, H.: *Fibre Reinforcement,* Akademisk Forlag, Copenhagen, 1964.

4. Balaguru, P.; and Shah, S.: *Fiber Reinforced Cement Composites*, McGraw-Hill, New York, NY, 1992.

5. "Standard Test Method for Tensile Properties of Plastics," *ASTM D 638–99*, 1999.

6. Beer, F.; and Johnston, R.: *Mechanics of Materials,* McGraw-Hill, New York, NY, 1981.

7. Allen, D.; and Haisler, W.: *Introduction to Aerospace Structural Analysis*, Wiley, NY, 1985.

8. Balaguru, P.: Private Communication, April 14, 2000.

9. Halpin, J.C.: *Primer on Composite Materials Analysis*, Technomic Publishing Co., Lancaster, PA, 1992.

10. Jones, R.M.: *Mechanics of Composite Materials*, McGraw-Hill, NY, 1975.

11. Tsai, S.W.: *Theory of Composites Design*, Think Composites, Dayton, OH, 1992.

12. "Standard Test Method for Tensile Properties of Metallic Material," *ASTM E8–99*, 1999.

13. Bulletin 309D, *Student Manual for Strain Gage Technology*, Measurement Group, Inc., Raleigh, NC, 1992.

14. "Strain Gage Installations for Concrete Structures," *Micro-Measurements Tech Tip TT–611*, 1998.

15. "Standard Test Method for Shear Properties of Composite Materials by the V-Notched Beam Method," *ASTM D 5379–93*, 1993.

16. Conant, N.; and Odom, E.: "An Improved Iosipescu Shear Test Fixture," *Journal of Composites Technology & Research*, Vol. 17, N1, pp. 50–55, January 1995.

17. Ifju, P.G.: "The Shear Gage: For Reliable Shear Modulus Measurements of Composite Materials," *Experimental Mechanics*, Vol. 34, N4, December 1994.

18. Ifju, P.G.: "The Shear Gage: For Reliable Shear Modulus Measurements of Composite Materials," *Proceedings of SEM Spring Conference on Experimental Mechanics*, Milwaukee, WI, June 1991.

19. Gurdal, Z.: *Design and Optimization of Laminated Composite Materials*, John Wiley & Sons, NY, 1999.

20. Nettles, A.T.: "Basic Mechanics of Laminated Composite Plates," *NASA Reference Publication 1351*, October 1994.

21. Matthews, F.L.; et al.: *Finite Element Modeling of Composite Materials and Structures*, WoodHead, Cambridge, England, 2000.

22. MSC/Software: *MacNeal, Schwendlec Corporation (MSC)/Nastran Finite Element Software*, Macneal-Schwendler Corporation, Los Angeles, CA, 2000.

23. Watson, R.B.: *"Factors Influencing the Measurement of Shear Properties When Using V-Notch Specimens With Strain Gages,"* Measurement Group Inc., P.O. Box 27777, Raleigh, NC, 27611, 1992.

24. *Mathcad 2000 Pro Software*, www.mathsoft.com, MathSoft Inc., Cambridge, MA, 2000.

REPORT DOCUMENTATION PAGE

Form Approved
OMB No. 0704-0188

1. AGENCY USE ONLY *(Leave Blank)*	2. REPORT DATE	3. REPORT TYPE AND DATES COVERED
	February 2002	Technical Memorandum

4. TITLE AND SUBTITLE

Analysis of Graphite-Reinforced Cementitious Composites

5. FUNDING NUMBERS

6. AUTHORS

R.E. Vaughan

7. PERFORMING ORGANIZATION NAMES(S) AND ADDRESS(ES)

George C. Marshall Space Flight Center
Marshall Space Flight Center, AL 35812

8. PERFORMING ORGANIZATION REPORT NUMBER

M–1040

9. SPONSORING/MONITORING AGENCY NAME(S) AND ADDRESS(ES)

National Aeronautics and Space Administration
Washington, DC 20546–0001

10. SPONSORING/MONITORING AGENCY REPORT NUMBER

NASA/TM—2002–211545

11. SUPPLEMENTARY NOTES

Prepared by Structures, Mechanics, and Thermal Department, Engineering Directorate

12a. DISTRIBUTION/AVAILABILITY STATEMENT

Unclassified-Unlimited
Subject Category 39
Nonstandard Distribution

12b. DISTRIBUTION CODE

13. ABSTRACT *(Maximum 200 words)*

Strategically embedding graphite meshes in a compliant cementitious matrix produces a composite material with relatively high tension and compressive properties as compared to steel-reinforced structures fabricated from a standard concrete mix. Although these composite systems are somewhat similar, the methods used to analyze steel-reinforced composites often fail to characterize the behavior of their more advanced graphite-reinforced counterparts. This Technical Memorandum describes some of the analytical methods being developed to determine the deflections and stresses in graphite-reinforced cementitious composites. It is initially demonstrated that the standard transform section method fails to provide accurate results when the elastic moduli ratio exceeds 20. An alternate approach is formulated by using the rule of mixtures to determine a set of effective material properties for the composite. Tensile tests are conducted on composite samples to verify this approach. When the effective material properties are used to characterize the deflections of composite beams subjected to pure bending, an excellent agreement is obtained. Laminated composite plate theory is investigated as a means for analyzing even more complex composites, consisting of multiple graphite layers oriented in different directions. In this case, composite beams are analyzed using the laminated composite plate theory with material properties established from tensile tests. Then, finite element modeling is used to verify the results. Considering the complexity of the samples, a very good agreement is obtained.

14. SUBJECT TERMS	15. NUMBER OF PAGES
laminated composite plates, rule of mixtures, experimental methods for composites	206
	16. PRICE CODE

17. SECURITY CLASSIFICATION OF REPORT	18. SECURITY CLASSIFICATION OF THIS PAGE	19. SECURITY CLASSIFICATION OF ABSTRACT	20. LIMITATION OF ABSTRACT
Unclassified	Unclassified	Unclassified	Unlimited

National Aeronautics and
Space Administration
AD33
George C. Marshall Space Flight Center
Marshall Space Flight Center, Alabama
35812